NEW TECHNOLOGIES FOR DETECTION, MONITORING AND TREATMENT OF PARKINSON'S DISEASE

EDITED BY: Martin J. McKeown, Xun Chen, Meeko Oishi and Aiping Liu
PUBLISHED IN: Frontiers in Aging Neuroscience, Frontiers in Neuroscience and Frontiers in Neurology

frontiers Research Topics

frontiers

ISSN 1664-8714
ISBN 978-2-88963-886-4
DOI 10.3389/978-2-88963-886-4

About Frontiers

Frontiers is more than just an open-access publisher of scholarly articles: it is a pioneering approach to the world of academia, radically improving the way scholarly research is managed. The grand vision of Frontiers is a world where all people have an equal opportunity to seek, share and generate knowledge. Frontiers provides immediate and permanent online open access to all its publications, but this alone is not enough to realize our grand goals.

Frontiers Journal Series

The Frontiers Journal Series is a multi-tier and interdisciplinary set of open-access, online journals, promising a paradigm shift from the current review, selection and dissemination processes in academic publishing. All Frontiers journals are driven by researchers for researchers; therefore, they constitute a service to the scholarly community. At the same time, the Frontiers Journal Series operates on a revolutionary invention, the tiered publishing system, initially addressing specific communities of scholars, and gradually climbing up to broader public understanding, thus serving the interests of the lay society, too.

Dedication to Quality

Each Frontiers article is a landmark of the highest quality, thanks to genuinely collaborative interactions between authors and review editors, who include some of the world's best academicians. Research must be certified by peers before entering a stream of knowledge that may eventually reach the public - and shape society; therefore, Frontiers only applies the most rigorous and unbiased reviews.
Frontiers revolutionizes research publishing by freely delivering the most outstanding research, evaluated with no bias from both the academic and social point of view. By applying the most advanced information technologies, Frontiers is catapulting scholarly publishing into a new generation.

What are Frontiers Research Topics?

Frontiers Research Topics are very popular trademarks of the Frontiers Journals Series: they are collections of at least ten articles, all centered on a particular subject. With their unique mix of varied contributions from Original Research to Review Articles, Frontiers Research Topics unify the most influential researchers, the latest key findings and historical advances in a hot research area! Find out more on how to host your own Frontiers Research Topic or contribute to one as an author by contacting the Frontiers Editorial Office: researchtopics@frontiersin.org

NEW TECHNOLOGIES FOR DETECTION, MONITORING AND TREATMENT OF PARKINSON'S DISEASE

Topic Editors:
Martin J. McKeown, University of British Columbia, Canada
Xun Chen, University of Science and Technology of China, China
Meeko Oishi, University of New Mexico, United States
Aiping Liu, University of British Columbia, Canada

Citation: McKeown, M. J., Chen, X., Oishi, M., Liu, A., eds. (2020). New Technologies for Detection, Monitoring and Treatment of Parkinson's Disease. Lausanne: Frontiers Media SA. doi: 10.3389/978-2-88963-886-4

Table of Contents

frontiers in Aging Neuroscience

ORIGINAL RESEARCH
published: 14 January 2019
doi: 10.3389/fnagi.2018.00438

Increased DJ-1 and α-Synuclein in Plasma Neural-Derived Exosomes as Potential Markers for Parkinson's Disease

Zhen-Hua Zhao[1†], Zhi-Ting Chen[2†], Rui-Ling Zhou[1], Xu Zhang[1], Qin-Yong Ye[2†] and Yin-Zhou Wang[1*†]*

[1] Department of Neurology, Fujian Provincial Hospital, Provincial Clinical College of Fujian Medical University, Fuzhou, China,
[2] Department of Neurology, Fujian Medical University Union Hospital, Fuzhou, China

The diagnosis of PD might be in difficulty, especially in the early stages. Therefore, the identification of novel biomarkers is imperative for the diagnosis and monitoring disease progression in PD. DJ-1 and α-synuclein, are two proteins that are critically involved in the pathogenesis of PD, and they have been examined as disease biomarkers in studies. However, no study exists regarding DJ-1 in plasma neural-derived exosomes. In the present study, the levels of DJ-1 and α-synuclein in plasma neural-derived exosomes were studied together in order to investigate novel biomarkers for PD. DJ-1 and α-synuclein in plasma and plasma neural-derived exosomes of the patients with PD and controls were quantified by ELISAs. The data revealed that the levels of DJ-1 and α-synuclein in plasma neural-derived exosomes and the ratio of plasma neural-derived exosomal DJ-1 to total DJ-1 were significantly higher in patients with PD, compared with controls, while levels of the two proteins in plasma exhibited no difference between the patients with PD and controls. However, no relationship was identified between biomarkers and disease progression. In addition, significant positive correlations between DJ-1 and α-synuclein in plasma neural-derived exosomes were found in the patients with PD and in healthy individuals. We hypothesize that DJ-1 in plasma neural-derived exosomes may be used as a potential biomarker as α-synuclein in PD and they might participate in the mechanism of PD together.

Keywords: α-synuclein, DJ-1, biomarker, plasma, exosome, Parkinson disease

OPEN ACCESS

Edited by:
Xun Chen,
University of Science and Technology of China, China

Reviewed by:
Liuqing Yang,
Johns Hopkins Medicine, United States
Deep R. Sharma,
SUNY Downstate Medical Center, United States
En Huang,
Temple University, United States

***Correspondence:**
Qin-Yong Ye
unionqyye@163.com
Yin-Zhou Wang
wphd@163.com

† These authors have contributed equally to this work

Received: *03 September 2018*
Accepted: *21 December 2018*
Published: *14 January 2019*

Citation:
Zhao Z-H, Chen Z-T, Zhou R-L, Zhang X, Ye Q-Y and Wang Y-Z (2019) Increased DJ-1 and α-Synuclein in Plasma Neural-Derived Exosomes as Potential Markers for Parkinson's Disease. Front. Aging Neurosci. 10:438. doi: 10.3389/fnagi.2018.00438

INTRODUCTION

Parkinson's disease (PD), characterized by a set of extrapyramidal motor features, is the second most common neurodegenerative disease worldwide. The beginning of disease-specific pathology occurs before the onset of classical clinical manifestations, and the symptoms of PD are not apparent until almost 60% of the dopamine neurons have died (Berardelli et al., 2013). PD in the early stages is prone to be misdiagnosed, due to a lack of suitable disease biomarkers and overt clinical symptoms. Consequently, there is still a substantial misdiagnosis rate.

Gene mutations of α-synuclein culminate in familial PD and α-synuclein has a close association with the pathogenic mechanism of heredofamilial and sporadic PD (Lucking and Brice, 2000; Braak and Del Tredici, 2017). DJ-1 is another gene product that has previously been

associated with both heredofamilial and sporadic PD, and appears to be associated with oxidative stress, which is an acritical process related to PD (Choi et al., 2006). Consequently, DJ-1 and α-synuclein have been considered to be leading biomarkers for PD (Hong et al., 2010). However, it is presently unknown whether the combination of DJ-1 and α-synuclein will be a more suitable combination for the diagnosis of PD.

Cerebrospinal fluid (CSF) has been reported to function as an accurate and reliable source for biomarkers in PD (Farotti et al., 2017). However, obtaining CSF is a cumbersome process compared to blood sampling in a regular clinical setting. Blood is an accessible source for application in a clinical setting (Mehta and Adler, 2016). However, a principal disadvantage of blood biomarkers is that they do not directly reflect the conditions in the central nerve system and are more easily affected by the peripheral environment.

Exosomes containing proteins and other constituents of their cellular origin are a means of communication between cells. Exosomes might be a pathway for neurons to divert proteins from neurons into the CSF or into the peripheral blood via blood–brain barrier. These materials associated with PD, including α-synuclein, maybe excessive and/or in a toxic or insoluble structure. To confirm this hypothesis, Shi and colleagues injected mice intracerebroventricularly with 125I-labeled α-synuclein or tau. And, they observed that 125I-labeled α-synuclein or tau could be detected in neural-derived blood exosomes which expressed the neuronal adhesion molecule L1CAM (Shi et al., 2014, 2016). Exosomal α-synuclein in neural-derived blood exosomes was increased in patients with PD (Shi et al., 2014). However, to the best of our knowledge, there are no relevant studies on exosomal DJ-1 in neural-derived blood exosomes.

In the present study, a combination of chemical and immunochemical methods were used to harvest and enrich neural-derived exosomes from small volumes of plasma in quantities that was enough to detect the implicated proteins in the pathogenic mechanism of PD. The levels of DJ-1 and α-synuclein in plasma neural-derived exosomes were analyzed in order to evaluate any potential associations with PD, and to assess their suitability as biomarkers for the disease. In addition, the levels of α-synuclein in plasma neural-derived exosomes were analyzed to investigate any associations between DJ-1 and α-synuclein, and the relationship between these proteins and the progression of PD were further investigated.

MATERIALS AND METHODS

Participants

This study was performed in the Department of Neurology of Fujian Provincial Hospital, Fuzhou, China, and was approved by the Ethics Committees of Fujian Provincial Hospital. Laboratorians and statistical analyst were blinded to any clinical information and the grouping. All individuals provided written informed consents.

From January 2016 to June 2017, a total of 39 PD patients were recruited. All patients with PD were diagnosed according to the United Kingdom Parkinson's Disease Society Brain Bank criteria (Hughes et al., 1992). The healthy controls were the patients' husbands or wifes, or healthy community volunteers. The individuals in the control group did not exhibit any signs or symptoms indicative of neurological disease. All individuals were excluded on the following criteria: the presence of (1) tumors, (2) essential tremors, secondary parkinsonism, or Parkinson-plus syndrome, (3) severe craniocerebral trauma, (4) inflammatory, infectious, or autoimmune diseases in the peripheral and central systems, (5) severe systemic diseases, such as anemia, hepatosis, heart failure, pulmonary disorders, and chronic renal failure, and (6) other neurodegenerative diseases.

All patients with PD and control subjects received an assessment which contained medical history, physical and neurological examinations, laboratory tests, and neuropsychological assessment. The laboratory evaluation consisted of routine blood parameters, serum electrolytes, blood urea nitrogen, creatinine, fasting blood glucose, vitamin B12 and thyroid stimulating hormone. The above results for all study participants were normal. All patients with PD were assessed using Hoehn-Yahr (H-Y) and Unified Parkinson's Disease Rating Scale-III (UPDRS-III) scores. The duration of disease since the time of initial diagnosis was available and used for subsequent analysis. Blood samples were collected at fasting state in the morning, after patients and controls were enrolled in the present study, and all plasmas were stored at −80°C.

Isolation of Plasma Neural-Derived Exosomes

Exosomes were isolated according to the experimental protocol described in a previous report (Goetzl et al., 2015). Briefly, 0.8 ml of plasma was incubated with 0.15 ml of thromboplastin-D (Thermo Fisher Scientific, Inc., Waltham, MA, United States) for 60 min. The plasma was then added to 0.35 ml of calcium- and magnesium-free Dulbecco's balanced salt solution (DBS-2) with protease inhibitor cocktail (Roche Applied Science, Inc., Madison, WI, United States) and phosphatase inhibitor cocktail (Thermo Scientific, Inc.). Following centrifugation at 1,500 × *g* for 20 min, the supernatant was mixed with 252 μl of ExoQuick exosome precipitation solution (EXOQ; System Biosciences, Inc., Palo Alto, CA, United States), and incubated for 1 h at 4°C. The resulting exosome suspensions were centrifuged at 1,500 × *g* for 30 min at 4°C, and each precipitation was re-suspended in 150 μl of DBS-2 with inhibitor cocktails and 100 μl of 3% bovine serum albumin. The suspensions were subsequently incubated for 1 h at 4°C with 1 μg of mouse anti-human CD171 (L1CAM neural adhesion protein) biotinylated antibody (clone 5G3, eBioscience; Thermo Fisher Scientific, Inc.) and 25 μl of streptavidin-agarose resin (Thermo Scientific, Inc.) with 50 μl of 3% BSA. Following being centrifuged at 200 × g for 10 min at 4°C and removal of the supernatant, each precipitation was suspended in 50 μl of 0.05 M glycine-HCl (pH 3.0) by vortexing for 10 s. Subsequently, 0.45 ml of DBS-2 with 2 g/100 ml of BSA, 0.10% Tween 20 and the inhibitor cocktails, was added to each suspension. After vortex-mixing, each suspension was incubated for 10 min at 37°C with. Samples were then stored at −80°C prior to ELISAs. The protein concentration of exosomes from the neural source was

determined using the Bradford protein assay (Tiangen Biotech, Co., Ltd., Beijing, China), with bovine serum albumin as a standard.

Transmission Electron Microscopy

The exosomes were placed in a droplet of 2.5% glutaraldehyde in PBS buffer at pH 7.2 and fixed for 2 h at 4°C. The samples were washed in 0.1 M PBS buffer and fixed in 1% osmium tetroxide for 2 h at 4°C. The samples were then dehydrated for 10 min in increasing concentrations of alcohol (50, 70, 90, and 100%, repeated three times), then infiltrated with alcohol/propylene oxide (1:1) and propylene oxide for 10 min at room temperature, respectively. The samples were embedded in Quetol-812 epoxy resin and polymerized at 40°C for 2 h, 60°C for 4 h, and 80°C for 10 h. Ultrathin sections (100 nm) were cut using a Leica UC6 ultra-microtome, and then were stained with uranyl acetate for 15 min and with lead citrate for 10 min at room temperature. The results were observed in a FEI TecnaiSPIRIT transmission electron microscope (Camcor, Eugene, OR, United States), operated at 120 kV.

ELISA Quantification of Exosome Proteins and Plasma Protein

The proteins in plasma neural-derived exosomes were quantified by ELISA kits for α-synuclein and human DJ-1 (R&D Systems, Inc., Minneapolis, MN, United States), according to the manufacturer's protocol. Plasma α-synuclein and human DJ-1 were also quantified, and the test for biomarker was repeated 3 times.

Data Analyses

In the present study, SPSS Statistics 19.0 (IBM, Corp., Armonk, NY, United States) was used for statistical analyses. $p < 0.05$ was accepted to be statistically significant in all cases. All continuous variables, including age, UPDRS-III scores, duration of disease, the levels of DJ-1 in exosomes, total DJ-1 in plasma, α-synuclein in exosomes, total α-synuclein in plasma, and their ratio are presented as the mean ± standard deviation (SD). A χ^2 test was used for comparing the differences between sexes. In order to compare the differences between age and biomarkers between the groups, a *t*-test was used to detect statistically significant differences when the data were normally distributed, and a Mann–Whitney *U*-test when the data were not normally distributed. In order to evaluate correlations among the biomarkers, Pearson's correlation coefficients for DJ-1 and α-synuclein of plasma were obtained. Spearman's correlation coefficients were also obtained to evaluate the correlations among the biomarkers of which the data do not conform to the normal distribution. Receiver operating characteristic (ROC) curves for the biomarkers were generated to evaluate their sensitivities and specificities in distinguishing PD from healthy controls. The "optimum" cut-off value for a ROC curve was the point associated with the maximal sum of sensitivity and specificity. ROC curves for the combination of DJ-1 and α-synuclein were also calculated using logistic regression analysis.

RESULTS

Evaluation of DJ-1 and/or α-Synuclein in Plasma and Plasma Neural-Derived Exosome as Biomarkers for PD

Plasma neural-derived exosomes were extracted and corroborated by transmission electron microscopy (**Figure 1A**). The concentrations of DJ-1 in the plasma neural-derived exosomes and plasma were measured using ELISAs. There was no significant difference in DJ-1 in the total plasma between patients with PD and controls in the total plasma (2.26 ± 0.65 vs. 2.49 ± 0.60 ng/ml, $p = 0.104$). The concentrations of DJ-1 in the plasma neural-derived exosomes were significantly higher in patients with PD compared with healthy controls (2.94 ± 0.96 vs. 2.34 ± 0.86 ng/mg, $p = 0.002$). The ratio of plasma neural-derived exosomal DJ-1 to total DJ-1 (exo/total) was also significantly higher in patients with PD, compared with the controls (1.39 ± 0.57 vs. 1.00 ± 0.50, $p = 0.001$) (**Table 1**).

The concentrations of α-synuclein in plasma neural-derived exosome and in plasma were also measured using ELISAs. Similar to the findings of a previous study (Shi et al., 2014), there was no significant difference in the plasma α-synuclein concentrations between patients with PD and controls (3.01 ± 1.51 vs. 3.01 ± 1.17 ng/ml, $p = 0.565$). However, the concentrations of α-synuclein in plasma neural-derived exosomes were significantly higher in patients with PD compared with healthy controls (7.75 ± 2.74 vs. 6.50 ± 1.17 ng/mg, $p = 0.018 < 0.05$) (**Table 1**).

To further evaluate the potential for DJ-1 and α-synuclein in plasma neural-derived exosomes to aid in the diagnosis of PD, ROC analysis was performed to characterize its sensitivity and specificity. The AUC for α-synuclein was 0.654, when the cut off value was 8.14 ng/mg, with a sensitivity of 48.7% and specificity of 85.0% (**Figure 1B**). The ROC analysis performance of DJ-1 in plasma neural-derived exosomes was identified to be moderate (AUC = 0.703, sensitivity = 79.5%, specificity = 57.5%) (**Figure 1C**), as the cut off values was 2.06 ng/mg. The exo/total DJ-1 generated a similar AUC result (0.724) with a sensitivity of 59.0% and a specificity of 82.5% at a cutoff value of 0.415 (**Figure 1D**). The AUC for the combination of DJ-1 and α-synuclein was 0.714 (**Figure 1E**), with a sensitivity of 82.1% and a specificity of 52.5% at a cutoff value of 0.35 on the predicted risk algorithm. The combination of these two proteins did not perform a significant discrimination.

Evaluating the Relationships Between DJ-1 and α-Synuclein Levels of Plasma and Plasma Neural-Derived Exosomes

To evaluate the relationships between DJ-1 and α-synuclein levels of plasma and plasma neural-derived exosomes, the present study conducted a correlation analysis. A significant positive correlation was identified between DJ-1 and α-synuclein levels of plasma neural-derived exosomes in patients with PD (**Figure 2A**) and controls (**Figure 2B**). No correlation was found between the plasma levels of DJ-1 and α-synuclein in patients with PD

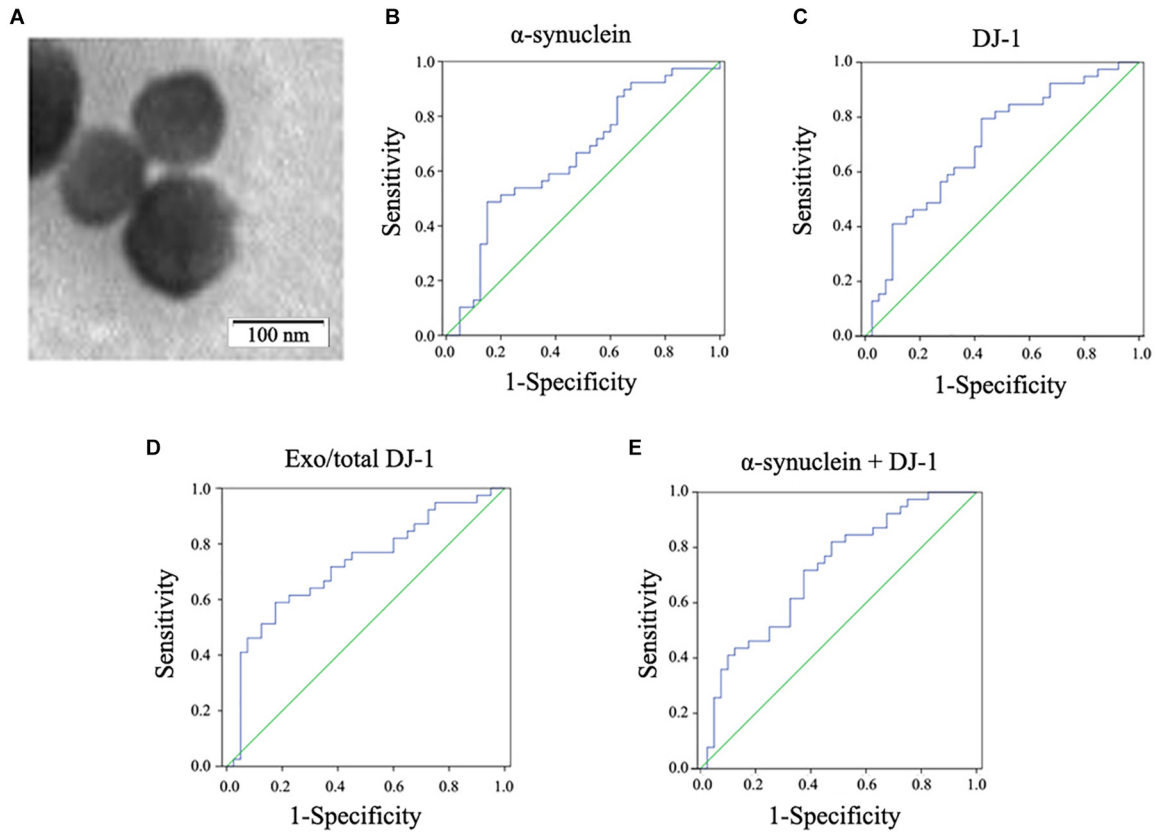

FIGURE 1 | Observation of plasma neural-derived exosomes and ROC analysis of biomarkers for PD diagnosis. Exosomes with lipid bilayer structure were observed under the transmission electron microscope (black arrow). Scale bars: 100 nm **(A).** In the whole cohort, α-synuclein in plasma neural-derived exosomes provided an AUC of 0.654 (sensitivity = 48.7%, specificity = 85.0%) for PD versus controls **(B)**. DJ-1 in plasma neural-derived exosomes performed similarly (AUC = 0.703, sensitivity = 79.5%, specificity = 57.5%) in the whole cohort **(C)**. The AUC of the ratio of plasma neural-derived exosomal DJ-1 to total DJ-1 was 0.724 with a sensitivity of 59.0% and a specificity of 82.5% **(D).** The AUC of α-synuclein +DJ-1 was 0.714 **(E)**.

(**Figure 2C**), but a weak correlation was found in controls (**Figure 2D**).

Correlation Between DJ-1 or α-Synuclein and the Progression of PD

Patients with PD were classified into H-Y stages 1–5 (Hoehn and Yahr, 1967), and were divided into two groups, early stage PD (H-Y 1 to 2) which included 22 patients and advanced stage PD (H-Y 3 to 5) which included 17 patients. Patients with PD in the advanced stage had a longer disease duration and higher UPDRS-III scores when compared with patients with PD in the early stage. However, no significant differences were identified in the neural-derived exosome and plasma levels of DJ-1 and α-synuclein between patients with PD at the early stage and advanced stages of disease (**Table 1**).

DISCUSSION

The development of effective biomarkers is an important and urgent task for PD in the early stage. A reliable biomarker can be conductive to identifying patients with PD in the early stage. And, it can also be used for the development of new therapy to treat the disease.

Plasma neural-derived exosomes may serve as a potentially sources that accurately reflects the changes of the central nervous system (CNS) (Shi et al., 2016). Exosomes from CNS which contain jettisoned and potentially toxic forms of α-synuclein or other disease-associated proteins that may be transported into the systemic circulation system (Shi et al., 2014). In addition, these exosomes may avoid the interferences from the blood contamination, system inflammation, and potential tumor. The study of Fiandaca et al. (2015) revealed that the exosomal levels of P-S396-tau, P-T181-tau and Aβ1-42 were significantly higher than in controls at one to 10 years prior to diagnosis with Alzheimer's disease. In a subsequent series of studies, astrocyte-derived exosomes or neural-derived exosomes were obtained from plasma by using the same method of polymer-based precipitation and combination of biotinylated antibody and streptavidin-agarose resin (Goetzl et al., 2015, 2016). In the present study, neural-derived exosomes were obtained using this method, and their origin was confirmed using transmission electron microscopy, and similar results were obtained when compared with a previous study (Shi et al., 2014). The principal

TABLE 1 | Compare of demographics and biomarkers between control subjects and PD.

		Parkinson's disease stage				
	Control	**Early**	**Advanced**	**Total**	***P*1**	***P*2**
Number of cases	40	22	17	39		
Sex (M/F)	17/23	15/7	8/9	23/16	0.143	0.184
Age (years)						
Mean ± SD	66.6 ± 8.8	65.2 ± 11.2	67.5 ± 6.8	67.5 ± 6.9	0.820[b]	0.445[b]
Range	46–80	39–79	58–82	39–82	–	–
Duration of disease (years)						
Mean ± SD	–	3.9 ± 2.5	6.4 ± 3.6	5.0 ± 3.2	–	0.016[a*]
Range	–	0.3–9	2–15	0.3–15	–	–
UPDRS-III scores	–	37.8 ± 15.2	62.6 ± 19.3	48.6 ± 21.0	–	< 0.001[b*]
Exosomes DJ-1 (ng/mg)	2.34 ± 0.86	2.97 ± 0.97	2.90 ± 0.97	2.94 ± 0.96	0.002[a*]	0.734[a]
Plasma DJ-1 (ng/ml)	2.49 ± 0.60	2.17 ± 0.51	2.39 ± 0.97	2.26 ± 0.65	0.104[b]	0.297[b]
Exo/total DJ-1	1.00 ± 0.50	1.44 ± 0.58	1.33 ± 0.58	1.39 ± 0.57	0.001[a*]	0.515[a*]
Exosomes α-syn (ng/mg)	6.50 ± 1.17	7.97 ± 2.97	7.46 ± 2.46	7.75 ± 2.74	0.018[a*]	0.650[a]
Plasma α-syn (ng/ml)	3.01 ± 1.17	3.04 ± 1.59	2.98 ± 1.44	3.01 ± 1.51	0.565[a]	0.820[a]
Exo/total α-syn	2.51 ± 1.45	3.19 ± 1.94	3.00 ± 1.68	3.11 ± 1.81	0.141[a]	0.777[a]

*exo, exosomes; α-syn, α-synuclein; [a]Mann–Whitney U-test; [b]Student's t-test; P1, compare between control subjects and PD; P2, compare between early stage PD and advanced stage PD. *p < 0.05.*

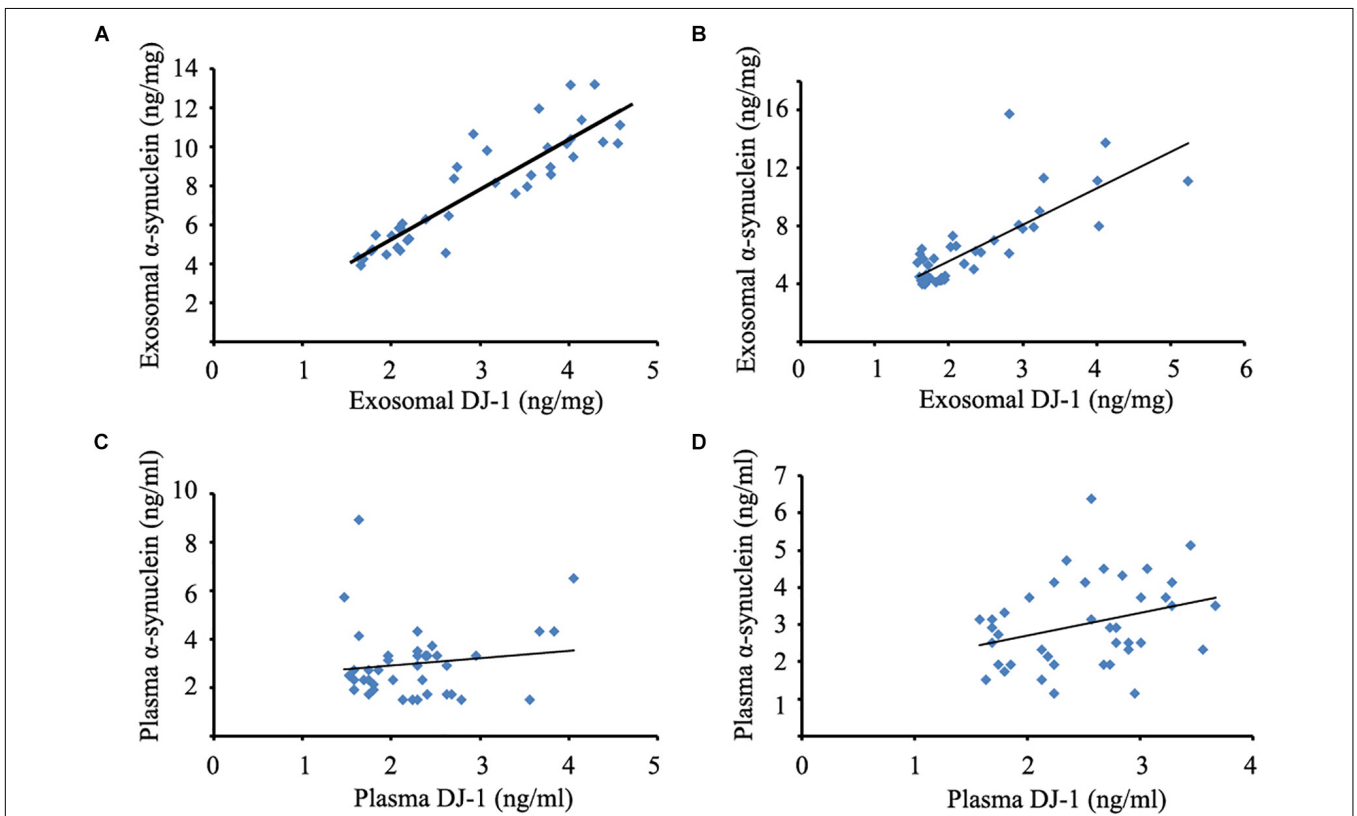

FIGURE 2 | Correlation analysis between DJ-1 and α-synuclein of plasma and plasma neural-derived exosomes. A significant positive correlation between DJ-1 and α-synuclein of plasma neural-derived exosomes was observed in patients with PD ($rs = 0.902$, $p < 0.001$) **(A)**, as well as DJ-1 and α-synuclein of plasma neural-derived exosomes in controls ($rs = 0.739$, $p < 0.001$) **(B)**. No correlation between DJ-1 and α-synuclein of plasma was observed in patients with PD ($rs = 0.059$, $p = 0.722$) **(C)**. A weak correlation between DJ-1 and α-synuclein of plasma in controls ($rs = 0.314$, $p = 0.048$) **(D)**.

advantage of this method using polymer-based precipitation, and combination of biotinylated antibody and streptavidin-agarose resin is that it is simple and can be easily performed in a typical laboratory without a Luminex workstation.

The α-synuclein in the CNS is associated with the progression of PD, and has been hypothesized to be secreted in means of exosomes (Marques and Outeiro, 2012; Gui et al., 2015). Previous studies have reported that plasma α-synuclein was not a suitable biomarker for PD (Lee et al., 2006; Li et al., 2007; Shi et al., 2010), as any peripheral cells containing abundant α-synuclein would affect the result (Barbour et al., 2008). In the present study, plasma α-synuclein levels exhibited no significant differences between patients with PD and controls. However, a higher level of α-synuclein was detected in plasma neural-derived exosomes in patients with PD by ELISA. These results were similar to those obtained by a previous study, in which the levels were detected by Luminex assays (Shi et al., 2014). As the results were free from methodological interference, the present study confirmed that α-synuclein in plasma neural-derived exosomes may function as a reliable biomarker for PD. However, there were limitations to the present study, namely that the sensitivity and specificity were not high enough. Therefore, the sample size needs to be expanded in future studies.

DJ-1 had previously been hypothesized to be associated with the mechanism of PD (Bonifati et al., 2003). Consequently, DJ-1 in biological fluids has garnered much interest as a promising biomarker for PD; however, the inconsistent results obtained by numerous studies regarding plasma DJ-1 suggest its unsuitability to be a reliable biomarker for PD (Waragai et al., 2007; An et al., 2018). Similar to α-synuclein, the plasmic level of DJ-1 is greatly affected by contamination due to its remarkably high content in erythrocytes (Shi et al., 2010). Therefore, researchers have focused on alternative sources of DJ-1. For example, a previous study reported that DJ-1 in saliva was increased in patients with PD compared with controls (Devic et al., 2011), and may present an association with disease progression (Kang et al., 2014). In a Korean study, the levels of DJ-1 in urinary exosomes in males were increased in patients with PD compared with controls and were increased with age in PD (Ho et al., 2014). Other forms of DJ-1, such as oxidized DJ-1 (Ogawa et al., 2014) and DJ-1 isoforms (Lin et al., 2012), have also been studied. To the best of our knowledge, the present study is the first to report that DJ-1 in plasma neural-derived exosomes was significantly increased in patients with PD compared with healthy controls. However, the combination of DJ-1 and α-synuclein in plasma neural-derived exosomes did not significantly enhance the performance of diagnosis.

In the present study, a significant positive correlation between DJ-1 and α-synuclein of plasma neural-derived exosomes was observed in patients with PD. The interaction of α-synuclein and DJ-1 serves an important role in heredofamilial and sporadic PD (Antipova and Bandopadhyay, 2017). A previous study reported that DJ-1 could be observed on the rim of Lewy bodies in patients with sporadic PD (Jin et al., 2005). The total level of DJ-1 protein is significantly increased in the brains of patients with PD compared with controls (Moore et al., 2005; Choi et al., 2006). In addition, DJ-1 can modulate the aggregation of α-synuclein and protect the neurons form cell toxicity of α-synuclein by chaperone-like activity (Sun et al., 2012) and physical interactions (Zondler et al., 2014). The knock-down or knock-out of DJ-1 has been demonstrated to increase α-synuclein toxicity, thus making neurons more vulnerable to the dopaminergic selective neurotoxin 6-hydroxydopamine (Batelli et al., 2015). The results of the present study further confirmed there is a correlation between DJ-1 and α-synuclein. Although the interactions between DJ-1 and α-synuclein have not been completely elucidated, DJ-1 and α-synuclein may participate together in the pathology of PD.

The mechanism for the increased α-synuclein and DJ-1 in the exosome is presently unclear. It has been hypothesized that α-synuclein may be secreted out of cell via exocytosis, exosomes, or other extracellular vesicles (Faure et al., 2006). In addition, there are several potential mechanisms for increasing α-synuclein in the exosome. Increasing α-synuclein synthesis may culminate in its increased secretion to the extracellular space in previous *in vitro* studies providing evidence for this potential mechanism. When neurons over-expressing α-synuclein would actively secrete an increased amount of α-synuclein into the extracellular space by the pathway of exosomes (Emmanouilidou et al., 2010; Reyes et al., 2015), α-synuclein induced cell death may be prevented by exosomal secretion. However, this self protective mechanism would damage neighboring cells (Lee et al., 2005). Another potential mechanism is the dysfunction of the autophagy-lysosomal pathway or macroautophagy. An example of this being ammonium chloride or bafilomycin A1, which inhibits lysosomal function, which would then increase the release of α-synuclein in exosomes (Alvarez-Erviti et al., 2011). This effect may also be observed in α-synuclein over-expressing SH-SY5Y cells treated with secretory carrier membrane protein 5, which is an autophagy inhibitor (Yang et al., 2017). If macroautophagy function was inhibited by silencing the key element autophagy related gene 5, the releasing of α-synuclein from cells by the pathway of exosomes would be observed as a kind of compensation (Fussi et al., 2018). The dysfunction of the endocytic pathway may be another mechanism for increasing α-synuclein secretion via the exosome. The glucocerebrosidase gene is a pathogenic gene in hereditary PD, and its mutation has been hypothesized to decrease glucocerebrosidase enzymatic activity and attenuate endocytic function. The inhibition of this enzymatic activity or expression of this mutant gene results in release of α-synuclein and its oligomers (Papadopoulos et al., 2018). Research regarding in exosomal DJ-1 is rare; however, we hypothesize that increasing DJ-1 in pathogenicity of α-synuclein maybe partially transferred with the exosome into extracellular space.

CONCLUSION

α-Synuclein and DJ-1 in plasma neural-derived exosomes may serve as potential biomarkers for PD. However, further studies should be conducted with larger patient cohorts in order to corroborate the significance of these findings and the relationship of these biomarkers and disease progression.

AUTHOR CONTRIBUTIONS

Z-HZ was responsible for the conception and design of the present study, execution of the experimental work, and wrote the first draft of the manuscript, and review and critique of the Manuscript. Z-TC undertook study design, execution of statistical analysis, execution of experimental work, and the review and critique of the manuscript. R-LZ and XZ organized the research project and reviewed and critiqued the manuscript. Y-ZW organized the research project and review and critiqued the statistical analysis and the manuscript. Q-YY was responsible for the conception of experiments, execution of experimental work, design and execution of statistical analysis, and the review and critique of the manuscript.

FUNDING

This work was supported by the Natural Science Foundation of Fujian Province (Grant No. 2015J01426) and Outstanding Youth Foundation of Fujian Provincial Hospital (Grant No. 2014060).

REFERENCES

Alvarez-Erviti, L., Seow, Y., Schapira, A. H., Gardiner, C., Sargent, I. L., Wood, M. J., et al. (2011). Lysosomal dysfunction increases exosome-mediated alpha-synuclein release and transmission. *Neurobiol. Dis.* 42, 360–367. doi: 10.1016/j.nbd.2011.01.029

An, C., Pu, X., Xiao, W., and Zhang, H. (2018). Expression of the DJ-1 protein in the serum of Chinese patients with Parkinson's disease. *Neurosci. Lett.* 665, 236–239. doi: 10.1016/j.neulet.2017.12.023

Antipova, D., and Bandopadhyay, R. (2017). Expression of DJ-1 in neurodegenerative disorders. *Adv. Exp. Med. Biol.* 1037, 25–43. doi: 10.1007/978-981-10-6583-5_3

Barbour, R., Kling, K., Anderson, J. P., Banducci, K., Cole, T., Diep, L., et al. (2008). Red blood cells are the major source of alpha-synuclein in blood. *Neurodegener. Dis.* 5, 55–59. doi: 10.1159/000112832

Batelli, S., Invernizzi, R. W., Negro, A., Calcagno, E., Rodilossi, S., Forloni, G., et al. (2015). The Parkinson's disease-related protein DJ-1 protects dopaminergic neurons in vivo and cultured cells from alpha-synuclein and 6-hydroxydopamine toxicity. *Neurodegener. Dis.* 15, 13–23. doi: 10.1159/000367993

Berardelli, A., Wenning, G. K., Antonini, A., Berg, D., Bloem, B. R., Bonifati, V., et al. (2013). EFNS/MDS-ES/ENS [corrected] recommendations for the diagnosis of Parkinson's disease. *Eur. J. Neurol.* 20, 16–34. doi: 10.1111/ene.12022

Bonifati, V., Rizzu, P., Van Baren, M. J., Schaap, O., Breedveld, G. J., Krieger, E., et al. (2003). Mutations in the DJ-1 gene associated with autosomal recessive early-onset parkinsonism. *Science* 299, 256–259. doi: 10.1126/science.1077209

Braak, H., and Del Tredici, K. (2017). Neuropathological staging of brain pathology in sporadic Parkinson's disease: separating the wheat from the chaff. *J. Parkinsons Dis.* 7, S71–S85. doi: 10.3233/JPD-179001

Chevallier, N., Jiracek, J., Vincent, B., Baur, C. P., Spillantini, M. G., Goedert, M., et al. (1997). Examination of the role of endopeptidase 3.4.24.15 in A beta secretion by human transfected cells. *Br. J. Pharmacol.* 121, 556–562. doi: 10.1038/sj.bjp.0701151

Choi, J., Sullards, M. C., Olzmann, J. A., Rees, H. D., Weintraub, S. T., Bostwick, D. E., et al. (2006). Oxidative damage of DJ-1 is linked to sporadic Parkinson and Alzheimer diseases. *J. Biol. Chem.* 281, 10816–10824. doi: 10.1074/jbc.M509079200

Devic, I., Hwang, H., Edgar, J. S., Izutsu, K., Presland, R., Pan, C., et al. (2011). Salivary α-synuclein and DJ-1: potential biomarkers for Parkinson's disease. *Brain* 134:e178. doi: 10.1093/brain/awr015

Emmanouilidou, E., Melachroinou, K., Roumeliotis, T., Garbis, S. D., Ntzouni, M., Margaritis, L. H., et al. (2010). Cell-produced alpha-synuclein is secreted in a calcium-dependent manner by exosomes and impacts neuronal survival. *J. Neurosci.* 30, 6838–6851. doi: 10.1523/JNEUROSCI.5699-09.2010

Farotti, L., Paciotti, S., Tasegian, A., Eusebi, P., and Parnetti, L. (2017). Discovery, validation and optimization of cerebrospinal fluid biomarkers for use in Parkinson's disease. *Expert Rev. Mol. Diagn.* 17, 771–780. doi: 10.1080/14737159.2017.1341312

Faure, J., Lachenal, G., Court, M., Hirrlinger, J., Chatellard-Causse, C., Blot, B., et al. (2006). Exosomes are released by cultured cortical neurones. *Mol. Cell. Neurosci.* 31, 642–648. doi: 10.1016/j.mcn.2005.12.003

Fiandaca, M. S., Kapogiannis, D., Mapstone, M., Boxer, A., Eitan, E., Schwartz, J. B., et al. (2015). Identification of preclinical Alzheimer's disease by a profile of pathogenic proteins in neurally derived blood exosomes: A case-control study. *Alzheimers Dement.* 11, 600–607. doi: 10.1016/j.jalz.2014.06.008

Fussi, N., Hollerhage, M., Chakroun, T., Nykanen, N. P., Rosler, T. W., Koeglsperger, T., et al. (2018). Exosomal secretion of alpha-synuclein as protective mechanism after upstream blockage of macroautophagy. *Cell Death Dis.* 9:757. doi: 10.1038/s41419-018-0816-2

Goetzl, E. J., Boxer, A., Schwartz, J. B., Abner, E. L., Petersen, R. C., Miller, B. L., et al. (2015). Altered lysosomal proteins in neural-derived plasma exosomes in preclinical Alzheimer disease. *Neurology* 85, 40–47. doi: 10.1212/WNL.0000000000001702

Goetzl, E. J., Mustapic, M., Kapogiannis, D., Eitan, E., Lobach, I. V., Goetzl, L., et al. (2016). Cargo proteins of plasma astrocyte-derived exosomes in Alzheimer's disease. *FASEB. J.* 30, 3853–3859. doi: 10.1096/fj.201600756R

Gui, Y., Liu, H., Zhang, L., Lv, W., and Hu, X. (2015). Altered microRNA profiles in cerebrospinal fluid exosome in Parkinson disease and Alzheimer disease. *Oncotarget* 6, 37043–37053. doi: 10.18632/oncotarget.6158

Ho, D. H., Yi, S., Seo, H., Son, I., and Seol, W. (2014). Increased DJ-1 in urine exosome of Korean males with Parkinson's disease. *Biomed Res. Int.* 2014: 704678. doi: 10.1155/2014/704678

Hoehn, M. M., and Yahr, M. D. (1967). Parkinsonism: onset, progression and mortality. *Neurology* 17, 427–442. doi: 10.1212/01.wnl.0000405146.06300.91

Hong, Z., Shi, M., Chung, K. A., Quinn, J. F., Peskind, E. R., Galasko, D., et al. (2010). DJ-1 and alpha-synuclein in human cerebrospinal fluid as biomarkers of Parkinson's disease. *Brain* 133, 713–726. doi: 10.1093/brain/awq008

Hughes, A. J., Daniel, S. E., Kilford, L., and Lees, A. J. (1992). Accuracy of clinical diagnosis of idiopathic Parkinson's disease: a clinico-pathological study of 100 cases. *J. Neurol. Neurosurg. Psychiatry* 55, 181–184. doi: 10.1136/jnnp.55.3.181

Jin, J., Meredith, G. E., Chen, L., Zhou, Y., Xu, J., Shie, F. S., et al. (2005). Quantitative proteomic analysis of mitochondrial proteins: relevance to Lewy body formation and Parkinson's disease. *Brain Res. Mol. Brain Res.* 134, 119–138. doi: 10.1016/j.molbrainres.2004.10.003

Kang, W. Y., Yang, Q., Jiang, X. F., Chen, W., Zhang, L. Y., Wang, X. Y., et al. (2014). Salivary DJ-1 could be an indicator of Parkinson's disease progression. *Front. Aging Neurosci.* 6:102. doi: 10.3389/fnagi.2014.00102

Lee, H. J., Patel, S., and Lee, S. J. (2005). Intravesicular localization and exocytosis of alpha-synuclein and its aggregates. *J. Neurosci.* 25, 6016–6024. doi: 10.1523/JNEUROSCI.0692-05.2005

Lee, P. H., Lee, G., Park, H. J., Bang, O. Y., Joo, I. S., and Huh, K. (2006). The plasma alpha-synuclein levels in patients with Parkinson's disease and multiple system atrophy. *J. Neural Transm.* 113, 1435–1439. doi: 10.1007/s00702-005-0427-9

Li, Q. X., Mok, S. S., Laughton, K. M., Mclean, C. A., Cappai, R., Masters, C. L., et al. (2007). Plasma alpha-synuclein is decreased in subjects with Parkinson's disease. *Exp. Neurol.* 204, 583–588. doi: 10.1016/j.expneurol.2006.12.006

Lin, X., Cook, T. J., Zabetian, C. P., Leverenz, J. B., Peskind, E. R., Hu, S. C., et al. (2012). DJ-1 isoforms in whole blood as potential biomarkers of Parkinson disease. *Sci. Rep.* 2:954. doi: 10.1038/srep00954

Lucking, C. B., and Brice, A. (2000). Alpha-synuclein and Parkinson's disease. *Cell. Mol. Life Sci.* 57, 1894–1908. doi: 10.1007/PL00000671

Marques, O., and Outeiro, T. F. (2012). Alpha-synuclein: from secretion to dysfunction and death. *Cell Death Dis.* 3:e350. doi: 10.1038/cddis.2012.94

Mehta, S. H., and Adler, C. H. (2016). Advances in biomarker research in Parkinson's disease. *Curr. Neurol. Neurosci. Rep.* 16:7. doi: 10.1007/s11910-015-0607-4

Moore, D. J., Zhang, L., Troncoso, J., Lee, M. K., Hattori, N., Mizuno, Y., et al. (2005). Association of DJ-1 and parkin mediated by pathogenic DJ-1 mutations and oxidative stress. *Hum. Mol. Genet.* 14, 71–84. doi: 10.1093/hmg/ddi007

Ogawa, I., Saito, Y., Saigoh, K., Hosoi, Y., Mitsui, Y., Noguchi, N., et al. (2014). [The significance of oxidized DJ-1 protein (oxDJ-1) as a biomarker for Parkinson's disease]. *Brain Nerve* 66, 471–477.

Papadopoulos, V. E., Nikolopoulou, G., Antoniadou, I., Karachaliou, A., Arianoglou, G., Emmanouilidou, E., et al. (2018). Modulation of beta-glucocerebrosidase increases alpha-synuclein secretion and exosome release in mouse models of Parkinson's disease. *Hum. Mol. Genet.* 27, 1696–1710. doi: 10.1093/hmg/ddy075

Reyes, J. F., Olsson, T. T., Lamberts, J. T., Devine, M. J., Kunath, T., and Brundin, P. (2015). A cell culture model for monitoring alpha-synuclein cell-to-cell transfer. *Neurobiol. Dis.* 77, 266–275. doi: 10.1016/j.nbd.2014.07.003

Shi, M., Kovac, A., Korff, A., Cook, T. J., Ginghina, C., Bullock, K. M., et al. (2016). CNS tau efflux via exosomes is likely increased in Parkinson's disease but not in Alzheimer's disease. *Alzheimers Dement.* 12, 1125–1131. doi: 10.1016/j.jalz.2016.04.003

Shi, M., Liu, C., Cook, T. J., Bullock, K. M., Zhao, Y., Ginghina, C., et al. (2014). Plasma exosomal alpha-synuclein is likely CNS-derived and increased in Parkinson's disease. *Acta Neuropathol.* 128, 639–650. doi: 10.1007/s00401-014-1314-y

Shi, M., Zabetian, C. P., Hancock, A. M., Ginghina, C., Hong, Z., Yearout, D., et al. (2010). Significance and confounders of peripheral DJ-1 and alpha-synuclein in Parkinson's disease. *Neurosci. Lett.* 480, 78–82. doi: 10.1016/j.neulet.2010.06.009

Sun, S. Y., An, C. N., and Pu, X. P. (2012). DJ-1 protein protects dopaminergic neurons against 6-OHDA/MG-132-induced neurotoxicity in rats. *Brain Res. Bull.* 88, 609–616. doi: 10.1016/j.brainresbull.2012.05.013

Waragai, M., Nakai, M., Wei, J., Fujita, M., Mizuno, H., Ho, G., et al. (2007). Plasma levels of DJ-1 as a possible marker for progression of sporadic Parkinson's disease. *Neurosci. Lett.* 425, 18–22. doi: 10.1016/j.neulet.2007.08.010

Yang, Y., Qin, M., Bao, P., Xu, W., and Xu, J. (2017). Secretory carrier membrane protein 5 is an autophagy inhibitor that promotes the secretion of alpha-synuclein via exosome. *PLoS One* 12:e0180892. doi: 10.1371/journal.pone.0180892

Zondler, L., Miller-Fleming, L., Repici, M., Goncalves, S., Tenreiro, S., Rosado-Ramos, R., et al. (2014). DJ-1 interactions with alpha-synuclein attenuate aggregation and cellular toxicity in models of Parkinson's disease. *Cell Death Dis.* 5:e1350. doi: 10.1038/cddis.2014.307

Conflict of Interest Statement: The authors declare that the research was conducted in the absence of any commercial or financial relationships that could be construed as a potential conflict of interest.

frontiers in Aging Neuroscience

ORIGINAL RESEARCH
published: 05 February 2019
doi: 10.3389/fnagi.2019.00018

N1 and P1 Components Associate With Visuospatial-Executive and Language Functions in Normosmic Parkinson's Disease: An Event-Related Potential Study

Yi-Qi Lin, Shi-Shuang Cui, Juan-Juan Du, Gen Li, Yi-Xi He, Ping-Chen Zhang, Yang Fu, Pei Huang, Chao Gao, Bin-Yin Li and Sheng-Di Chen**

Department of Neurology and Institute of Neurology, Ruijin Hospital Affiliated to Shanghai Jiao Tong University School of Medicine, Shanghai, China

Background: Hyposmia is one of the most important clinical markers of Parkinson's disease (PD) with a prevalence ranging from 50 to 96% of PD patients. A significant association was found between hyposmia and cognitive impairment of PD. However, there were no reports of event-related potentials (ERP) performance in PD patients with and without hyposmia for cognitive functions assessment.

Purpose: The aim of our study was to compare ERP performance and its association with cognitive domains between PD with and without hyposmia.

Methods: Olfactory functions were assessed by Sniffin' Sticks test-16 (SS-16). Twenty-four subjects were included in PD with hyposmia group and nineteen were in PD without hyposmia group. ERP measures were recorded during a delayed match to sample (DMS) task with Chinese characters. The parameters of ERP components including N1, N2, P1, P2, and P3 in retrieval epoch were compared between the two groups and the correlation between ERP results and MOCA item score was also analyzed.

Results: No significant difference was found in ERP performance between PD with and without hyposmia. Among all participants, N1 latency was significantly negatively related to visuospatial-executive item score of Montreal Cognitive Assessment (MOCA) ($r_S = -0.381$, $P = 0.012$) and P1 amplitude was positively associated with language item score of MOCA ($r_S = 0.302$, $P = 0.049$). Within the normosmic group, a significant association was found between N1 latency and visuospatial-executive item score ($r_S = -0.619$, $P = 0.005$) and there was also a correlation between language score and P1 amplitude ($r_S = 0.537$, $P = 0.018$). In the hyposmic group, only a significant correlation was found between N1 latency and clock drawing test performance ($r_S = -0.413$, $P = 0.045$) rather than visuospatial-executive item score. Furthermore, SS-16 score was not found to be significantly associated with either visuospatial-executive or language item score of MOCA.

OPEN ACCESS

Edited by:
Aiping Liu,
The University of British Columbia, Canada

Reviewed by:
Yi Li,
New York University, United States
Niels Janssen,
Universidad de La Laguna, Spain

***Correspondence:**
Bin-Yin Li
libinyin@126.com
Sheng-Di Chen
chensd@rjh.com.cn

Received: *06 September 2018*
Accepted: *21 January 2019*
Published: *05 February 2019*

Citation:
Lin Y-Q, Cui S-S, Du J-J, Li G, He Y-X, Zhang P-C, Fu Y, Huang P, Gao C, Li B-Y and Chen S-D (2019) N1 and P1 Components Associate With Visuospatial-Executive and Language Functions in Normosmic Parkinson's Disease: An Event-Related Potential Study. Front. Aging Neurosci. 11:18. doi: 10.3389/fnagi.2019.00018

Conclusion: No significant difference was found in ERP components between PD with and without hyposmia. N1 latency and P1 amplitude were respectively associated with visuospatial-executive and language functions in the normosmic group while in the hyposmic group, only a significant correlation was found between N1 latency and clock drawing test performance rather than visuospatial-executive item score in MOCA.

Keywords: hyposmia, Parkinson's disease, event-related potentials, working memory, visuospatial function, language

INTRODUCTION

Hyposmia is one of the most important non-motor symptoms of Parkinson's disease (PD) with a prevalence ranging from 50 to 96% of PD patients (Doty et al., 1988; Wenning et al., 1995; Hawkes et al., 1997; Boesveldt et al., 2008; Duda, 2010). It generally predates motor symptoms and the olfactory testing is useful in differentiating PD from non-PD patients with a sensitivity ranging from 79 to 100% and a specificity from 80 to 89% (Doty, 2012). Therefore, hyposmia is reported to be a critical clinical marker of PD.

In recent years olfactory dysfunction is found to be associated with other non-motor symptoms in PD patients such as chronic constipation, clinical possible rapid eye movement behavior disorder (RBD) (Chen et al., 2015) and psychotic symptoms (Morley et al., 2011). Notably, increasing evidence suggests that hyposmia is strongly associated with cognitive impairment in PD patients and may be a risk factor for PD dementia (Bohnen et al., 2010; Stephenson et al., 2010; Morley et al., 2011; Parrao et al., 2012; Domellof et al., 2017). In fact, the association between olfaction and cognition has been long reported in mild cognitive impairment and Alzheimer's disease which was evidenced by prominent atrophy in the primary olfactory cortex and hippocampus (Vasavada et al., 2015) as well as a strong correlation between tau pathology in the olfactory bulb and limbic systems (Attems et al., 2005). However, the role of hyposmia in cognitive impairment in PD patients is not clear.

Event-related potentials (ERP) have been widely used for assessing cognitive functions and brain ability. ERP wave latency and amplitude represent respectively the length of time spent and the amount of neural resources participating during information processing. There were increasing studies of ERP in PD patients owning to its independence of motor speed and disability. The abnormal P300 was reported to be associated with cognitive impairment in PD (Katsarou et al., 2004; Matsui et al., 2007) while other ERP measures were barely studied in PD. It remained unclear whether the ERP components were altered in PD with hyposmia, especially the early ERP components reflecting visuospatial processing which was one of the mostly impaired cognitive domains in PD.

The delayed match to sample (DMS) task, one of the most popular tasks during ERP records in PD patients (Seer et al., 2016), was used in our study to test working memory which related to several cognitive abilities including storage capacity, retrieval strategies (Unsworth and Engle, 2007) and visuospatial attention (Bleckley et al., 2003; Giuliano et al., 2014). And Chinese characters applied in our DMS task were more acceptable for Chinese participants and more dependable on visual working memory (Opitz et al., 2014). What's more, we focused on retrieval epoch rather than encoding epoch in view of impaired retrieval process and reserved encoding ability of memory deficit in PD (Mahurin et al., 1993).

To our knowledge, there was no research focusing on cognitive ERP measures in PD patients with hyposmia. The aim of this study was to improve our understanding of the role of hyposmia in cognitive impairment in PD using the ERP technique with DMS task. Our study investigated difference in ERP components and its association with cognitive domains between PD patients with and without hyposmia.

MATERIALS AND METHODS

Subject

Idiopathic PD patients aging from 50 to 80 were recruited from movement disorder clinic of the Department of Neurology, Ruijin Hospital affiliated to Shanghai Jiao Tong University School of Medicine from September 2016 to October 2017. PD was diagnosed according to the clinical Movement Disorder Society (MDS) diagnostic criteria (Postuma et al., 2015) by senior Movement Disorder Specialist. Exclusion criteria included history of head injury, stroke, psychiatric disorder, poor vision, nasal and paranasal disease or other factors affecting olfactory function. Patients with less than 6 years of education or Mini-Mental State Examination (MMSE) score less than 24 were also excluded.

Finally 43 PD patients were enrolled in our study. Hyposmia was defined with score of Sniffin' Sticks test-16 (SS-16) (Burghart Messtechnik, Wedel, Germany) less than 8.3 (Chen et al., 2012) which was consistent with previous researches in our department (Chen et al., 2015). There were 24 subjects in PD with hyposmia group and 19 in PD without hyposmia group. All participants were informed of the research protocol and this study was carried out in accordance with the recommendations of Ethical Review of Biomedical Research Involving Human Subjects by China's Ministry of Health with written informed consent from all subjects. The protocol was approved by Ethics Committee of Ruijin Hospital affiliated to Shanghai Jiao Tong University School of Medicine, Shanghai, China.

Neuropsychological Assessment

Demographic characters including age, sex, education years and disease duration were recorded (**Table 1**). The disease progression was assessed by modified Hoehn and Yahr (H-Y) scale (Hoehn and Yahr, 1967) and levodopa equivalent dose (LED) which was calculated as reported (Tomlinson et al., 2010). Motor subtypes were divided into tremor dominant type and non-tremor dominant type. Montreal Cognitive Assessment (MOCA) Beijing version was used to evaluate cognitive performance (Yu et al., 2012). Night sleep quality was assessed by Parkinson's disease Sleep Scale (PDSS) (Wang et al., 2008). Rapid Eye Movement Sleep Behavior Disorder Questionnaire-Hong Kong (RBD-HK) (Shen et al., 2014) and Epworth Sleepiness Scale (ESS) (Kumar et al., 2003) were used to evaluate RBD and excessive daytime sleepiness (EDS). The anxiety symptoms were evaluated by Hamilton Anxiety Rating Scale (HAMA) (Thompson, 2015) and 17-item Hamilton Rating Scale for Depression (HAMD-17) (Hamilton, 1960) was used for depression screening.

TABLE 1 | Demographics and clinical characteristics in PD with and without hyposmia groups (mean ± standard deviation).

	PD without hyposmia (*n* = 19)	PD with hyposmia (*n* = 24)	*P*
Age (years)	62.37 ± 6.19	64.71 ± 5.89	0.213
Sex (M/*n*)	8/19	11/24	0.807
Disease duration (years)	5.31 ± 5.46	5.63 ± 4.29	0.835
LED (mg)	269.66 ± 260.57	280.65 ± 174.76	0.871
Education (years)	12.05 ± 2.30	12.92 ± 2.50	0.250
H-Y stage	1.68 ± 0.71	1.75 ± 0.59	0.742
Motor subtype (tremor type/*n*)	7/19	11/22	0.553
SS-16	10.58 ± 1.64	6.00 ± 2.02	0.000
PDSS	126.84 ± 20.61	117.75 ± 16.59	0.116
RBD-HK	14.84 ± 17.58	13.13 ± 14.00	0.723
ESS	5.95 ± 4.76	5.71 ± 4.84	0.872
HAMD-17	3.74 ± 3.96	3.83 ± 4.06	0.938
HAMA	5.16 ± 4.80	3.75 ± 3.18	0.255
MOCA	25.79 ± 1.93	26.79 ± 2.64	0.173
MMSE	28.68 ± 1.46	28.46 ± 2.06	0.688

The Delayed Match to Sample Task

Each participant was required to participate in a practice block before the test block during the DMS task (**Figure 1**). In each trial, after a single of "+" in the screen of 500 ms, a set of six visually similar and easily confused Chinese characters (sample stimulus) presented for 2000 ms which should be remembered by subjects. After a blank for 3000 ms, a character (probe stimulus) demonstrated in the middle of the screen could either be a member of the previous set of characters (answer "yes") or be another similar-looking one (answer "no"). The character presented until a response before 2000 ms or until 2000 ms without response. Subjects were asked to answer "yes" by pressing the button of "1" or "no" by pressing the button of "2" on a keyboard as soon as the response was ensured. The "yes" and "no" answers were randomized and 50% of the correct answers were "yes" and the rest was "no" in each block. The inter-trial interval was 5000 ms. Patients were allowed to begin the test until the accuracy of the practice block was higher than 50%. Each test contained 100 trials. This DMS task was programmed by E-Prime 2.0 software (Psychology Software Tools, Inc., Pittsburgh, PA, United States) in which reaction time and accuracy of each subject were also recorded. The retrieval period of our study was defined from 200 ms before probe stimulus onset to 1000 ms after.

EEG Recordings and Data Analysis

ERP was recorded from 32 Ag-AgCl electrodes (Fp1, Fp2, F3, F4, C3, C4, P3, P4, O1, O2, F7, F8, T7, T8, P7, P8, Fz, FCz, Cz, Pz, FC1, FC2, CP1, CP2, FC5, FC6, CP5, CP6, FT9, FT10, TP9, TP10) which were placed according to the international 10–20 system with a 32-channel amplifier (BrainAmp by Brain Products, Munich, Germany).

All channels were digitized at 500 Hz with 200 ms-long prestimulus baseline used for baseline correction. The filter band-pass was 0.1–70 Hz. Electro-oculogram (EOG) was also recorded to correct ocular artifacts. A semi-automatic check was used in artifact rejection. Trials were rejected if EEG voltage step was

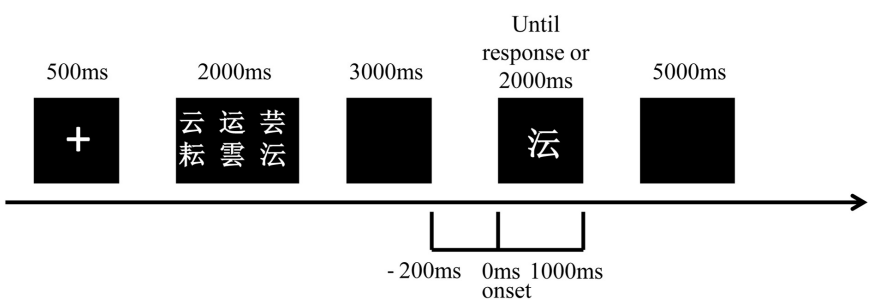

FIGURE 1 | Schematic representation of the visual DMS task used for ERP recordings. A set of six Chinese characters (sample stimulus) was displayed after a single of "+" and was required to be remembered by participants. After a blank for 3000 ms, a character (probe stimulus) presented for 2000 ms and the answer of "yes" or "no" was required to decide whether this character was a member of the set of characters or not. The inter-trial interval was 5000 ms. The retrieval period is from 200 ms before probe stimulus onset to 1000 ms after.

higher than 50 μV/ms or if difference of values in intervals was higher than 200 μV or lower than 0.5 μV. The mean rejection rate for all participants was higher than 1%. ERPs were based on correct trials and data not rejected for artifacts.

The five ERP components including N1, N2, P1, P2, and P300 were analyzed in reference of early studies, meanwhile, electrodes with maximal amplitude were chosen, which was consistent with the previous report of our center using the same paradigm (Li et al., 2016). N1 amplitude was measured as the maximal negative peak within the latency window of 150–210 ms on P7, P8 electrodes. P1 amplitude was identified at the most positive peak on O1, O2, P7 and P8 within 84–140 ms after the stimulus onset. N2 amplitude was considered at the maximal negative peak on F3, F4, C3, C4, CZ, FZ and FCz within the latency window of 230–300 ms. P2 amplitude was identified at the maximal positive peak on FC1, FC2, CZ, FZ and FCz within the latency window of 150–250 ms. The P300component amplitude was analyzed as the maximal positive peak within 250–450 ms on O1, O2 and Pz electrodes. The N1P2 amplitude was summed absolute amplitude of the N1 and P2 peaks on P7, P8, FC1, FC2, CZ, FZ and FCz electrodes. The N1P2 amplitude divided by average noise level yielded the signal-to-noise (S/N) ratio.

Statistical Analysis

All statistical analysis was performed by SPSS 19.0 (IBM, Armonk, NY). Demographic characteristics and clinical variables were compared between the two groups using the independent sample *t*-test or chi square analysis. The Spearman's correlation was analyzed between each ERP component parameter and MOCA item score. The association between SS-16 and MOCA item score was also analyzed by Spearman's correlation. All ERP components parameters were compared between the two groups using independent Mann–Whitney *U*-test. All tests were 2-tailed and *P*-values < 0.05 were considered statistically significant.

RESULTS

Demographics and Clinical Characteristics

There was no significant group difference in demographic characters including age, sex, and education degree. No significant difference was revealed in disease duration, H-Y stage, tremor subtype and LED between PD with and without hyposmia. Questionnaire results of sleep disorder (PDSS, RBD-HK and ESS) as well as anxiety (HAMA) and depression (HAMD-17) were similar between the two groups. No significant difference was found in total score of MMSE or MOCA (**Table 1**).

Task Performance and Brain Activity

There was no significant difference between PD patients with and without hyposmia regarding number of valid trials, reaction time and accuracy. No significant difference was found in parameters of ERP components including N1, N2, P1, P2 and P300 between the two groups (**Table 2** and **Figure 2**). Notably, the N1P2 amplitude did not differ between the two groups. And the mean S/N ratio was 4.90 in the normosmic group and 5.17 in the hyposmic group and no difference was found between the two groups (**Table 2**).

TABLE 2 | Task performance and parameters of ERP components in PD with and without hyposmia groups (mean ± standard deviation).

	PD without hyposmia (*n* = 19)	PD with hyposmia (*n* = 24)	*P*
Number of valid trials	1625	2048	0.954
Accuracy (%)	89.79 ± 8.38	88.21 ± 19.39	0.742
Reaction time (s)	1590.49 ± 226.51	1549.82 ± 246.54	0.581
N1 latency (ms)	162.16 ± 12.05	158.54 ± 7.75	0.265
N1 amplitude (μV)	−6.05 ± 3.30	−7.17 ± 3.92	0.391
N2 latency (ms)	261.98 ± 15.06	262.42 ± 21.12	0.940
N2amplitude (μV)	−1.94 ± 3.29	−1.89 ± 2.88	0.964
P1 latency (ms)	98.58 ± 8.00	99.83 ± 9.30	0.643
P1 amplitude (μV)	4.98 ± 3.31	4.77 ± 2.75	0.818
P2 latency (ms)	169.43 ± 20.04	173.35 ± 28.51	0.615
P2 amplitude (μV)	5.39 ± 3.97	5.63 ± 2.63	0.807
P3 latency (ms)	372.25 ± 54.80	391.53 ± 46.93	0.221
P3 amplitude (μV)	5.03 ± 2.96	6.40 ± 4.01	0.220
N1P2 amplitude (μV)	8.28 ± 4.83	8.23 ± 3.19	0.509
S/N	4.90 ± 2.32	5.17 ± 2.53	0.826

Correlation Between ERPs and Cognitive Ability

Correlation was analyzed between ERP component parameter and cognitive performance in all participants (**Tables 3**, **4**). N1 latency was significantly negatively related to visuospatial-executive item score of MOCA ($r_s = -0.381$, $P = 0.012$). Among three visuospatial-executive tests, a significant negative correlation between N1 latency and test score was found in cube copy test ($r_s = -0.401$, $P = 0.008$) and clock drawing ($r_s = -0.451$, $P = 0.002$) but not in trail making test. What's more, a significant positive correlation was found between P1 amplitude and language item score of MOCA ($r_s = 0.302$, $P = 0.049$). There was no correlation between MOCA total score and N1 or P1 parameters. Parameters of other ERP components including N2, P2 and P300 were not found significantly associated with MOCA score or MOCA item score. Then the correlations between N1 latency and P1 amplitude and visuospatial-executive and language item score were also analyzed in separate groups (**Table 5**). There was a significant negative correlation between N1 latency and visuospatial-executive item score within the normosmic group ($r_s = -0.619$, $P = 0.005$) but not within the hyposmic group. Among three visuospatial tests, a significant negative correlation with N1 latency was found in both cube copy test ($r_s = -0.585$,

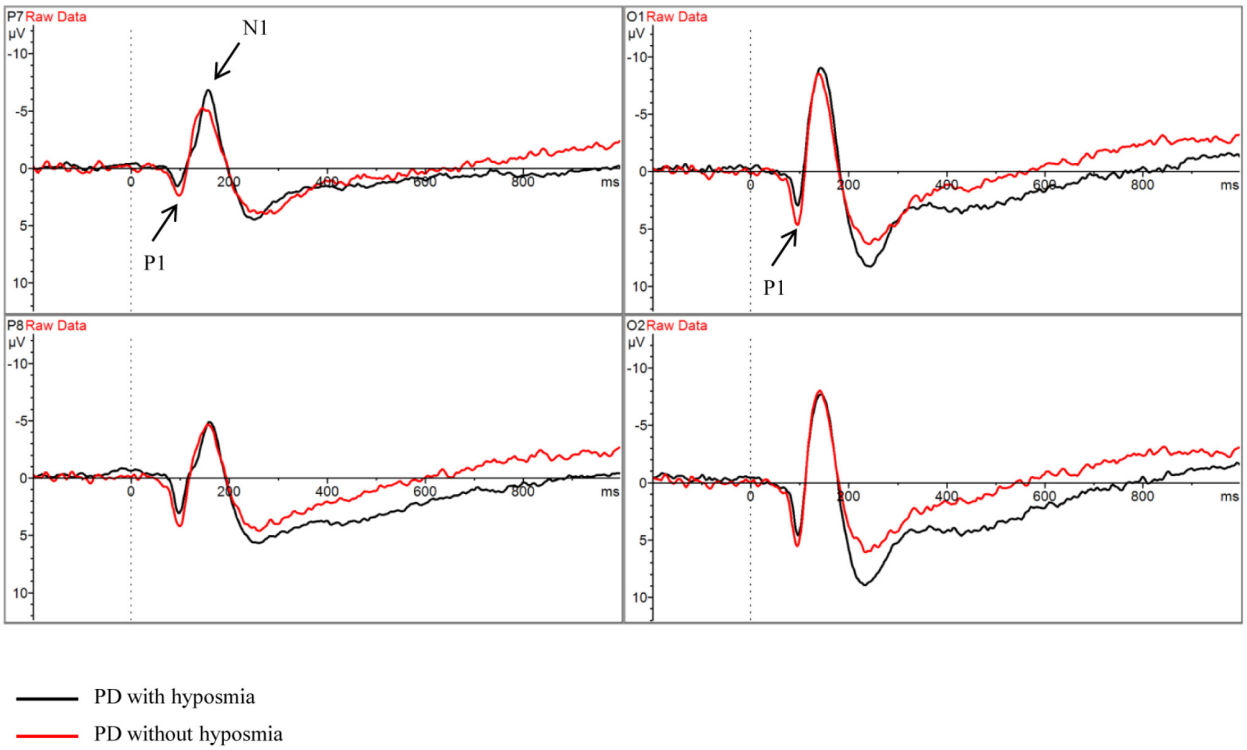

FIGURE 2 | Grand average ERP waveform in PD with hyposmia (black line) and PD without hyposmia (red line) during retrieval period in DMS task. Latency was recorded in milliseconds with stimulus onset at 0. Amplitude was recorded in micro-voltage.

P = 0.008) and clock drawing test (r_s = −0.523, P = 0.022) within the normosmic group and only in clock drawing test (r_s = −0.413, P = 0.045) within the hyposmic group. In addition, a significant correlation between P1 amplitude and language item score was found within the normosmic group (r_s = 0.537, P = 0.018) but not within the hyposmic group. Furthermore, SS-16 score was not found to be significantly associated with visuospatial-executive or language item score of MOCA (**Table 6**).

Correlation was also analyzed between parameters of N1 and P1 components and clinical characteristics in all subjects (**Table 7**). N1 latency was found to be significantly negatively related to education degree (r_s = −0.326, P = 0.033). There was a significant positive correlation between HAMA score and N1 amplitude (r_s = 0.360, P = 0.018). No significant correlation was found between other component parameters and clinical characteristics.

TABLE 3 | Correlation analysis between ERP latency and MOCA score in all participants (correlation coefficient r_s).

	N1	N2	P1	P2	P3
Visuospatial-executive	−0.381*	0.085	−0.068	−0.104	0.121
Visuospatial-executive (trail making test)	−0.105	0.107	−0.067	0.103	0.079
Visuospatial-executive (cube copy)	−0.401**	0.178	−0.009	0.000	0.094
Visuospatial-executive (clock drawing)	−0.451**	0.021	−0.037	−0.207	0.069
Naming	−0.044	0.084	−0.038	−0.191	0.164
Attention	0.092	−0.131	0.000	0.041	−0.023
Language	0.101	−0.027	0.036	0.020	0.237
Abstraction	−0.232	−0.125	0.051	−0.088	0.193
Delayed Recall	0.034	0.199	−0.003	0.136	0.236
Orientation	−0.206	0.080	−0.004	−0.067	−0.098
Total score	−0.217	0.100	−0.024	−0.003	0.223

*$P < 0.05$; **$P < 0.01$.

DISCUSSION

To our knowledge, our study was the first to compare cognitive ERP measures between PD patients with and without hyposmia. No significant difference in ERP performance was found between the two groups. Among all subjects, N1 latency was significantly negatively related to visuospatial-executive function and there was a significant positive correlation between P1 amplitude and language ability. Within the normosmic group, N1 and P1 also associated with visuospatial-executive and language functions while a significant correlation was only found between N1 latency and clock drawing test performance rather than visuospatial-executive item score in the hyposmic group. What's more, odor identification ability was not found to be significantly related to visuospatial-executive function or language ability.

TABLE 4 | Correlation analysis between ERP amplitude and MOCA score in all participants (correlation coefficient r_s).

	N1	N2	P1	P2	P3
Visuospatial-executive	0.010	−0.077	−0.185	−0.288	−0.147
Visuospatial-executive (trail making test)	−0.100	−0.079	−0.234	−0.188	−0.205
Visuospatial-executive (cube copy)	0.053	0.193	−0.094	−0.164	−0.228
Visuospatial-executive (clock drawing)	0.035	−0.067	−0.018	−0.179	−0.016
Naming	0.059	−0.206	0.193	0.037	0.200
Attention	0.053	0.003	−0.161	−0.034	0.081
Language	−0.195	−0.120	0.302*	0.231	0.075
Abstraction	−0.140	−0.069	−0.033	−0.038	0.222
Delayed Recall	0.142	0.226	−0.114	0.088	0.040
Orientation	−0.214	0.071	−0.089	0.169	−0.169
Total score	0.005	0.089	−0.053	0.020	0.002

*$P < 0.05$.

TABLE 5 | Correlation analysis between parameters of ERP components (N1 and P1) and MOCA item (visuospatial-executive and language items) score in PD with and without hyposmia groups (correlation coefficient r_s).

	PD without hyposmia		PD with hyposmia	
	N1 latency	P1 amplitude	N1 latency	P1 amplitude
Visuospatial- executive	−0.619**	−0.182	−0.161	−0.121
Visuospatial- executive (trail making test)	−0.303	−0.207	0.119	−0.153
Visuospatial- executive (cube copy)	−0.585**	−0.184	−0.153	0.044
Visuospatial- Executive (clock drawing)	−0.523*	0.040	−0.413*	−0.059
Language	0.104	0.537*	0.098	0.032

*$P < 0.05$; **$P < 0.01$.

TABLE 6 | Correlation analysis between SS-16 score and MOCA item (visuospatial-executive and language items) score in all participants (correlation coefficient r_s).

	SS-16
Visuospatial-executive	−0.088
Visuospatial-executive (trail making test)	−0.034
Visuospatial-executive (cube copy)	−0.118
Visuospatial-executive (clock drawing)	−0.125
Language	−0.201
Total score	−0.099

TABLE 7 | Correlation analysis between parameters of ERP components (N1 and P1) and clinical characteristics in all participants (correlation coefficient r_s).

	N1 latency	N1 amplitude	P1 latency	P1 amplitude
Age (years)	−0.177	0.143	0.058	0.175
Disease duration (years)	0.037	−0.105	0.203	0.076
Education degree (years)	−0.326*	−0.091	−0.232	−0.058
LED (mg)	0.086	0.028	0.162	0.134
ESS	0.089	0.041	0.287	0.086
PDSS	0.260	−0.128	−0.046	0.226
RBD-HK	−0.047	0.163	0.003	0.191
H-Y stage	0.091	0.149	0.236	0.051
HAMA	0.127	0.360*	0.035	0.047
HAMD-17	−0.074	0.191	−0.045	−0.095

*$P < 0.05$.

Hyposmia is an important clinical biomarker of PD and there are four subtypes of olfactory dysfunction reported in PD including impairment of odor identification, odor discrimination, odor threshold detection and odor recognition memory (Mesholam et al., 1998; Haehner et al., 2009). Odor identification deficit is the most prevalent form of hyposmia and is tested mainly by University of Pennsylvania Smell Identification Test (UPSIT) in PD patients (Doty et al., 1988) and SS-16 (Haehner et al., 2009) which was used in our study considering its advantage in cross-cultural application.

Previous studies found a significant association between hyposmia and cognitive impairment in PD patients. The percentage of cognitive decline was significantly higher in PD patients with hyposmia than those without (Bohnen et al., 2010; Stephenson et al., 2010; Morley et al., 2011; Parrao et al., 2012). And olfactory dysfunction significantly increased the risk of dementia in PD patients regardless the cognitive functions at baseline according to a 10-year follow up study (Domellof et al., 2017). The underlying mechanism remained unclear. The olfactory bulb was known to be one of the onset sites with appearance of Lewy body pathology during PD progression in Braak's stage (Braak et al., 2003). And over expression of alpha-synuclein in the olfactory bulb was reported to initiate hyposmia and other prodromal symptoms of PD in rats (Niu et al., 2018). A hypothesis was proposed that severe olfactory dysfunction might be related to abundant cortical Lewy body deposition (Morley et al., 2011) which was found to be associated with PD dementia (Tsuboi et al., 2007). What's more, the relation between hyposmia and cognitive impairment could also be explained by cholinergic denervation of the limbic archicortex (Bohnen et al., 2010) and dopaminergic denervation of the hippocampus (Bohnen et al., 2008). In our study, no significant difference was found in MMSE or MOCA score between PD with and without hyposmia, which may be associated with limits of our sample size and sensitivities of MMSE and MOCA in cognitive impairment of PD patients (Burdick et al., 2014; Wyman-Chick et al., 2017). Interestingly, no significant difference was found in parameters of ERP components including N1, N2, P1, P2 and P300 recorded during DMS tasks between these two groups. Therefore, the association between cognitive domains and ERP measures in PD with and without hyposmia was important to be investigated.

N1 and P1 were found to respectively associate with visuospatial-executive functions and language in our study while no significant correlation was found between the other components including P2, N2, and P300 and specific cognitive

functions. N1 and P1 are the earliest components in ERP representing visual sensory input. The generator of visual N1 is probably located in lateral extrastriate cortex (Gomez Gonzalez et al., 1994), dorsal occipito-parietal and ventral occipito-temporal areas (Yamazaki et al., 2000) and the visual P1 may be generated in fusiform gyrus (Heinze et al., 1994). N1 and P1 were reported to be associated with visual perceptual processing (Vogel and Luck, 2000; Taylor, 2002) especially in visuospatial attention according to previous reports (Naatanen and Picton, 1987; Luck et al., 1990). Luck et al. (1990) found that N1 was related to attention orienting to relevant stimulus and P1 possibly reflected a facilitation of early sensory processing with attention already focused. On the other hand, several studies demonstrated the role of N1 and P1 in language perception. Selpien et al. (2015) found that N1 and P1 were significantly related to language lateralization. In an auditory ERP study, the association between P1 amplitude and attention was found in linguistic probes stimulation but not in non-linguistic probes (Giuliano et al., 2014).

Abnormal N1 and P1 components in PD patients were observed in several studies. Wright et al. (1996) found attenuated N1 amplitudes during Auditory Oddball Task in 17 PD patients. However, enlarged N1 and P1 amplitudes as well as shortened N1 latency in 34 PD patients were demonstrated in a visual ERP study with oddball and S1–S2 tasks (Li et al., 2003). The discrepancy may be explained by the differences of tasks used in ERP, sample size and analytical approach of component parameters. Unfortunately, the clinical significance of N1 and P1 components in PD patients was investigated in very few studies. Wang et al. (2001) reported the association between N1 and cognitive visual processing in PD patients evidenced by its correlation with the regional cerebral blood flow. Consistent to previous studies, our study found a significant negative correlation between N1 latency and visuospatial-executive function in PD patients and P1 amplitude was significantly positively related to language ability. Therefore N1 latency and P1 amplitude during DMS task were possible to be used for assessing visuospatial-executive functions and language abilities in PD patients. Interestingly, the significant association between these cognitive functions and N1 and P1 components were also found in the normosmic group while in the hyposmic group, there was only a significant correlation between N1 and clock drawing test score rather than visuospatial-executive item score. To explain difference in clinical significance of N1 and P1 components between the two groups, one hypothesis could be that there exists different cognitive processing between these normosmic and hyposmic participants. Increasing evidence shows that PD with and without hyposmia may be two subtypes of PD patients. Lee et al. (2015) found that normosmic PD represented a unique clinical phenotype with a more benign with fewer motor deficits and higher dopamine transporter activity. On the other hand, hyposmia in PD was reported to be associated with tremor-dominant type (Iijima et al., 2011), SNCA rs11931074 and specific non-motor symptoms such as RBD and chronic constipation (Chen et al., 2015). From the aspect of cognition, a good olfactory performance in PD was found to compensate gray matter volume loss (Lee et al., 2014) and there were cholinergic and dopaminergic denervations in PD with hyposmia (Bohnen et al., 2008, 2010). Therefore, some components underlying a cognitive process such as visuospatial-executive and language functions could be different between PD with and without hyposmia.

The impaired cognitive domains in PD with hyposmia were under debate. Bohnen et al. (2010) found that UPSIT scores were significantly related to episodic verbal learning in 58 PD patients but not other cognitive performance including visuospatial function, visual non-verbal memory, attention and executive function. However, poorer memory and executive functions were reported to be associated with worse olfactory identification in other studies (Morley et al., 2011; Parrao et al., 2012). Our study demonstrated no significant association between SS-16 score and visuospatial-executive or language item score of MOCA in PD patients. The discrepancy is possibly explained by difference in sample size and neurocognitive test batteries which may be avoided by using ERP measures.

There were several limitations of our study. A larger sample size is expected in further studies to confirm our results. In addition, only MOCA with relatively high reliability and validation reported (Nie et al., 2012) was used for cognitive assessment in our study as the psychometric properties of neurocognitive test batteries were rarely studied in Chinese PD patients. What's more, only odor identification was tested which was the mostly impaired olfactory function in PD (Doty et al., 1988). However, in view of possibly different mechanisms underlying four subtypes of hyposmia (Kareken et al., 2003; Hedner et al., 2010), the association between cognitive domains and the other three olfactory functions in PD warrants further investigation.

In conclusion, our study compared ERP measures recorded during DMS tasks at retrieval period and its association with cognitive domains between PD patients with and without hyposmia. No significant difference in ERP components was found between the two groups in the present study. Among all participants, N1 latency was significantly negatively related to visuospatial-executive functions and there was also a significantly positive correlation between P1 amplitude and language ability. In PD without hyposmia, N1 latency and P1 amplitude were respectively associated with visuospatial-executive and language functions while in PD with hyposmia, only a significant correlation was found between N1 latency and clock drawing test performance rather than visuospatial-executive item score in MOCA. What's more, no significant association was found between odor identification ability and visuospatial-executive or language item score of MOCA.

AUTHOR CONTRIBUTIONS

All the authors cooperated and contributed to the design and plan of the present study. Y-QL, S-SC, J-JD, GL, Y-XH, P-CZ, YF, PH, and CG performed the research. S-DC was in charge of clinical diagnosis. Y-QL and B-YL analyzed the data. Y-QL wrote the original article. S-DC and B-YL were in charge of manuscript verifying.

FUNDING

This work was supported by grants from the National Natural Science Foundation of China (Nos. 81430022 and 81771374).

ACKNOWLEDGMENTS

The authors thank the patients for their participation in the project.

REFERENCES

Attems, J., Lintner, F., and Jellinger, K. A. (2005). Olfactory involvement in aging and Alzheimer's disease: an autopsy study. *J. Alzheimers Dis.* 7, 149–157; discussion 173–180. doi: 10.3233/JAD-2005-7208

Bleckley, M. K., Durso, F. T., Crutchfield, J. M., Engle, R. W., and Khanna, M. M. (2003). Individual differences in working memory capacity predict visual attention allocation. *Psychon. Bull. Rev.* 10, 884–889. doi: 10.3758/BF03196548

Boesveldt, S., Verbaan, D., Knol, D. L., Visser, M., Van Rooden, S. M., Van Hilten, J. J., et al. (2008). A comparative study of odor identification and odor discrimination deficits in Parkinson's disease. *Mov. Disord.* 23, 1984–1990. doi: 10.1002/mds.22155

Bohnen, N. I., Gedela, S., Herath, P., Constantine, G. M., and Moore, R. Y. (2008). Selective hyposmia in Parkinson disease: association with hippocampal dopamine activity. *Neurosci. Lett.* 447, 12–16. doi: 10.1016/j.neulet.2008.09.070

Bohnen, N. I., Muller, M. L., Kotagal, V., Koeppe, R. A., Kilbourn, M. A., Albin, R. L., et al. (2010). Olfactory dysfunction, central cholinergic integrity and cognitive impairment in Parkinson's disease. *Brain* 133, 1747–1754. doi: 10.1093/brain/awq079

Braak, H., Del Tredici, K., Rub, U., De Vos, R. A., Jansen Steur, E. N., and Braak, E. (2003). Staging of brain pathology related to sporadic Parkinson's disease. *Neurobiol. Aging* 24, 197–211. doi: 10.1016/S0197-4580(02)00065-9

Burdick, D. J., Cholerton, B., Watson, G. S., Siderowf, A., Trojanowski, J. Q., Weintraub, D., et al. (2014). People with Parkinson's disease and normal MMSE score have a broad range of cognitive performance. *Mov. Disord.* 29, 1258–1264. doi: 10.1002/mds.25924

Chen, W., Chen, S., Kang, W. Y., Li, B., Xu, Z. M., Xiao, Q., et al. (2012). Application of odor identification test in Parkinson's disease in China: a matched case-control study. *J. Neurol. Sci.* 316, 47–50. doi: 10.1016/j.jns.2012.01.033

Chen, W., Kang, W. Y., Chen, S., Wang, Y., Xiao, Q., Wang, G., et al. (2015). Hyposmia correlates with SNCA variant and non-motor symptoms in Chinese patients with Parkinson's disease. *Parkinsonism Relat. Disord.* 21, 610–614. doi: 10.1016/j.parkreldis.2015.03.021

Domellof, M. E., Lundin, K. F., Edstrom, M., and Forsgren, L. (2017). Olfactory dysfunction and dementia in newly diagnosed patients with Parkinson's disease. *Parkinsonism Relat. Disord.* 38, 41–47. doi: 10.1016/j.parkreldis.2017.02.017

Doty, R. L. (2012). Olfaction in Parkinson's disease and related disorders. *Neurobiol. Dis.* 46, 527–552. doi: 10.1016/j.nbd.2011.10.026

Doty, R. L., Deems, D. A., and Stellar, S. (1988). Olfactory dysfunction in parkinsonism: a general deficit unrelated to neurologic signs, disease stage, or disease duration. *Neurology* 38, 1237–1244. doi: 10.1212/WNL.38.8.1237

Duda, J. E. (2010). Olfactory system pathology as a model of Lewy neurodegenerative disease. *J. Neurol. Sci.* 289, 49–54. doi: 10.1016/j.jns.2009.08.042

Giuliano, R. J., Karns, C. M., Neville, H. J., and Hillyard, S. A. (2014). Early auditory evoked potential is modulated by selective attention and related to individual differences in visual working memory capacity. *J. Cogn. Neurosci.* 26, 2682–2690. doi: 10.1162/jocn_a_00684

Gomez Gonzalez, C. M., Clark, V. P., Fan, S., Luck, S. J., and Hillyard, S. A. (1994). Sources of attention-sensitive visual event-related potentials. *Brain Topogr.* 7, 41–51. doi: 10.1007/BF01184836

Haehner, A., Boesveldt, S., Berendse, H. W., Mackay-Sim, A., Fleischmann, J., Silburn, P. A., et al. (2009). Prevalence of smell loss in Parkinson's disease–a multicenter study. *Parkinsonism Relat. Disord.* 15, 490–494. doi: 10.1016/j.parkreldis.2008.12.005

Hamilton, M. (1960). A rating scale for depression. *J. Neurol. Neurosurg. Psychiatry* 23, 56–62. doi: 10.1136/jnnp.23.1.56

Hawkes, C. H., Shephard, B. C., and Daniel, S. E. (1997). Olfactory dysfunction in Parkinson's disease. *J. Neurol. Neurosurg. Psychiatry* 62, 436–446. doi: 10.1136/jnnp.62.5.436

Hedner, M., Larsson, M., Arnold, N., Zucco, G. M., and Hummel, T. (2010). Cognitive factors in odor detection, odor discrimination, and odor identification tasks. *J. Clin. Exp. Neuropsychol.* 32, 1062–1067. doi: 10.1080/13803391003683070

Heinze, H. J., Mangun, G. R., Burchert, W., Hinrichs, H., Scholz, M., Munte, T. F., et al. (1994). Combined spatial and temporal imaging of brain activity during visual selective attention in humans. *Nature* 372, 543–546. doi: 10.1038/372543a0

Hoehn, M. M., and Yahr, M. D. (1967). Parkinsonism: onset, progression and mortality. *Neurology* 17, 427–442. doi: 10.1212/WNL.17.5.427

Iijima, M., Kobayakawa, T., Saito, S., Osawa, M., Tsutsumi, Y., Hashimoto, S., et al. (2011). Differences in odor identification among clinical subtypes of Parkinson's disease. *Eur. J. Neurol.* 18, 425–429. doi: 10.1111/j.1468-1331.2010.03167.x

Kareken, D. A., Mosnik, D. M., Doty, R. L., Dzemidzic, M., and Hutchins, G. D. (2003). Functional anatomy of human odor sensation, discrimination, and identification in health and aging. *Neuropsychology* 17, 482–495. doi: 10.1037/0894-4105.17.3.482

Katsarou, Z., Bostantjopoulou, S., Kimiskidis, V., Rossopoulos, E., and Kazis, A. (2004). Auditory event-related potentials in Parkinson's disease in relation to cognitive ability. *Percept. Mot. Skills* 98, 1441–1448. doi: 10.2466/pms.98.3c.1441-1448

Kumar, S., Bhatia, M., and Behari, M. (2003). Excessive daytime sleepiness in Parkinson's disease as assessed by Epworth Sleepiness Scale (ESS). *Sleep Med.* 4, 339–342. doi: 10.1016/S1389-9457(03)00105-9

Lee, D. H., Oh, J. S., Ham, J. H., Lee, J. J., Lee, I., Lee, P. H., et al. (2015). Is normosmic Parkinson disease a unique clinical phenotype? *Neurology* 85, 1270–1275. doi: 10.1212/WNL.0000000000001999

Lee, J. E., Cho, K. H., Ham, J. H., Song, S. K., Sohn, Y. H., and Lee, P. H. (2014). Olfactory performance acts as a cognitive reserve in non-demented patients with Parkinson's disease. *Parkinsonism Relat. Disord.* 20, 186–191. doi: 10.1016/j.parkreldis.2013.10.024

Li, B.-Y., Tang, H.-D., and Chen, S.-D. (2016). Retrieval deficiency in brain activity of working memory in amnesic mild cognitive impairment patients: a brain event-related potentials study. *Front. Aging Neurosci.* 8:54. doi: 10.3389/fnagi.2016.00054

Li, M., Kuroiwa, Y., Wang, L., Kamitani, T., Takahashi, T., Suzuki, Y., et al. (2003). Early sensory information processes are enhanced on visual oddball and S1–S2 tasks in Parkinson's disease: a visual event-related potentials study. *Parkinsonism Relat. Disord.* 9, 329–340. doi: 10.1016/S1353-8020(02)00094-9

Luck, S. J., Heinze, H. J., Mangun, G. R., and Hillyard, S. A. (1990). Visual event-related potentials index focused attention within bilateral stimulus arrays. II. Functional dissociation of P1 and N1 components. *Electroencephalogr. Clin. Neurophysiol.* 75, 528–542. doi: 10.1016/0013-4694(90)90139-B

Mahurin, R. K., Feher, E. P., Nance, M. L., Levy, J. K., and Pirozzolo, F. J. (1993)."Cognition in Parkinson's disease and related disorders," *in Neuropsychology of Alzheimer's Disease and Other Dementias*. New York, NY: Oxford University Press, 308–349.

Matsui, H., Nishinaka, K., Oda, M., Kubori, T., and Udaka, F. (2007). Auditory event-related potentials in Parkinson's disease: prominent correlation with attention. *Parkinsonism Relat. Disord.* 13, 394–398. doi: 10.1016/j.parkreldis.2006.12.012

Mesholam, R. I., Moberg, P. J., Mahr, R. N., and Doty, R. L. (1998). Olfaction in neurodegenerative disease: a meta-analysis of olfactory functioning in Alzheimer's and Parkinson's diseases. *Arch. Neurol.* 55, 84–90. doi: 10.1001/archneur.55.1.84

Morley, J. F., Weintraub, D., Mamikonyan, E., Moberg, P. J., Siderowf, A. D., and Duda, J. E. (2011). Olfactory dysfunction is associated with neuropsychiatric manifestations in Parkinson's disease. *Mov. Disord.* 26, 2051–2057. doi: 10.1002/mds.23792

Naatanen, R., and Picton, T. (1987). The N1 wave of the human electric and magnetic response to sound: a review and an analysis of the

component structure. *Psychophysiology* 24, 375–425. doi: 10.1111/j.1469-8986.1987.tb00311.x

Nie, K., Zhang, Y., Wang, L., Zhao, J., Huang, Z., Gan, R., et al. (2012). A pilot study of psychometric properties of the Beijing version of Montreal Cognitive Assessment in patients with idiopathic Parkinson's disease in China. *J. Clin. Neurosci.* 19, 1497–1500. doi: 10.1016/j.jocn.2011.11.039

Niu, H., Shen, L., Li, T., Ren, C., Ding, S., Wang, L., et al. (2018). Alpha-synuclein overexpression in the olfactory bulb initiates prodromal symptoms and pathology of Parkinson's disease. *Transl. Neurodegener.* 7:25. doi: 10.1186/s40035-018-0128-6

Opitz, B., Schneiders, J. A., Krick, C. M., and Mecklinger, A. (2014). Selective transfer of visual working memory training on Chinese character learning. *Neuropsychologia* 53, 1–11. doi: 10.1016/j.neuropsychologia.2013.10.017

Parrao, T., Chana, P., Venegas, P., Behrens, M. I., and Aylwin, M. L. (2012). Olfactory deficits and cognitive dysfunction in Parkinson's disease. *Neurodegener. Dis.* 10, 179–182. doi: 10.1159/000335915

Postuma, R. B., Berg, D., Stern, M., Poewe, W., Olanow, C. W., Oertel, W., et al. (2015). MDS clinical diagnostic criteria for Parkinson's disease. *Mov. Disord.* 30, 1591–1601. doi: 10.1002/mds.26424

Seer, C., Lange, F., Georgiev, D., Jahanshahi, M., and Kopp, B. (2016). Event-related potentials and cognition in Parkinson's disease: an integrative review. *Neurosci. Biobehav. Rev.* 71, 691–714. doi: 10.1016/j.neubiorev.2016.08.003

Selpien, H., Siebert, C., Genc, E., Beste, C., Faustmann, P. M., Gunturkun, O., et al. (2015). Left dominance for language perception starts in the extrastriate cortex: an ERP and sLORETA study. *Behav. Brain Res.* 291, 325–333. doi: 10.1016/j.bbr.2015.05.050

Shen, S. S., Shen, Y., Xiong, K. P., Chen, J., Mao, C. J., Huang, J. Y., et al. (2014). Validation study of REM sleep behavior disorder questionnaire-Hong Kong (RBDQ-HK) in east China. *Sleep Med.* 15, 952–958. doi: 10.1016/j.sleep.2014.03.020

Stephenson, R., Houghton, D., Sundararajan, S., Doty, R. L., Stern, M., Xie, S. X., et al. (2010). Odor identification deficits are associated with increased risk of neuropsychiatric complications in patients with Parkinson's disease. *Mov. Disord.* 25, 2099–2104. doi: 10.1002/mds.23234

Taylor, M. J. (2002). Non-spatial attentional effects on P1. *Clin. Neurophysiol.* 113, 1903–1908. doi: 10.1016/S1388-2457(02)00309-7

Thompson, E. (2015). Hamilton Rating Scale for Anxiety (HAM-A). *Occup. Med.* 65:601. doi: 10.1093/occmed/kqv054

Tomlinson, C. L., Stowe, R., Patel, S., Rick, C., Gray, R., and Clarke, C. E. (2010). Systematic review of levodopa dose equivalency reporting in Parkinson's disease. *Mov. Disord.* 25, 2649–2653. doi: 10.1002/mds.23429

Tsuboi, Y., Uchikado, H., and Dickson, D. W. (2007). Neuropathology of Parkinson's disease dementia and dementia with Lewy bodies with reference to striatal pathology. *Parkinsonism Relat. Disord.* 13(Suppl. 3), S221–S224. doi: 10.1016/S1353-8020(08)70005-1

Unsworth, N., and Engle, R. W. (2007). The nature of individual differences in working memory capacity: active maintenance in primary memory and controlled search from secondary memory. *Psychol. Rev.* 114, 104–132. doi: 10.1037/0033-295X.114.1.104

Vasavada, M. M., Wang, J., Eslinger, P. J., Gill, D. J., Sun, X., Karunanayaka, P., et al. (2015). Olfactory cortex degeneration in Alzheimer's disease and mild cognitive impairment. *J. Alzheimers Dis.* 45, 947–958. doi: 10.3233/JAD-141947

Vogel, E. K., and Luck, S. J. (2000). The visual N1 component as an index of a discrimination process. *Psychophysiology* 37, 190–203. doi: 10.1111/1469-8986.3720190

Wang, G., Cheng, Q., Zeng, J., Bai, L., Liu, G. D., Zhang, Y., et al. (2008). Sleep disorders in Chinese patients with Parkinson's disease: validation study of a Chinese version of Parkinson's disease sleep scale. *J. Neurol. Sci.* 271, 153–157. doi: 10.1016/j.jns.2008.04.008

Wang, L., Kuroiwa, Y., Li, M., Wang, J., and Kamitani, T. (2001). Do P1 and N1 evoked by the ERP task reflect primary visual processing in Parkinson's disease? *Doc. Ophthalmol.* 102, 83–93.

Wenning, G. K., Shephard, B., Hawkes, C., Petruckevitch, A., Lees, A., and Quinn, N. (1995). Olfactory function in atypical parkinsonian syndromes. *Acta Neurol. Scand.* 91, 247–250. doi: 10.1111/j.1600-0404.1995.tb06998.x

Wright, M. J., Geffen, G. M., and Geffen, L. B. (1996). ERP measures of stimulus processing during an auditory oddball task in Parkinson's disease: evidence for an early information processing deficit. *Parkinsonism Relat. Disord.* 2, 13–21. doi: 10.1016/1353-8020(95)00024-0

Wyman-Chick, K. A., Martin, P. K., Barrett, M. J., Manning, C. A., and Sperling, S. A. (2017). Diagnostic accuracy and confidence in the clinical detection of cognitive impairment in early-stage parkinson disease. *J. Geriatr. Psychiatry Neurol.* 30, 178–183. doi: 10.1177/0891988717701001

Yamazaki, T., Kamijo, K., Kenmochi, A., Fukuzumi, S., Kiyuna, T., Takaki, Y., et al. (2000). Multiple equivalent current dipole source localization of visual event-related potentials during oddball paradigm with motor response. *Brain Topogr.* 12, 159–175. doi: 10.1023/A:1023467806268

Yu, J., Li, J., and Huang, X. (2012). The Beijing version of the Montreal Cognitive Assessment as a brief screening tool for mild cognitive impairment: a community-based study. *BMC Psychiatry* 12:156. doi: 10.1186/1471-244X-12-156

Conflict of Interest Statement: The authors declare that the research was conducted in the absence of any commercial or financial relationships that could be construed as a potential conflict of interest.

frontiers in Aging Neuroscience

ORIGINAL RESEARCH
published: 13 February 2019
doi: 10.3389/fnagi.2019.00022

Progressive Gait Deficits in Parkinson's Disease: A Wearable-Based Biannual 5-Year Prospective Study

*Markus A. Hobert[1,2,3], Susanne Nussbaum[2,3], Tanja Heger[2,3], Daniela Berg[1,2,3], Walter Maetzler[1,2,3] and Sebastian Heinzel[1]**

[1] Department of Neurology, Christian-Albrechts-University zu Kiel, Kiel, Germany, [2] Department of Neurodegenerative, Hertie Institute for Clinical Brain Research, University of Tübingen, Tübingen, Germany, [3] German Center for Neurodegenerative Diseases (DZNE), Tübingen, Germany

Background: Gait changes occur during all Parkinson's disease (PD) stages and wearable sensor-derived gait parameters may quantify PD progression. However, key aspects that may qualify quantitative gait parameters as progression markers in PD remain elusive.

Objectives: Longitudinal changes in gait parameters from a lower-back sensor under convenient and challenging walking conditions in early- and mid-stage PD patients (E-PD, M-PD) compared to controls were investigated.

Methods: Normal- and fast-pace parameters (step: number, time, velocity, variability) were assessed every 6 months for up to 5 years in 22 E-PD (<4 years baseline disease duration), 18 M-PD (>5 years) and 24 controls. Parameter trajectories and associations with MDS-UPDRS-III were tested using generalized estimating equations.

Results: Normal-pace step number (annual change in E-PD: 2.1%, Time*Group: $p = 0.001$) and step time variability (8.5%, $p < 0.05$) longitudinally increased in E-PD compared to controls (0.7%, −12%). For fast pace, no significant progression differences between groups were observed. Longitudinal changes in M-PD did not differ significantly from controls. MDS-UPDRS-III was largely associated with normal-pace parameters in M-PD.

Conclusion: Wearables can quantify progressive gait deficits indicated by increasing step number and step time variability in E-PD. In M-PD, and for fast-pace, gait parameters possess limited potential as PD progression markers.

Keywords: Parkinson's disease, progression marker, gait, wearable sensor, prospective study

OPEN ACCESS

Edited by:
Martin James McKeown, The University of British Columbia, Canada

Reviewed by:
Richard Camicioli, University of Alberta, Canada
Antonio Suppa, Sapienza University of Rome, Italy

***Correspondence:**
Sebastian Heinzel
s.heinzel@neurologie.uni-kiel.de

Received: *29 October 2018*
Accepted: *28 January 2019*
Published: *13 February 2019*

Citation:
Hobert MA, Nussbaum S, Heger T, Berg D, Maetzler W and Heinzel S (2019) Progressive Gait Deficits in Parkinson's Disease: A Wearable-Based Biannual 5-Year Prospective Study. Front. Aging Neurosci. 11:22. doi: 10.3389/fnagi.2019.00022

INTRODUCTION

Progression markers in Parkinson's disease (PD) are key to advances in PD prognosis and novel treatment efficacy measures. Yet, objective, reliable and quantitative markers of progressive motor deficits are still largely missing. Commonly, semiquantitative rating scales such as the MDS-UPDRS (Goetz et al., 2007) are used to assess motor symptoms and effects of disease modifyers. However,

such clinical ratings are to some extent subjective, substantially placebo-responsive (Shin et al., 2016), partly rater-dependent (Post et al., 2005) and therefore prone to bias. Previously, stopwatch-based motor performance measures have been suggested as progression markers, specifically "turning pegs" and "inserting pegs" in functional dexterity/pegboard tests as measures of upper extremity brady- and hypokinesia (Haaxma et al., 2010). These timed measures have been shown to worsen significantly in early-stage (E-PD) but not mid-stage PD (M-PD) patients over 4 years compared to controls (Heinzel et al., 2017). For timed axial measures, including gait speed and timed-up-and-go-test, progression differences were not significant. However, using wearable sensors (so-called "wearables") gait can be quantified more specifically and more precisely suggesting promising potential of wearables-based progression markers. Previously, quantitative gait parameters have been prospectively assessed in de-novo PD patients (Galna et al., 2015). While not compared to healthy controls (HC), step length and swing time during convenient gait significantly decreased in PD from baseline to month 18. A subsequent 36-month analysis also including HC showed significant group differences between time points regarding step time, length and width variability (Rochester et al., 2017). One other study with unstandardized follow-up intervals compared gait parameters with the change of the item "gait" of the MDS-UPDRS-III and found an association between the worsening in the item "gait" and a decrease of stride length (Schlachetzki et al., 2017). However, key aspects that may qualify these quantitative gait parameters as progression markers in PD remain elusive. In particular, short interval progression characteristics over longer periods, progression in M-PD, and unspecific longitudinal changes in HC need further investigation. Moreover, whether the assessment of gait under convenient or challenging conditions best reveals progressive gait deficits in PD is still unknown.

The present prospective longitudinal study therefore investigated normal- and fast-pace gait as assessed with a lower-back wearable and a validated algorithm deriving gait parameters in E-PD, M-PD, and HC. Assessments were performed 6-monthly for up to 5 years. Differences in longitudinal changes of gait parameters in the PD groups relative to HC were analyzed.

MATERIALS AND METHODS

Prospective Study Design and Participants

Prospective data of the MODEP study (MODeling Epidemiological data to study Parkinson's disease progression) (Heinzel et al., 2016, 2017) with standardized biannual clinical and gait assessments over up to 5 years (10 visits) were analyzed. Forty patients with PD according United Kingdom Brain Bank criteria (Hughes et al., 1993), and 24 age- and sex-matched HC were included. Since symptom progression can depend on PD duration (Haaxma et al., 2010), patients were recruited as and *a priori* stratified into E-PD (<4 years baseline disease duration, $n = 22$) and M-PD (>5 years, $n = 18$) as suggested by neuropathological findings (Kordower et al., 2013). The study was approved by the local ethical committee (University of Tübingen; No 46/2010). All participants gave written informed consent.

Clinical Assessment

Clinical assessments comprised current medication, height, weight, clinical ratings of PD motor symptoms (MDS-UPDRS-III) (Goetz et al., 2007), and Hoehn and Yahr stage. For axial scores, MDS-UPDRS-III axial items (3.9/3.10/3.12/3.13/3.14) were summed (Levy et al., 2000). Levodopa equivalent daily dose [LEDD; mg/day] was calculated (Tomlinson et al., 2010). Visits differed in ON/OFF medication state (E-PD: 18%; M-PD: 25% of visits in ON state) which was accounted for in statistical analyses. Moreover, the freezing of gait (FOG) questionnaire (Giladi et al., 2009) and the Montreal Cognitive Assessment (MoCA) (Nasreddine et al., 2005) were assessed. For FOG a score of 3 or higher in item #3, and for mild cognitive impairment a MoCA score of 22 or lower scores were considered (Carson et al., 2018).

Gait Assessment

Participants were instructed to walk 20 m, first with normal (convenient) pace and then with fast pace (individual maximum), along a 2 m-wide straight corridor. Both conditions were performed twice, and gait parameters were averaged for the two trials. The wearable (Dynaport Hybrid, McRoberts B.V., The Hague, Netherlands) was fixed with a belt to the participants' lower back. The Dynaport Hybrid is an inertial measurement unit containing a 3D-accelerometer and a 3D-gyroscope with 100 Hz sampling frequency. Reliability of the sensor system and derived movement parameters has been shown previously using a instrumented Timed Up and Go (TUG) tests (van Lummel et al., 2016). After discarding acceleration and deceleration periods of walks (first and last 15% of the data; about 3 m each) (Lindemann et al., 2008), the company-provided validated gait analysis algorithm (Zijlstra and Hof, 2003; Brandes et al., 2006; Dijkstra et al., 2008; Houdijk et al., 2008; Hobert et al., 2017) was applied to extract the following gait parameters: step number, step time, step velocity, and measures of gait variability, i.e., step time variability (calculated as coefficient of variation), gait asymmetry (Yogev et al., 2007; Plotnik et al., 2009) and phase coordination index (PCI) (Plotnik et al., 2007).

Statistical Approach

Longitudinal data of gait parameters were analyzed using generalized estimating equations (GEE) with identity-link functions with normal distributions and exchangeable working correlation structure (Zeger et al., 1988; Hardin and Hilbe, 2003). GEE models comprised the subject ID, the within-subject variable Time (visit 1 to 10; centered), the factor Group (E-PD vs. HC; M-PD vs. HC), the interaction term Time*Group (i.e., group difference in progression) and the covariates age (at baseline), ON/OFF medication state, weight, height, body-mass-index were considered. Parameters for normal- and fast-pace gait were selected as dependent variables. Group effects are related to the median of the observational period. The significance

level was α = 5% (two-sided). Bonferroni-corrections for multiple testing were applied considering two group comparisons and two gait conditions ($p < 0.0125$, significance threshold; $0.0125 < p < 0.05$, statistical trend). Moreover, gait parameters were tested for associations with clinical PD parameters (MDS-UPDRS-III total score, axial score, Hoehn and Yahr stage, LEDD). Here, GEE models were calculated for the overall PD sample, and separately for E-PD and M-PD, comprising the respective clinical parameter and aforementioned covariates (except Group). For these exploratory analyses no correction for multiple testing was considered ($p < 0.05$). We used IBM SPSS Statistics, V22.0 (Armonk, NY, IBM Corp.) for statistical analyses.

RESULTS

E-PD and M-PD did not differ significantly in age and sex-ratio compared to HC. M-PD differed significantly in disease duration, but also in LEDD, MDS-UPDRS-III scores and Hoehn and Yahr stage (**Supplementary Table S1**).

PD groups showed a significantly larger step number and lower velocity compared to HC for normal-pace (E-PD: $p = 0.001$; M-PD: $p < 0.001$) and for fast-pace gait ($p < 0.001$). For GEE analyses, see **Supplementary Tables S2**, **S3**. Moreover, normal-pace step time CoV was significantly higher in M-PD compared to HC ($p = 0.002$). None of the other gait parameters showed significant differences between the PD groups and HC ($p > 0.05$), neither for normal- nor for fast-pace gait.

Longitudinal changes of the quantitative gait parameters are shown in **Figure 1**. Significant differences in longitudinal changes ($p < 0.0125$; Bonferroni-corrected) were only observed between HC and E-PD, and only for normal pace. Specifically, the progression in normal-pace step number differed significantly between E-PD and HC (Time*Group, $p = 0.001$), with a significant increase over time only in E-PD (Time: $p < 0.001$), but not HC (Time: $p = 0.070$). Moreover, E-PD and HC differed regarding the longitudinal changes in normal-pace step time CoV (Time*Group, $p = 0.002$), gait asymmetry ($p = 0.009$), and for trend, PCI ($p = 0.028$). However, while HC showed a decrease over time in gait variability parameters (step time CoV, $p < 0.001$; gait asymmetry, $p = 0.003$; PCI, $p = 0.015$), no significant change over time was observed in E-PD ($p > 0.05$). For fast-pace, none of the longitudinal changes of gait parameters differed significantly between groups.

Excluding individuals who at least once fulfilled the criteria for mild cognitive impairment (3 HC, 5 E-PD, 2 M-PD) or entering MoCA scores as additional factor into GEE analyses largely did not change the main results. Similarly, excluding individuals who reported freezing of gait (2 E-PD, 4 M-PD) or excluding visits in ON medication state resulted in the main findings of progression group differences in normal-pace step number and step time CoV, which remained significant and showed similar effect sizes. To further test the reliability of the results, we analyzed the performances in single gait trials instead of the average of the two trials. For each of the two single trials the interaction effect (Time*Group) was observed ($p < 0.05$) for normal-pace step number and step time CoV in E-PD versus HC comparisons. Analyses of the ratio of normal/fast-pace gait parameters showed the longitudinal changes of ratio values to be less pronounced and with larger variability between visits and individuals compared to normal-pace parameters alone.

Associations between clinical parameters and wearables-based gait parameters partly differed between gait conditions (normal/fast-pace) and PD groups (**Table 1**). For normal pace, gait variability in E-PD, and in M-PD additionally step number and velocity showed significant associations with clinical parameters. For fast pace, E-PD but not M-PD showed associations of gait variability with clinical parameters. In M-PD, axial scores showed larger associations with fast-pace compared to normal-pace step number and velocity.

DISCUSSION

The present prospective observational study with 6-month intervals over a period of up to 5 years investigated the potential of quantitative gait parameters for the assessment of changes in normal- and fast-pace gait, respectively, in early- and mid-stage PD patients.

This study supports and extends previous findings suggesting longitudinal changes of normal-pace step number as a potential progression marker in E-PD (Galna et al., 2015; Schlachetzki et al., 2017). Changes were significantly larger in E-PD (2.1%/year) than in HC (0.7%/year), and, importantly, showed linear progression over the 5-year observation period. These findings remained robust when also accounting for further potential confounders and when excluding individuals with mild cognitive impairment and freezing of gait. This makes step number during normal pace a very promising and robust progression parameter for routine diagnostics and clinical trials.

Gait variability parameters may also possess potential as a progression marker in early phases of clinical PD. Significant differences in longitudinal changes were observed between E-PD and HC, however, this finding was not (only) due to a (non-significant) increase in PD (8.5%/year) but partly driven by HC decreasing in gait variability over time. Our finding supports our clinical impression that variability of gait shows relevant changes in short time periods in many PD patients, and may be one of the best predictors of disease milestones like falls (Hausdorff et al., 2003; Callisaya et al., 2011; Henderson et al., 2016). Indeed, previous cross-sectional analyses showed increased gait variability to be associated with PD duration (Hausdorff et al., 2003). Thus, the potential as PD progression marker should be further evaluated in future studies.

M-PD did not show any significant gait changes compared to HC during the relatively long observation period. With increasing PD duration between-patient differences in PD severity and phenotypes might become more apparent, thus single PD progression markers might not be valid for all PD patients (Fereshtehnejad et al., 2015). Overall, our results argue

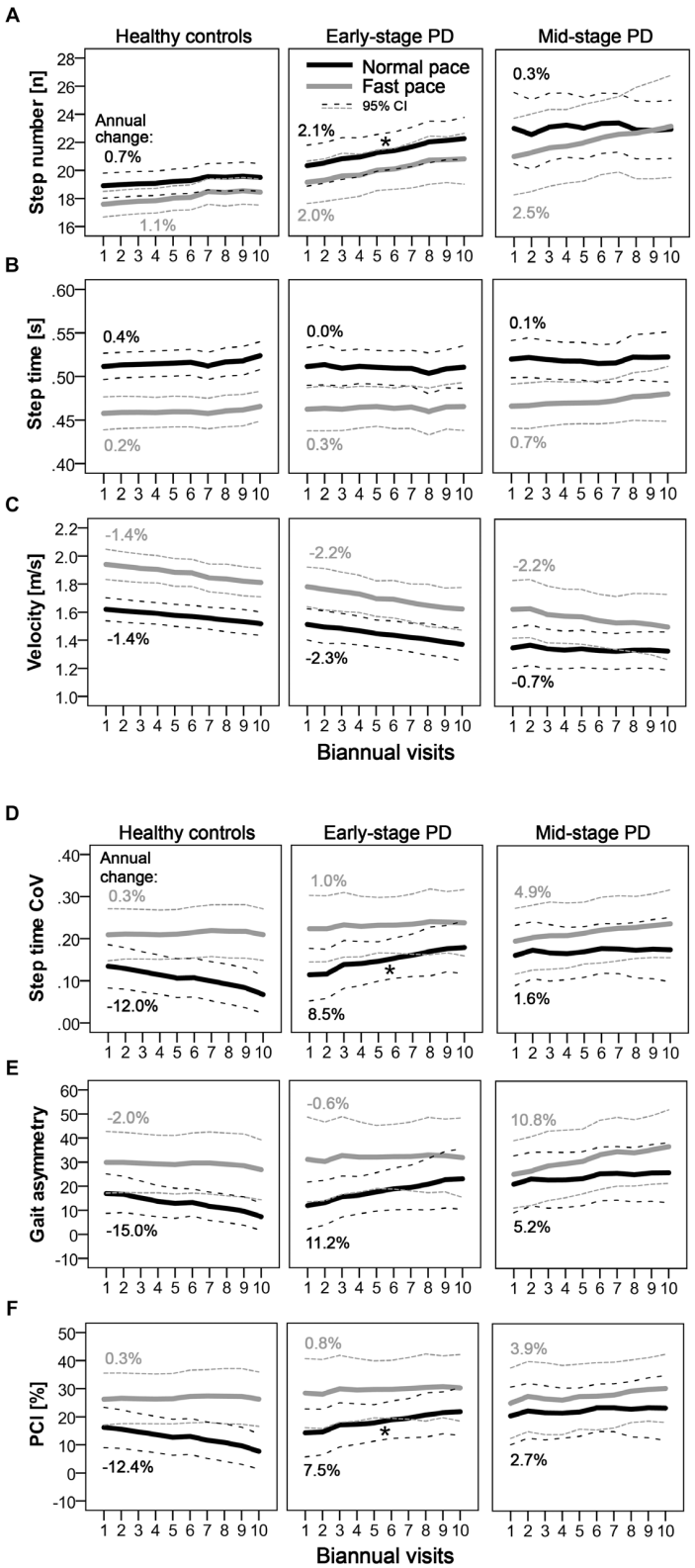

FIGURE 1 | Longitudinal progression of quantitative gait characteristics as indicated by step number **(A)** step time **(B)** velocity **(C)** and parameters of gait variability. **(D–F)** Mean values per visit and 95% confidence intervals are shown for normal pace (black) and fast pace (gray) conditions for PD groups (early-stage and mid-stage) and controls. Annual changes [%] of gait parameters are indicated. Asterisks denote significant (Time*Group: $p < 0.0125$; Bonferroni-corrected) differences in longitudinal changes compared to controls.

TABLE 1 | Associations of wearables-based and clinical parameters of gait deficits.

Gait condition	Clinical parameter (defined unit)	All PD patients	Relative and absolute change per 1-unit change of clinical parameter (mean ± S.E.)	E-PD	Relative and absolute change per 1-unit change of clinical parameter (mean ± S.E.)	M-PD	Relative and absolute change per 1-unit change of clinical parameter (mean ± S.E.)
Normal pace	**MDS-UPDRS-III**	Step number	3%, 0.67 ± 0.19			Step number	4%, 0.80 ± 0.24
	(Unit: 10 scores of	Velocity	−3%, −0.04 ± 0.01			Velocity	−3%, −0.04 ± 0.01
	max. 120)	Step time CoV	14%, 0.02 ± 0.01			Step time CoV	13%, 0.02 ± 0.01
		Gait asym.	18%, 3.71 ± 1.36			Gait asym.	18%, 4.34 ± 1.95
		PCI	17%, 3.38 ± 1.16			PCI	15%, 3.40 ± 1.19
	AXIAL	Step number	8%, 1.84 ± 0.43	Step time CoV	47%, 0.07 ± 0.03	Step number	10%, 2.21 ± 0.51
	(Unit: 5 scores of	Velocity	−7%, −0.09 ± 0.02	PCI	53%, 9.19 ± 3.93	Velocity	−8%, −0.11 ± 0.02
	max. 20)	Step time CoV	33%, 0.05 ± 0.01			Step time CoV	29%, 0.05 ± 0.01
		Gait asym.	44%, 8.87 ± 2.27			Gait asym.	46%, 10.92 ± 4.18
		PCI	36%, 7.14 ± 2.27			PCI	32%, 7.13 ± 2.63
	H and Y	Step time CoV	26%, 0.04 ± 0.01	Gait asym.	27%, 4.59 ± 1.93	Step time CoV	25%, 0.04 ± 0.01
	(Unit: 1 stage of	Gait asym.	34%, 6.91 ± 1.56			Gait asym.	34%, 8.06 ± 2.66
	max. 5)	PCI	29%, 5.79 ± 1.60			PCI	28%, 6.27 ± 1.27
	LEDD			Step time CoV	8%, 0.01 ± 0.00		
	(Unit: 100 mg/day)			PCI	7%, 1.25 ± 0.60		
Fast pace	**MDS-UPDRS-III**	Step number	3%, 0.66 ± 0.19	CoV	−7%, −0.02 ± 0.01	Step number	5%, 1.04 ± 0.31
	(Unit: 10 scores of	Velocity	−3%, −0.04 ± 0.01	Gait asym.	-10%, −3.05 ± 1.44	Velocity	−4%, −0.06 ± 0.02
	max. 120)						
	AXIAL	Step number	14%, 2.89 ± 0.75			Step number	17%, 3.64 ± 0.95
	(Unit: 5 score of	Velocity	−9%, 0.16 ± 0.03			Velocity	−13%, −0.20 ± 0.04
	max. 20)						
	H and Y	Step number	5%, 1.07 ± 0.33			Step number	8%, 1.74 ± 0.55
	(Unit: 1 stage of					Velocity	−6%, −0.10 ± 0.05
	max. 5)						
	LEDD	Step number	1%, 0.21 ± 0.10	Step time CoV	9%, 0.02 ± 0.01		
	(Unit: 100 mg/day)			PCI	9%, 2.74 ± 1.04		

Significant associations ($p < 0.05$) between clinical measures of Parkinson's disease and wearables-based gait parameters are shown. Upper part: normal-pace parameters; lower part: fast-pace parameters. The parameter name and the relative (in %) and the absolute change of the parameter that occurred with one unit change of the respective clinical measure (shown on the left) are indicated. In columns, analysis results are shown for the entire PD group (left), and when only considering E-PD or M-PD groups. H and Y, Hoehn and Yahr stage; CoV, coefficient of variance; E-PD, early-stage Parkinson's disease; gait asym., gait asymmetry; LEDD, levodopa equivalent daily dose; MDS-UPDRS-III, Movement Disorder Society sponsored Unified Parkinson's Disease Rating Scale, part 3, motor examination; M-PD, mid-stage Parkinson's disease; PCI, phase coordination index; S.E., standard error.

against a relevant potential of quantitative gait analysis for the evaluation of disease progression in mid-stage PD.

Interestingly, normal-pace walking was more sensitive to gait-related changes than fast-pace walking. Compared to normal-pace, fast-pace gait might be more challenging and stressful, which may increase (behavioral) variability and confounding with unspecific age-related factors. Therefore, we recommend normal-pace walking to be included in, e.g., clinical trials to assess PD progression, and to omit challenging walking conditions and normal/fast-pace comparisons.

Established clinical PD parameters showed associations with the quantitative wearables-based gait parameters thereby supporting their value and clinical relevance. Associations were largely observed in M-PD, and for normal-pace conditions. Differences in associations might be due to lower variance of the clinical data in E-PD than in M-PD. Moreover, MDS-UPDRS-III total and axial sum scores may less specifically indicate motor symptoms compared to quantitative gait parameters, and in E-PD more specific quantification of motor symptoms may be required. Fast-pace conditions might introduce unspecific (error) variance into gait variability parameter data, thus compared to normal-pace their associations with clinical measures might be weaker.

These present results might also provide future clinical and scientific perspectives. Parameters that allow to quantify disease progression, such as kinetic gait parameters derived from wearable devices, could serve as objective outcome markers of pharmacological treatment and other interventions. In this regard reliable quantitative markers of PD motor symptoms and their progression are highly promising as (at least secondary) outcomes in the clinical routine as well as in clinical intervention trials (Moreau et al., 2018). These measures have the potential of increasing sensitivity and objectivity while reducing costs of these clinical trials (Merchant et al., 2018). Importantly,

wearable-based motor measures possess a high relevance for daily living and quality of life (Van Uem et al., 2016), and studies based on such measures may therefore yield results that benefit PD patients.

This study faces some limitations. First, the sample was relatively small. However, the thorough and high-frequency evaluation of participants may partially compensate for this limitation, especially as parameters are needed that are robust even in smaller samples. Second, PD is a heterogeneous disease and further subgroups and non-motor symptoms potentially influencing gait, e.g., depression, were not accounted for. Also, multi-facetted interventions were not controlled for in this observational study. Longitudinal differences in pharmacological and non-pharmacological treatments and their efficacy over time may additionally contribute to the heterogeneity in PD, particularly in advanced PD. While accounting for ON/OFF medication state in statistical analyses modeling of individual treatments is complex. Thus, subtle gait changes and factors contributing to progression differences between PD patients might have remained undetected.

To conclude, number of steps and possibly also gait variability measures as assessed during normal-pace walking with a lower-back wearable are robust and promising progression markers in the early phase of PD.

AUTHOR CONTRIBUTIONS

DB and WM conceived the study. DB, WM, TH, and SN organized the study. WM, TH, SN, and MH executed the study. SH and MH designed the statistical analysis. SH executed the statistical analysis. DB, WM, and MH critically reviewed the results. MH and SH wrote the first draft of the manuscript. DB, WM, and MH critically reviewed the manuscript.

FUNDING

The MODEP study was initially supported by Solvay Pharmaceuticals and received financial support by Teva Pharmaceutical Industries Ltd. The analysis of the MODEP data was supported by Lundbeck. The funders were not involved in study design, data collection and analysis, decision to publish, and preparation of the manuscript. None of the authors reports any financial interests or potential conflicts of interest related to this study.

ACKNOWLEDGMENTS

We thank the participants for participation in the study. We would also like to thank Dr. Maren Ellerbork, Dr. Jana Godau, Dr. Sandra E. Hasmann, Dr. Miriam Maechtel and Irénée Kanyiki for performing assessments during the active data collection phase. Moreover, we acknowledge financial support by Land Schleswig-Holstein within the funding program Open Access Publikationsfonds.

SUPPLEMENTARY MATERIAL

The Supplementary Material for this article can be found online at: https://www.frontiersin.org/articles/10.3389/fnagi.2019.00022/full#supplementary-material

REFERENCES

Brandes, M., Zijlstra, W., Heikens, S., van Lummel, R., and Rosenbaum, D. (2006). Accelerometry based assessment of gait parameters in children. *Gait Posture* 24, 482–486. doi: 10.1016/j.gaitpost.2005.12.006

Callisaya, M. L., Blizzard, L., Schmidt, M. D., Martin, K. L., McGinley, J. L., Sanders, L. M., et al. (2011). Gait, gait variability and the risk of multiple incident falls in older people: a population-based study. *Age Ageing* 40, 481–487. doi: 10.1093/ageing/afr055

Carson, N., Leach, L., and Murphy, K. J. (2018). A re-examination of Montreal Cognitive Assessment (MoCA) cutoff scores. *Int. J. Geriatr. Psychiatry* 33, 379–388. doi: 10.1002/gps.4756

Dijkstra, B., Zijlstra, W., Scherder, E., and Kamsma, Y. (2008). Detection of walking periods and number of steps in older adults and patients with parkinson's disease: accuracy of a pedometer and an accelerometry-based method. *Age Ageing* 37, 436–441. doi: 10.1093/ageing/afn097

Fereshtehnejad, S.-M., Romenets, S. R., Anang, J. B. M., Latreille, V., Gagnon, J.-F., and Postuma, R. B. (2015). New clinical subtypes of parkinson disease and their longitudinal progression. *JAMA Neurol.* 72, 863–873. doi: 10.1001/jamaneurol.2015.0703

Galna, B., Lord, S., Burn, D. J., and Rochester, L. (2015). Progression of gait dysfunction in incident Parkinson's disease: impact of medication and phenotype. *Mov. Disord.* 30, 359–367. doi: 10.1002/mds.26110

Giladi, N., Tal, J., Azulay, T., Rascol, O., Brooks, D. J., Melamed, E., et al. (2009). Validation of the freezing of gait questionnaire in patients with Parkinson's disease. *Mov. Disord.* 24, 655–661. doi: 10.1002/mds.21745

Goetz, C. G., Fahn, S., Martinez-Martin, P., Poewe, W., Sampaio, C., Stebbins, G. T., et al. (2007). Movement disorder society-sponsored revision of the unified parkinson's disease rating scale (MDS-UPDRS): process, format, and clinimetric testing plan. *Mov. Disord.* 22, 41–47. doi: 10.1002/mds.21198

Haaxma, C. A., Bloem, B. R., Overeem, S., Borm, G. F., and Horstink, M. W. (2010). Timed motor tests can detect subtle motor dysfunction in early Parkinson's disease. *Mov. Disord.* 25, 1150–1156. doi: 10.1002/mds.23100

Hardin, J., and Hilbe, J. (2003). *Generalized Estimating Equations*, Boca Raton, FL: CRC Press.

Hausdorff, J. M., Balash, J., and Giladi, N. (2003). Effects of cognitive challenge on gait variability in patients with Parkinson's disease. *J. Geriatr. Psychiatry Neurol.* 16, 53–58.

Heinzel, S., Bernhard, F. P., Roeben, B., Nussbaum, S., Heger, T., Martus, P., et al. (2017). Progression markers of motor deficits in Parkinson's disease: a biannual 4-year prospective study. *Mov. Disord.* 32, 1254–1256. doi: 10.1002/mds.27062

Heinzel, S., Maechtel, M., Hasmann, S. E., Hobert, M. A., Heger, T., Berg, D., et al. (2016). Motor dual-tasking deficits predict falls in Parkinson's disease: a prospective study. *Park. Relat. Disord.* 26, 73–77. doi: 10.1016/j.parkreldis.2016.03.007

Henderson, E. J., Lord, S. R., Brodie, M. A., Gaunt, D. M., Lawrence, A. D., Close, J. C. T., et al. (2016). Rivastigmine for gait stability in patients with Parkinson's disease (ReSPonD): a randomised, double-blind, placebo-controlled, phase 2 trial. *Lancet Neurol.* 15, 249–258. doi: 10.1016/S1474-4422(15)00389-0

Hobert, M. A., Meyer, S. I., Hasmann, S. E., Metzger, F. G., Suenkel, U., Eschweiler, G. W., et al. (2017). Gait is associated with cognitive flexibility: a dual-tasking study in healthy older people. *Front. Aging Neurosci.* 9:154. doi: 10.3389/fnagi.2017.00154

Houdijk, H., Appelman, F. M., Van Velzen, J. M., Van der Woude, L. H. V., and Van Bennekom, C. A. M. (2008). Validity of dynaport gaitmonitor for assessment of spatiotemporal parameters in amputee gait. *J. Rehabil. Res. Dev.* 45, 1335–1342.

Hughes, A. J., Daniel, S. E., Blankson, S., and Lees, A. J. (1993). A clinicopathologic study of 100 cases of Parkinson's disease. *Arch. Neurol.* 50, 140–148.

Kordower, J. H., Olanow, C. W., Dodiya, H. B., Chu, Y., Beach, T. G., Adler, C. H., et al. (2013). Disease duration and the integrity of the nigrostriatal system in Parkinson's disease. *Brain* 136, 2419–2431. doi: 10.1093/brain/awt192

Levy, G., Tang, M. X., Cote, L. J., Louis, E. D., Alfaro, B., Mejia, H., et al. (2000). Motor impairment in PD: relationship to incident dementia and age. *Neurology* 55, 539–544.

Lindemann, U., Najafi, B., Zijlstra, W., Hauer, K., Muche, R., Becker, C., et al. (2008). Distance to achieve steady state walking speed in frail elderly persons. *Gait Posture* 27, 91–96. doi: 10.1016/j.gaitpost.2007.02.005

Merchant, K. M., Cedarbaum, J. M., Brundin, P., Dave, K. D., Eberling, J., Espay, A. J., et al. (2018). A proposed roadmap for parkinson's disease proof of concept clinical trials investigating compounds targeting alpha-synuclein. *J. Parkinsons. Dis.* doi: 10.3233/JPD-181471 [Epub ahead of print].

Moreau, C., Duce, J. A., Rascol, O., Devedjian, J.-C., Berg, D., Dexter, D., et al. (2018). Iron as a therapeutic target for Parkinson's disease. *Mov. Disord.* 33, 568–574. doi: 10.1002/mds.27275

Nasreddine, Z. S., Phillips, N. A., Bedirian, V., Charbonneau, S., Whitehead, V., Collin, I., et al. (2005). The montreal cognitive assessment, MoCA: a brief screening tool for mild cognitive impairment. *J. Am. Geriatr. Soc.* 53, 695–699. doi: 10.1111/j.1532-5415.2005.53221.x

Plotnik, M., Giladi, N., and Hausdorff, J. M. (2007). A new measure for quantifying the bilateral coordination of human gait: effects of aging and Parkinson's disease. *Exp. Brain Res.* 181, 561–570. doi: 10.1007/s00221-007-0955-7

Plotnik, M., Giladi, N., and Hausdorff, J. M. (2009). Bilateral coordination of gait and Parkinson's disease: the effects of dual tasking. *J. Neurol. Neurosurg. Psychiatry* 80, 347–350. doi: 10.1136/jnnp.2008.157362

Post, B., Merkus, M. P., de Bie, R. M. A., de Haan, R. J., and Speelman, J. D. (2005). Unified Parkinson's disease rating scale motor examination: are ratings of nurses, residents in neurology, and movement disorders specialists interchangeable? *Mov. Disord.* 20, 1577–1584. doi: 10.1002/mds.20640

Rochester, L., Galna, B., Lord, S., Yarnall, A. J., Morris, R., Duncan, G., et al. (2017). Decrease in Aβ42 predicts dopa-resistant gait progression in early Parkinson disease. *Neurology* 88, 1501–1511. doi: 10.1212/WNL.0000000000003840

Schlachetzki, J. C. M., Barth, J., Marxreiter, F., Gossler, J., Kohl, Z., Reinfelder, S., et al. (2017). Wearable sensors objectively measure gait parameters in Parkinson's disease. *PLoS One* 12:e0183989. doi: 10.1371/journal.pone.0183989

Shin, C. W., Hahn, S., Park, B.-J., Kim, J.-M., Park, E. O., and Jeon, B. (2016). Predictors of the placebo response in clinical trials on Parkinson's disease: a meta-analysis. *Parkinsonism Relat. Disord.* 29, 83–89. doi: 10.1016/j.parkreldis.2016.05.019

Tomlinson, C. L., Stowe, R., Patel, S., Rick, C., Gray, R., and Clarke, C. E. (2010). Systematic review of levodopa dose equivalency reporting in Parkinson's disease. *Mov. Disord.* 25, 2649–2653. doi: 10.1002/mds.23429

van Lummel, R. C., Walgaard, S., Hobert, M. A., Maetzler, W., van Dieën, J. H., Galindo-Garre, F., et al. (2016). Intra-rater, inter-rater and test-retest reliability of an instrumented timed up and go (itug) test in patients with parkinson's disease. *PLoS One* 11:e0151881. doi: 10.1371/journal.pone.0151881

Van Uem, J. M. T., Walgaard, S., Ainsworth, E., Hasmann, S. E., Heger, T., Nussbaum, S., et al. (2016). Quantitative timed-up-and-go parameters in relation to cognitive parameters and health-related quality of life in mild-to-moderate parkinson's disease. *PLoS One* 11:e0151997. doi: 10.1371/journal.pone.0151997

Yogev, G., Plotnik, M., Peretz, C., Giladi, N., and Hausdorff, J. M. (2007). Gait asymmetry in patients with Parkinson's disease and elderly fallers: when does the bilateral coordination of gait require attention? *Exp. Brain Res.* 177, 336–346. doi: 10.1007/s00221-006-0676-3

Zeger, S. L., Liang, K. Y., and Albert, P. S. (1988). Models for longitudinal data: a generalized estimating equation approach. *Biometrics* 44, 1049–1060.

Zijlstra, W., and Hof, A. L. (2003). Assessment of spatio-temporal gait parameters from trunk accelerations during human walking. *Gait Posture* 18, 1–10. doi: 10.1016/S0966-6362(02)00190-X

Conflict of Interest Statement: The authors declare that the research was conducted in the absence of any commercial or financial relationships that could be construed as a potential conflict of interest.

frontiers in Neurology

ORIGINAL RESEARCH
published: 20 March 2019
doi: 10.3389/fneur.2019.00271

Hydralazine Protects Nigrostriatal Dopaminergic Neurons From MPP+ and MPTP Induced Neurotoxicity: Roles of Nrf2-ARE Signaling Pathway

*Xingfang Guo[1], Chao Han[2], Kai Ma[1], Yun Xia[1], Fang Wan[1], Sijia Yin[1], Liang Kou[1], Yadi Sun[1], Jiawei Wu[1], Junjie Hu[1], Jinsha Huang[1], Nian Xiong[1] and Tao Wang[1]**

[1] Department of Neurology, Union Hospital,Tongji Medical College, Huazhong University of Science and Technology, Wuhan, China, [2] Department of Neurology, The First Affiliated Hospital of USTC and Division of Life Sciences and Medicine, University of Science and Technology of China, Hefei, China

OPEN ACCESS

Edited by:
Martin James McKeown,
University of British Columbia, Canada

Reviewed by:
Margarida Castro-Caldas,
New University of Lisbon, Portugal
Petr A. Slominsky,
Institute of Molecular Genetics (RAS), Russia

***Correspondence:**
Tao Wang
wangtaowh@hust.edu.cn

Specialty section:
This article was submitted to Neurodegeneration, a section of the journal Frontiers in Neurology

Received: 18 September 2018
Accepted: 28 February 2019
Published: 20 March 2019

Citation:
Guo X, Han C, Ma K, Xia Y, Wan F, Yin S, Kou L, Sun Y, Wu J, Hu J, Huang J, Xiong N and Wang T (2019) Hydralazine Protects Nigrostriatal Dopaminergic Neurons From MPP+ and MPTP Induced Neurotoxicity: Roles of Nrf2-ARE Signaling Pathway. Front. Neurol. 10:271. doi: 10.3389/fneur.2019.00271

Although the pathogenic mechanisms of Parkinson's disease (PD) remain unclear, ample empirical evidence suggests that oxidative stress is involved in the pathogenesis of this disease. The nuclear factor E2-related factor 2 (Nrf2) is known to activate several antioxidant response element (ARE)-driven antioxidative genes that prevents oxidative stress *in vitro* and *in vivo*. Moreover, it was documented that hydralazine is a potent Nrf2 activator. In this study, we tested whether hydralazine can attenuate 1-Methyl-4-phenylpyridinium (MPP^+) and 1-methyl-4-phenyl-1,2,3,6-tetrahydropyridine (MPTP)- induced neurotoxicity *in vitro* and *in vivo* by activating Nrf2 and its downstream network of antioxidative genes. We found that treatment with hydralazine attenuated MPP^+ or H_2O_2-induced loss of cell viability in human neuroblastoma cell line (SH-SY5Y). In addition, hydralazine significantly promoted the nuclear translocation of Nrf2, and upregulated the expression of its downstream antioxidative genes. Further, knockout of Nrf2 abolished the protection conferred by hydralazine on MPP^+ -induced cell death. Similar findings were observed *in vivo*. Before, during, and after MPTP 30 mg/kg (i.p.) administration for 7 days, the mice were given hydralazine (Hyd) 51.7 mg/kg per day by oral gavage for 3 weeks. Oral administration of hydralazine ameliorated oxidative stress, MPTP-induced behavioral disorder, and loss of neurons of dopaminergic system in the substantia nigra (SN) and striatum, all of which were attributed to its ability to activate the Nrf2-ARE pathway. Hydralazine increased the migration of Nrf2 to the nucleus in dopaminergic neurons, enhanced the expression of its downstream antioxidative genes. Together, these datasets show that the Nrf2-ARE pathway mediates the protective effects of hydralazine on Parkinson's disease.

Keywords: Parkinson's disease, hydralazine, neuroprotection, Nrf2-ARE signaling pathway, MPTP, MPP^+

HIGHLIGHTS

- Hydralazine prevents the MPP^+ and H_2O_2-induced cell death in SH-SY5Y cells, and activates Nrf2-ARE signaling in both treated and non-treated MPP^+ cells *in vitro*.
- Hydralazine activate Nrf2-ARE signaling and attenuate MPP^+-mediated cytotoxicity in an Nrf2-dependent pattern.
- Hydralazine confers protection in dopaminergic neurons in the MPTP model of Parkinson's disease.
- Hydralazine alleviate oxidative stress and activates Nrf2-triggered gene expression *in vivo*.

INTRODUCTION

Currently, the pathogenesis of Parkinson's disease (PD) is elusive. It has been postulated that prolonged increased in reactive oxygen species (ROS) plays important role in modulating the occurrence of the disease (1, 2). This is because ROS compromises the mechanisms that balances oxidant and antioxidant systems (3). One of the mechanisms that prevent cell damage caused by oxidative stress is the antioxidant defense system. By increasing the level of antioxidant enzymes, phase II detoxifying enzymes, quinone oxidoreductase 1 (NQO1), NAD(P)H, heme oxygenase-1 (HMOX1), glutamate-cysteine ligase subunits (GCLC and GCLM), the nuclear factor E2-related factor 2 (Nrf2) modulates the pathophysiological and physiological processes of various diseases (4). These enzymes are involved in glutathione (GSH) synthesis and maintains the form of GSH by suppressing its oxidized form GSSG (5, 6). Several structural and molecular studies on Nrf2 revealed that Nrf2 is expressed in the cytoplasm in physiological conditions via a Kelch-like ECH-associated protein 1 (Keap1)-dependent ubiquitination-proteasomal degradation, and this process is enhanced by electrophiles and oxidants (7, 8). It was revealed that the N terminal region and double glycine repeat domain (DGR) of Keap1 contains the bric-a-brac, tramtrack, broad-complex (BTB) domain, termed as Kelch repeats in the C terminal region. Keap1 keeps the Nrf2 within the cytoplasm in normal cellular conditions by binding to a scaffold protein of Nrf2 ubiquitin ligase (E3), Cul3 through its BTB domain, and binding to the substrate of Nrf2 through its DGR domain, which causes Nrf2 degradation (9) and ubiquitination (10). When stimulated by oxidants or electrophiles, Nrf2 undergoes modifications by some mechanisms which compromise Keap1/Nrf2 interactions, which leads to the dissociation of Nrf2 from Keap1 complex, become stabilized, and then moves into the nucleus. This is followed by binding to the antioxidant response elements (AREs), a consensus gene sequence located in the promoter region of several genes that encode antioxidant enzymes (11). Several studies have provided evidence that Nrf2-ARE signal transduction participates in PD (12, 13). Downregulation of Nrf2 renders the dopaminergic neurons susceptible to oxidative stress damage (14–16), while activation of Nrf2 confers neuroprotection (17–21). Based on this background, the Nrf2-ARE interaction is thought to play important role in neurodegenerative conditions including PD.

Administration of pharmacological antioxidants seem to be the most direct approach to suppress oxidative damage. However, clinical trials on antioxidants e.g., N-acetylcysteine, vitamin E, glutathione, and vitamin C have revealed rather disappointing results for PD (22–25). One possible reason is that the efficacy of these antioxidants is largely based on their ability to stoichiometrically scavenge for oxidants. An alternative promising therapeutic strategy of restoring redox homeostasis in PD by activating the transcription factor Nrf2 may have significant advantages over conventional strategies. Hydralazine (Hyd), an FDA approved treatment for hypertension, is a water-soluble carbonyl-scavenger due to its nucleophilic hydrazine group (26). Because of this, hydralazine has been found to be a powerful antioxidant properties (27–29), Moreover, it was reported that hydralazine could activate the Nrf2 signaling pathway *in vitro* [human neuroblastoma cell line (SH-SY5Y)] and *in vivo* (Caenorhabditis elegans) model system (30), and possesses anti-aging properties (31). As mentioned above, oxidative stress and the deregulation of Nrf2-ARE signaling pathways are both involved in PD. Thus, we hypothesized that hydralazine may provide strong neuroprotective effects in Parkinson's disease in both *in vitro* and *in vivo* settings. To test this possibility, we investigated the mechanisms that orchestrate the neuroprotective effects of hydralazine using an 1-Methyl-4-phenylpyridinium (MPP^+)-induced cytotoxicity model and 1-methyl-4-phenyl-1,2,3,6-tetrahydropyridine (MPTP)-induced mice model of PD. We found that hydralazine displayed promising therapeutic efficacy toward PD by activating the Nrf2 signaling pathway.

EXPERIMENTAL PROCEDURES

Preparation of Human Neuroblastoma SH-SY5Y Cells

SHSY5Y cells were obtained from ATCC (ATCCCRL-2266) and grown in DMEM/F12 medium (hyclone) supplemented with 10% FBS (EVERY GREEN, Zhejiang Tianhang Biotechnology Co., Ltd, China), 100 μg/mL streptomycin, and 100 U/ml penicillin (Beijing solarbio science & technology co., Ltd) in high humidity condition with 5% CO_2 at 37°C. After culturing the cells in 100 mm dishes to reach a ∼70% confluence, they were subjected to hydralazine, H_2O_2 or MPP^+ treatment. The dose and duration of application of hydralazine, H_2O_2 or MPP^+ are provided in the figures and text. SiRNA interference were performed by treating the cells with Nrf2 SiRNA (sc-37030) or control SiRNA (sc-37007) (Santa Cruz Biotechnology, Santa Cruz, CA) in 6-well plates for 24 h using the Lipofectamine 3000 reagent (Thermo Fisher Scientific Co., Carlsbad, CA, USA) as indicated in the instructions provided by the manufacturer. After transfection for approximately 24 h, SHSY5Y cells were exposed to hydralazine with or without MPP^+. After these treatments, cells were used for biochemical analysis.

Cell Viability Evaluation by CCK-8 Assay

The cell counting kit-8 solution (CCK-8) assay was performed to determine the cell viability. Briefly, after seeding the SH-SY5Y

cells in 96-well plates at a density of 1×10^4 cells/well, they were treated with reagents. This was followed by incubating with 10 μl CCK-8 buffer for 1 h at 37 C following the instructions provided by the kit company. A microplate reader (BioTek, Winooski, VT, USA) was used to measure the absorbance at 450 nm. All samples were assessed in triplicate.

Quantitative Real-Time PCR

Total RNA was isolated from SHY-SY5 cells using RNAiso Plus (TaKaRa, Japan). Total RNA (2 μg) was reverse transcribed to cDNA using the PrimeScript™ II 1st Strand cDNA Synthesis Kit (TaKaRa, Japan) to determine the mRNA expressions of Nrf2 by qRT-PCR using SYBR Green reagent (TaKaRa, Japan). The PCR condition was as follows: 95°C for 5 min, 60°C for 20 s, 40 amplification cycles. Housekeeping gene β-actin served as an internal control. Data analysis is based on the ΔΔCt method with normalization of raw data to β-actin. Each reaction was run in triplicate. Nrf2 primer: forward, 5′-CAGTCAGCGACGGAA AGAGT-3′; reverse, 5′-ACGTAGCCGAAGAAACCTCA-3′; β-actin primer: forward, 5′- AGCCATGTA CGTAGCCATCC−3′; reverse, 5′- CTCTCAGCTGTGGTGGTGAA -3′.

Animals and Treatment

The mice used in this study were kept and handled according to the guidelines of the NIH Guide regarding the Use and Care of Laboratory Animals. All animals were given free water and food *ad libitum*, and the housing conditions were regulated to a 12 h dark-light cycle and temperature of (22 ± 2°C). This study conformed to the guidelines of the Animal Care and Use Committees of Maximum efforts of Huazhong University of Science and Technology (HUST). Care was taken to use few animals and reduce discomfort. Male C57/BL6 mice, 8 weeks old, were used all of which were obtained from Beijing Vital River Laboratory Animal Technology Co., Ltd. There are four groups ($n = 8$ or 9 for per group) in this experiment. The first group mice (MPTP group) only received injections of MPTP-HCl (30 mg/kg, i.p., Sigma) in saline for consecutive 7 days, an MPTP model of PD was generated as previously described (32). The second group mice (Hyd+MPTP group) were administered hydralazine (51.7 mg/kg per day in saline, Sigma) (33) by oral gavage for 3 weeks before, during, and after MPTP administration. The third group mice (Hyd group) were administered hydralazine (51.7 mg/kg per day in saline, Sigma) (33) by oral gavage for 3 weeks, and the fourth group (Control group) received vehicle only. Behavioral test of the animals were performed after the last oral gavage, after behavior test, mice were killed (**Figure 3A**).

Rotarod Testing

The general motor deficits were evaluated using the rotarod test. Mice were put in a rod which was 7 cm in diameter, and then tested at a constant speed of 30 rpm. In each test, the mouse was subjected to the rod for 1 min prior to the test. Each animal was put on the roller for 5 min, and then the latency to fall off the rolling rod was calculated. Prior to assessing the behavior of the animals, they were given pre-trials for habituation to the test system for 4 days. An average of five trials were performed for each mouse.

Pole Testing

Each mouse was placed on the top of a vertical pole (50 cm long and 1 cm in diameter) wrapped with gauze to avoid slip and fall. After pre-trials for habituation to the test system for 4 days, time of the mouse head orient downward (named as Turn) and total time climbing down the pole as an indication of the locomotion activity (TLA) were recorded. Each mouse received five successive trials for average.

Tissue Preparation

One day after the behavior test, animals were killed by decapitation under anesthesia. Afterwards, brains were removed immediately was fixed in 4% buffered paraformaldehyde and embedded in paraffin for the next immunofluorescent staining. The ventral midbrain containing the substantia nigra and striatum of the other mice were dissected and frozen immediately in liquid nitrogen and stored at −80°C for protein extraction.

Immunofluorescent Staining

After isolation, the substantia nigra and striatum tissues were embedded in paraffin and sectioned to 5 μm thickness. The sections were deparaffinized with xylene, followed by dehydration using ethanol. Finally, EDTA (PH 9.0) antigen retrieval buffer was used for antigen retrieval. These section were put on slices followed by treatment with 3% BSA at room temperature for 30 min, before they were incubated with the following primary antibodies at 4°C overnight, mouse polyclonal anti-TH (1:200, Proteintech, China), rabbit polyclonal anti-Nrf2 (1:200, Genetex), rabbit monoclonal anti-IBA1(1:200, Abcam), rabbit monoclonal anti-GFAP (1:200, Abcam). Subsequently, secondary antibodies, Alexa Fluor 488-conjugated (1:500, Life Technologies) and/or Alexa Fluor 647-conjugated (1:500, Life Technologies) were added and incubated for 1 h at room temperature. SH-SY5Y cell were fixed with 4% paraformaldehyde for 30 min, washed in PBS, and permeabilized with 0.3% Triton X-100 in PBS for 10 min at room temperature. The cells were treated with rabbit polyclonal anti-Nrf2 (1:200, Genetex) antibody overnight at 4°C after blocking with 10% normal goat serum for 1 h, and then incubated with Alexa Fluor 488-conjugated (1:500, Life Technologies) secondary antibody for 1 h at room temperature. Images from the sections were examined on an OLYMPUS IX71 fluorescent microscope. Then quantitative analysis of the optical density and of number positive neurons was performed using Image pro plus.

Determination of Protein Expression

Nuclear and cytosolic fractions were extracted from the substantia nigra, striatum specimen and human neuroblastoma SH-SY5Y cells using cytoplasmic and nuclear protein extraction kit (Beyotime, Beijing, China) following the instructions given by the manufacturer. Briefly, cells were subjected to various treatments and then suspended in PBS. The next step involved the addition of the cytoplasmic protein isolation reagents A and B. The cytosolic fraction was obtained by centrifugation. The nuclei pellets were suspended in the isolation reagent for nuclear protein. Similarly, the nuclear fraction was obtained by centrifugation. All the isolated proteins from mouse striatum,

ventral, and SH-SY5Y cells were treated on ice with RIPA lysis buffer comprising of phosphatase inhibitor A and B, protease inhibitor PMSF (PMSF:RIPA = 1:99), cocktail (Servicebio, Wuhan, China), followed by centrifugation at 12,000 g, for 15 min at 4°C, to obtain the supernatants. BCA Protein Assay Kit was applied to measure the protein concentration. This was followed by denaturation of the protein specimen using the sodium dodecyl sulfate solution together with boiling for 5 min at 98°C. About 30 μg sample was loaded onto SDS-PAGE after which electrophoresis was performed to transfer the proteins to a PVDF membrane. Thereafter, 5% milk was using to block the membranes at room temperature for 1 h before primary antibodies, rabbit monoclonal anti-β-actin (1:3000, Antgene, China), rabbit polyclonal anti-Histone H3 (1:1000, Servicebio, China), mouse monoclonal anti-GCLC (1:500, Santa Cruz), rabbit polyclonal anti-Nrf2 (1:1000, Genetex), rabbit monoclonal anti-NQO1 (1:10000, Abcam), rabbit monoclonal anti-HMOX1 (1:2000, Abcam), rabbit monoclonal anti-GCLM (1:5000, Abcam), and rabbit polyclonal tyrosine hydroxylase antibody (1:1000, Proteintech, China) were added and incubated overnight at 4°C. Finally, HRP-conjugated secondary anti-mouse antibody (1:5000, Antgene, China) or HRP-conjugated secondary anti-rabbit (1:5000, Antgene, China) was added to the membranes after washing with TBST thrice (5 min/each time) for 1 h at room temperature. After washing, ECL was loaded onto the membrane to detect the immunoreaction using the Bio-Rad imaging system. The branes were analyzed with Imagine J software. Relative band intensities were measured with β-actin or Histone H3 serving as internal control.

Determination of the Oxidative Activity by Lipid Peroxidation Assay

The generation of malondialdehyde (MDA) was measured using the lipid peroxidation commercial assay kit following the instructions provided by the manufacturer. Briefly, and tissue were homogenized, sonicated, and centrifuged. The MDA concentration on in the supernatants was measured as well as the protein concentration. The protein concentration was determined using the assay kit (Bio-Rad Laboratories, Hercules, USA). This was followed by performance of the MDA assay following the instructions provided with the Lipid Peroxidation MDA assay kit (Beyotime). The multimode microplate reader was used to quantify the MDA levels in the samples at 532 nm.

Determination of Cellular Levels of GSSG and GSH Using HPLC

Substantia nigra samples were homogenized, sonicated and centrifuged. In brief, 30 μl supernatant was isocratically eluted through a 4.6 × 150 mm C18 column (ESA, Inc.) with a mobile phase containing 50 mM LiH_2PO_4, 1.0 mM 1-octanesulfonic acid, and 1.5% (v/v) methanol, and then detected by a 2-channel Coulochem III electrochemical detector (ESA, Inc), set with a guard cell potential 950 mV, Channel 1 potential for GSH detection and Channel 2 potential 880 mV for GSSG detection (34). The quantities of GSSG and GSH were presented as nmol per mg protein.

Data Analysis

All data are expressed as mean ± SEM and were performed using the SPSS20 software. Between-group comparisons were conducted by Student's *t*-test, while the one-way ANOVAs was used to compare three or more groups followed by Tukey's multiple comparison test. A *P*-value of < 0.05 was considered to be statistically significant.

RESULTS

Hydralazine Prevents the MPP^+ and H_2O_2-Induced Cell Death in SH-SY5Y Cells, and Activates Nrf2-ARE Signaling in Both Treated and Non-treated MPP^+ Cells *in vitro*

Analysis of the influence of MPP^+ on SH-SY5Y viability revealed that the cell viability decreased to about 50% or below based on CCK-8 assays when exposed to 1000 μM (1 mM) MPP^+ for 24 or 36 h (**Figure 1A**). Therefore, we treated SH-SY5Y cells with MPP^+ 1 mM for 24 h to establish a model of MPP^+-induced cytotoxicity. Next, the effects of hydralazine on the survival of cells following exposure to MPP^+ were tested. Four doses of hydralazine (2.5, 5, 10, or 20 μM) were tested against MPP^+. Hydralazine alone at the micromolar range (2.5–20 μM) had no overt effects on these cells. But, hydralazine (10 and 20 μM) conferred significant protection against MPP^+ according to the CCK-8 assays (**Figure 1B**). Moreover, we chose H_2O_2 (100 μM) as another control of toxicity (30). Similarly, hydralazine protected the cells from H_2O_2-induced cytotoxicity (**Figure 1C**). Moreover, we observed that hydralazine (10 and 20 μM) alone increased the viability of SH-SY5Y in the absence of MPP^+ and H_2O_2 (**Figures 1B,C**). It is well-known that during cellular metabolism, spontaneous oxidative damage to unsaturated lipids generates many electrophilic carbonyl compounds which are potential threats to cell survival. Since hydralazine is a well-known carbonyl scavenger (35), we speculated that it can improve SH-SY5Y viability by scavenging Carbonyl moieties.

Thereafter, we tested the ability of hydralazine to induce nuclear translocation of Nrf2. SH-SY5Y cells were treated with 10 μM hydralazine with or without MPP^+, but the control groups were treated with saline following Nrf2 partition quantification and subcellular fractionation. Hydralazine treatment increased the nuclear translocation of Nrf2, which was accompanied by a corresponding decreased in the cytosolic fraction relative to the nuclear Nrf2 fraction (**Figures 1D–F**). The same phenomenon of nuclear translocation was observed based on immunofluorescence (**Figure 1G**). As showed in **Figures 1D–G**, treatment with hydralazine alone triggered a remarkable increase in the nuclear translocation of Nrf2, but the reasons for this effect remain unclear. It is likely that Nrf2 was modified by hydralazine in a way that disrupted the Nrf2:Keap1 interaction, and then, translocated to the nucleus. Further studies are required to answer this question. Next, we determined whether hydralazine (10 μM) would increase the downstream protein of the Nrf2-ARE pathway,

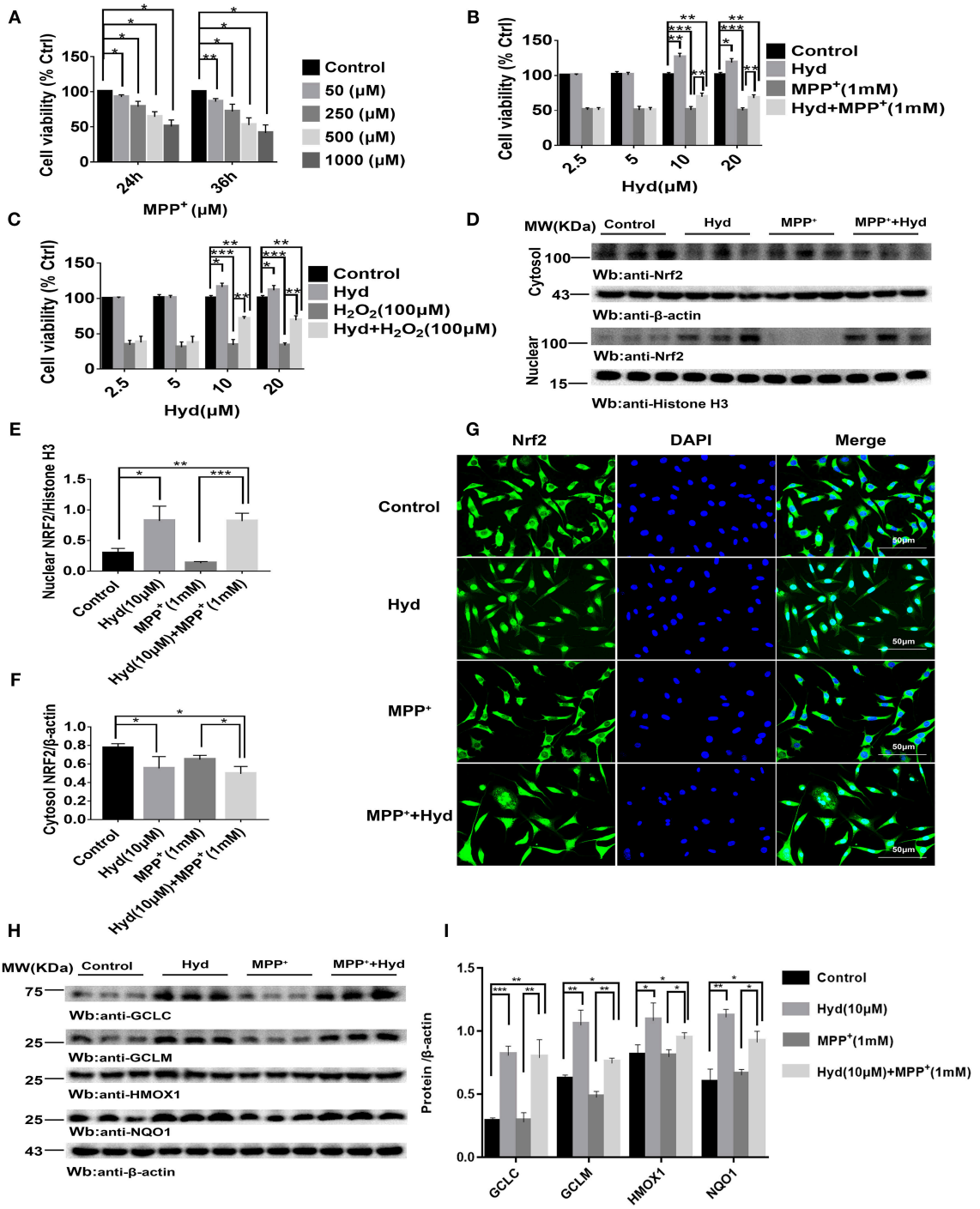

FIGURE 1 | Hydralazine prevents the MPP^+ and H_2O_2-induced cell death in SH-SY5Y cells, and activates Nrf2-ARE signaling in both treated and non-treated MPP^+ cells *in vitro*. SH-SY5Y cells were incubated with various concentrations of MPP^+ for 24, 36 h **(A)**. Cell viability was determined by CCK-8 assay. $^*p < 0.05$, $^{**}p < 0.01$, $n = 6$, compared with the two indicated groups. SH-SY5Y cells were incubated with or without hydralazine (2.5, 5, 10, 20 μM) in the absence or presence of 1 mM MPP^+ for 24 h **(B)**. The viability of cells under MPP^+-mediated cytotoxicity was significantly improved with hydralazine (10 and 20 μM) treatment. $^*p < 0.05$, $^{**}p < 0.01$, $^{***}p < 0.001$, $n = 6$, significant difference between the two indicated groups. SH-SY5Y cells were incubated with or without hydralazine (2.5, 5, 10, 20 μM) in the absence or presence of H_2O_2 (100 μM) for 24 h **(C)**. The viability of cells under H_2O_2 -induced cytotoxicity was significantly improved with hydralazine (10 and 20 μM) treatment. $^*p < 0.05$, $^{**}p < 0.01$, $^{***}p < 0.001$ $n = 6$, significant difference between the two indicated groups. The results of immunofluorescence and western blot analysis indicated Nrf2 translocated to the nucleus with hydralazine treatment when exposured to MPP^+ or not in SH-SY5Y **(D–G)**. Scale bar =500 μm. Treated cells were subjected to cell fractionation and western blot analysis. β-actin or Histonen H3 served as a loading control. $^*p < 0.05$, $^{**}p < 0.01$, $^{***}p < 0.001$, $n = 6$, significant difference between the two indicated groups. Hydralazine induces expression of Nrf2-dependent antioxidant enzymes measured by western blot analysis **(H,I)**. $^*p < 0.05$, $^{**}p < 0.01$, $^{***}p < 0.001$, $n = 6$, significant difference between the two indicated groups. Data were presented as mean ± SEM.

GCLC, GCLM, HMOX1, and NQO1 by western blot analysis. All four protein levels of target genes were significantly increased (**Figures 1H,I**). Collectively, the *in vitro* findings indicate that hydralazine induce nuclear translocation of Nrf2 which activates the ARE genes, thereby conferring protection against MPP^+.

Hydralazine Activate Nrf2-ARE Signaling and Attenuate MPP^+-Mediated Cytotoxicity in an Nrf2-Dependent Pattern

To confirm whether the Nrf2-dependent pathway mediated the neuroprotective effects of hydralazine, the inhibitory effect of hydralazine on MPP^+ neurotoxicity was assessed in SH-SY5Y cells after transfection with either control SiRNA or Nrf2 SiRNA. Results from western blotting and real-time PCR indicated that Nrf2 was successfully knocked-down in SH-SY5Y cells by Nrf2 SiRNA compared to control SiRNA (**Figures 2A–C**). Treatment with hydralazine alone triggered a remarkable increase in the nuclear translocation of Nrf2 (**Figures 2D–F**). However, Nrf2 interference abolished the increase in nuclear Nrf2 caused by hydralazine in SH-SY5Y cells. On the other hand, cytosolic Nrf2 displayed a corresponding decrease relative to the control group transfected with control SiRNA. Furthermore, the hydralazine-induced increase in expression of Nrf2-mediated ARE genes, such as GCLC, GCLM, HMOX1, and NQO1 were inhibited following Nrf2 SiRNA in SH-SY5Y cells based on western blot analysis (**Figures 2G,H**). According to these results, we speculate hydralazine activate Nrf2-ARE signaling in an Nrf2-dependent manner.

Meanwhile, our results indicated that hydralazine treatment increased cell viability, which is opposite to the CCK8 assay results recorded in MPP^+ exposure alone group in SH-SY5Y cells transfected with control SiRNA (**Figure 2I**, $p < 0.01$). However, hydralazine failed to increase cell viability following Nrf2 knockdown and MPP^+ exposure (**Figure 2I**). Nrf2 SiRNA transfection in SH-SY5Y cells increased their vulnerability to MPP^+ neurotoxicity as compared to the control SiRNA transfection group (**Figure 2I**, $p < 0.05$). These data reveal that the protective effect of hydralazine on SH-SY5Y cells exposed to MPP^+ neurotoxicity is dependent on the Nrf2 pathway.

Hydralazine Confers Protection in Dopaminergic Neurons in the MPTP Model of Parkinson's Disease

To explore the therapeutic effect of hydralazine in PD, the MPTP mice model was used. Mice were divided into four groups ($n = 9$ for per group) for this experiment. The first group mice (MPTP group) only received injections of MPTP-HCl (30 mg/kg, i.p., Sigma) in saline for consecutive 7 days, an MPTP model of PD was generated as previously described (32). The second group of mice (Hyd+MPTP group) were administered with hydralazine (51.7 mg/kg per day in saline, Sigma) (33) by oral gavage for 3 weeks before, during, and after MPTP administration. The third group mice (Hyd group) were administered with hydralazine (51.7 mg/kg per day in saline, Sigma) (33) by oral gavage for 3 weeks, and the fourth group mice (Control group) received vehicle only. The pretreatment paradigm in the MPTP-induced PD Model was utilized (**Figure 3A**). We observed that the weight of MPTP-treated mice was much lower compared to normal group due to the neurotoxicity of MPTP. But administration of hydralazine alleviated the loss of weight (**Figure 3B**). Behavior testing of the animals was performed after the last oral gavage (**Figure 3A**). The rotarod test was applied to evaluate motor and coordination abilities. In this test, the decrease in latent time on the rod in the MPTP mice compared to the vehicle treated control mice ($p < 0.001$) was reversed by hydralazine treatment ($p < 0.01$) (**Figure 3C**). Similar results were obtained in Pole test. The time to orient downward (Turn) and to descend (TLA) was increase in the MPTP mice compared to the control mice ($p < 0.05$), indicating a motor deficit, and this effect was reversed by hydralazine ($p < 0.05$) (**Figure 3D**). These results suggested that hydralazine conferred protection in locomotion function.

After the behavioral tests, we tested whether *in vivo* hydralazine can maintain the integrity of dopaminergic neurons in the SNpc and their terminal fibers in striatum. Thus, we performed immunofluorescence staining using dopaminergic neuronal specific marker, anti-TH antibody. MPTP administration caused remarkable loss of dopaminergic neurons in the SNpc (**Figures 3E,F**) and striatal DA terminal fibers (**Figures 3I,J**) when compared to control. Meanwhile, we found that reduction of TH-positive neurons was abolished in the similar anatomic level sections of SN in the MPTP mice treated with hydralazine than MPTP alone (**Figure 3E**). Quantification analysis using the cell counting kit in a double blind way indicated a statistically significant preservation of TH positive dopaminergic SN neurons in the MPTP-treated mice with hydralazine groups compared with MPTP mice (**Figure 3F**, $p < 0.01$). This observation was further confirmed by western blotting assay on SN lysates (**Figure 3G**). The ratio of TH/β-action in the MPTP group was significantly lower than in control group ($p < 0.001$) and MPTP mice with hydralazine groups (**Figure 3H**, $p < 0.05$). Hydralazine-treated mice in the presence of MPTP showed significant reductions in the loss of the TH positive DA terminals in the striatal region when compared to MPTP alone mice (**Figures 3I,J**, $p < 0.01$). Consistent with TH-immunofluorescent in the striatal region, western blotting of the striatum lysates rescued the loss of TH positive DA terminals in the hydralazine-treated mice with MPTP compared to MPTP alone mice (**Figures 3K,L**, $p < 0.001$), Taken together, these findings provide evidence that hydralazine confers protection on nigrostriatal dopaminergic neurons in the subacute model of MPTP neurotoxicity.

Hydralazine Alleviate Oxidative Stress and Activates Nrf2-Triggered Gene Expression *in vivo*

Subsequently, we investigated whether hydralazine activates Nrf2-ARE pathway *in vivo* using mice. Mice were treated as described above to assess the level of MDA, a key product produced from membrane lipid oxidation. Mice treated

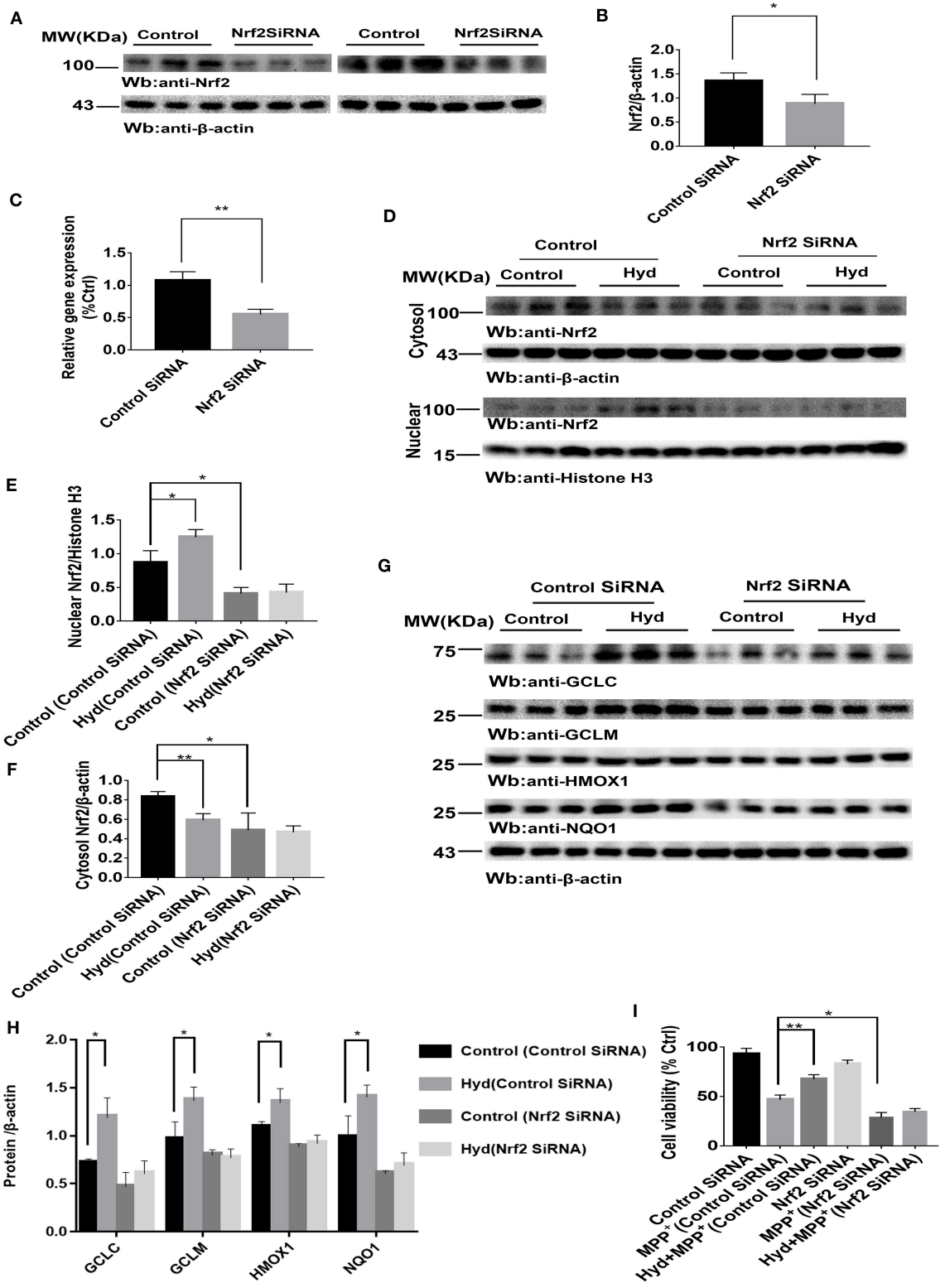

FIGURE 2 | Hydralazine activate Nrf2-ARE signaling and attenuate MPP^+-mediated cytotoxicity in an Nrf2-dependent pattern. SH-SY5Y cells were treated with either an Nrf2 SiRNA or a control SiRNA. The protein and mRNA levels of Nrf2 were measured by western blotting and real-time PCR **(A–C)**. $^*p < 0.05$, $^{**}p < 0.01$, $n = 6$, significant difference between the two indicated groups. Hydralazine treatment alone induced a remarkable increase in the nuclear translocation of Nrf2, however, Nrf2 interference abolished the increase in nuclear Nrf2 induced by hydralazine in SH-SY5Y **(D,E)**, in the meantime, cytosolic Nrf2 had corresponding decrease in contrast

(Continued)

FIGURE 2 | with control group transfected with control SiRNA **(D,F)** by western blot analysis. *$p < 0.05$, **$p < 0.01$, n=6, significant difference between the two indicated groups. Selective activation of Nrf2 mediated gene transcription by hydralazine in SH-SY5Y cells transfected by control SiRNA, but not in SH-SY5Y cells transfected by Nrf2 SiRNA measured by western blotting **(G,H)**. *$p < 0.05$, $n = 6$, significant difference between the two indicated groups. Hydralazine significantly protected SH-SY5Y cells from MPP^+ induced death in an Nrf2-dependent manner measured by CCK-8 assay **(I)**. *$p < 0.05$, **$p < 0.01$, $n = 6$, significant difference between the two indicated groups. Data were presented as mean ± SEM.

with MPTP displayed a remarkably increase in MDA levels which were suppressed by hydralazine treatment in the SNpc (**Figure 4A**) and in striatum (**Figure 4B**). Glutathione (GSH) is an antioxidant which has the capacity to prevent damage to important cellular components. Glutathione disulfide (GSSG) is its oxidized form and the ratio of oxidized glutathione to reduced glutathione is frequently used to evaluate oxidative stress. MPTP decreased GSH levels and increased GSSH levels and these effects were reversed by hydralazine in the SNpc, as supported by the increased ratio of GSH/GSSG (**Figures 4C,D**). It can be inferred that Nrf2-ARE signaling suppressed cellular oxidative stress caused by several factors. These experimental results demonstrate that hydralazine suppresses oxidative stress triggered by MPTP.

We further explored whether this effect was due to regulation of the Nrf2-ARE signaling pathway. **Figures 4E–G**, shows that hydralazine induced a dramatic increase in the nuclear translocation of Nrf2 in the SNpc of hydralazine-treated mice with MPTP, compared with the MPTP mice ($p < 0.001$), corresponding decrease in cytosolic Nrf2 fraction ($p < 0.01$). Moreover, hydralazine treatment alone enhanced the nuclear Nrf2 levels when compared to control (**Figures 4E,F**, $p < 0.01$). The cytosolic Nrf2 fraction decreased slightly compared to nuclear Nrf2 fraction (**Figures 4E,G**). This observation was further confirmed by double immunofluorescence (**Figure 4H**) in the SNpc. Consistent with SNpc, western blotting assay on the striatum lysates showed a statistically significant increase in the Nrf2 nuclear translocation, and a corresponding decrease in cytosolic Nrf2 fraction, in both hydralazine-treated mice with MPTP and hydralazine alone mice when compared to control (**Figures 4I,J**). Based on these results, it was observed that hydralazine activated Nrf2-ARE signaling. Moreover, we observed that Nrf2 colocalized with TH (dopaminergic neuron marker) in the SNpc, but not with ionized calcium binding adapter molecule 1 (IBA1, microglial cell marker) or glial fibrillary acidic protein (GFAP, astrocyte marker) as revealed by double immunofluorescence in the SNpc of hydralazine-treated mice with MPTP. Hydralazine increased the nuclear translocation of Nrf2 in the dopaminergic neuron (**Figure 4L**), which explained why hydralazine protected dopaminergic neurons from MPTP induced neurotoxicity to a certain extent.

In the hydralazine treatment group, western blot assay revealed that Nrf2-ARE targeted genes, NQO1, HMOX1, GCLM, and GCLC, were significantly increased in the SNpc (**Figures 4M,N**) and in striatum (**Figures 4O,P**) after compare with MPTP alone. Additionally, treatment with hydralazine alone increased the expression of above ARE genes compared to control group in both SNpc (**Figures 4M,N**) and striatum (**Figures 4O,P**). Based on the above discussion, the mechanism by which hydralazine activated Nrf2-ARE signaling even in the absence of toxicant was not clear. This should be explored in further studies. In conclusion, these data provide *in vivo* evidence that hydralazine can activate the Nrf2-mediated ARE gene transcription which provides antioxidant effects *in vivo*.

DISCUSSION

Current treatment for PD are primarily designed relief some of the clinical symptoms which hardly translated to improved quality of life in most patients. In addition, there is no known therapy that prevents the pathogenesis and progress of neurodegeneration. Although several studies have been performed to assess the etiology of PD, the associated mechanisms are still not fully understood. Mounting evidence suggests that oxidative stress appears to be involved in the pathogenesis of PD (36). Consequently, we have reasons to believe that increasing the capacity of dopaminergic neurons to confront oxidants could serve as an important strategy to prevent the onset and/or to delay the progression of PD. However, the prevailing knowledge from clinical trials on antioxidants such as ubiquinone, glutathione, N-acetylcysteine, vitamin C, and vitamin E reveals there are conflicting outcomes on their efficacy (22–25). It is likely that oxidants may exert influence by activating death-related pathways rather than directly killing dopaminergic neurons (37), relying only on stoichiometric scavenging of oxidants has proved to be ineffective. The Nrf2 signaling cascade modulates transcriptional expression of oxidative stress to restore redox homeostasis and is a versatile pathway for neurotherapeutics. Several genetic studies have demonstrated that a functional haplotype in the Nrf2 gene promoter, which conferred high transcriptional activity had a protective effect (38), and the deficiency of Nrf2 increased hypersensitivity of the dopaminergic neurons to neurotoxicity caused by MPTP (14, 39, 40) and 6-OHDA (15) in animal models. Moreover, *in vitro* Nrf2 activation also provides neuroprotective effect against the neurotoxins paraquat (41), 6-OHDA (42, 43), and MPP^+ (44). These datasets imply that the Nrf2 pathway may provide neuroprotection which can be exploited to develop drugs that treat PD.

Hydralazine, which was developed by Swiss researchers in the early 1950s (45), was approved drug by FDA for antihypertensive treatment. In this study, we demonstrate that hydralazine displays remarkable neuroprotective effects in a model of PD *in vivo* and *in vitro*. Oral administration of hydralazine decreased MDA levels, increased the ratio of GSH/GSSG, alleviated weight loss and the associated motor deficits, attenuated dopaminergic neurons loss and activated Nrf2 signaling pathways, all of which exerted profound neuroprotective activities in MPTP model of PD (**Figure 3**), and these effects were further confirmed in human

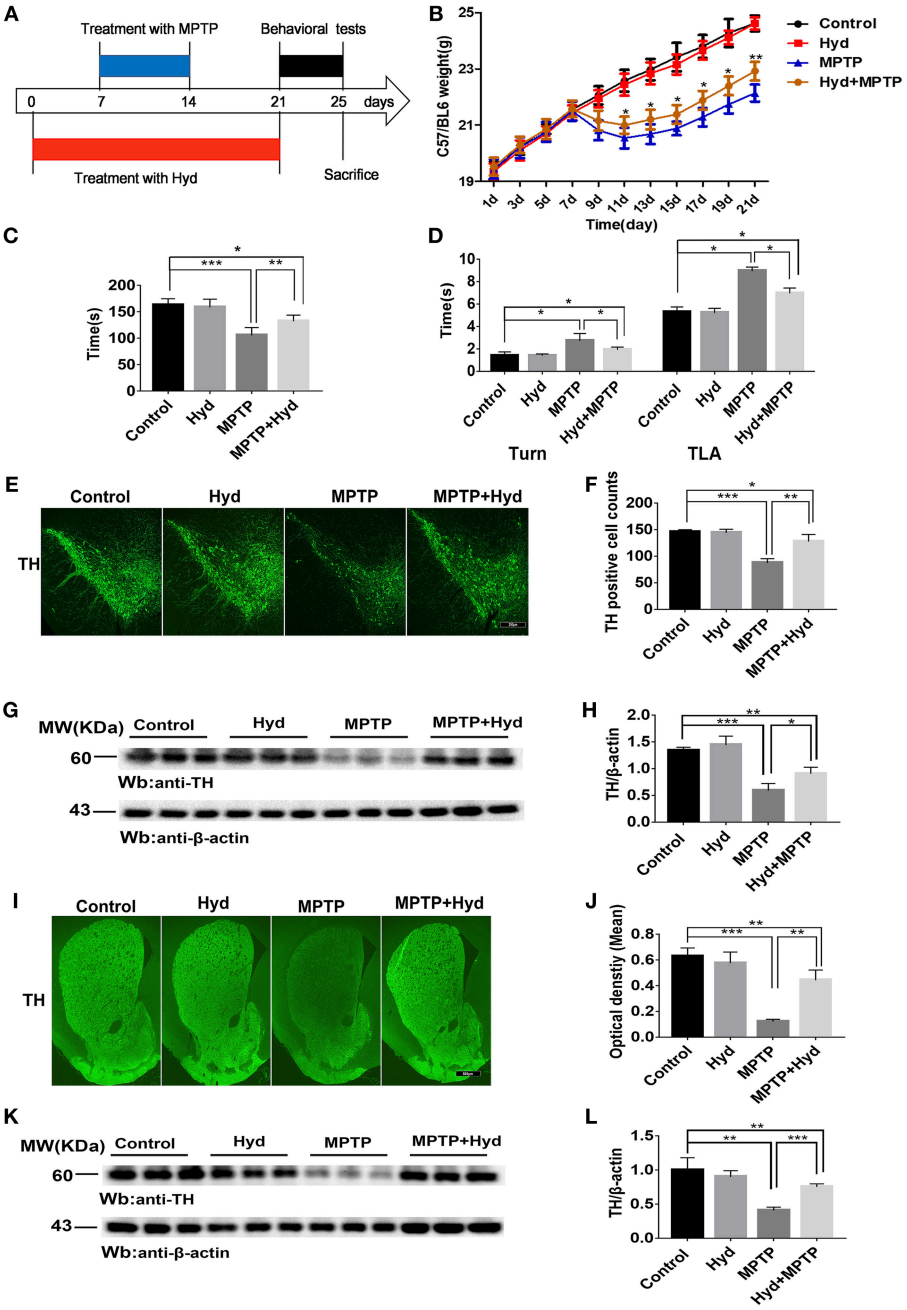

FIGURE 3 | Hydralazine confers protection in dopaminergic neurons in the MPTP model of Parkinson's disease. Schematic representation of the MPTP model experimental design **(A)**. Hydralazine alleviated MPTP-induced weight loss **(B)**. $^{*}p < 0.05$, significant difference between the two indicated groups ($n = 8$). Hydralazine ameliorated MPTP-induced behavior disorder **(C,D)**. Performance on the rotarod and pole test was impaired in MPTP-treated group. However, impairment was ameliorated in MPTP model treated with hydralazine. $^{*}p < 0.05$, $^{**}p < 0.01$, $^{***}p < 0.001$, significant difference between the two indicated groups ($n = 8$). Tyrosine hydroxylase immunofluorescence of substantia nigra pars compacta (SNpc). Scale bar = 250 μm. We found that there were fewer TH positive neurons in the similar anatomic level sections of SN in the MPTP mice than hydralazine- treated mice, MPTP mice with hydralazine and control mice, compared to the MPTP mice group, MPTP mice with hydralazine group significantly attenuated the loss of dopaminergic neurons in SNpc **(E,F)**. $^{*}p < 0.05$, $^{**}p < 0.01$, $^{***}p < 0.001$, $n = 6$, very significant difference between the two indicated groups. The western blotting of TH in SN further reconfirmed the findings (G and H). $^{*}p < 0.05$, $^{***}p < 0.001$ $n = 6$, significant difference between the two indicated groups. The MPTP neurotoxicity also resulted the decrease of the TH positive DA terminals in the striatal region of the MPTP mice group compared with MPTP mice with hydralazine group. **(I,J)**. Scale bar = 500 μm. $^{**}p < 0.01$, $^{***}p < 0.001$, $n = 6$, very significant difference between the two indicated groups. Immunoblotting also validated this observation **(K,L)**. $^{**}p < 0.01$, $^{***}p < 0.001$, $n = 6$, compared with the two indicated groups. Data were presented as mean ± SEM.

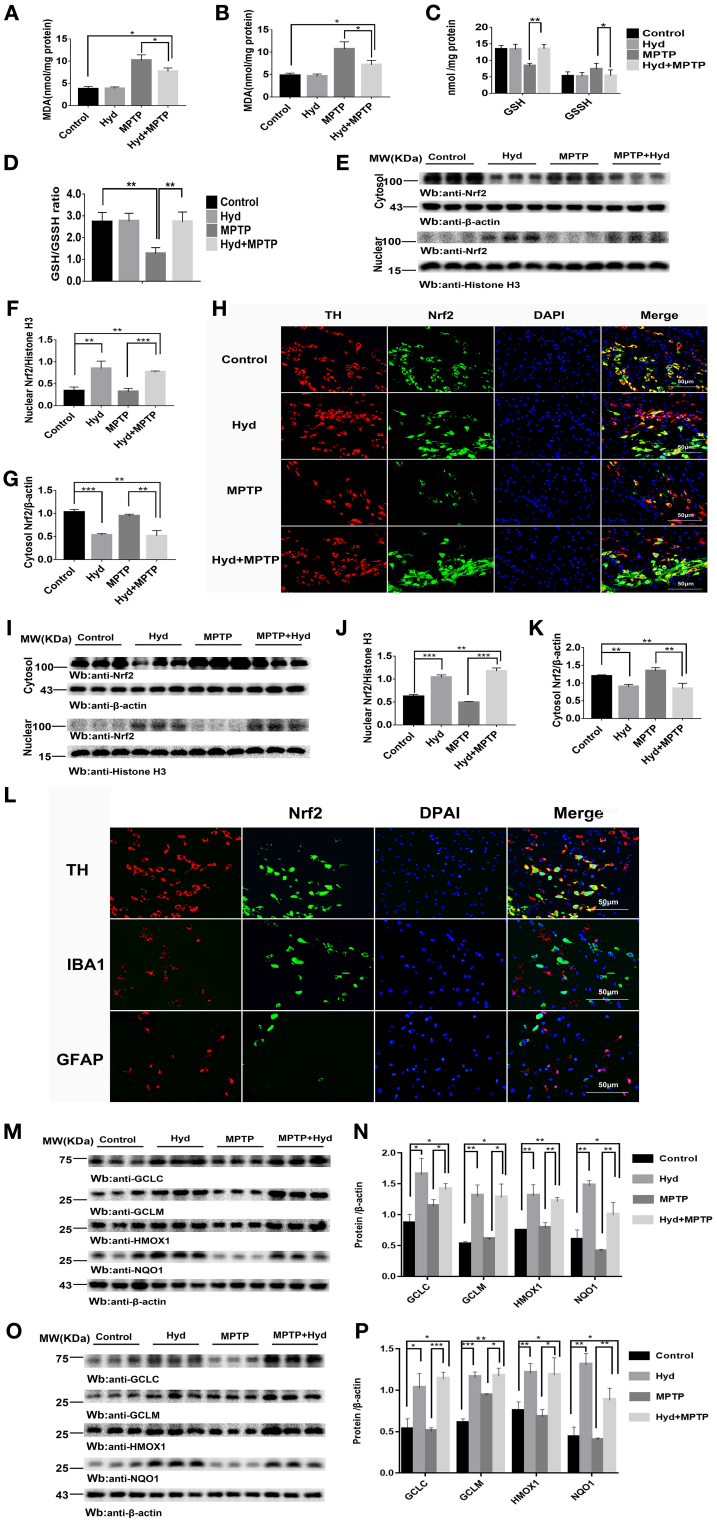

FIGURE 4 | Hydralazine alleviate oxidative stress and activates Nrf2-triggered gene expression *in vivo.* Hydralazine significantly decreased MDA in the substantia nigra (A) and striatum(B) of MPTP mice treated with hydralazine compared with MPTP mice. *$p < 0.05$, $n = 5$, significant difference between the two indicated groups. MPTP administration showed a remarkable decrease in GSH levels and increase in GSSH that was inhibited by hydralazine in the SNpc, corresponding increase in the ratio of GSH/GSSG **(C,D)**. *$p < 0.05$, **$p < 0.01$, $n = 5$, significant difference between the two indicated groups. Hydralazine treatment leads to a shift in Nrf2 migration and increases nuclear Nrf2 Protein levels, in the meantime, cytosolic Nrf2 had corresponding decrease in the substantia nigra **(E–H)** and striatum **(I–K)** of

(Continued)

FIGURE 4 | MPTP-treated mice. $^{**}p < 0.01$, $^{***}p < 0.001$. $n = 6$, significant difference between the two indicated groups. Nrf2 colocalized with TH in the SNpc, not with IBA1, GFAP by double immunofluorescence **(L)** in the SNpc of hydralazine-treated mice with MPTP, hydralazine can increase nuclear translocation of Nrf2 in the dopaminergic neuron **(L)**. Protein levels of Nrf2 were analyzed by Western blot. β-actin and Histonen H3 are used as markers for cytosolic and nuclear fractions, respectively. Hydralazine treatment increased the expression of Nrf2 downstream target in the substantia nigra **(M,N)** and striatum **(O,P)** of MPTP-treated mice. $^{*}p < 0.05$, $^{**}p < 0.01$, $^{***}p < 0.001$, $n = 6$, significant difference between the two indicated groups. Data were presented as mean ± SEM.

neuroblastoma SH-SY5Y cells (**Figure 1**). The cell viability was increased following hydralazine treatment when exposed to MPP^+ or H_2O_2. Among the key Nrf2-regulated genes stimulated by hydralazine were NQO1, HMOX1, GCLM, GCLC. It was reported NQO1 ameliorated the baleful effects of DA quinines, and had various antioxidant properties (46, 47). HMOX1 has been implicated in the metabolism of the pro-oxidant heme to form the antioxidant pigment biliverdin which confers resistance to chronic oxidative stress and apoptosis in dopaminergic neurons (48, 49). GCLC and GCLM regulates the production of cellular antioxidant glutathione (50). These proteins are involved in oxidative stress and redox homeostasis. Nrf2 SiRNA transfection was performed to explore the function of Nrf2 in the protective effect of hydralazine against neurotoxicity MPP^+ induced in SHSY5Y cells. Nrf2 SiRNA2 transfection treatment abolished the hydralazine-induced ARE genes expression and increased the vulnerability to MPP^+ neurotoxicity (**Figure 2**). However, we lacked Nrf2 knockout mice and Nrf2 knockin mutant mice to perform more confirmatory experiments.

A noteworthy phenomenon is that hydralazine treatment alone increased nuclear translocation of Nrf2 and elevated the Nrf2-mediated ARE gene transcription *in vitro* and *in vivo* (**Figures 1**, **2**, **4**). But the mechanism for this effect remains elusive. It is possible that Nrf2 was modified by hydralazine in a way that disrupted the Nrf2:Keap1 interaction, which then allowed it to translocate to the nucleus where it binds the antioxidant response elements (AREs), a consensus gene sequence present in the promoter region of a large number of genes encoding antioxidant enzymes (11). In the future, we will further explore this concept. In addition, we found that hydralazine increased the migration of Nrf2 to the nucleus in dopaminergic neurons, induced the expression of its downstream antioxidative genes, although we did not observe this phenomenon in microglial cells and astrocytes. Collectively, our experimental results demonstrate the ability of hydralazine to modulate key antioxidant genes which are crucial to the survival of SH-SY5Y cells and dopaminergic neurons in PD model.

Hydralazine has been known to act as an antioxidant which eliminates acrolein, an agent that transduces oxidative stress signals (51, 52) and a potent Nrf2 activator (30). Here, we demonstrate that Nrf2 activation is a novel mechanism by which hydralazine exerts protection in PD. However, additional investigations are required to explain how this nucleophilic drug activates the Nrf2 pathway. One possibility is that hydralazine directly disrupts the interaction between Keap-1 and Nrf2 (53). It is also likely that hydralazine activates Nrf2 pathway through other pathways e.g., Notch or AMP kinase pathways, nuclear factor-kappa B (NF-κB), synoviolin, the GSK-3-β-TrCP, and PI3K/Akt pathway (54), which are reported to interact with Nrf2 elements. Another possibility is that the "adduct-trapping" properties of hydralazine which involves the classic electrophile-mediated pathway to increase the degradation of Keap1, thus accelerate Nrf2 liberation (55). Certainly, there is little evidence that hydrazaline crosses the Blood-Brain Barrier, However, this drug has been studied in the Alzheimer's disease mouse model (33). Together with the findings obtained in this study, we speculate that hydrazaline has some degree of permeability through the Blood-Brain Barrier. To improve its clinical application, its oral bioavailability, *in vivo* pharmacokinetic profiles, permeability through Blood-Brain Barrier and the potential side effects need to be explored.

CONCLUSION

This study shows that hydralazine as a potent Nrf2 activator, increases the expression of Nrf2 downstream ARE target genes and confers strong neuroprotection in model of PD both *in vitro* and *vivo* in a Nrf2 -independent manner. These datasets provide novel insights that have high therapeutic value for Parkinson's disease.

ETHICS STATEMENT

All animal procedures were in strict accordance with the National Institutes of Health's Guidelines for Care and were approved by the Animal Care and Use Committees of Huazhong University of Science and Technology (HUST).

AUTHOR CONTRIBUTIONS

XG participated in all aspects of the experimental design, implementation, analysis, and writing including obtaining, analyzing, and interpreting data and making significant contributions to the writing of the manuscript. CH contributed to the experimental design. KM, YX, FW, SY, LK, YS, JW, and JuH contributed to the experimental implementation. JiH and NX contributed to data analysis. The whole experiment was completed under the guidance of TW.

ACKNOWLEDGMENTS

This work was supported by grants 81471305 and 81671260 from the National Natural Science Foundation of China (to TW), and grants 2016YFC1306000 and 2017YFC1310200 from the National Key Plan for Scientific Research and Development of China (to TW).

REFERENCES

1. Bokov A, Chaudhuri A, Richardson A. The role of oxidative damage and stress in aging. *Mech Ageing Dev.* (2004) 125:811–26. doi: 10.1016/j.mad.2004.07.009
2. Dias V, Junn E, Mouradian MM. The role of oxidative stress in Parkinson's disease. *J Parkinsons Dis.* (2013) 3:461–91. doi: 10.3233/JPD-130230
3. Goswami SK, Maulik N, Das DK. Ischemia-reperfusion and cardioprotection: a delicate balance between reactive oxygen species generation and redox homeostasis. *Ann Med.* (2007) 39:275–89. doi: 10.1080/07853890701374677
4. Kaspar JW, Niture SK, Jaiswal AK. Nrf2:INrf2 (Keap1) signaling in oxidative stress. *Free Radic Biol Med.* (2009) 47:1304–9. doi: 10.1016/j.freeradbiomed.2009.07.035
5. Lu SC. Regulation of glutathione synthesis. *Mol Aspects Med.* (2009) 30:42–59. doi: 10.1016/j.mam.2008.05.005
6. Sheehan D, Meade G, Foley VM, Dowd CA. Structure, function and evolution of glutathione transferases: implications for classification of non-mammalian members of an ancient enzyme superfamily. *Biochem J.* (2001) 360:1–16. doi: 10.1042/bj3600001
7. Itoh K, Wakabayashi N, Katoh Y, Ishii T, Igarashi K, Engel JD, et al. Keap1 represses nuclear activation of antioxidant responsive elements by Nrf2 through binding to the amino-terminal Neh2 domain. *Genes Dev.* (1999) 13:76–86. doi: 10.1101/gad.13.1.76
8. Taguchi K, Motohashi H, Yamamoto M. Molecular mechanisms of the Keap1-Nrf2 pathway in stress response and cancer evolution. *Genes Cells.* (2011) 16:123–40. doi: 10.1111/j.1365-2443.2010.01473.x
9. Kensler TW, Wakabayashi N, Biswal S. Cell survival responses to environmental stresses via the Keap1-Nrf2-ARE pathway. *Annu Rev Pharmacol Toxicol.* (2007) 47:89–116. doi: 10.1146/annurev.pharmtox.46.120604.141046
10. Kumar H, Kim IS, More SV, Kim BW, Choi DK. Natural product-derived pharmacological modulators of Nrf2/ARE pathway for chronic diseases. *Nat Prod Rep.* (2013) 31:109–39. doi: 10.1039/C3NP70065H
11. Sykiotis GP, Bohmann D. Stress-activated cap'n'collar transcription factors in aging and human disease. *Sci Signal.* (2011) 3:re3. doi: 10.1126/scisignal.3112re3
12. Cuadrado A, Morenomurciano P, Pedrazachaverri J. The transcription factor Nrf2 as a new therapeutic target in Parkinson's disease, Expert Opinion on Therapeutic Targets, Informa Healthcare. *Expert Opin Ther Targets.* (2009) 13:319–29. doi: 10.1517/13543780802716501
13. Williamson TP, Johnson DA, Johnson JA. Activation of the Nrf2-ARE pathway by siRNA knockdown of Keap1 reduces oxidative stress and provides partial protection from MPTP-mediated neurotoxicity. *Neurotoxicology.* (2012) 33:272–9. doi: 10.1016/j.neuro.2012.01.015
14. Burton N, Kensler TR. *In vivo* modulation of the Parkinsonian phenotype by Nrf2. *Neurotoxicology.* (2006) 27:1094–100. doi: 10.1016/j.neuro.2006.07.019
15. Jakel RJ, Townsend JA, Kraft AD, Johnson JA. Nrf2-mediated protection against 6-hydroxydopamine. *Brain Res.* (2007) 1144:192–201. doi: 10.1016/j.brainres.2007.01.131
16. Rojo AI, Innamorato NG, Martín-Moreno AM, De Ceballos ML, Yamamoto M, Cuadrado A. Nrf2 regulates microglial dynamics and neuroinflammation in experimental Parkinson's disease. *Glia.* (2010) 58:588–98. doi: 10.1002/glia.20947
17. Lee JA, Son HJ, Kim JH, Park KD, Shin N, Kim HR, et al. A novel synthetic isothiocyanate ITC-57 displays antioxidant, anti-inflammatory, and neuroprotective properties in a mouse Parkinson's disease model. *Free Radic Res.* (2016) 50:1188–99. doi: 10.1080/10715762.2016.1223293
18. Lee JA, Kim JH, Woo SY, Son HJ, Han SH, Jang BK, et al. A novel compound VSC2 has anti-inflammatory and antioxidant properties in microglia and in Parkinson's disease animal model. *Br J Pharmacol.* (2015) 172:1087–100. doi: 10.1111/bph.12973
19. Lee JA, Son HJ, Park KD, Han SH, Shin N, Kim JH, et al. A novel compound ITC-3 activates the Nrf2 signaling and provides neuroprotection in Parkinson's disease models. *Neurotox Res.* (2015) 28:1–14. doi: 10.1007/s12640-015-9550-z
20. Skibinski G, Hwang V, Ando DM, Daub A, Lee AK, Ravisankar A, et al. From the cover: Nrf2 mitigates LRRK2- and Î±-synucleinâ"induced neurodegeneration by modulating proteostasis. *Proc Natl Acad Sci USA.* (2017) 114:1165. doi: 10.1073/pnas.1522872114
21. Son HJ, Choi JH, Lee JA, Kim DJ, Shin KJ, Hwang O. Induction of NQO1 and neuroprotection by a novel compound KMS04014 in Parkinson's disease models. *J Mol Neurosci.* (2015) 56:263–72. doi: 10.1007/s12031-015-0516-7
22. Kamat CD, Gadal S, Mhatre M, Williamson KS, Pye QN, Hensley K. Antioxidants in central nervous system diseases: preclinical promise and translational challenges. *J Alzheimers Dis.* (2008) 15:473–93. doi: 10.3233/JAD-2008-15314
23. Shen L, Ji HF. Insights into the disappointing clinical trials of antioxidants in neurodegenerative diseases. *J Alzheimers Dis.* (2010) 19:1141–2. doi: 10.3233/JAD-2010-1307
24. Shults CW, Haas R. Clinical trials of coenzyme Q10 in neurological disorders. *Biofactors.* (2010) 25:117–26. doi: 10.1002/biof.5520250113
25. Storch A, Jost WH, Vieregge P, Spiegel J, Greulich W, Durner J, et al. Randomized, double-blind, placebo-controlled trial on symptomatic effects of coenzyme Q in Parkinson disease. *Arch Neurol.* (2007) 64:938–44. doi: 10.1001/archneur.64.7.nct60005
26. Burcham PC. Potentialities and pitfalls accompanying chemico-pharmacological strategies against endogenous electrophiles and carbonyl stress. *Chem Res Toxicol.* (2008) 21:779–86. doi: 10.1021/tx700399q
27. Hamann K, Nehrt G, Ouyang H, Duerstock B, Shi R. Hydralazine inhibits compression and acrolein-mediated injuries in *ex vivo* spinal cord. *J Neurochem.* (2010) 104:708–18. doi: 10.1111/j.1471-4159.2007.05002.x
28. Hamann K, Durkes A, Ouyang H, Pond A, Shi R. Critical role of acrolein in secondary injury following *ex vivo* spinal cord trauma. *J Neurochem.* (2010) 107:712–21. doi: 10.1111/j.1471-4159.2008.05622.x
29. Liusnyder P, Borgens RB, Shi R. Hydralazine rescues PC12 cells from acrolein-mediated death. *J Neurosci. Res.* (2010) 84:219–27. doi: 10.1002/jnr.20862
30. Dehghan E, Zhang Y, Saremi B, Yadavali S, Hakimi A, Dehghani M, et al. Hydralazine induces stress resistance and extends C. elegans lifespan by activating the NRF2/SKN-1 signalling pathway. *Nat Commun.* (2017) 8:2223. doi: 10.1038/s41467-017-02394-3
31. Maheshwari M, Roberts JK, Desutter B, Duong K, Tingling J, Fawver JN, et al. Hydralazine modifies Aβ fibril formation and prevents modification by lipids *in vitro*. *Biochemistry.* (2010) 49:10371. doi: 10.1021/bi101249p
32. Jacksonlewis V, Przedborski S. Protocol for the MPTP mouse model of Parkinson's disease. *Nat Protoc.* (2007) 2:141–51. doi: 10.1038/nprot.2006.342
33. Wang J, Zhao Z, Lin E, Zhao W, Qian X, Freire D, et al. Unintended effects of cardiovascular drugs on the pathogenesis of Alzheimer's disease. *PLoS ONE.* (2013) 8:e65232. doi: 10.1371/journal.pone.0065232
34. Yang L, Calingasan NY, Thomas B, Chaturvedi RK, Kiaei M, Wille EJ, et al. Neuroprotective effects of the triterpenoid, CDDO methyl amide, a potent inducer of Nrf2-mediated transcription. *PLoS ONE.* (2009) 4:e5757. doi: 10.1371/journal.pone.0005757
35. Burcham PC. Carbonyl scavengers as pharmacotherapies in degenerative disease: hydralazine repurposing and challenges in clinical translation. *Biochem Pharmacol.* (2018) 154:397–406. doi: 10.1016/j.bcp.2018.06.006
36. Jenner P. Oxidative stress in Parkinson's disease. *Ann Neurol.* (2003) 53 (Suppl. 3):S26. doi: 10.1002/ana.10483
37. Zhou C, Huang Y, Przedborski S. Oxidative stress in Parkinson's Disease: a mechanism of pathogenic and therapeutic significance. *Ann N Y Acad Sci.* (2008) 1147:93–104. doi: 10.1196/annals.1427.023
38. Otter MV, Landgren S, Nilsson S, Celojevic D, Bergström P, Håkansson A, et al. Association of Nrf2-encoding NFE2L2 haplotypes with Parkinson's disease. *BMC Med Genet.* (2010) 11:36. doi: 10.1186/1471-2350-11-36
39. Chen PC, Vargas MR, Pani AK, Smeyne RJ, Johnson DA, Kan YW, et al. Nrf2-mediated neuroprotection in the MPTP mouse model of Parkinson's disease: Critical role for the astrocyte. *Proc Natl Acad Sci USA.* (2009) 106:2933–8. doi: 10.1073/pnas.0813361106
40. Kaidery NA, Banerjee R, Yang L, Smirnova NA, Hushpulian DM, Liby KT, et al. Targeting Nrf2-Mediated gene transcription by extremely potent synthetic triterpenoids attenuate dopaminergic neurotoxicity in the MPTP mouse model of Parkinson's disease. *Antioxid Redox Signal.* (2013) 18:139–57. doi: 10.1089/ars.2011.4491
41. Nisosantano M, Gonzálezpolo RA, BravoSan Pedro JM, Gómezsánchez R, Lastresbecker I, Ortizortiz MA, et al. Activation of apoptosis signal-regulating kinase 1 is a key factor in paraquat-induced cell death: modulation by the Nrf2/Trx axis. *Free Radic Biol Med.* (2010) 48:1370–81. doi: 10.1016/j.freeradbiomed.2010.02.024

42. Hara H, Ohta M, Adachi T. Apomorphine protects against 6-hydroxydopamine-induced neuronal cell death through activation of the Nrf2-ARE pathway. *J Neurosci Res.* (2010) 84:860–6. doi: 10.1002/jnr.20974
43. Hwang YP, Jeong HG. The coffee diterpene kahweol induces heme oxygenase-1 via the PI3K and p38/Nrf2 pathway to protect human dopaminergic neurons from 6-hydroxydopamine-derived oxidative stress. *Febs Lett.* (2008) 582:2655–62. doi: 10.1016/j.febslet.2008.06.045
44. Wruck CJ, Claussen M, Fuhrmann G, Römer L, Schulz A, Pufe T, et al. Luteolin protects rat PC 12 and C6 cells against MPP+ induced toxicity via an ERK dependent Keapl-Nrf2-ARE pathway. *J Neural Transm Suppl.* (2007) 72:57–67. doi: 10.1007/978-3-211-73574-9_9
45. Sneader W. *Drug Discovery: A History*. Chichester: John Wiley & Sons Ltd. (2005). doi: 10.1002/0470015535
46. Kapinya KJ, Harms U, Harms C, Blei K, Katchanov J, Dirnagl U, et al. Role of NAD(P)H:quinone oxidoreductase in the progression of neuronal cell death *in vitro* and following cerebral ischaemia *in vivo*. *J Neurochem.* (2010) 84:1028–39. doi: 10.1046/j.1471-4159.2003.01601.x
47. Van FM, Kuiperij HB. The Nrf2-ARE Signalling pathway: promising drug target to combat oxidative stress in neurodegenerative disorders. *Curr Drug Targets CNS Neurol Disord.* (2005) 4:267–81. doi: 10.2174/1568007054038238
48. Ferris CD, Jaffrey SR, Sawa A, Takahashi M, Brady SD, Barrow RK, et al. Haem oxygenase-1 prevents cell death by regulating cellular iron. *Nat Cell Biol.* (1999) 1:152–7. doi: 10.1038/11072
49. Otterbein LE, Soares MP, Yamashita K, Bach FH. Heme oxygenase-1: unleashing the protective properties of heme. *Trends Immunol.* (2003) 24:449–55. doi: 10.1016/S1471-4906(03)00181-9
50. Franklin CC, Backos DS, Mohar I, White CC, Forman HJ, Kavanagh TJ. Structure, function, and post-translational regulation of the catalytic and modifier subunits of glutamate cysteine ligase. *Mol Aspects Med.* (2009) 30:86–98. doi: 10.1016/j.mam.2008.08.009
51. Hamann K, Shi R. Acrolein scavenging: a potential novel mechanism of attenuating oxidative stress following spinal cord injury. *J Neurochem.* (2010) 111:1348–56. doi: 10.1111/j.1471-4159.2009.06395.x
52. Luo J, Shi R. Acrolein induces oxidative stress in brain mitochondria. *Neurochem Int.* (2005) 46:243–52. doi: 10.1016/j.neuint.2004.09.001
53. Marcotte D, Zeng W, Hus JC, Mckenzie A, Hession C, Jin P, et al. Small molecules inhibit the interaction of Nrf2 and the Keap1 Kelch domain through a non-covalent mechanism. *Bioorg Med Chem.* (2013) 21:4011–9. doi: 10.1016/j.bmc.2013.04.019
54. O'Connell MA, Hayes JD. The Keap1/Nrf2 pathway in health and disease: from the bench to the clinic. *Biochem Soc Trans.* (2015) 43:687–9. doi: 10.1042/BST20150069
55. Ma Q. Role of Nrf2 in oxidative stress and toxicity. *Annu Rev Pharmacol Toxicol.* (2013) 53:401–26. doi: 10.1146/annurev-pharmtox-011112-140320

Conflict of Interest Statement: The authors declare that the research was conducted in the absence of any commercial or financial relationships that could be construed as a potential conflict of interest.

frontiers in Aging Neuroscience

CLINICAL STUDY PROTOCOL
published: 05 April 2019
doi: 10.3389/fnagi.2019.00077

Voluntary Saccade Training Protocol in Persons With Parkinson's Disease and Healthy Adults

*Paul B. Camacho[1], Ronald Carbonari[2], Sa Shen[3], Cindy Zadikoff[4], Arthur F. Kramer[2,5] and Citlali López-Ortiz[1,2,3,6]**

[1] Department of Kinesiology and Community Health, University of Illinois at Urbana–Champaign, Urbana, IL, United States, [2] Beckman Institute for Advanced Science and Technology, University of Illinois at Urbana–Champaign, Champaign, IL, United States, [3] Center on Health, Aging and Disability, University of Illinois at Urbana–Champaign, Champaign, IL, United States, [4] Department of Neurology, Northwestern University Feinberg School of Medicine, Chicago, IL, United States, [5] Center for Cognitive and Brain Health, Department of Psychology, Northeastern University, Boston, MA, United States, [6] Joffrey Ballet Academy, The Official School of the Joffrey Ballet, Chicago, IL, United States

Background: Voluntary saccade function gradually decreases during both the progression of Parkinson's disease (PD) and neurologically healthy adult aging. Voluntary saccades display decreased length and increased saccade latency, duration, and the number of compensatory saccades in aging and PD. Saccades serve as the key eye movement for maintaining salient features of the visual environment on the high visual acuity fovea of the retina. Abnormal saccade behavior has been associated with freezing of gait in PD. We have not identified any studies that have investigated improvement in voluntary saccade function using voluntary saccade training.

Objective: We report an experimental protocol that tests a training paradigm following the principle of specificity to improve voluntary saccade velocity and amplitude, while decreasing latency and the number of compensatory saccades.

Methods: Persons with PD (n = 22) and persons with no known neurological disorders (n = 22) between the ages of 40 and 65 years will be recruited. In a randomized-block study design, all participants will perform voluntary saccades to targets in eight cardinal and intercardinal directions. In each of the eight sessions during the four-week intervention period, participants will train at three target amplitudes. Participants will perform 40 trials for each amplitude block, consisting of five randomly presented repetitions for each direction. Voluntary and reflexive saccades will be recorded pre- and post-intervention, along with clinical mobility assessment using the Movement Disorder Society Unified Parkinson's Disease Rating Scale. Mobility scores, the amplitude, latency, and duration of the first saccade, and the number of saccades to reach the fixation target will be analyzed using an ANOVA of mixed effects.

Discussion: This protocol holds promise as a potential method to improve voluntary saccade function in persons with PD. Should persons with PD not improve on any outcome following the intervention, this lack of response may support the use of saccade assessment as a response biomarker for the diagnosis of PD.

OPEN ACCESS

Edited by:
Daniel Ortuño-Sahagún, Universidad de Guadalajara, Mexico

Reviewed by:
Yasuo Terao, Kyorin University, Japan
José M. Delgado-García, Universidad Pablo de Olavide, Spain

***Correspondence:**
Citlali López-Ortiz
lopezort@illinois.edu

Received: *05 December 2018*
Accepted: *19 March 2019*
Published: *05 April 2019*

Citation:
Camacho PB, Carbonari R, Shen S, Zadikoff C, Kramer AF and López-Ortiz C (2019) Voluntary Saccade Training Protocol in Persons With Parkinson's Disease and Healthy Adults. Front. Aging Neurosci. 11:77. doi: 10.3389/fnagi.2019.00077

Trial Registration: This protocol was retrospectively registered at ISRCTN (ISRCTN.com) since July 25, 2018. The first participant was recruited March 12, 2016. The protocol identifier is 17784042.

Descriptive Title: A two-arm, pre/post-protocol to compare the effects of a four-week voluntary saccade training intervention in persons with Parkinson's disease and healthy adults aged forty years or older.

Keywords: eye movements, saccades, Parkinson's disease, training, voluntary saccades, healthy adults, saccade latency, saccade amplitude

INTRODUCTION

Voluntary Saccade Function Impairment in Parkinson's and Healthy Aging Adults

Visual function is a major area of decline in Parkinson's disease (PD) progression and healthy aging adults (Terao et al., 2011; Dowiasch et al., 2015). One element of visual function that has been correlated with PD progression and neurologically healthy aging by a number of studies is saccade behavior (Terao et al., 2011; Dowiasch et al., 2015; Seferlis et al., 2015; Noiret et al., 2017). Saccades are the ballistic eye movements that allow the high acuity fovea of the retina to quickly orient toward salient elements of the visual environment. Persons with PD exhibit lower saccade amplitude, higher saccadic latencies, and longer durations to achieve targets (Mosimann et al., 2005; Terao et al., 2011). Deficits in voluntary saccade control contribute to mobility impairments related to turning during navigation (Ambati et al., 2016; Nemanich and Earhart, 2016). It has been noted that turning during navigation in persons with PD increases instability and risk of falling (Stack and Ashburn, 1999). Voluntary saccade function deficits are also present to a lesser extent in neurologically healthy aging adults (Chen and Machado, 2016; Fernandez-Ruiz et al., 2017).

Existing Treatments

Various treatments, including electrical brain stimulation, have been suggested for improving voluntary saccade function in PD (Chen and Machado, 2016). An eye-movement training protocol consisting of horizontal saccades to increasingly distant points and cognitively more challenging targets, such as letters and words, was shown to increase reading speed in older adults with age-related macular degeneration (Seiple et al., 2005). Other treatments include the anti-saccade paradigm, which requires the suppression of a saccade to a stimulus and voluntary saccade to a location of equal eccentricity in the opposite direction (Jamadar et al., 2015). However, such studies focus on accuracy and error rate and do not address hypometria as is needed for navigation (Jamadar et al., 2015; Ambati et al., 2016).

Need for a Trial

Recent work has investigated the difference between smooth-pursuit performance in persons with PD and persons with no known neurological disorders (Ito et al., 2013; Fukushima et al., 2015). However, the current literature does not include voluntary saccade practice as a method of comparing potential improvements in voluntary saccade function for persons with PD and healthy aging adults. While we cannot predict if there will be immediate short- or long-term benefits to the participants in the study, exercising eye movements can potentially benefit eye movement control. As with any other movement training, exercise increases circulation to the muscles and improves their physiological function. Physical mobility is of the utmost importance for the quality of life in the general population. Furthermore, recent PD literature indicates that abnormal saccade behavior is associated with the freezing of gait and difficulty in navigation (Lohnes and Earhart, 2011; Ambati et al., 2016; Nemanich and Earhart, 2016; Stuart et al., 2017). Improving abnormal saccade behavior may affect freezing of gait and other motor-related PD symptoms. Improving these outcomes for persons with PD has the potential to improve the same daily activities as those in healthy aging persons, as well as increasing walking ability (Lohnes and Earhart, 2011; Stuart et al., 2017). Further, saccade function has been demonstrated as a key factor in the slowing of reading, decrease in driving abilities, and eye-hand coordination in several studies (Schmitt et al., 2015; Coats et al., 2016).

Saccade Biomarker Potential

Identifying non-invasive biomarkers of PD onset is imperative for disease treatment. Saccadic abnormalities have been suggested as a diagnostic tool for PD, including early stage progression marking and differential diagnosis from other tremor disorders such as essential tremor (Yerram et al., 2013). Saccade abnormalities may also be useful as markers for frontal cortex and basal ganglia malfunction and degeneration in PD, as well as changes in the cerebellum (Terao et al., 2013). van Stockum et al. (2012) later suggested that due to the differences in reports of saccadic latency deficiencies and facilitation, the hypometria seen across different saccadic paradigms may be a better measure for the effect of PD on saccades. Control of voluntary saccades has also been highlighted as a promising area of motor control in general (Baird-Gunning and Lueck, 2018). Diagnosis in the early stages will benefit individuals with PD, enabling prompt disease treatment and management to slow disease progression. In addition to the person diagnosed with PD, this also benefits their immediate family and support network.

One criticism against saccade measurements as a diagnostic tool for PD is that the abnormalities seen in saccadic movements tend to differ based on the experimental context (MacAskill and Anderson, 2016). Abnormalities in saccade latency and

amplitude are known to occur in multiple neurodegenerative disorders, which could lessen biomarker specificity (MacAskill and Anderson, 2016). However, recent reviews outlined differential characteristics of saccadic performance in PD and several other neurodegenerative diseases (Termsarasab et al., 2015; MacAskill and Anderson, 2016). Additionally, research into the characteristic relationship between saccade duration, peak velocity, and amplitude has not been extensively undertaken in PD. This "main sequence" is believed to characteristically optimize the costs of speed and saccadic accuracy at a given amplitude (Bahill et al., 1975; Harris and Wolpert, 2006). If the main sequence relationship is affected by training differences in persons with PD compared to neurologically healthy persons, the biomarker potential for voluntary saccade training response would be further supported. One benefit of saccadic measurements as a PD biomarker is that assessments of eye tracking systems are non-invasive, unlike biochemical markers, which require blood or CSF extraction. Additionally, saccade testing could occur in a clinical setting without the need for physician supervision and biochemical testing facilities, with the most common side effect being possible fatigue from eye movement.

Risks/Benefits Comparison

Risks associated with eye training include the possibility of eye strain and orbital myositis, which is a rare autoimmune disorder that may result from inflammation due to vigorous exercise. These risks are minimal and reduced by the progressive periodization of amplitudes in the training regimen. The potential benefits of improved eye coordination, range of motion, and responsivity to visual stimuli outweigh the minimal risk for eye strain/injury. The greatest amount of risk in the study is associated with performing OFF-state assessments in participants with PD. The OFF-state occurs when the motor effects of levodopa and other dopaminergic medications are not present due to delayed intake of these medications. During the OFF-state, intensified motor symptoms that may be uncomfortable – such as dyskinesia, rigidity, spasticity, bradykinesia, dystonia, and freezing – may be present. However, discomfort and possible risk of falls are mitigated by limiting the inclusion criteria to only include individuals in the early stage of the disease (H&Y score 1–2; see **Table 1** for criteria) where these symptoms are not severe in general or in the OFF-state. Neurologist clearance – as well as facilitation of dialogue between participant and neurologist, participant and researchers, and researchers and neurologists – will provide an informed environment for how to manage the two-hour disruption in medication. Further, risks of discomfort and falling will be minimized through the use of wheel chairs, gait belts, and secure seating during the eye-tracking assessment.

It is common practice to perform assessments in the OFF-state in the field of PD clinical research because the methodology provides a controlled environment for assessing the disease without the influence of movement-modifying medications that mask the disease condition. This is especially important in biomarker research of PD patients. Assessment in the OFF-state condition increases relevance and generalizability of the study evidence to populations with undiagnosed and untreated PD. Generalizability of results may lead to greater instances of early detection and allow for informed diagnoses of individuals not yet receiving movement-modifying medications. The increased applicability of data collected in OFF-state assessments far outweighs the risks.

TABLE 1 | Criteria for Hoehn & Yahr stages one and two.

H&Y: Stage One	H&Y: Stage Two
1. Signs and symptoms on one side only	1. Symptoms are bilateral
2. Symptoms are mild	2. Minimal disability
3. Symptoms are inconvenient but not disabling	3. Posture and gait affected
4. Usually presents with tremor of one limb	
5. Friends have noticed changes in posture, locomotion, and facial expression	

Saccade Training Time Selection

Due to the current lack of literature studying voluntary saccade training through practice, the training dose of 30 min, twice per week, for four weeks was chosen based on training doses seen in other eye training protocols (Fischer and Hartnegg, 2000; Bibi and Edelman, 2009; Jamadar et al., 2015; Knox and Wolohan, 2015; Kleiser et al., 2017; Johannesson et al., 2018). The limit of 30 min of practice per day was chosen to reduce the likelihood of eye strain.

Explanation for Choice of Comparators

There will be no comparator intervention used in this study. The effects of the voluntary saccade training intervention in persons with PD will be compared to those in persons with no known neurological disorders so that we can determine whether the group with PD is more responsive to the intervention. A greater response in the participants with PD would indicate a significant improvement in saccade performance. A lack of response to the intervention would indicate a resistance to improvement in saccade performance that may be characteristic of persons with PD.

Objectives

Research Hypothesis

We hypothesize that before and after comparisons of voluntary and reflexive saccade performance will show a greater decrease in latency and the number of saccades needed to reach the target, along with a greater increase in saccade amplitude and velocity in Parkinson's disease participants as compared to participants with no known neurological disorders.

Study Objectives

Primary objective

To determine whether voluntary saccade training decreases voluntary latency, reflexive latency, and number of saccades needed to reach a target amplitude and increases saccade amplitude in persons with PD compared to persons with no known neurological disorders.

Secondary objectives

To determine whether training voluntary saccades affects motor disability in persons with PD. We will also investigate whether training voluntary saccades affects the relationship of the main sequence. Should statistical analysis reveal that these improvements are absent in participants with PD, we propose that saccade performance would be a potential early PD biomarker.

Trial Design

This trial is designed as a two-arm, pre-post, single center pilot trial with an equal number of participants with PD and participants with no known neurological disorders (control), which will be analyzed using an analysis of variance (ANOVA) with mixed effects.

METHODS: PARTICIPANTS, INTERVENTIONS, AND OUTCOMES

Study Setting

All data collection and participant training will be conducted in the Neuroscience of Dance in Health and Disability (NDHD) Laboratory at the University of Illinois at Urbana–Champaign. Access to the laboratory space is limited to the research team and participants, with a partitioned area for saccade training and eye tracking data collection. This protocol has been approved by the local IRB and all NDHD laboratory staff have completed the ethics and best practices training required by the local IRB and the University of Illinois. Due to the small size of this study, Champaign County, Illinois will be sufficient for the recruitment of both study groups. The adult population of Champaign County is approximately 170000 persons and is largely rural. We will attempt to representatively recruit participants according to the ethnicity data provided by the US Census Bureau: 72.4% White, 13.4% Black or African American, 0.4% Native American, 10.9% Asian, 0.1% Native Hawaiian and other Pacific Islander, 2.8% two or more races, and 6.0% Hispanic or Latino[1].

Eligibility Criteria

A final decision on inclusion will be made in consultation with the principal investigator once all screening materials are complete (see **Figure 2** for a full timeline). During the initial contact interview, the research assistants will read a script describing the study and assessment procedures; if interested, they will be provided via email with the physician release form to be completed by the participant and physician along with the consent form for the participant's review. Once all questions from the participant regarding the study procedures have been answered by the research team, the consent form is completed, and the physician release form is received via U.S. mail, email, or by hand and reviewed by the principal investigator, a determination will be made whether to proceed with screening using the MoCA and Modified Hoehn & Yahr levels. Only if all inclusion criteria are met, the participant will continue with the study (see **Table 2** for eligibility criteria). Research shows that the prevalence of PD in men is 1.5 times greater than in women. Therefore, we expect that ratio will be reflected in our recruitment.

TABLE 2 | Eligibility criteria for protocol.

Inclusion Criteria

1. To be medically stable with diagnosis of PD by meeting the United Kingdom PD Society Brain Bank Criteria OR- no known neuromuscular disorders for the for the control group.
2. To have a Modified Hoehn & Yahr stage 1–2 (with unilateral involvement only, unilateral and axial involvement, and bilateral involvement without impairment of balance) in the conventionally defined OFF medication state.
3. To have medical clearance form from their physician for participation in the study.
4. To be in a stable regimen of PD medication 30 days prior to the initiation of the study and until the completion of the study.
5. To be willing and able to provide informed consent.
6. To be of age 40 and up.
7. Must have a caregiver/family member present for OFF-state assessment sessions.

Exclusion Criteria

1. Presence of dementia based on The Montreal Cognitive Assessment (MOCA) – score of less than 25.
2. Diagnosis of comorbid neurological disorder such as epilepsy.
3. History of neurological injury such as stroke.
4. History of brain surgery such as deep brain stimulation.
5. Concurrent severe medical illness which in the opinion of the research team will preclude participation in the study (such illnesses may include but not limited to severe or uncontrolled cardiovascular disease, hypertension, pulmonary disease, or diabetes).
6. Inability to attend and participate in at least seven of the training sessions.
7. Uncorrected vision, history of retinal disease (e.g., macular degeneration), presence of optic neuropathy due to glaucoma or ischemic optic neuropathy, pseudoexfoliation syndrome, ocular surgery, ocular trauma, visually significant cataract, orbital myositis, blindness or refractive errors outside –5 to +3 D.
8. Indication by the participant s neurologist in the medical release form that testing the participant in the OFF-medication state would put PD participants at significant risk for medical complications.

Voluntary Saccade Training Intervention

Equipment

Training and testing will be performed using the SR EyeLink II eye tracking system (SR Research). The EyeLink II system for assessments and training has two cameras on a head mount located directly below eye level. The pupil is tracked by a device that captures infrared light reflected off the lens and cornea of the eyes. The lens, cornea, and other parts of the eye absorb a small amount of energy from infrared light, but the energy is less than 18% of the Maximum Permissible Exposure level as certified by the American Standards Institute (ANSI Z 136.1-1973). The EyeLink II system will be mounted to the participant's head using the adjustable straps, such that the head camera bar will be parallel to the display screen, on which four infrared emitters will be placed in a rectangle. The participant will be then positioned, using a chin rest support, so that the participant's resting focus point will be at the center fixation target display on the screen in the middle of the rectangle of emitters. The experimenter will position the eye tracker on the participant's head so that

[1]https://www.census.gov/quickfacts/fact/table/champaigncountyillinois,US/PST120217

the participant can see targets displayed at the amplitude of interest. The chin rest also serves to isolate eye-movements from head movements during eye tracking and maintain a set distance from the display screen. A Sharp Aquos 178.5 cm by 100 cm television will be used as the display for the participant (Sharp Corporation, Sakai-ku, Sakai, Japan). This screen mirrors the computer display visible to the experimenter during training and testing sessions. A second host computer runs the SR Research data capture and processing during sessions. The host computer also displays pupil position and the view of the left and right eye cameras in real time. After adjusting the eye cameras and pupil threshold to track the pupils moving in the eight cardinal and intercardinal directions, the cameras will be then calibrated using the SR Research program. The experimenter will then perform a validation of the camera calibration prior to beginning a training or testing block.

Training

Over the course of the four-week intervention period, participants will undergo eight training sessions of 30 min each. During each training session, three target amplitudes will be trained on the six target amplitudes: 10°, 20°, 30°, 40°, 45°, and 50°. Each amplitude will be trained in two different training sessions over the course of the intervention period. This follows an intercalated training schedule of progressive and regressing load design (see **Table 3**). For each amplitude, the participants perform saccades to each of the eight cardinal and intercardinal directions. Each direction will be indicated five times for a total of 40 trials per amplitude per session. Participants will place their head on a chin rest 40 cm away from the screen in order to isolate the movement of the eyes. Training will involve a visual display designed to initiate only voluntary saccades. Training will begin with a warm-up for the eyes in order to reduce the possibility of injury. Participants will foveate on a central fixation starting point and wait for an instructional arrow that points to one of eight visual targets arranged in eight cardinal points in the perimeter of a circle.

Every trial consists of a fixation period, target circle presentation period, direction indication period, and resetting period (see **Figure 1**). During the fixation period the participant is instructed to focus on the center of a circular fixation bulls-eye target. Next, in the target circle presentation period, a circle of targets in each of the eight directions is presented around the central fixation target. The central fixation target is then replaced by an arrow indicating which direction to look in and fixate on the target there located. After the fixation is recorded at the indicated target, the resetting period follows with the

TABLE 3 | Training schedule of amplitudes. On both sessions of each week, the same three amplitudes will be trained.

Week	Amplitudes Trained
1	10°, 20°, 30°
2	10°, 20°, 40°
3	20°, 30°, 45°
4	20°, 40°, 50°

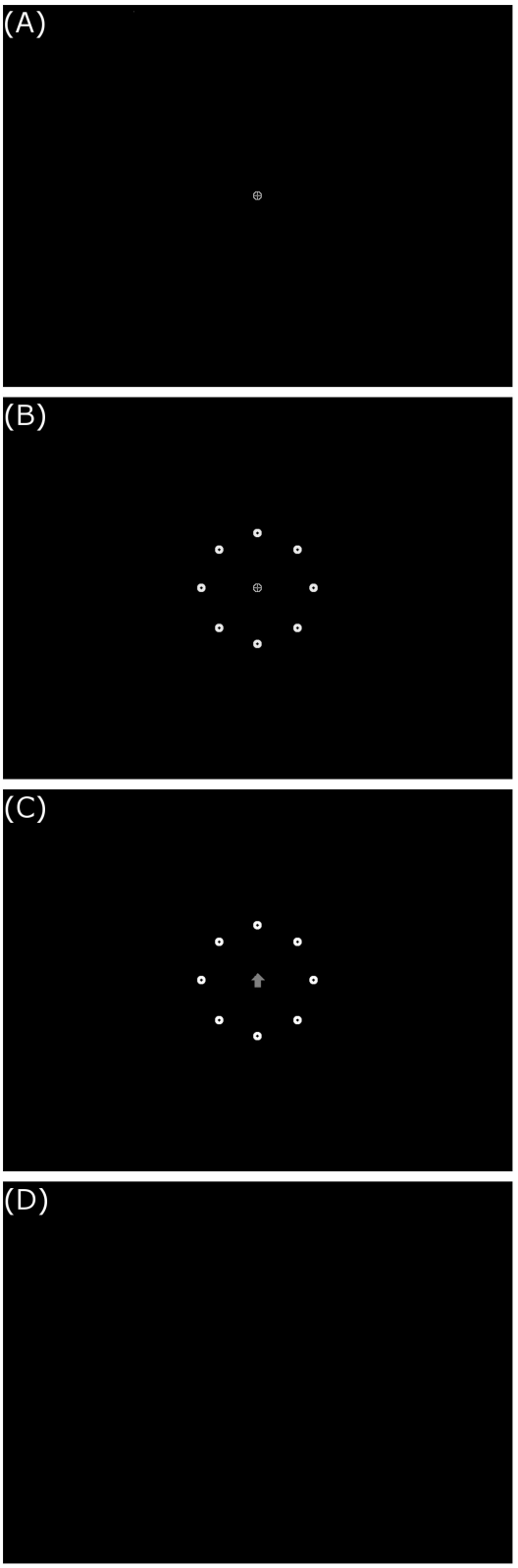

FIGURE 1 | Example training/testing trial display sequence. **(A)** Central fixation target, **(B)** 20° target circle, **(C)** northern direction indication arrow, and (D) blank reset screen. All images presented in 800 × 600 resolution on screen.

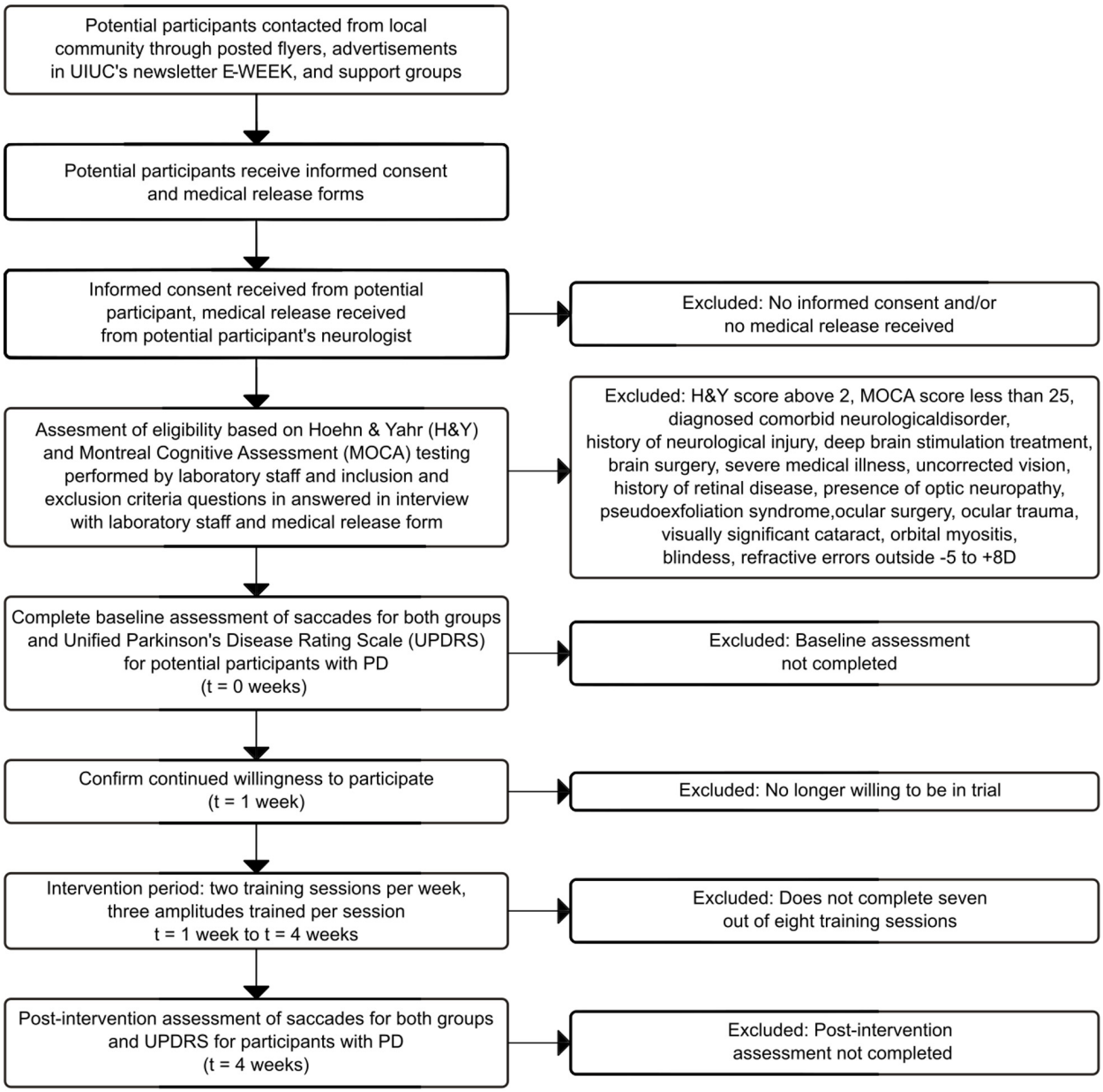

FIGURE 2 | Participant flow timeline.

presentation of the sole central fixation target. Due to the nature of mass-practice of eye movements, there is an inherent risk of eye fatigue or strain in participants. However, participants in this study will be instructed to rest at the first sign of any eye pain or fatigue, to minimize the risk and influence of strain or fatigue on the outcomes of the experiment.

Participants who are unable to complete seven of the eight training sessions due to fatigue or other events related to the intervention will be omitted from the study and receive prorated compensation. The intervention is designed to minimize fatigue by providing rest breaks regularly and as the participant indicates a need for rest. During both the training and testing sessions, eye tracking data will be collected by the SR Eyelink II system and stored. While only testing session data will be analyzed to determine the effects of the intervention, training session data can be used to check that training sessions will be completed per the protocol instructions. This check data includes the number of trials per direction per amplitude, amplitudes trained, and collection dates for each session.

Modifications

In the unlikely case of an unexpected event, the research team, in consultation with the participant's physician, will make the decision to modify or terminate the trial. As this is a

pilot trial, there will be no adjustment to sample size in the course of the study.

Concomitant Care

(1) Involvement in other interventional studies will not be permitted for participants in either group.
(2) Participants will continue their physician prescribed treatment during their participation.

Outcomes

Primary Outcome Measures

The primary outcomes of this study are four measures of voluntary and reflexive saccade performance: (1) the normalized amplitude calculated as the amplitude of the saccade divided by the target eccentricity, (2) the mean normalized saccadic velocity calculated as the mean normalized amplitude divided by saccade duration, (3) saccadic latency calculated as the time from the presentation of the directional cue to the saccade onset. The saccade onset is calculated as the time between the presentation of the directional arrow and the first eye movement crossing the velocity threshold of 30°/s and the acceleration threshold of 8000°/s^2 specified by the EyeLink® II User Manual (Jainta et al., 2011). The fourth outcome is the number of saccades needed to reach the target. The first three outcomes are only calculated on the first saccade toward the target.

Secondary Outcome Measures

One secondary outcome for this study is Movement Disorder Society-sponsored new version of the Unified Parkinson's Disease Rating Scale (MDS-UPDRS). The MDS-UPDRS assesses motor examination and complications, motor aspects of daily living, and non-motor aspects of daily living using a combination of questionnaire and task performance assessment (Goetz et al., 2008; Martinez-Martin et al., 2013). The MDS-UPDRS will only be assessed in participants with PD, as participants with no known neurological disorders should not present disability measurable with these instruments. Additionally, the peak saccadic velocity, duration, and amplitude will be analyzed as a measure of changes to the main sequence (Bahill et al., 1975).

Primary outcomes will be assessed by a member of the NDHD laboratory staff blinded to secondary outcome assessment, which will be performed on a separate day (see **Table 5** for investigator team timeline). Secondary outcome assessors will be blinded to primary outcomes and will not be involved in training sessions. Changes after the four-week intervention from the initial value of each primary and secondary outcome measure will be analyzed using an ANOVA of mixed effects.

Participant Timeline

Table 4 contains a full timeline of participant involvement.

Sample Size

There will be two groups with the same treatment: (1) a control group of participants with no known neurological disorders and (2) a test group comprised of participants with PD that have H&Y levels 1–2. In the absence of existing data in the literature to estimate the required same sample size for a protocol of this nature, the estimation is based on the number of eyes tested and trained in other eye movement studies and a 10% attrition rate seen in other studies performed by the authors (Hall et al., 2010; Knox and Wolohan, 2015; Ivanov et al., 2016; Heath et al., 2017).

Recruitment

Persons with PD (n = 22) and neurologically healthy persons (n = 22), between the ages of 40 and 65 years will be recruited. Participants will be recruited from the local community through posted flyers, advertisements in UIUC s newsletter E-WEEK, and support groups (in a 60-mile radius around the UIUC campus).

TABLE 4 | Timeline of participant involvement.

	Study Period					
	Enrolment	Allocation	Post-allocation			
Timepoint	*Week –1*	*Week 0*	*Week 1*	*Week 2*	*Week 3*	*Week 4*
Enrolment:						
Eligibility screen	X					
Informed consent	X					
Medical release	X					
Allocation		X				
Intervention:						
Parkinson's group			X	X	X	X
Healthy group			X	X	X	X
Assessments:						
Clinical Screening		X				
Saccades			X			X
Clinical			X			X

METHODS: DATA COLLECTION, MANAGEMENT, AND ANALYSIS

Saccade Function Testing

During the week prior to and the week following the intervention period, participants will be tested for both voluntary and reflexive saccade performance (see **Table 6** for summary of saccade testing). Voluntary saccade testing will involve the same task as the training sessions, in the 10°, 20°, and 30° amplitudes only. In the reflexive saccade testing session, the same amplitudes will be tested following the reflexive testing protocol. As in the voluntary saccade testing, each amplitude will be tested for the eight cardinal and intercardinal directions. Five trials will be performed per direction, resulting in 40 trials per amplitude in a testing session. The structure of each trial consisted of the initial fixation period, followed by the simultaneous disappearance of the central fixation target and appearance of the reflexive target, and finally the resetting period. Unlike in the voluntary saccade trials, there is no presentation of the circle of targets prior to the appearance of the reflexive target and no arrow to indicate the direction of movement to be performed (see **Figure 3**). Assessments will begin with a warm-up for the eyes in order to minimize the risk of injury. Participants with no known neurological disorders (see **Supplementary Material Data Sheet 2** sample physician release

TABLE 5 | Investigator team activity timeline.

Activity/assessment	PD Only (Yes/ No)	Staff member	Approximate time to complete (min)	Prestudy screening/ consent	Basline/ Intervention week 1	Intervention week 2	Intervention week 3	Intervention week 4/ conclusion
Prescreening consent		Study coordinator	5	X				
Screening checklist		Study coordinator	10	X				
Consent form		Study coordinator	45	X				
Medical release and relevant medical history	Yes	Potential participant's neurologist	30	X				
Hoehn and Yahr scale	Yes	Clinical assessors	30		X			
Montreal Cognitive Assessment	Yes	Clinical assessors	30		X			
Unified Parkinson's Disease Rating Scale	Yes	Clinical assessors	30		X			
Voluntary saccade assessment		Staff member	45		X			
Reflexive saccade assessment		Staff member	45		X			
Voluntary saccade training intervention		Staff member	45		XX	XX	XX	XX
Termination form		Study coordinator	N/A					X
Serious adverse event form		Study coordinator	N/A	As needed throughout protocol				
Progress note		All team members	N/A	X	X	X	X	X
Communication log		All team members	N/A	Every phone or in-person contact outside of regular study visits				

form) will complete only the eye-tracking related assessments. There will be one pre-training assessment and one post-training assessment, totaling two assessment periods for the control group protocol. Each assessment period should last no longer than 1.5 h including rest periods.

Participants will perform eye-tracking related assessments in ON and OFF motor-related medication states in order to completely characterize the effects of eye-movement training in PD (see **Table 7** for OFF-state timeline). Participants will continue regular intake of any medications that are unrelated to motor symptoms in PD.

Clinical Mobility Testing for Participants With Parkinson's

Following completion of eye-tracking related assessments, the participant's motor function will be assessed using the Movement Disorder Society-United Parkinson's Disease Rating Scale (MDS-UPDRS) in the OFF-state for an accurate description of PD stage. To achieve the OFF-state, participants will be instructed to take their last dose of medication approximately 8 h before their scheduled morning assessment. This approach will time the initiation of the OFF-state with the beginning of data collection. Immediately following the OFF-state eye-tracking assessment, the MDS-UPDRS will be administered to participants in the NDHD Laboratory which is equipped with ballet barres for support. Immediately after the MDS-UPDRS administration, participants will be instructed to take their medication and take a 60 min long break while they return to their normal ON-state. This protocol will mitigate the time spent in the OFF-state to approximately 2 h. Sixty-minutes after the intake of medication, participants will complete a final eye-tracking assessment in the ON-state. In total, pre/post-assessments will last at most 4 and a half hours, including the 60 min break and assessment beaks. A summary of an example Parkinson's pre-training and post-training assessment timeline follows: If the participant takes medications in a schedule other than every 8 h, the participant will time the start of the experiment with their regular time of medication intake and withhold from taking their regular dosage for the first 2 h of the experiment. After those 2 h, the participant will resume regular medication intake.

TABLE 6 | Saccade testing summary table.

VOLUNTARY	REFLEXIVE
Amplitudes: 10°, 20°, and 30°	**Amplitudes**: 10°, 20°, and 30°
Directions (*Cardinal*): North, Northwest, West,	**Directions (*Cardinal*):** North, Northwest, West,
Southwest, South, Southeast, East, Northeast [8 total]	Southwest, South, Southeast, East, Northeast [8 total]
Repetitions PER Direction: 5×	**Repetitions PER Direction**: 5×
Total Trials: 120	**Total Trials**: 120
Task: Voluntary Saccade	**Task**: Reflexive Saccade

Combination of voluntary and reflexive eye-tracking related assessments will last approximately 1.5 h including rest time.

Processing

Eye tracking data for both the left and right eyes is first converted to ASCII files, which will be then converted into two types of ASCII files: gaze data, which consisted of pupil position relative to the room, and head referenced (*href*) data, which consists of pupil position relative to the head. In order to

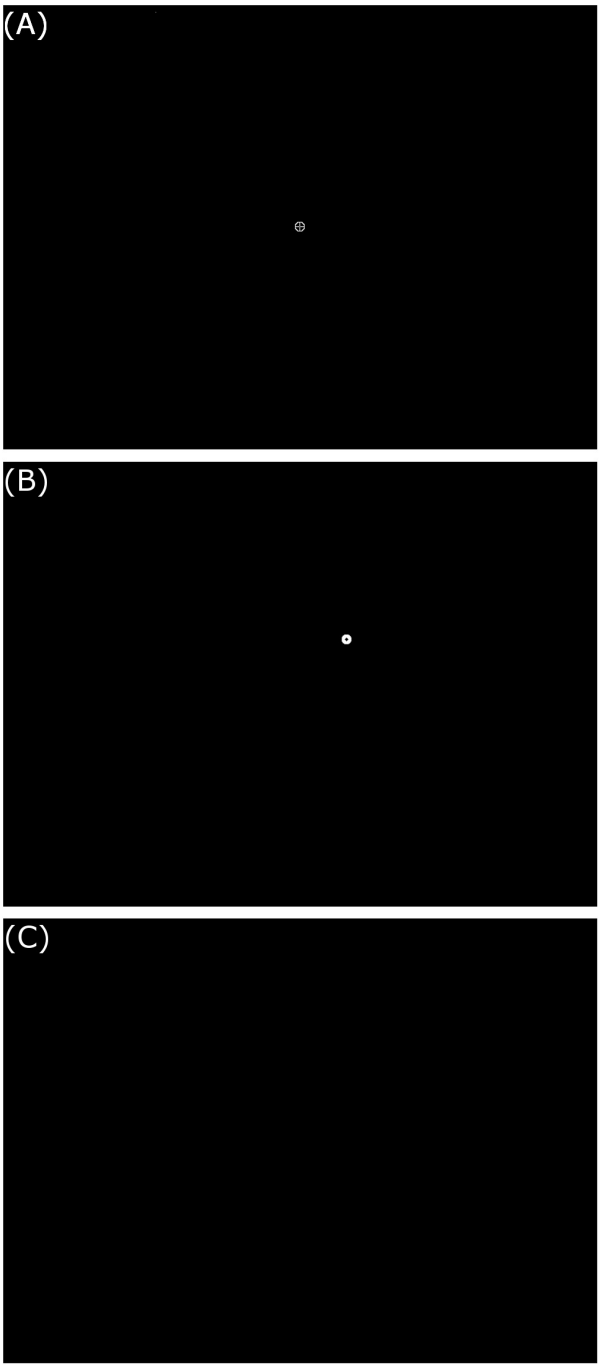

FIGURE 3 | Example reflexive testing trial display sequence. **(A)** Central fixation target, **(B)** 20° northeast target, and **(C)** blank reset screen. All images presented in 800 × 600 resolution on screen.

TABLE 7 | OFF-state testing timeline for participants.

Night Before	7:00 AM	8:30 AM	9:00 AM	10:00 AM
Take last dose of medication at 11 PM (taken 8 h before morning assessment)	Eye-Tracking Assessment (OFF-state)	MDS-UPDRS Assessment	**RETURN TO MEDICATION (60-min break)**	Eye-Tracking Assessment (ON-state)

TABLE 8 | IRB protocol revision chronology.

Original Submission	July 2, 2015	
Approval date	January 15, 2016	
Amendment 01	February 16, 2016	Update of research team list.
Amendment 02	October 3, 2016	Change in research location to Freer Hall room 250.
Amendment 03	July 31, 2017	Addition of testing in the off-medication state for participants with PD.
Amendment 04	April 9, 2018	Update of research team list.
Amendment 05	July 19, 2018	Medical release form specific to healthy controls added.

minimize false positive detection of saccades caused by head movement, the *href* data is then used for further processing. This data is then processed in MATLAB (MathWorks, Inc., Natick, MA, United States) using a program developed by Ronald Carbonari. This program converts eye tracking data from pixel measurements of movement distances to radial distance based on the fixed distance of the participant from the experiment display. The program also uses median pupil position during fixation to find the center of the visual focus for each trial to calculate real saccade distances, removing the assumption that the center of the visual fixation target is the center of actual fixation. Blinks and their subsequent movements will be detected and removed using a data-driven blink finder in the MATLAB program. Saccade latency is calculated as the time between presentation of the directional arrow and the first eye movement crossing the velocity threshold of 30°/s and the acceleration threshold of 8000°/s^2, as specified by the EyeLink® II User Manual (Jainta et al., 2011). The program then removed faulty fixations and appended the start of each saccade to occur 1.6 ms after the end of the previous fixation. This auto-cleaned data will be then stored and plotted, allowing the data to be visualized for each trial and cleaned on a per trial basis using an additional section of the MATLAB script edited by the user. This script allows users to, on either eye, delete trials missing excessive position data or delete false saccades not detected by the automated cleaning process. Additionally, users could shift the start and/or end of a fixation to match visually determined correct times based on the plot of radial position versus time. Saccades are automatically shifted along with the endpoints for adjusted fixations. The user can also move individual saccades and insert fixation-saccade pairs to match visually determined significant pupil movements. Only the first three saccades in each trial will be analyzed since this was a sufficient number of saccades to reach the target in preliminary tests.

Data Management

All participants will be assigned a code for de-identification for all data collected. The participant code will be stored in a locked cabinet and destroyed when the study procedures are completed. Data analyses will be conducted on the coded non-identifiable data. All data will be kept in a locked file cabinet or

TABLE 9 | Trial registration data.

Primary registry and trial identifying number: 17784042
Date of registration in primary registry: July 25, 2018
Secondary identifying numbers: N/A
Source(s) of monetary or material support: Unfunded
Primary sponsor: University of Illinois at Urbana–Champaign
Secondary sponsor(s): None
Contact for public queries: CLO, Ph.D., MA lopezort@illinois.edu
Contact for scientific queries: CLO, Ph.D., MA University of Illinois at Urbana–Champaign
Public title: Voluntary saccade training in persons with Parkinson's disease and healthy adults
Scientific title: Voluntary saccade training in persons with Parkinson's disease and healthy adults – two-arm, pre/post-trial
Countries of recruitment: United States of America
Health condition(s) or problem(s) studied: Parkinson's disease, voluntary saccades, reflexive saccades
Intervention: Voluntary saccade training
Key inclusion and exclusion criteria: Ages eligible for study: ≥40 years; Sexes eligible for study: both; Accepts healthy volunteers: yes
Inclusion criteria: For participants with PD: (1) medically stable with diagnosis of PD by meeting the United Kingdom PD Society Brain Bank Criteria, (2) to have a Modified Hoehn & Yahr stage 1–2 (with unilateral involvement only, unilateral and axial involvement, and bilateral involvement without impairment of balance) in the conventionally defined OFF medication state, (3) to have medical clearance form from their physician for participation in the study, (4) to be in a stable regimen of PD medication 30 days prior to the initiation of the study and until the completion of the study, (5) to be willing and able to provide informed consent, (6) to be of age 40 and up, and (7) must have a caregiver/family member present for OFF-state assessment sessions.
For neurologically healthy participants: (1) no known neuromuscular disorders, (2) to have medical clearance form from their physician for participation in the study, (3) to be willing and able to provide informed consent, and 4) to be of age 40 and up.
Exclusion criteria: (1) presence of dementia based on The Montreal Cognitive Assessment (MOCA) –score of less than 25, (2) diagnosis of comorbid neurological disorder such as epilepsy, (3) history of neurological injury such as stroke, (4) history of brain surgery such as deep brain stimulation, (5) concurrent severe medical illness which in the opinion of the research team will preclude participation in the study (such illnesses may include but not limited to severe or uncontrolled cardiovascular disease, hypertension, pulmonary disease, or diabetes), (6) inability to attend and participate in at least seven of the training sessions, (7) uncorrected vision, history of retinal disease (e.g., macular degeneration), presence of optic neuropathy due to glaucoma or ischemic optic neuropathy, pseudoexfoliation syndrome, ocular surgery, ocular trauma, visually significant cataract, orbital myositis, blindness or refractive errors outside –5 to +3 D, (8) indication by the participant's neurologist in the medical release form that testing the participant in the OFF-medication state would put PD participants at significant risk for medical complications.
Study type: Interventional
Allocation: no randomization; Intervention model: two-arm pre-post; Masking: non-masked
Primary purpose: eye movement training
Study Phase: Phase 0
Date of first enrolment: March 12, 2016
Target sample size: 44
Recruitment status: Recruiting
Primary outcome(s): For both voluntary and reflexive saccades: number of saccades needed to reach target amplitude, for first saccade: latency, normalized mean velocity, normalized amplitude
Key secondary outcomes: Unified Parkinson's Disease Rating Scale

in encrypted, password protected research computers. We will retain all screening data for those who qualify and volunteer and destroy the screening data for those who are excluded or do not choose to participate in the study. The informed consent, medical clearance, and verification of PD diagnosis will be stored together in a locked cabinet.

Statistical Methods

After data cleaning is completed using the automatic and user-guided portions of the MATLAB program, the cleaned data for all trials, which contains pupil position data for both eyes, will undergo statistical analysis. Using SAS, an ANOVA with mixed effects will be performed using the finalized data concerning four variables of interest for both voluntary and reflexive saccades: (1) normalized mean velocity, (2) normalized angular distance, (3) latency for the first saccade in a trial, and (4) saccade count to target (SAS Institute Inc., Cary, NC, United States). For participants with PD, the UPDRS scores before and after the intervention will be included with the eight saccade variables in the ANOVA with mixed effects to determine if any significant clinical mobility improvements occur. In secondary analyses, saccade-related measurements will be compared between the voluntary and reflexive saccades and by target amplitude. In the case of non-normality, non-parametric statistical methods will be used. Saccade data that are not viable for statistical analysis due to problems in recording eye movements, such as blinks obscuring saccades and loss of fovea tracking during a saccade initiation or endpoint, will not be included in the statistical analyses. Main sequence analysis will be included as a secondary form of analysis. Due to the comparatively weaker relationship seen between peak velocity and amplitude in the range that will be recorded, analysis of the relationship between mean velocity and amplitude and the relationship between duration and amplitude will be included (Bahill et al., 1975).

METHODS: MONITORING

Data Monitoring

Due to the low risk of this protocol, no data monitoring committee is required.

Should the intervention cause orbital myositis or other physical injuries in any of the participants, the research team, in consultation with the patient's physician, will make the final decision to terminate the trial.

Harms

Data collected with the eye tracker during assessments in the study will not give an immediate indication about participant risk. However, participant comfort and concern for their own health will be continuously monitored verbally by research personnel throughout the assessment. If the participant expresses concern all research procedures will stop and research personnel will call 911 with the participant's consent. In case of such an adverse event the IRB will be immediately notified. The participants are required to have a caregiver/family member present during OFF-assessments. There will be an area on

the physician clearance form (**Supplementary Material Data Sheet 3** sample physician release form for PD) for instructions to minimize risk during the OFF-state as well as a schedule for the administration of medications before and after the OFF period. The medical waiver will include an additional area for any special instructions to research assistants as necessary. Patients that could be at significant risk for medical complications by withdrawing from medications will be excluded from the study.

Auditing

The trial will be audited by compliance entities associated with the University of Illinois at Urbana–Champaign system.

DISCUSSION

Improvement in voluntary saccade function may occur due to changes at multiple levels of the saccade. Saccade improvements may occur due to increased eye muscle strength as well as better nervous system planning and control of saccades. Three sets of extraocular muscles are involved in performing saccades depending on their component composition (Sparks, 2002). The medial and lateral rectus muscles generate horizontal saccade movements (Sparks, 2002). The superior and inferior rectus muscles function with the superior and oblique muscle pairs for production of vertical saccade components (Sparks, 2002). Production of oblique saccades requires all three pairs of muscles to coordinate together (Sparks, 2002). Functional improvement of these muscles may impact the ability to perform movements of different horizontal and/or vertical components depending on which muscles are affected. At the nervous system level, communication between areas involved in the generation of saccades may increase to produce better coordination between the horizontal and vertical saccade systems. Control over peak saccadic velocity may also change as the training task aims to facilitate larger voluntary saccadic amplitudes, potentially inducing a change to the main sequence that has been seen previously in voluntary control of reflexive saccades (Muhammed et al., 2018).

The superior colliculus (SC) has been identified as a key area for target and timing selection for saccades in primates (Port and Wurtz, 2009). Neurons in the SC are thought to form a map of saccades by direction and amplitude, requiring the activity of a group of SC neurons to form a saccade of the correct amplitude and direction (Sparks, 2002). SC neurons receive cortical and subcortical input and communicate output to the midbrain and pontine areas, as well as all premotor areas associated with control of eye and head movements (Sparks, 2002). The cortical frontal eye fields – while not necessary for saccade initiation – contribute to saccade control, through activity mediated by the SC (Sparks, 2002). The cerebellum plays a key role by creating the error signal for saccades, which contributes to saccade accuracy, speed, and lack of variability (Robinson and Fuchs, 2001). This signal is also generated by different areas of the cerebellum depending on whether the saccade has a horizontal or vertical direction (Robinson and Fuchs, 2001). The posterior vermis and caudal fastigial nucleus generate horizontal saccade signals, while vertical saccade information is handled by the interpositus nucleus (Robinson and Fuchs, 2001). Through these signals, the cerebellum adds correction information to saccade commands prior to initiation of movement to achieve accurate saccades of the necessary speed (Robinson and Fuchs, 2001).

A lack of response to voluntary saccade training in the primary or secondary outcome measures would support the use of this protocol for testing saccades as part of a biomarker assessment for early detection and diagnosis of PD. An added dimension of biomarker potential may come from a differential response of the main sequence to the training between the two groups as measured by changes in characteristic peak velocity for given saccadic amplitudes. This would create a more robust saccade-based biomarker by adding a treatment-response dimension to the characterization suggested as a diagnostic tool by previous studies (Terao et al., 2013; Yerram et al., 2013; Termsarasab et al., 2015).

CONCLUSION

This intervention holds significant promise as a low-cost, low resource-demand tool to improve motor functions of the eyes in persons with PD and adults with no known neurological disorders as well as mobility outcomes associated with eye function in persons with PD. Should persons with PD not show improvements on any metric following the intervention, a lack of response to voluntary saccade training may support saccade assessment as a biomarker for early detection and diagnosis of PD.

ETHICS AND DISSEMINATION

Research Ethics Approval

All methods have been approved by the local IRB committee (see **Table 8** for a full IRB revision history as of the publication of this article). All subjects will provide written informed consent (see **Supplemental Materials Data Sheet 1** sample informed consent for informed consent form) in accordance with the Declaration of Helsinki. This protocol has been designed in accordance with SPIRIT guidelines for clinical trial protocols (see **Table 9** for a summary of SPIRIT-required trial registration information).

Protocol Version

IRB# 16033
Issue date: July 19th, 2018
Protocol amendment number: 06
Authors: Paul B. Camacho *(PBC),* Ronald Carbonari *(RC),* Sa Shen *(SS),* Cindy Zadikoff *(CZ),* Arthur F. Kramer *(AK),* Citlali López-Ortiz *(CLO)*

Protocol Amendments

Important protocol modifications will be approved by the local IRB and communicated to co-investigators, trial participants, trial registries, the clinical trial publishing journal.

Consent or Assent

The written informed consent will be completed by the participant before enrolling in the study and undertaking baseline data collection. The participants will have the opportunity to read the informed consent and ask any questions about the procedures to the PI before participation in the study. We will provide the participant with a copy of the signed informed consent document. We will give a period of at least 24 h for review of the consent form. This will assure that the participant has had ample time in reviewing and understanding the consent form prior to signing. The PI will be available to answer any questions regarding the consent form.

Confidentiality

All biographical and medical information about potential participants will be stored in paper form in a locked cabinet. We will retain all screening data for those who qualify and volunteer. We will destroy the screening data for those who are excluded or do not choose to participate in the study. All participants will be assigned a random identification number for all data collection. The participant identification code will be stored in paper form and destroyed when the study procedures are completed. Clinical measures taken to as part of the recruitment process and study will be deidentified, using assigned participant numbers, and completed in paper form. Raw eye tracking data will be collected and stored by participant number on a computer, which will have no internet connection. Access to the NDHD laboratory is restricted to trained staff and, during training or testing, the participants and their caregivers. At no point will anyone who is not a member of the NDHD staff have access to any collected data. Data analyses will be conducted on the coded non-identifiable data. The data will be kept for 5 years after publication, as required by the American Psychological Association. Only deidentified data will be released after the trial as part of peer-reviewed scientific journal articles and storage in a data repository.

Access to Data

The final trial de-identified dataset will be available to members of the NDHD laboratory staff and stored in an online data repository. To minimize bias, investigators performing data processing of eye tracking data will not have access to clinical measure outcomes or identifying information until the end of the study. Similarly, clinical assessors will not have access to eye tracking data or other information that could bias assessment.

Ancillary and Post-trial Care

Study participants will continue with regular, prescribed medical care throughout the experiment. In the event of physical injury, their physician will be contacted.

Dissemination Policy

The proposed forms of dissemination are presentations at scientific conferences and publications in scientific journals. Only deidentified data will be released after the trial as part of peer-reviewed scientific journal articles and storage in a data repository. To be eligible for authorship, all potential authors must meaningfully contribute to and approve the final manuscript. All authors are expected to contribute to the shaping of the protocol and performance of some aspect of the study. The full protocol and statistical code will be accessible via an online data repository, along with the participant-level dataset for the purposes of study reproducibility.

SPONSOR CONTACT INFORMATION

Trial Sponsor: University of Illinois at Urbana–Champaign
Sponsor's Reference: N/A
Contact name: Dr. Citlali López-Ortiz
Address: 221 Freer Hall 906 S Goodwin Ave. Urbana, IL 61801
Telephone: (217) 300-1022
Email: lopezort@illinois.edu

Sponsor Responsibilities

The sponsor will have no direct role in study design, data collection, management, analysis, interpretation of data, writing of the report, or decision to submit the report for publication.

AUTHOR CONTRIBUTIONS

CL-O conceived the study and design and involved in all aspects of the study. AK supervised the experiments design. CZ assisted with medical aspects of the protocol design. PBC helped refine the study design and wrote the manuscript. RC set up the eye tracker and computing systems and developed the data processing software. RC and PBC helped with implementation. SS contributed with statistical expertise. All authors contributed to refinement of the study protocol, approved the final manuscript, and agreed to be accountable for the content of the manuscript.

FUNDING

This work was supported by the College of Applied Health Sciences and Beckman Institute for Advance Science and Technology at the University of Illinois at Urbana–Champaign.

ACKNOWLEDGMENTS

We express our gratitude to the staff of the Neuroscience of Dance in Health and Disability Laboratory for their assistance in testing the experimental set up and other aspects of this protocol, along with Reika McNish and Nathaniel Speidel for their assistance in proofreading and editing this manuscript. We thank the staff of the Department of Kinesiology and Community Health, the College of Applied Health Sciences, the Center on

Health Aging and Disability, and the Beckman Institute for Advanced Science and Technology at the University of Illinois at Urbana–Champaign for equipment support. We also thank the participants, current and future, for participation in this protocol.

SUPPLEMENTARY MATERIAL

The Supplementary Material for this article can be found online at: https://www.frontiersin.org/articles/10.3389/fnagi.2019.00077/full#supplementary-material

REFERENCES

Ambati, V. N., Saucedo, F., Murray, N. G., Powell, D. W., and Reed-Jones, R. J. (2016). Constraining eye movement in individuals with Parkinson's disease during walking turns. *Exp. Brain Res.* 234, 2957–2965. doi: 10.1007/s00221-016-4698-1

Bahill, A. T., Clark, M. R., and Stark, L. (1975). The main sequence, a tool for studying human eye movements. *Math. Biosci.* 24, 191–204. doi: 10.1016/0025-5564(75)90075-9

Baird-Gunning, J. J. D., and Lueck, C. J. (2018). Central control of eye movements. *Curr. Opin. Neurol.* 31, 90–95.

Bibi, R., and Edelman, J. A. (2009). The influence of motor training on human express saccade production. *J. Neurophysiol.* 102, 3101–3110. doi: 10.1152/jn.90710.2008

Chen, P. L., and Machado, L. (2016). Age-related deficits in voluntary control over saccadic eye movements: consideration of electrical brain stimulation as a therapeutic strategy. *Neurobiol. Aging* 41, 53–63. doi: 10.1016/j.neurobiolaging.2016.02.010

Coats, R. O., Fath, A. J., Astill, S. L., and Wann, J. P. (2016). Eye and hand movement strategies in older adults during a complex reaching task. *Exp. Brain Res.* 234, 533–547. doi: 10.1007/s00221-015-4474-7

Dowiasch, S., Marx, S., Einhauser, W., and Bremmer, F. (2015). Effects of aging on eye movements in the real world. *Front. Hum. Neurosci.* 9:46. doi: 10.3389/fnhum.2015.00046

Fernandez-Ruiz, J., Peltsch, A., Alahyane, N., Brien, D. C., Coe, B. C., Garcia, A., et al. (2017). Age related prefrontal compensatory mechanisms for inhibitory control in the antisaccade task. *Neuroimage* 165, 92–101. doi: 10.1016/j.neuroimage.2017.10.001

Fischer, B., and Hartnegg, K. (2000). Effects of visual training on saccade control in dyslexia. *Perception* 29, 531–542. doi: 10.1068/p2666c

Fukushima, K., Ito, N., Barnes, G. R., Onishi, S., Kobayashi, N., Takei, H., et al. (2015). Impaired smooth-pursuit in Parkinson's disease: normal cue-information memory, but dysfunction of extra-retinal mechanisms for pursuit preparation and execution. *Physiol. Rep.* 3:e12361. doi: 10.14814/phy2.12361

Goetz, C. G., Tilley, B. C., Shaftman, S. R., Stebbins, G. T., Fahn, S., Martinez-Martin, P., et al. (2008). Movement disorder society-sponsored revision of the Unified Parkinson's Disease Rating Scale (MDS-UPDRS): scale presentation and clinimetric testing results. *Mov. Disord.* 23, 2129–2170. doi: 10.1002/mds.22340

Hall, C. D., Heusel-Gillig, L., Tusa, R. J., and Herdman, S. J. (2010). Efficacy of gaze stability exercises in older adults with dizziness. *J. Neurol. Phys. Ther.* 34, 64–69. doi: 10.1097/NPT.0b013e3181dde6d8

Harris, C. M., and Wolpert, D. M. (2006). The main sequence of saccades optimizes speed-accuracy trade-off. *Biol. Cybern.* 95, 21–29. doi: 10.1007/s00422-006-0064-x

Heath, M., Shellington, E., Titheridge, S., Gill, D. P., and Petrella, R. J. (2017). A 24-week multi-modality exercise program improves executive control in older adults with a self-reported cognitive complaint: evidence from the antisaccade task. *J. Alzheimers Dis.* 56, 167–183. doi: 10.3233/JAD-160627

Ito, N., Barnes, G. R., Fukushima, J., Fukushima, K., and Warabi, T. (2013). Cue-dependent memory-based smooth-pursuit in normal human subjects: importance of extra-retinal mechanisms for initial pursuit. *Exp. Brain Res.* 229, 23–35. doi: 10.1007/s00221-013-3586-1

Ivanov, I. V., Mackeben, M., Vollmer, A., Martus, P., Nguyen, N. X., and Trauzettel-Klosinski, S. (2016). Eye movement training and suggested gaze strategies in tunnel vision – A randomized and controlled pilot study. *PLoS One* 11:e0157825. doi: 10.1371/journal.pone.0157825

Jainta, S., Vernet, M., Yang, Q., and Kapoula, Z. (2011). The pupil reflects motor preparation for saccades – even before the eye starts to move. *Front. Hum. Neurosci.* 5:97. doi: 10.3389/fnhum.2011.00097

Jamadar, S. D., Johnson, B. P., Clough, M., Egan, G. F., and Fielding, J. (2015). Behavioral and neural plasticity of ocular motor control: changes in performance and fMRI activity following antisaccade training. *Front. Hum. Neurosci.* 9:653. doi: 10.3389/fnhum.2015.00653

Johannesson, O. I., Edelman, J. A., Sigurthornorsson, B. D., and Kristjansson, A. (2018). Effects of saccade training on express saccade proportions, saccade latencies, and peak velocities: an investigation of nasal/temporal differences. *Exp. Brain Res.* 236, 1251–1262. doi: 10.1007/s00221-018-5213-7

Kleiser, R., Stadler, C., Wimmer, S., Matyas, T., and Seitz, R. J. (2017). An fMRI study of training voluntary smooth circular eye movements. *Exp. Brain Res.* 235, 819–831. doi: 10.1007/s00221-016-4843-x

Knox, P. C., and Wolohan, F. D. (2015). Temporal stability and the effects of training on saccade latency in express saccade makers. *PLoS One* 10:e0120437. doi: 10.1371/journal.pone.0120437

Lohnes, C. A., and Earhart, G. M. (2011). Saccadic eye movements are related to turning performance in Parkinson disease. *J. Parkinsons Dis.* 1, 109–118.

MacAskill, M. R., and Anderson, T. J. (2016). Eye movements in neurodegenerative diseases. *Curr. Opin. Neurol.* 29, 61–68. doi: 10.1097/WCO.0000000000000274

Martinez-Martin, P., Rodriguez-Blazquez, C., Alvarez-Sanchez, M., Arakaki, T., Bergareche-Yarza, A., and Chade, A. (2013). Expanded and independent validation of the movement disorder society-unified parkinson's disease rating scale (MDS-UPDRS). *J. Neurol.* 260, 228–236. doi: 10.1007/s00415-012-6624-1

Mosimann, U. P., Muri, R. M., Burn, D. J., Felblinger, J., O'Brien, J. T., and McKeith, I. G. (2005). Saccadic eye movement changes in Parkinson's disease dementia and dementia with Lewy bodies. *Brain* 128(Pt 6), 1267–1276. doi: 10.1093/brain/awh484

Muhammed, K., Dalmaijer, E., Manohar, S., and Husain, M. (2018). Voluntary modulation of saccadic peak velocity associated with individual differences in motivation. *Cortex* (in press). doi: 10.1016/j.cortex.2018.12.001

Nemanich, S. T., and Earhart, G. M. (2016). Freezing of gait is associated with increased saccade latency and variability in Parkinson's disease. *Clin. Neurophysiol.* 127, 2394–2401. doi: 10.1016/j.clinph.2016.03.017

Noiret, N., Vigneron, B., Diogo, M., Vandel, P., and Laurent, E. (2017). Saccadic eye movements: what do they tell us about aging cognition? *Neuropsychol. Dev. Cogn. B Aging Neuropsychol. Cogn.* 24, 575–599. doi: 10.1080/13825585.2016.1237613

Port, N. L., and Wurtz, R. H. (2009). Target selection and saccade generation in monkey superior colliculus. *Exp. Brain Res.* 192, 465–477. doi: 10.1007/s00221-008-1609-0

Robinson, F. R., and Fuchs, A. F. (2001). The role of the cerebellum in voluntary eye movements. *Annu. Rev. Neurosci.* 24, 981–1004. doi: 10.1146/annurev.neuro.24.1.981

Schmitt, K. U., Seeger, R., Fischer, H., Lanz, C., Muser, M., Walz, F., et al. (2015). Saccadic eye movement performance as an indicator of driving ability in elderly drivers. *Swiss Med. Wkly* 145, w14098. doi: 10.4414/smw.2015.14098

Seferlis, F., Chimona, T. S., Papadakis, C. E., Bizakis, J., Triaridis, S., and Skoulakis, C. (2015). Age related changes in ocular motor testing in healthy subjects. *J. Vestib. Res.* 25, 57–66.

Seiple, W., Szlyk, J. P., McMahon, T., Pulido, J., and Fishman, G. A. (2005). Eye-movement training for reading in patients with age-related macular degeneration. *Invest. Ophthalmol. Vis. Sci.* 46, 2886–2896. doi: 10.1167/iovs.04-1296

Sparks, D. L. (2002). The brainstem control of saccadic eye movements. *Nat. Rev. Neurosci.* 3, 952–964. doi: 10.1038/nrn986

Stack, E., and Ashburn, A. (1999). Fall events described by people with Parkinson's disease: implications for clinical interviewing and the research agenda. *Physiother. Res. Int.* 4, 190–200. doi: 10.1002/pri.165

Stuart, S., Galna, B., Delicato, L. S., Lord, S., and Rochester, L. (2017). Direct and indirect effects of attention and visual function on gait impairment in Parkinson's disease: influence of task and turning. *Eur. J. Neurosci.* 46, 1703–1716. doi: 10.1111/ejn.13589

Terao, Y., Fukuda, H., Ugawa, Y., and Hikosaka, O. (2013). New perspectives on the pathophysiology of Parkinson's disease as assessed by saccade performance: a clinical review. *Clin. Neurophysiol.* 124, 1491–1506. doi: 10.1016/j.clinph.2013.01.021

Terao, Y., Fukuda, H., Yugeta, A., Hikosaka, O., Nomura, Y., Segawa, M., et al. (2011). Initiation and inhibitory control of saccades with the progression of Parkinson's disease – Changes in three major drives converging on the superior colliculus. *Neuropsychologia* 49, 1794–1806. doi: 10.1016/j.neuropsychologia.2011.03.002

Termsarasab, P., Thammongkolchai, T., Rucker, J. C., and Frucht, S. J. (2015). The diagnostic value of saccades in movement disorder patients: a practical guide and review. *J. Clin. Mov. Disord.* 2:14. doi: 10.1186/s40734-015-0025-4

van Stockum, S., MacAskill, M. R., and Anderson, T. J. (2012). Impairment of voluntary saccades and facilitation of reflexive saccades do not co-occur in Parkinson's disease. *J. Clin. Neurosci.* 19, 1119–1124. doi: 10.1016/j.jocn.2011.10.014

Yerram, S., Glazman, S., and Bodis-Wollner, I. (2013). Cortical control of saccades in Parkinson disease and essential tremor. *J. Neural Transm. (Vienna)* 120, 145–156. doi: 10.1007/s00702-012-0870-3

Conflict of Interest Statement: The authors declare that the research was conducted in the absence of any commercial or financial relationships that could be construed as a potential conflict of interest.

frontiers in Neuroscience

METHODS
published: 29 April 2019
doi: 10.3389/fnins.2019.00396

Use of Overlapping Group LASSO Sparse Deep Belief Network to Discriminate Parkinson's Disease and Normal Control

Ting Shen[1], Jiehui Jiang[1,2], Wei Lin[3], Jingjie Ge[4], Ping Wu[4], Yongjin Zhou[1], Chuantao Zuo[4,5,6]*, Jian Wang[7]*, Zhuangzhi Yan[1] and Kuangyu Shi[8,9]*

[1] Shanghai Institute for Advanced Communication and Data Science, Shanghai University, Shanghai, China, [2] Key laboratory of Specialty Fiber Optics and Optical Access Networks, Joint International Research Laboratory of Specialty Fiber Optics and Advanced Communication, Shanghai University, Shanghai, China, [3] Department of Neurosurgery, 904 Hospital of PLA, Anhui Medical University, Wuxi, China, [4] PET Center, Huashan Hospital, Fudan University, Shanghai, China, [5] Institute of Functional and Molecular Medical Imaging, Fudan University, Shanghai, China, [6] Human Phenome Institute, Fudan University, Shanghai, China, [7] Department of neurology, Huashan Hospital, Fudan University, Shanghai, China, [8] Department of Nuclear Medicine, University Hospital Bern, Bern, Switzerland, [9] Department of Nuclear Medicine, Technische Universitat Munchen, Munich, Germany

OPEN ACCESS

Edited by:
Xun Chen,
University of Science and Technology of China, China

Reviewed by:
Cheng-Yu Wei,
Chang Bing Show Chwan Memorial Hospital, Taiwan
Maria Eugenia Caligiuri,
Università degli Studi Magna Graecia, Italy

***Correspondence:**
Jiehui Jiang
jiangjiehui@shu.edu.cn
Chuantao Zuo
zuochuantao@fudan.edu.cn
Jian Wang
wangjian336@hotmail.com

Specialty section:
This article was submitted to Neurodegeneration, a section of the journal Frontiers in Neuroscience

Received: 18 January 2019
Accepted: 08 April 2019
Published: 29 April 2019

Citation:
Shen T, Jiang J, Lin W, Ge J, Wu P, Zhou Y, Zuo C, Wang J, Yan Z and Shi K (2019) Use of Overlapping Group LASSO Sparse Deep Belief Network to Discriminate Parkinson's Disease and Normal Control. Front. Neurosci. 13:396. doi: 10.3389/fnins.2019.00396

As a medical imaging technology which can show the metabolism of the brain, 18F-fluorodeoxyglucose (FDG)-positron emission tomography (PET) is of great value for the diagnosis of Parkinson's Disease (PD). With the development of pattern recognition technology, analysis of brain images using deep learning are becoming more and more popular. However, existing computer-aided-diagnosis technologies often over fit and have poor generalizability. Therefore, we aimed to improve a framework based on Group Lasso Sparse Deep Belief Network (GLS-DBN) for discriminating PD and normal control (NC) subjects based on FDG-PET imaging. In this study, 225 NC and 125 PD cohorts from Huashan and Wuxi 904 hospitals were selected. They were divided into the training & validation dataset and 2 test datasets. First, in the training & validation set, subjects were randomly partitioned 80:20, with multiple training iterations for the deep learning model. Next, Locally Linear Embedding was used as a dimension reduction algorithm. Then, GLS-DBN was used for feature learning and classification. Different sparse DBN models were used to compare datasets to evaluate the effectiveness of our framework. Accuracy, sensitivity, and specificity were examined to validate the results. Output variables of the network were also correlated with longitudinal changes of rating scales about movement disorders (UPDRS, H&Y). As a result, accuracy of prediction (90% in Test 1, 86% in Test 2) for classification of PD and NC patients outperformed conventional approaches. Output scores of the network were strongly correlated with UPDRS and H&Y ($R = 0.705$, $p < 0.001$; $R = 0.697$, $p < 0.001$ in Test 1; $R = 0.592$, $p = 0.0018$, $R = 0.528$, $p = 0.0067$ in Test 2). These results show the GLS-DBN is feasible method for early diagnosis of PD.

Keywords: Parkinson's disease, Deep Belief Network, overlapping group LASSO, sparse representation, deep learning, early diagnose

INTRODUCTION

Parkinson's disease (PD) is a long-term degenerative disease of the central nervous system which effects 2–3% of the world's population over 65 years old, and its incidence is increasing in recent years(Postuma and Berg, 2017). Accurate early diagnosis of PD is crucial for treatment and prognosis.

Imaging disease-specific patterns of regional glucose metabolism with 18F-fluorodeoxyglucose (FDG)-positron emission tomography (PET) allows for accurate diagnosis of PD, this has been increasingly acknowledged in recent years (Eckert et al., 2005; Dabrowska et al., 2015; Meyer et al., 2017; Politis et al., 2017). Some studies (Juh et al., 2004; Brajkovic et al., 2017) used voxel-based statistical analyses or network analysis in comparison to normal control (NC). For example, Juh et al. used statistical parametric mapping to determine useful metabolic patterns in diagnosing PD (Juh et al., 2004). Brajkovic et al. combined visual assessment of individual scans with statistical parametric mapping (Brajkovic et al., 2017). These researches showed that compared with NC, glucose metabolism of PD patients in sensorimotor cortex, lateral frontal and parietooccipital areas was decreased (Meles et al., 2017), which is of great value for the early diagnose of PD.

Currently, with the development of artificial intelligence and data-driven analysis, various computer-aided-diagnosis systems based on machine learning or deep learning(Chandra and Sharma, 2016; Chen et al., 2017) methods have been developed to identify brain disease related alterations in neuroimaging datasets. For instance, some studies (Tang et al., 2010; Garraux et al., 2013; Tripathi et al., 2015) classify PD patients based on automated statistical analysis. Garraux et al. applied logistic regression based on the expression of metabolic covariance patterns. Tripathi et al. used a relevance vector machine in combination with bootstrap resampling for multiclass classification. Also, in Matthews's research (Matthews et al., 2018), two machine learning approaches (Canonical Variates Analysis and Scaled Subprofile Model) were used to represent the difference in motor symptoms between NC and PD patients. Methods using deep learning have also been explored to extract latent features from PET images. For example, Liu et al. extracted potential features from 83 regions of interest in magnetic resonance imaging and PET scans and trained a multilayer neural network of multiple auto-encoders to combine multimodal features for classification (Siqi et al., 2015). Suk et al. presented that a stacked auto-encoder can be used to learn the underlying non-linear complicated patterns in low-level features, for example, the relationship between features (Suk et al., 2015). Also, in Brosch et al.'s study, in order to find the modes of variation between disease parameters and demography, they proposed a low-dimensional manifold of brain volumes based DBN model (Brosch et al., 2014).

While previous studies have claimed that existing machine learning and deep learning methods achieved an acceptable classification accuracy to discriminate PD and normal controls (NC), these methods are still hampered by over-fitting and poor generalizability, due to few labeled samples in neuroimaging datasets. To solve above problems, scholars have used deep learning models with multi-parameters, e.g., deep belief network (DBN), to avoid models' poor generalizability from traditional machine learning methods (Yoshida and Miyato, 2017; Xu et al., 2018). In addition, they have also proposed to add regular terms to the objective function, which could optimize the loss function, reduce the complexity of deep learning models, and prevent models' over-fitting (Mei et al., 2015). For these reasons, considering the feature distribution of PET images, in this paper, based on DBN, we add the Group Lasso Sparse (GLS) model as a regular term to the objective function to prevent the model over-fitting, and at the same time, to learn the multi-level imaging features such as texture or edge information for classifying PD vs. NC. To evaluate the effectiveness of our method, we also compared our model with other deep learning models.

GROUP LASSO SPARSE DEEP BELIEF NETWORK (GLS-DBN) ALGORITHM

In this paper, we propose an improved DBN method, Group Lasso Sparse Deep Belief Network (GLS-DBN), for feature learning and classification of PET images. As a deep architecture, DBN is suitable to deliver non-linear and complicated machine learning information (Liu et al., 2011; Rui and Yang, 2017; Zheng and Lu, 2017; Prasetio et al., 2018). Sparsity has become a key ingredient for improving DBN because compared with non-sparse representations, sparse representations are more efficient from the point of view of information theory, which allow the change of the effective number of bits per example in a fixed-size representation (Ranzato et al., 2007; Luo et al., 2010; Halkias et al., 2013). Sparsity is generally introduced into DBN by adding a sparse penalty to the objective function and considering it as a convex optimization problem. For example, based on the DBNs of Hinton et al. (2006), Lee et al. proposed a sparse DBN which faithfully simulating some properties of visual region V2 (Lee et al., 2007). Ji et al. proposed a sparse-response DBN based on rate distortion theory, in which the distortion function was based on Kullback-Leibler divergence between equilibrium distribution in DBN model and data distribution, then a small code rate was realized by adding sparse response regularization (Ji et al., 2014). Xu et al. examined the problem of invariance existing in sparse regular term and proposed an improved sparse DBN (Xu et al., 2018). This model uses Laplace distribution to induce the sparse state of hidden layer nodes, and uses location parameters in the distribution to control the intensity of sparsity. In addition to these, Keyvanrad et al added normal regularization term in DBN which make the whole model has different response according to difference between hidden units' activation and fixed value (Keyvanrad and Homayounpour, 2017). Compared with base DBN model (without sparse penalty), all of these models achieved better performance in natural image recognition, but it is unknown whether these methods can be applied to PET images. Therefore, to evaluate PET image patterns, we combined traditional DBN with the overlapping group lasso model and propose a novel sparse DBN model(Rao et al., 2015; Jian et al., 2017; Liu et al., 2017; Yuan et al., 2018),

GLS-DBN, adding a sparse penalty to learn useful low-level feature representations.

GLS-DBN is based on GLS Restricted Boltzmann Machine (GLS-RBM). As an improved Restricted Boltzmann Machine (RBM) (Fischer and Igel, 2012), GLS-RBM combines the overlapping group lasso model with the pre-training of traditional RBM, grouping its hidden units according to the same overlap ration of each group. Through this, GLS-RBM connects similar features between groups. When a large number of similar features exist discretely in multiple groups, multiple groups are activated simultaneously, effectively solving the problem of over fitting in the traditional learning model and improving the recognition rate of the model.

We implement the GLS-RBM model by adding a sparse penalty to the objective function. In this paper, we also use the Cauchy distribution to replace the traditional L1 normal form between groups in the overlapping groups Lasso model, making the entire model sparser at the group level (Lü et al., 2016). For sample collection: $\{v^1, v^2 \dots v^m\}$, the optimization model of unsupervised pre-training of GLS-RBM is:

$$F = F_{unsup} + \tau F_{sprase} \tag{1}$$

$$F_{sprase} = \lambda F_{Lasso} + \varphi F_{Cachy} \tag{2}$$

Where F_{unsup} is the likelihood function of the RBM. The new objective function of the optimization GLS-RBM model after adding a sparse penalty is:

$$\text{minimize}_{\{w_{ij},b_i,c_j\}} F = -\frac{1}{m}\sum_{l=1}^{m} log \sum_{h} P\left(v^{(l)}, h^{(l)}\right) + \tau \sum_{l=1}^{m} F_{sprase} \tag{3}$$

For a GLS-RBM model, all hidden units $\{h_1, h_2 \dots h_n\}$ are evenly distributed to I overlapping groups. Each group has the same number of nodes, and there is overlap between each group. The degree of overlapping is determined by α (between-group and group). **Figure 1** shows a simple GLS-RBM model based overlapping group lasso.

The F_{sprase} in the whole layer becomes:

$$\begin{aligned} F_{sprase} &= \lambda F_{Lasso} + \varphi F_{Cachy} \\ &= \lambda \sum_{i=1}^{I} \sqrt{\sum_{n\in Group_i} p\left(h_n = 1 \mid v\right)^2} + \varphi \sum_{j=1}^{n} L\left(\gamma, \mu, p_j\right) \end{aligned} \tag{4}$$

$$\mathrm{L}\left(\gamma, \mu, p\right) = \frac{1}{\pi}\frac{\gamma}{(x-\mu)^2 + \gamma^2} = \frac{1}{\pi\gamma}\frac{1}{\left[1 + \left(\frac{p_j-\mu}{\gamma}\right)^2\right]} \tag{5}$$

Where p is the probability distribution of the hidden unit, γ is the scale parameter, which controls the degree of sparsity, and μ is the location parameter.

The Gradient descent algorithm is used to iteratively solve and update parameters of the function. We use the objective function with penalty to update the weight w, and the hidden layer bias b. The visible layer bias is obtained according to the original objective function. The gradient of the objective function is solved as follows:

$$\frac{\partial F}{\partial W_{ij}} = \frac{\partial}{\partial W_{ij}}\left(\frac{1}{m}\sum_{l=1}^{m} ln\left(P\left(v^{(l)}\right)\right) + \frac{\partial F_{sprase}}{\partial W_{ij}}\right) \tag{6}$$

$$\frac{\partial F}{\partial b_j} = \frac{\partial}{\partial b_j}\left(\frac{1}{m}\sum_{l=1}^{m} ln\left(P\left(v^{(l)}\right)\right) + \frac{\partial F_{sprase}}{\partial b_j}\right) \tag{7}$$

$$\frac{\partial F}{\partial a_j} = \frac{\partial}{\partial a_j}\left(\frac{1}{\mathrm{m}}\sum_{l=1}^{m} ln\left(P\left(v^{(l)}\right)\right)\right) \tag{8}$$

Because

$$\begin{aligned} \frac{\partial F_{sprase}}{\partial p_j} = & \frac{1}{2}\sum_{i=1}^{I}\frac{2 \times p_j^{(l)}}{\sqrt{\sum_{j\in Group_i} p_j^{(l)^2}}} \\ & + \frac{1}{2m}\sum_{l=1}^{m}\sum_{i=1}^{I}\frac{2 \times p_j^{(l)}}{\sqrt{\sum_{j\in Group_i} p_j^{(l)^2}}} - \frac{1}{\pi\gamma^2} \\ & \times \frac{1}{m}\sum_{l=1}^{m}\frac{2\left(\frac{p_j^{(l)}-\mu}{\gamma}\right)}{\left(1 + \left(\frac{p_j^{(l)}-\mu}{\gamma}\right)^2\right)^2} \end{aligned} \tag{9}$$

The second item with sparse penalty is expanded as follows:

$$\frac{\partial F_{sprase}}{\partial W_{ij}} = \sum_{j=1}^{n}\frac{\partial F_{sprase}}{\partial p_j} \times \frac{1}{m}\sum_{l=1}^{m} p_j^l\left(1 - p_j^l\right) v_i^l \tag{10}$$

$$\frac{\partial F_{sprase}}{\partial b_j} = \sum_{j=1}^{n}\frac{\partial F_{sprase}}{\partial p_j} \times \frac{1}{m}\sum_{l=1}^{m} p_j^l\left(1 - p_j^l\right) \tag{11}$$

In whole GLS-DBN, multiple basic GLS-RBMs can be stacked upon each other to form a deep hierarchy. The output of each GLS-RBM serves as the input of the next basic GLS-RBM at successive levels. In the last layer of GLS-DBN, a back propagation (BP) network is set, receiving the output feature vector of GLS-RBM as learned features, and adopting a gradient descent algorithm to fine-tune the weight of the whole network, thereby coordinating and optimizing the parameters of the whole DBN. The feature vector mapping of GLS-DBN is optimized and the size of the input space is simplified.

MATERIALS AND METHODS

Materials

Two different cohorts of PD and NC subjects was included in this study. The first cohort came from Huashan Hospital, Fudan University, Shanghai, China. Subjects were recruited from Chinese populations and totaled 300 participants: 200 NC and 100 PD patients. Before the study, follow-up data for at least 1 year from all participants was collected. Then clinicians who

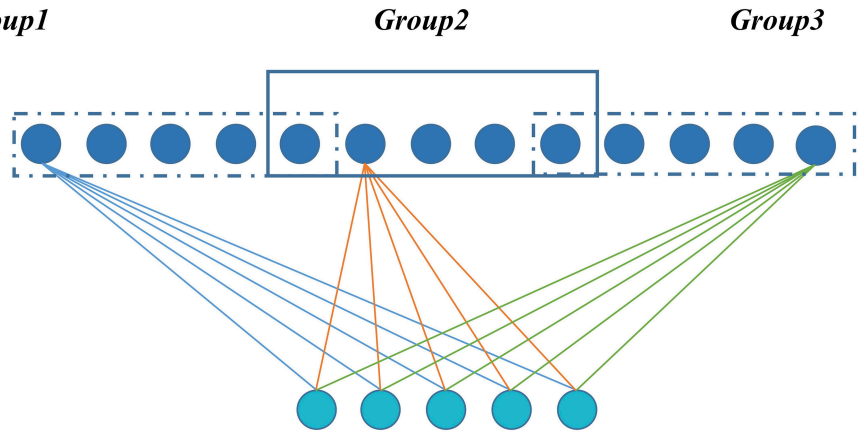

FIGURE 1 | A simple RBM model based overlapping Group Lasso model. All visible units are evenly divided into three groups, and overlapping rate is 0.2.

were unaware of the imaging results were followed up to further confirm the clinical diagnosis. Healthy controls in this study were accepted by senior movement disorders expert neurological examination, to rule out a history of psychiatric or neurologic disorders. All participants had no drug use or exposed to antipsychotic drugs.

The subjects in the Huashan cohort were randomly divided into training & validation and test (Test 1) datasets. The Test 1 dataset consisted of 50 subjects, including 25 PD patients and 25 NC subjects. Due to the variability of sampling when grouping data sets, the random cross validation method is used in the training & validation dataset, which included 75 PD patients and 175 NC subjects randomly partitioned into deep learning model training (80%) and validation (20%), with 50 iterations. The purpose of multiple cross-validation was to find the optimal parameter combination. Finally, the Test 1 dataset was used to verify the performance of the trained model.

The second cohort was from 904 Hospital in Wuxi, China, and included 25 NC and 25 PD patients, enrolled between 2011 and 2015. Also, before the study, necessary screening and clinical examinations from the two senior investigators of movement disorders were used to select eligible subjects. All subjects in the Wuxi cohort were used as a test dataset (Test 2) to verify the reliability and robustness of the deep learning model.

The demographic information and clinical data of two cohorts are shown in **Table 1**. The clinical characteristics (HY, UPDRS) were not significantly different among Training & Validation dataset and test datasets (Test 1 and Test 2) for PD or NC ($P > 0.05$). The study was ethically approved by the Institutional Review Boards at North Shore University Hospital and Huashan Hospital. The study was conducted in accordance with the Code of Ethics of the World Medical Association (Declaration of Helsinki) and the standards set by the local Institutional Review board and funding agencies. After a detailed explanation of the scanning procedure, each subject received written consent from each institution. During or after data collection, authors can access information that could identify all participants.

PET Imaging Acquisition

All participants were asked to fast before imaging. And the whole experiment was carried out in a dimly-lit room. The equipment used in this study was Siemens Biograph 64 PET/computed tomography (CT; Siemens, Germany). After 45 min of intravenous injection of 185 MBq of FDG, the scans were performed for about 10 min. Hanning filter is used for image reconstruction and then projection, with an axial and transaxial cut-off frequency of 0.5.

PET Pre-processing

The pre-processing of original PET data was completed by SPM5 software (Wellcome Department of Imaging Neuroscience, Institute of Neurology, London, UK). And the software platform is implemented in Matlab7.4.0 (Mathworks Inc., Sherborn, MA). First, through linear and non-linear transformations, PET scans from all samples were spatially normalized into Montreal Neurological Institute brain space. Then, a Gaussian filter of 10 mm FWHM was used for smooth images over three-dimension space. After that, an automated anatomic labeling template was used to remove unrelated regions in PET images. Due to individual variation in FDG uptake, finally, each PET image was normalized to the range of 0 to 1 through following formula, where v is the voxel value of the image:

$$v_{normalization} = \frac{v - v_{min}}{v_{\max} - v_{min}} \tag{12}$$

Data Dimension Reduction

Locally linear embedding (LLE) (Roweis and Saul, 2000; Xin et al., 2005) was used to reduce the dimensionality of pre-processed PET data in all subjects, including the Huashan and Wuxi cohorts. Since high-dimensional features are often associated with many redundant and hidden important relationships, we need a more concise PET data representation. LLE is a typical manifold learning algorithm that has been used to reduce the dimensionality of medical images (Liu et al., 2013). LLE solves globally non-linear problems using locally linear

TABLE 1 | Demographic and clinical information of Huashan hospital control and Wuxi 904 hospital cohort.

	Cohort		*N*	Gender(M/F)	Age(years)	H&Y	UPDRS
Huashan Hospital Cohort	Training & Validation dataset	NC	175	98/77	49.5 (29)	N/A	N/A
		PD	75	51/24	56.5 (14.5)	2 (1)	20 (19.05)
		P-Value	–	0.9217[a]	0.593[b]	–	–
	Test dataset (Test 1)	NC	25	10/15	50 (22.5)	N/A	N/A
		PD	25	14/11	55 (16)	2.5 (1.5)	25 (19.5)
		P-Value	–	0.4218[a]	0.258[b]	–	–
Wuxi 904 Hospital Cohort	Test dataset (Test 2)	NC	25	12/13	59 (9)	N/A	N/A
		PD	25	19/6	65 (11.5)	2.5 (1.5)	28 (18.5)
		P-Value	–	0.1884[a]	0.771[b]	–	–

Age and clinical ratings are given as. Median (Interquartile range). H & Y, Hoehn and Yahr scale; UPDRS, Unified Parkinson's Disease Rating Scale; P[a], The chi-square test; P[b], The two-sample t-test.

fitting, which means a sample x1 can be represented linearly by several samples from its k neighborhoods:

$$x_1 = w_{12}x2 + w_{13}x_3 + \ldots + w_{1k}x_k \quad (13)$$

Through LLE, we projected x_1, x_2, x_3 … x_k onto a lower dimensional space x_1', x_2', x_3' … x_k' keeping the same linear relationship:

$$x_1' \approx w_{12}x_2' + w_{13}x_3' + \ldots + w_{1k}x_k' \quad (14)$$

For high-dimensional data, LLE can maintain the local linear characteristics of the sample in the case of dimensionality reduction and map it to a low-dimensional global coordinate system, establishing a bridge between the high-dimensional data space and the low-dimensional latent space. In this paper, we use LLE to get a laconic representation of PET data. An automated method was used to optimize the LLE parameters number of neighbors, K, and corresponding dimensionality, D (Kayo, 2006).

GLS-DBN for Feature Learning and Classification

Based on the proposed GLS-RBM model, we used three GLS-RBM stacks to form a sparse GLS-DBN network for feature relearning and classification of PD and NC samples. The input of the GLS-DBN model is the low-dimensional feature learned from original PET data using the LLE algorithm, and the output is the prediction result.

Figure 2 shows the structure of our GLS-DBN for PD classification. We used a greedy layer-wise algorithm for pre-training of the GLS-DBN. First, the weights (W1) were optimized to represent the distribution of the input data. Then the weights were frozen, the first level output was generated after input data through them. This output was used to train the next GLS-RBM, with training performed in the same way. Finally, on the top of the GLS-DBN, a SoftMax layer was added, all the layers performed supervised fine-tuning as one deep neural network.

In the training progress, all the training steps shared the same BP approach. The training set was randomly divided into several mini-batches or subsets, and the cost function was minimized using mini-batch gradient descent. At every iteration, only one mini-batch was used for minimization. After all the samples were used once for training, the training set was divided again so that batches in each echo had different samples. The initial learning rate was set to 0.0001.

The training progress of the model was carried out on the training & validation dataset from the Huashan cohort. Parameters were optimized through the mean accuracy of the validation dataset. Finally, the two test datasets (Test 1 and Test 2) were used to verify the performance of the trained model.

Correlation Analyses

Before passing through the last layer of GLS-DBN, SoftMax function, the values of the two nodes indicate scores for PD and NC, respectively (Choi and Jin, 2018). The quantitative value of the PD node was defined as RiskScore, a score that indicates the proximity of PET data to PD or NC. In addition, RiskScore was correlated with Hoehn and Yahr scale (H&Y) and Unified Parkinson's Disease Rating Scale (UPDRS), in which Pearson correlation was used.

Experimental Comparison

To verify the reliability of our algorithm, we compared it to traditional DBN and improved sparse DBN networks. The sparse representation capability in various improved models was examined, including Lee's model, based on a quadratic regularization term (Lee et al., 2007), Ji's model, based on rate distortion theory (Ji et al., 2014), Keyvanrad's model, based on normal distribution (Keyvanrad and Homayounpour, 2017), and Xu's model (Xu et al., 2018), based on Laplace distribution. In addition, we compared our model with traditional DBN (without sparse penalty), Cauchy distribution, and group lasso distribution to examine the effectiveness of overlapping group lasso model. All of these methods are based on different regularization term definitions.

In all experiments, the DBN-based algorithm used the same structure, namely the same layers and the same hidden units. Weights and biases were initialized to uniformly distributed random numbers.

We used the sparsity measurement method proposed by Hoyer to accurately calculate the sparsity of the feature

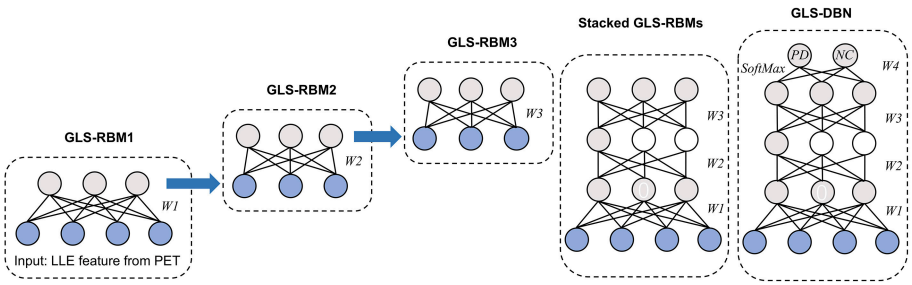

FIGURE 2 | Structure of GLS-DBN for PD classification.

representation learned by the model (Hoyer, 2004). The sparsity measurement method is as follows:

$$\text{sparseness}\,(x) = \frac{\sqrt{n} - \left(\sum_{i=1}^{n} |x_i|\right) / \sqrt{\sum_{i=1}^{n} x_i^2}}{\sqrt{n} - 1} \qquad (15)$$

Where x is the input data, n is the dimension of input data, and the value range of sparsity is [0,1]. The closer to 1, the sparser x is. The sparsity of activation probability of hidden units in batch data was calculated first, and then the average sparsity of activation probability of all data hidden units was calculated.

Sensitivity, specificity and accuracy of the test datasets (Test 1 and Test 2) were used as indicators to measure the performance of the model. In order to further evaluate the performance of the proposed method, we used receiver operating characteristic (ROC) graph to visualize the result of contrast experiments. The area under the curve (AUC) of the ROC was also computed to quantitatively evaluate the classification performance.

In addition, to verify the robust of our proposed method, we conducted a second experiment analysis and reassigned the distribution of the training & validation set and test dataset according to the H&Y. **Appendix A** shows the demographic and clinical information on the second experiment analysis. Similar to the first experiment analysis, we repeated above steps to calculate sensitivity, specificity, accuracy and AUC of the training & validation and test datasets (Test 1 and Test 2).

RESULTS

Determination of Parameters

Following an automated method (Kayo, 2006), the number of dimensions and nearest neighbors in LLE were set to 350 and 10.

To determine the optimal structure and parameters of the GLS-DBN model, including the scale parameter, location parameter, overlapping rate, and the number of hidden units, the greedy search algorithm was used in the whole training progress until the average accuracy of the validation dataset was optimized. These were chosen as the initial parameters for fine-tuning of the GLS-DBN.

Finally, hyper-parameters were set: number of hidden units, scale parameter, location parameter, and overlapping rate were set to 500, 1, 0.025, and 0.2. The maximum number of iterations of GLS-RBM and BP network were 50 and 300. Using features from LLE and GLS-DBN as classifiers, the classification experiment achieved 94% accuracy distinguishing PD and NC in the validation dataset.

Classification Results

Two different batches of data from the Huashan and Wuxi cohorts were used to validate the model's performance. **Figure 3** and **Table 2** show the final classification performance on the validation dataset, Test dataset 1, and Test dataset 2 under hyper-parameters in two experiments. Using features from LLE and GLS-DBN as classifiers, in Experiment 1, the classification experiment distinguishing PD and NC achieved 90.0% accuracy, 96% sensitivity, 84% specificity, and AUC of 0.9120 in Test dataset 1 and 86% accuracy, 92% sensitivity, 80% specificity, and AUC of 0.8992 in Test dataset 2; while in Experiment 2, the classification experiment distinguishing PD and NC achieved 88.0% accuracy, 92% sensitivity, 84% specificity, and AUC of 0.9320 in Test dataset 1 and 84% accuracy, 88% sensitivity, 80% specificity, and AUC of 0.8947 in Test dataset 2. As a result, we observed that the effect of different data distribution was slight for the classification. It means that our proposed model may have good robustness for other datasets.

Experimental Comparison

To verify the recognition ability of the algorithm, the classification accuracies of different models were compared. The results are shown in **Figures 4**, **5** and **Table 3**.

As shown in **Table 3**, **Figures 4**, **5**, GLS-DBN achieved the best accuracy on the training and test datasets when using the same network structure. GLS-DBN resulted in improved performance when compared to the traditional DBN classifier. Although the best sensitivities in the test dataset were seen in DBN models based on quadratic regularization and rate distortion, the specificities of these models were quite low (0.56 and 0.50) indicating that the rate of missed diagnosis is low but the rate of misdiagnosis is high. Improved DBN model-based group lasso achieved the best sensitivity, but the specificity was relatively low. These results indicate that our model has the ability to balance specificity and sensitivity when the best accuracy is reached. The accuracy in the Test 2 dataset was not significantly lower than the accuracy in the Test 1 dataset, demonstrating the generalizability of our model. Our model also achieved the best AUC in the Test 2 dataset and close to the optimal result in the Test 1 dataset.

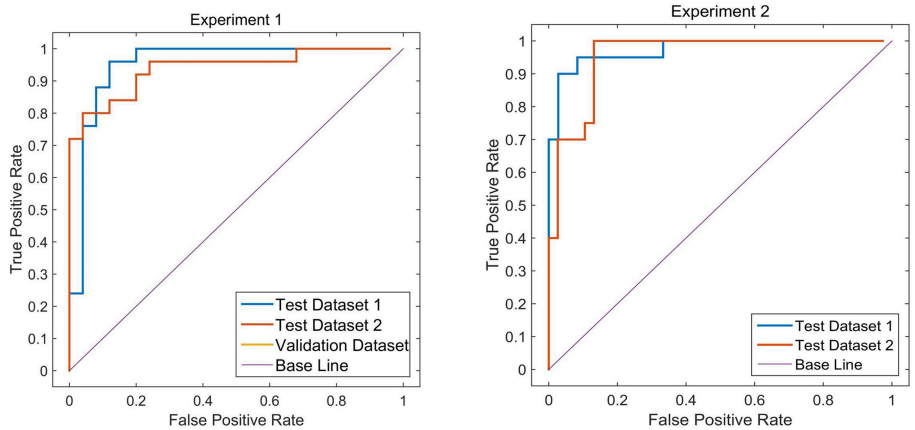

FIGURE 3 | ROC curves on Validation dataset, Test dataset 1 and Test dataset 2.

TABLE 2 | Classification performance on Validation and Test datasets.

		Accuracy	Sensitivity	Specificity	AUC
Experiment 1	Validation dataset	0.924	0.973	0.80	0.9325
	Test dataset 1	0.90	0.96	0.84	0.9120
	Test dataset 2	0.86	0.92	0.80	0.8992
Experiment 2	Validation dataset	0.9380	0.9642	0.834	0.9634
	Test dataset 1	0.88	0.92	0.84	0.9320
	Test dataset 2	0.84	0.88	0.80	0.8947

In a comprehensive sense, compared with other sparse DBN models based on different sparse penalties, our model optimizes the prediction of PD diagnosis.

Correlation Analyses

RiskScore calculated from the GLS-DBN model was significantly correlated with clinical scale value in the Test dataset, shown in **Figure 6**. RiskScore was significantly positively correlated with UPDRS (r =0 .705, $P < 0.0001$), and HY ($r = 0.697$, $p < 0.0001$) in Test 1, UPDRS ($r = 0.592$, $P = 0.0018$), and HY ($r = 0.528$, $p = 0.0067$) in Test 2.

These results show that RiskScore could be used as a quantitative biomarker for early diagnosis of Parkinson's disease.

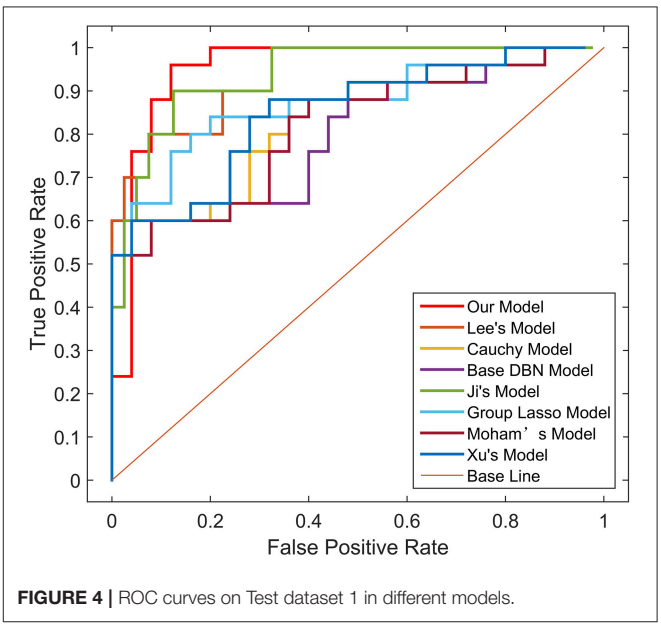

FIGURE 4 | ROC curves on Test dataset 1 in different models.

DISCUSSION

In this paper, we used an improved sparse DBN named GLS-DBN for the diagnosis of PD. Compared with other sparse DBN models based on different sparse penalties, our model showed better performance in classification of PD and NC, demonstrating that GLS-DBN can be used for effectively learning superior feature representation from small neuroimaging data. Results from other datasets also proved the preferable generalizability of GLS-DBN.

In addition, we compared the results of other similar studies to our results. Due to differences in datasets, number of samples, and methods of feature selection and reduction, while the accuracy was not the best, our proposed method still exceeded most relevant studies. Further, the sensitivity of our result was significantly higher than those automated classifications (96 vs. 86.67%, 96 vs. 84.4%) (Fung and Stoeckel, 2007; Rana et al., 2015). And the accuracy is closer to those methods based on voxel statistical analyses (90 vs. 90.9%, 90 vs. 86.5%) (Eckert et al., 2005). Our results also show a better specificity compared with automated classifications. Our automated method based deep learning performs better than traditional CAD methods and approaches results with manual diagnosis.

In terms of feature extraction and dimension reduction, the research of Rana et al. considered five brain areas, while the features used in our experiment were chosen from the whole brain (Rana et al., 2015). For high-dimensional PET data, LLE has

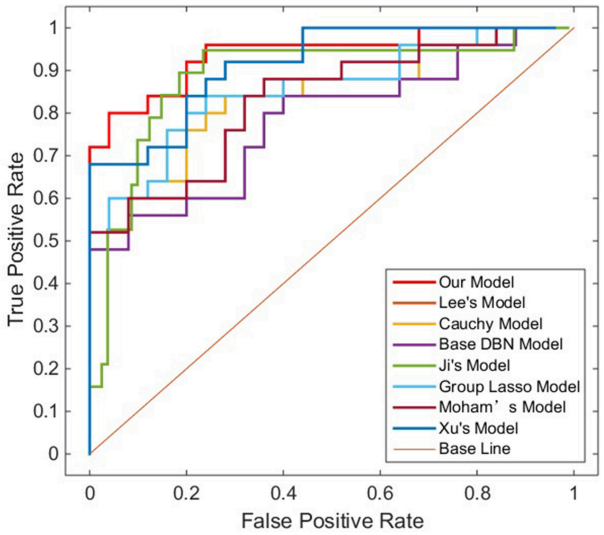

FIGURE 5 | ROC curves on Test dataset 2 in different models.

TABLE 3 | Classification performance on test datasets in different sparse models.

Model	Dataset	Accuracy	Sensitivity	Specificity	AUC
Base DBN model	Validation	0.7596	0.7845	0.6843	0.7769
	Test 1	0.66	0.72	0.60	0.7568
	Test 2	0.68	0.68	0.68	0.7408
Lee's model	Validation	0.9245	0.9353	0.8247	0.9275
	Test 1	0.88	0.925	0.70	0.91
	Test 2	0.84	**0.9630**	0.56	0.8726
Moham's model	Validation	0.7968	0.7164	0.6852	0.8087
	Test 1	0.70	0.72	0.68	0.7744
	Test 2	0.72	0.72	0.72	0.7904
Ji's model	Validation	0.8727	0.8867	0.7589	0.8977
	Test 1	0.86	**0.9750**	0.500	**0.9125**
	Test 2	0.84	0.96	0.45	0.8726
Xu's model	Validation	0.8443	0.8847	0.7964	0.8876
	Test 1	0.74	0.72	0.76	0.8096
	Test 2	0.80	0.80	0.80	0.8752
Cauchy model	Validation	0.8034	0.8181	0.7443	0.8232
	Test 1	0.72	0.72	0.72	0.7824
	Test 2	0.76	0.72	0.80	0.8016
Group Lasso model	Validation	0.898	0.9341	0.7877	0.9012
	Test 1	0.80	0.72	**0.88**	0.8320
	Test 2	0.78	0.72	**0.84**	0.8160
Our model	Validation	0.935	0.925	0.85	0.9487
	Test 1	**0.90**	0.96	0.84	0.9120
	Test 2	**0.86**	0.92	0.80	**0.8992**

The bold values represents means the highest value of accuracy, sensitivity, specificity and AUC on test dataset 1 and test dataset 2 in different models.

learned the potential non-linear expression in PET image data and embedded the features after dimensionality reduction into linear coordinates, which can map the PET data of PD and NC to different feature spaces, that is, subjects with different clinical manifestations have different distribution of brain features (Roweis and Saul, 2000). So, LLE reduces the recognition error caused by redundant information and significantly improves the feature difference between PD and NC samples, which is crucial for later feature learning and classification.

In terms of feature learning, almost all studies using pattern recognition in PD diagnosis use features directly for classification, without the progress of feature relearning. In this study, the GLS-DBN model based on a deep learning algorithm can re-encode features before classification, which improves accuracy. The experimental results also show that GLS-DBN can learn more appropriate features in PET data compared with the traditional RBM and DBN algorithms. One possible reason is that sparse coding learns helpful low-dimensional feature representations from unlabeled data. By constraining the hidden layer, GLS-RBM can obtain a simpler and more structured weight pattern, thus avoiding the redundant and sequential-value code that RBM may produce that RBM may produce. **Figure 7** shows the activation probability of hidden units caused by an input data, in other words, the representation of this input data obtained by traditional RBM and GLS-RBM. As we can see from **Figure 7**, the activation probability of RBM approaching is much lower than that of GLS-RBM, while the activation probability of the hidden units in sparse-RBM is very close to 0, which means DBN-based sparse penalty can learn a sparser representation of input data. **Table 4** shows the results of sparseness in different improved DBN models. Although Lee's model and Ji's model achieved the best sparseness (0.8594, 0.8239), classification performance in **Table 3** showed high sensitivity (0.925, 0.9750 in Test 1, 0.9630, 0.96 in Test 2) but low specificity (0.70, 0.56 in Test 1, 0.50, 0.45 in Test 2). Compared with other sparse models, our model achieved the highest sparseness (0.8011 vs. 0.6619, 0.7145, 0.7473, 0.7963, 0.7852) and also the best classification performance. The results in **Table 4** show that the sparsest DBN model does not represent the most suitable model for learning useful low-level feature representation of PET image patterns. Combining the results of **Table 3**, through the adjustment of parameters, the GLS-DBN base overlapping group lasso model can achieve optimal sparseness, and balance specificity and sensitivity while ensuring the accuracy of the model.

PD reflects in a small part of the brain pathology, causing differences in only part of the brain compared to healthy people. When using LLE dimensionality reduction for 3D PET images, there may be a group relationship between features; moreover, it is possible that there is overlap of features between groups. The overlapping group lasso model takes this relationship into account, and using a sparse penalty term effectively suppresses expression of some redundant features. This increases the feature difference between PD and NC samples, achieving improved classification. The results of Test 1 from the Huashan cohort show the excellent performance of our model. The results of Test 2 from the Wuxi cohort show the reliability of the model, and also its generalizability to other datasets.

Considering the clinical effectiveness of the results, including HY and UPDRS, this paper analyzed the correlation between RiskScore and the clinical scale, shown in **Figure 6**. RiskScore

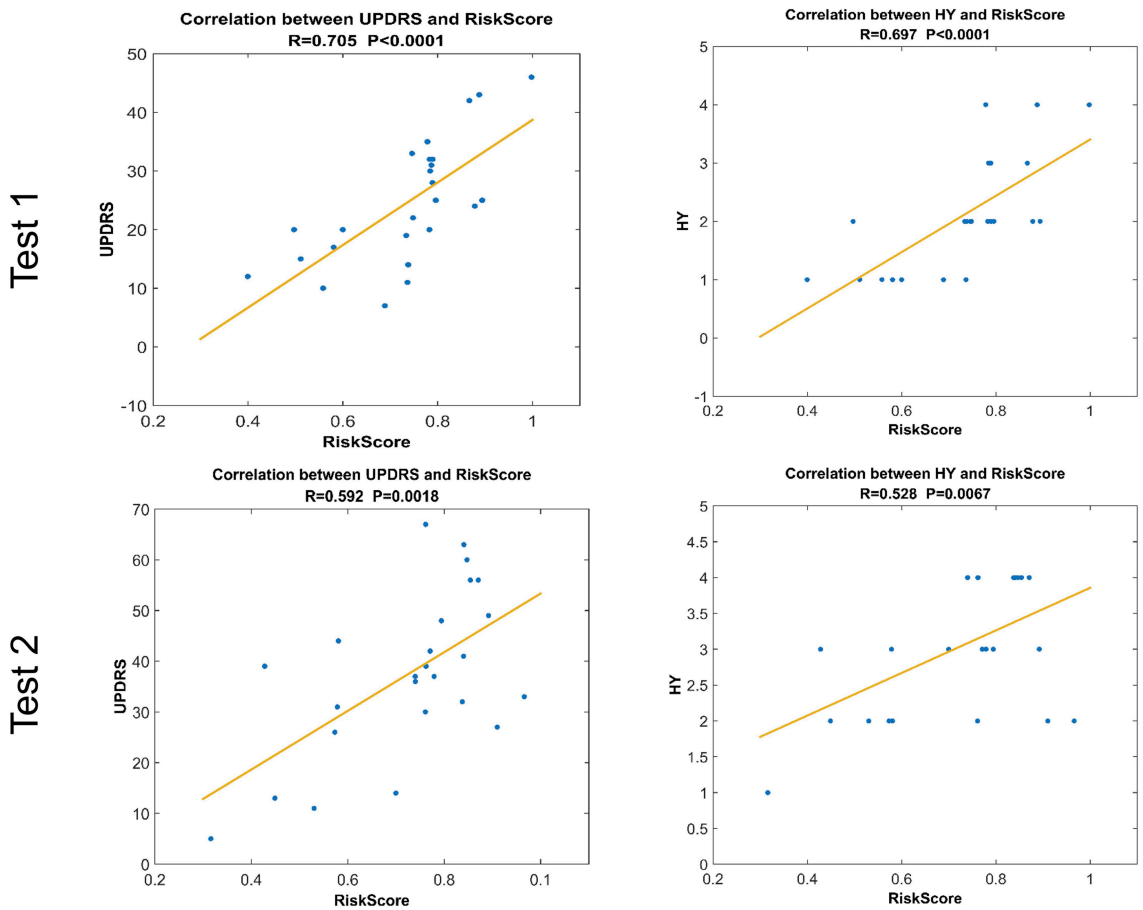

FIGURE 6 | Correlation between output of the network and clinical scale value.The last layer provides an output score for NC or PD converter, defined as RiskScore.

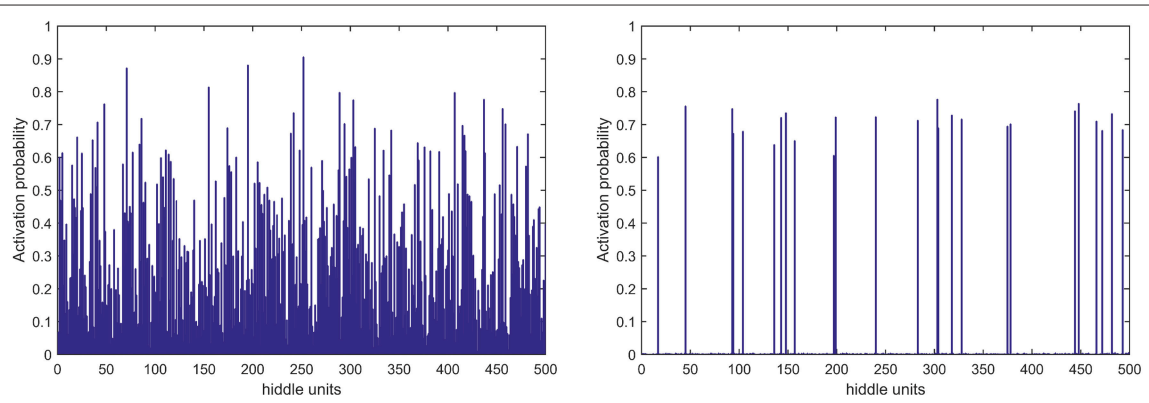

FIGURE 7 | Activation probability of hidden units obtained by RBM (left) and GLS-RBM (right).

calculated from the GLS-DBN model was significantly correlated with clinical scale value (0.705, 0.697, $p < 0.001$; 0.592, 0.528, $p < 0.01$) in the Test dataset, indicating that the features learned by GLS-DBN correlate with clinical information. To better describe the discriminability of the results, we conducted a statistical analysis of the risk values, and the distribution of RiskScore in PD and NC are shown in **Figures 8**, **9**. RiskScore of PD was significantly higher than that of NC (0.31 ± 0.23 and 0.73 ± 0.14, $p < 0.01$ in Test 1, 0.26 ± 0.22 and 0.72 ± 0.17, $p < 0.01$ in Test 2). These results indicate that this method can effectively classify

TABLE 4 | Average sparseness of different models.

Model	Base DBN model	Lee's model	Ji's model	Xu's model	Cauchy model	Keyvanrad's model	Group Lasso model	Our model
Sparseness	0.6619	0.8594	0.8239	0.7145	0.7473	0.7963	0.7852	0.8011

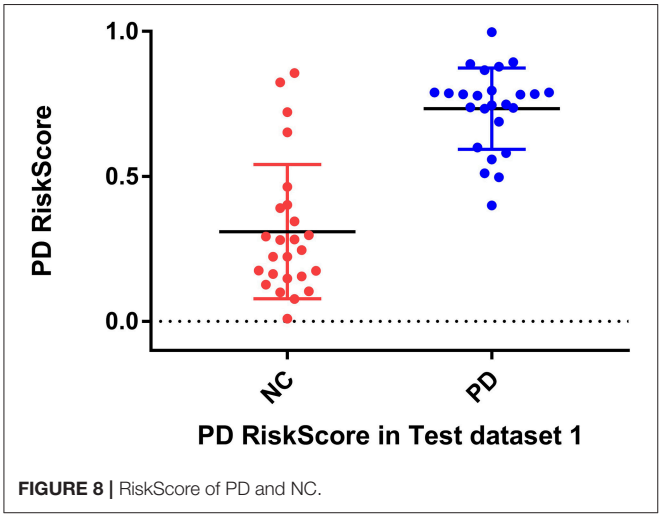

FIGURE 8 | RiskScore of PD and NC.

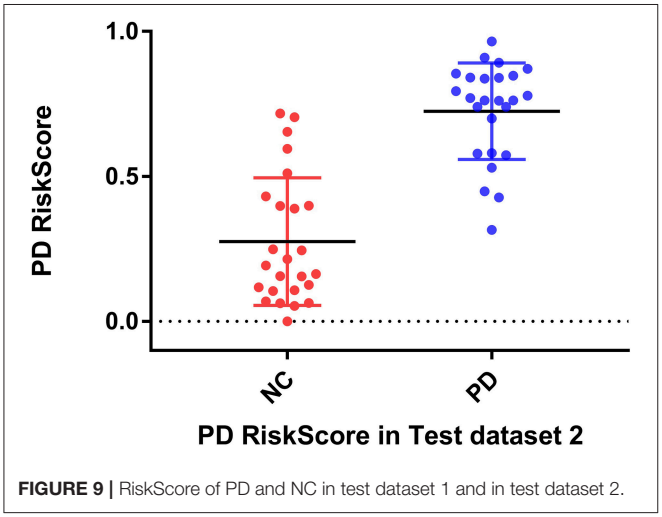

FIGURE 9 | RiskScore of PD and NC in test dataset 1 and in test dataset 2.

PD and NC, and that RiskScore can be used as a quantitative biomarker for early diagnosis of PD.

LIMITATIONS

Despite the impressive performance of the proposed method, the method also has some limitations and disadvantages. First, trial and error was used to determine the learning rate, and the parameter values in the network structure were optimized through a large number of experiments, causing a relatively large time complexity of the algorithm. Proper selection of parameters merits further studies; we propose using optimization algorithms such as a grid search algorithm to search for the optimal parameter combination as a next step. Second, while our work has a large number of subjects compared with several recent studies, it's still not enough to generalize our experimental results. Further, our work focuses on PET features only. Multimodal data, such as MRI and diffusion tensor imaging features, can be used for feature confusion and classification. Third, our classifier is a BP network, and other classifiers such as extreme learning machine and support vector machine can be combined with DBN. Combining other classifiers with DBN would allow the last layer before BP to be features learned from the DBN model and as an input for traditional classifiers, possibly improving classification results. Finally, as our study is based on PD and NC samples, it would be meaningful and of vital importance to further grade of different forms of Parkinson's disease or distinguish idiopathic Parkinson's disease from other forms of degenerative Parkinson's disease.

CONCLUSION

In this paper, we introduced a sparse feature learning framework in PD early diagnosis. GLS-DBN model accurately classifies patients into diagnostic groups with limited image processing and provides a quantitative biomarker which can predict early Parkinson's disease. Longitudinal changes of rating scales about movement disorders (UPSRS and H&Y), was significantly correlated with the output value of prediction model. In the future, our approach may be used in independent cohorts, and as an accurate biomarker, it could identify appropriate prodromal patients who might benefit from early intervention.

ETHICS STATEMENT

This study was carried out in accordance with the recommendations of Ethics committee of longhua hospital affiliated to University of Traditional Chinese Medicine with written informed consent from all subjects. All subjects gave written informed consent in accordance with the Declaration of Helsinki. The protocol was approved by the longhua hospital affiliated to University of Traditional Chinese Medicine.

AUTHOR CONTRIBUTIONS

All authors listed have made a substantial, direct and intellectual contribution to the work, and approved it for publication.

FUNDING

This study was supported by grants from the National Natural Science Foundation of China (Nos. 61603236, 81671239,

81361120393, 81401135, 81771483, and 81361120393), the National Key Research and Development Program of China (Nos. 2016YFC1306305, 2016YFC1306500 and 2018YFC1707704) from Ministry of Science and Technology of China, Shanghai Technology and Science Key Project in Healthcare (No. 17441902100), Science and Technology Commission of Shanghai Municipality (17JC1401600), and the Open Project Funding of Human Phenome Institute (No. HUPIKF2018203), Fudan University.

SUPPLEMENTARY MATERIAL

The Supplementary Material for this article can be found online at: https://www.frontiersin.org/articles/10.3389/fnins.2019.00396/full#supplementary-material

REFERENCES

Brajkovic, L., Kostic, V., Sobicsaranovic, D., Stefanova, E., Jecmenicalukic, M., Jesic, A., et al. (2017). The utility of FDG-PET in the differential diagnosis of Parkinsonism. *Neurol. Res.* 39, 675–684. doi: 10.1080/01616412.2017.1312211

Brosch, T., Yoo, Y., Li, D. K. B., Traboulsee, A., and Tam, R. (2014). Modeling the variability in brain morphology and lesion distribution in multiple sclerosis by deep learning. *Med Image Comput Comput. Assist Interv.* 17(Pt 2):462–9. doi: 10.1007/978-3-319-10470-6_58

Chandra, B., and Sharma, R. K. (2016). Fast learning in deep neural networks. *Neurocomputing* 171, 1205–1215. doi: 10.1016/j.neucom.2015.07.093

Chen, Y., Lin, Z., Xing, Z., Gang, W., and Gu, Y. (2017). Deep learning-based classification of hyperspectral data. *IEEE J. Select. Top. Appl. Earth Observ. Remote Sens.* 7, 2094–2107. doi: 10.1109/JSTARS.2014.2329330

Choi, H., and Jin, K. H. (2018). Predicting cognitive decline with deep learning of brain metabolism and amyloid imaging. *Behav. Brain Res.* 344, 103–109. doi: 10.1016/j.bbr.2018.02.017

Dabrowska, M., Schinwelski, M., Sitek, E. J., Muraszko-Klaudel, A., Brockhuis, B., Jamrozik, Z., et al. (2015). The role of neuroimaging in the diagnosis of the atypical parkinsonian syndromes in clinical practice. *Neurol. Neurochir. Pol.* 49, 421–431. doi: 10.1016/j.pjnns.2015.10.002

Eckert, T., Barnes, A., Dhawan, V., Frucht, S., Gordon, M. F., Feigin, A. S., et al. (2005). FDG PET in the differential diagnosis of parkinsonian disorders. *Neuroimage* 26, 912–921. doi: 10.1016/j.neuroimage.2005.03.012

Fischer, A., and Igel, C. (2012). "An introduction to restricted Boltzmann machines," in *Iberoamerican Congress on Pattern Recognition* (Buenos Aires). doi: 10.1007/978-3-642-33275-3_2

Fung, G., and Stoeckel, J. (2007). SVM feature selection for classification of SPECT images of Alzheimer's disease using spatial information. *Knowled. Inform. Syst.* 11, 243–258. doi: 10.1007/s10115-006-0043-5

Garraux, G., Phillips, C., Schrouff, J., Kreisler, A., Lemaire, C., Degueldre, C., et al. (2013). Multiclass classification of FDG PET scans for the distinction between Parkinson's disease and atypical parkinsonian syndromes ⋆⋆. *Neuroimage Clin.* 2, 883–893. doi: 10.1016/j.nicl.2013.06.004

Halkias, X., Paris, S., and Glotin, H. (2013). Sparse penalty in deep belief networks: using the mixed norm constraint. *Comput Sci.* Available online at: http://arxiv.org/abs/1301.3533

Hinton, G. E., Osindero, S., and Teh, Y. W. (2006). A fast learning algorithm for deep belief nets. *Neural Comput.* 18, 1527–1554. doi: 10.1162/neco.2006.18.7.1527

Hoyer, P. O. (2004). Non-negative matrix factorization with sparseness constraints. *J. Mach. Learn. Res.* 5, 1457–1469. doi: 10.1016/j.neucom.2011.09.024

Ji, N. N., Zhang, J. S., and Zhang, C. X. (2014). A sparse-response deep belief network based on rate distortion theory. *Pattern Recognit.* 47, 3179–3191. doi: 10.1016/j.patcog.2014.03.025

Jian, W., Cai, Q., Chang, Q., and Zurada, J. M. (2017). Convergence analyses on sparse feedforward neural networks via group lasso regularization ⋆. *Inform. Sci. Int. J.* 381, 250–269. doi: 10.1016/j.ins.2016.11.020

Juh, R., Kim, J., Moon, D., Choe, B., and Suh, T. (2004). Different metabolic patterns analysis of Parkinsonism on the 18F-FDG PET. *Eur. J. Radiol.* 51, 223–233. doi: 10.1016/S0720-048X(03)00214-6

Kayo, O. (2006). Locally linear embedding algorithm – Extensions and applications. *Value Eng.* Available online at: http://jultika.oulu.fi/Record/isbn951-42-8041-5

Keyvanrad, M. A., and Homayounpour, M. M. (2017). Effective sparsity control in deep belief networks using normal regularization term. *Knowl. Inf. Syst.* 53, 533–550. doi: 10.1007/s10115-017-1049-x

Lee, H., Ekanadham, C., and Ng, A. Y. (2007). "Sparse deep belief net model for visual area V2," in *International Conference on Neural Information Processing Systems* (Vancouver, BC). doi: 10.1.1.87.2404&rep=rep1&type=pdf

Liu, X., Peng, C., Yang, J., Zhao, D., and Zaiane, O. (2017). "Group guided sparse group lasso multi-task learning for cognitive performance prediction of Alzheimer?s disease," in International Conference on Brain Informatics (Beijing). doi: 10.1007/978-3-319-70772-3_19

Liu, X., Tosun, D., Weiner, M. W., Schuff, N., and Alzheimer's Disease Neuroimaging, I. (2013). Locally linear embedding (LLE) for MRI based Alzheimer's disease classification. *Neuroimage* 83, 148–157. doi: 10.1016/j.neuroimage.2013.06.033

Liu, Y., Zhou, S., and Chen, Q. (2011). Discriminative deep belief networks for visual data classification. *Pattern Recognit.* 44, 2287–2296. doi: 10.1016/j.patcog.2010.12.012

Lü, R., Guan, X., Li, X., and Hwang, I. (2016). A large-scale flight multi-objective assignment approach based on multi-island parallel evolution algorithm with cooperative coevolutionary. *Sci. China Inform. Sci.* 59:072201. doi: 10.1007/s11432-015-5495-3

Luo, H., Shen, R., and Niu, C. (2010). Sparse group restricted boltzmann machines. *Statistics*. Available online at: https://arxiv.org/pdf/1008.4988.pdf

Matthews, D. C., Hedva, L., Ana, L., Andrews, R. D., Anat, M., Wernick, M. N., et al. (2018). FDG PET Parkinson's disease-related pattern as a biomarker for clinical trials in early stage disease. *NeuroImage Clin.* 20, 572–579. doi: 10.1016/j.nicl.2018.08.006

Mei, X., Yong, M., Fan, F., Chang, L., Liu, C., Huang, J., et al. (2015). Infrared ultraspectral signature classification based on a restricted Boltzmann machine with sparse and prior constraints. *Int. J. Remote Sens.* 36, 4724–4747. doi: 10.1080/01431161.2015.1079664

Meles, S. K., Teune, L. K., De Jong, B. M., Dierckx, R. A., and Leenders, K. L. (2017). Metabolic imaging in parkinson disease. *J. Nucl. Med. Off. Public. Soc. Nuclear Med.* 58, 23–28. doi: 10.2967/jnumed.116.183152

Meyer, P. T., Frings, L., Rucker, G., and Hellwig, S. (2017). (18)F-FDG PET in parkinsonism: differential diagnosis and evaluation of cognitive impairment. *J. Nucl. Med.* 58, 1888–1898. doi: 10.2967/jnumed.116.186403

Politis, M., Pagano, G., and Niccolini, F. (2017). Imaging in Parkinson's Disease. *Int. Rev. Neurobiol.* 132:233–274. doi: 10.1016/bs.irn.2017.02.015

Postuma, R. B., and Berg, D. (2017). The new diagnostic criteria for parkinson's disease. *Int. Rev. Neurobiol.* 132, 55–78. doi: 10.1016/bs.irn.2017.01.008

Prasetio, M. D., Hayashida, T., Nishizaki, I., and Sekizaki, S. (2018). "Deep belief network optimization in speech recognition," in *International Conference on Sustainable Information Engineering and Technology* (Malang). doi: 10.1109/SIET.2017.8304124

Rana, B., Juneja, A., Saxena, M., Gudwani, S., Senthil Kumaran, S., Agrawal, R. K., et al. (2015). Regions-of-interest based automated diagnosis of Parkinson's disease using T1-weighted MRI. *Expert Syst. Appl.* 42, 4506–4516. doi: 10.1016/j.eswa.2015.01.062

Ranzato, M., Boureau, Y. L., and Lecun, Y. (2007). "Sparse feature learning for deep belief networks," in *International Conference on Neural Information Processing Systems* (Vancouver, BC). Available online at: https://dl.acm.org/citation.cfm?id=2981672

Rao, N. S., Nowak, R., Cox, C., and Rogers, T. (2015). Classification with the Sparse Group Lasso. *IEEE Transac. Signal Process.* 64, 448–463. doi: 10.1109/TSP.2015.2488586

Roweis, S. T., and Saul, L. K. (2000). Nonlinear dimensionality reduction by locally linear embedding. *Science* 290, 2323–2326. doi: 10.1126/science.290.5500.2323

Rui, X., and Yang, L. (2017). A multi-task learning framework for emotion recognition using 2D continuous space. *IEEE Transact. Affect. Comput.* 8, 3–14. doi: 10.1109/TAFFC.2015.2512598

Siqi, L., Sidong, L., Weidong, C., Hangyu, C., Sonia, P., Ron, K., et al. (2015). Multimodal neuroimaging feature learning for multiclass diagnosis of Alzheimer's disease. *IEEE Transac. Biomed. Eng.* 62, 1132–1140. doi: 10.1109/TBME.2014.2372011

Suk, H. I., Lee, S. W., Shen, D., and Initiative, T. (2015). Latent feature representation with stacked auto-encoder for AD/MCI diagnosis. *Brain Struct. Func.* 220, 841–859. doi: 10.1007/s00429-013-0687-3

Tang, C. C., Poston, K. L., Eckert, T., and Feigin, A. (2010). Differential diagnosis of parkinsonism: a metabolic imaging study using pattern analysis. *Lancet Neurol.* 9, 130–131. doi: 10.1016/S1474-4422(10)70002-8

Tripathi, M., Tang, C. C., Feigin, A., Lucia, I. D., Nazem, A., Dhawan, V., et al. (2015). Automated differential diagnosis of early parkinsonism using metabolic brain networks: a validation study. *J. Nuclear Med.* 57, 60–66. doi: 10.2967/jnumed.115.161992

Xin, G., De-Chuan, Z., and Zhi-Hua, Z. (2005). Supervised nonlinear dimensionality reduction for visualization and classification. *IEEE Transac. Syst. Man Cybernet. Part B Cybernet. Publicat. IEEE Syst. Man Cybernet. Soc.* 35, 1098–1107. doi: 10.1109/TSMCB.2005.850151

Xu, Y., Li, B. B., and Song, W. (2018). Research on improved deep belief network classification algorithm. *J. Front. Comput. Sci. Technol.* 13, 596–607. doi: 10.3778/j.issn.1673-9418.1804002

Yoshida, Y., and Miyato, T. (2017). Spectral norm regularization for improving the generalizability of deep learning. Available online at: https://arxiv.org/pdf/1705.10941.pdf

Yuan, L., Yu, L., Yi, Z., and Yue, C. (2018). Speech bottleneck feature extraction method based on overlapping group lasso sparse deep neural network. *Speech Commun.* 99, 56–61. doi: 10.1016/j.specom.2018.02.005

Zheng, W. L., and Lu, B. L. (2017). Investigating critical frequency bands and channels for EEG-based emotion recognition with deep neural networks. *IEEE Trans. Auton. Ment. Dev.* 7, 162–175. doi: 10.1109/TAMD.2015.2431497

Conflict of Interest Statement: The authors declare that the research was conducted in the absence of any commercial or financial relationships that could be construed as a potential conflict of interest.

frontiers in Aging Neuroscience

ORIGINAL RESEARCH
published: 27 May 2019
doi: 10.3389/fnagi.2019.00106

Regional High Iron in the Substantia Nigra Differentiates Parkinson's Disease Patients From Healthy Controls

Kiarash Ghassaban[1†], Naying He[2†], Sean Kumar Sethi[3], Pei Huang[4], Shengdi Chen[4], Fuhua Yan[2] and Ewart Mark Haacke[1,2,3]*

[1] Department of Radiology, Wayne State University, Detroit, MI, United States, [2] Department of Radiology, Ruijin Hospital, Shanghai Jiao Tong University School of Medicine, Shanghai, China, [3] Magnetic Resonance Innovations, Inc., Bingham Farms, MI, United States, [4] Department of Neurology & Institute of Neurology, Ruijin Hospital, Shanghai Jiao Tong University School of Medicine, Shanghai, China

OPEN ACCESS

Edited by:
Xun Chen,
University of Science and Technology of China, China

Reviewed by:
Sabina Capellari,
University of Bologna, Italy
Cathy W. Levenson,
Florida State University, United States

***Correspondence:**
Fuhua Yan
yfh11655@rjh.com.cn

[†] These authors have contributed equally to this work

Received: 30 January 2019
Accepted: 23 April 2019
Published: 27 May 2019

Citation:
Ghassaban K, He N, Sethi SK, Huang P, Chen S, Yan F and Haacke EM (2019) Regional High Iron in the Substantia Nigra Differentiates Parkinson's Disease Patients From Healthy Controls. Front. Aging Neurosci. 11:106. doi: 10.3389/fnagi.2019.00106

Background: Iron is important in the pathophysiology of Parkinson's disease (PD) specifically related to degeneration of the substantia nigra (SN). Magnetic resonance imaging (MRI) can be used to measure brain iron in the entire structure but this approach is insensitive to regional changes in iron content.

Objective: The goal of this work was to use quantitative susceptibility mapping (QSM) and R2* to quantify both global and regional brain iron in PD patients and healthy controls (HC) to ascertain if regional changes correlate with clinical conditions and can be used to discriminate patients from controls.

Methods: Susceptibility and R2* maps of 25 PD and 24 HC subjects were reconstructed from data collected on a 3T GE scanner. For the susceptibility maps, three-dimensional regions-of-interest (ROIs) were traced on eight deep gray matter (DGM) structures and an age-based threshold was applied to define regions of high iron content. The same multi-slice ROIs were duplicated on the R2* maps as well. Mean susceptibility values of both global and regional high iron (RII) content along with global R2* values were measured and compared not only between the two cohorts, but also to susceptibility and R2* baselines as a function of age. Finally, clinical features were compared for those PD patients lying above and below the upper 95% regional susceptibility-age prediction intervals.

Results: The SN was the only structure showing significantly higher susceptibility in PD patients compared to controls globally ($p < 0.01$) and regionally ($p < 0.001$). The R2* values were also higher only in the SN of PD patients compared to the healthy cohort ($p < 0.05$). Furthermore, those patients with abnormal susceptibility values lying above the upper 95% prediction intervals had significantly higher united Parkinson's diagnostic

rating scores. R2* values had larger errors and showed larger dispersion as a function of age than QSM data for global analysis while the dispersion was significantly less for QSM using the RII iron content.

Conclusion: Abnormal iron deposition in the SN, especially in RII areas, could serve as a biomarker to distinguish PD patients from HC and to assess disease severity.

Keywords: brain, iron, magnetic resonance imaging, Parkinson's disease, substantia nigra, deep gray matter, quantitative susceptibility mapping, relaxometry

INTRODUCTION

Parkinson's disease (PD) is believed to be the second most common neurodegenerative disease in developed countries (Shulman and De Jager, 2009). Research has shown that the substantia nigra (SN) is one of the most important structures playing a vital role in the pathophysiology of PD patients (Ghassaban et al., 2018). Neuronal loss and lack of dopamine content in this midbrain nucleus generally lead to movement disorders in these patients (Wang et al., 2016; Martin-Bastida et al., 2017). The loss of neuromelanin in particular has been thought to lead to an increase in iron content in the SN which has been implicated in a number of PD studies (Castellanos et al., 2015; Huddleston et al., 2017; Langley et al., 2017). In fact, the SN seems to be the only reliable brain structure through which a meaningful relationship with neuronal loss has been found (Ghassaban et al., 2018). Since the onset of PD is generally late and brain iron levels tend to increase as a function of age in deep gray matter (DGM) structures even under normal conditions, (Hallgren and Sourander, 1958; Li et al., 2014; Liu et al., 2016) it is important to account for these age-dependent changes (Acosta-Cabronero et al., 2017).

A number of magnetic resonance imaging (MRI) techniques can be used to quantify iron content in the human body. Conventionally, R2 and R2* relaxation rate mapping along with phase information have been utilized to measure iron deposition in different regions of the human body *in vivo* (Ghassaban et al., 2018). However, one of the most popular approaches today is the use of quantitative susceptibility mapping (QSM); a post-processing technique that generates susceptibility maps using phase information and, unlike other conventional quantification techniques, is independent of imaging parameters such as geometry, echo time, spatial resolution, field strength, and signal-to-noise ratio (SNR) (Haacke et al., 2015). QSM also appears to have the greatest reliability and robustness compared to other MR-based *in vivo* methods (Haacke et al., 2015; Du et al., 2016; Langkammer et al., 2016). Specifically, in terms of consistency, QSM has been shown to have high repeatability and less variability compared to R2* (Feng et al., 2018).

Liu et al. (2016) investigated a cohort of 174 healthy adults using QSM with the purpose of assessing the effects of normal aging on the iron levels in seven DGM structures. In addition to their evaluation of mean susceptibility from the entire 3D region covered by each nucleus as a function of age (also known as the global analysis) in the basal ganglia and midbrain, they introduced a new age- and structure-dependent high iron susceptibility-age baseline (also known as the regional analysis). The regional analysis appeared to be more robust and sensitive to age-related changes compared to the global analysis (Liu et al., 2016). Furthermore, by applying the same methodology, Ghassaban et al. (2018) established the global and regional susceptibility-age baselines for the dentate nucleus using 81 healthy adults. Therefore, we hypothesized that this regional analysis may also be more sensitive to changes in iron for PD patients.

In this study, using QSM and R2* techniques, we compare the iron content in the DGM structures between a cohort of PD patients and a group of healthy controls (HC). Additionally, using QSM maps we investigate the iron deposition rates of PD patients compared to the corresponding global and regional normal baselines established by Liu et al. (2016) and Ghassaban et al. (2018) Similarly, R2* maps are used to compare global measurements to those of the healthy population established by Li et al. (2014). Also, susceptibility measurements in terms of increased iron deposition are compared to the clinical status of PD patients. Finally, the QSM data are compared directly to the R2* across the different DGM nuclei using the HC data. This study could potentially pave the way for developing future iron-based diagnostic studies and better understanding the etiology of PD.

MATERIALS AND METHODS

Data Collection

This study was approved by the local ethics committee at Ruijin Hospital and all subjects signed consent forms. A total of 49 subjects were evaluated: 25 PD patients (61.8 ± 6.4 years old) and 24 HC subjects (63.4 ± 8.0 years old). All of the PD patients were recruited from local movement disorder clinics. The inclusion criteria were: (1) a diagnosis of idiopathic PD, (2) Mini-Mental State Exam (MMSE) score equal to or more than 24, and (3) Hoehn and Yahr (H&Y) scale of one through three as patients with higher scores had more severe symptoms and would have trouble staying still in the magnet for the duration of the scans. The exclusion criteria were: (1) symptoms of secondary or atypical parkinsonism, or (2) a history of cerebrovascular disease, seizures, brain surgery, brain tumor, moderate-to-severe head trauma, or hydrocephalus, or (3) treatment with antipsychotic drugs or with any other drug possibly affecting clinical evaluation. Data were collected using a 16 echo, gradient echo imaging sequence on a 3T GE Signa HDxt

from an eight-channel receive-only head coil with the following imaging parameters: TE1 = 2.69 ms with ΔTE = 2.87 ms, TR = 59.3 ms, pixel bandwidth = 488 Hz/pixel, flip angle = 12°, slice thickness = 1 mm, matrix size = 256 × 256, and an in-plane resolution of 0.86 × 0.86 mm^2.

Data Processing

QSM Processing

The susceptibility maps were created using the first eight echoes and were reconstructed for each echo individually using SMART v2.0 (MRI Institute for Biomedical Research, Bingham Farms, MI, United States) followed by a weighted average of the resultant QSM images based on their SNRs. Only 8 echoes were used because of severe frontal signal loss at echo times longer than roughly 20 ms. The reconstruction steps included the brain extraction tool (BET) to segment only the brain tissue using the fourth echo magnitude data,(Smith, 2002) quality guided 3D phase unwrapping algorithm (3DSRNCP) for phase unwrapping, (Abdul-Rahman et al., 2007) sophisticated harmonic artifact reduction for phase data (SHARP) for background field removal with a threshold of 0.05 and a deconvolution kernel of 6, (Schweser et al., 2011) and a truncated k-space division (TKD) approach (threshold = 0.1) referred to as susceptibility weighted imaging and mapping (SWIM) for inverse filtering (Haacke et al., 2010). The DGM nuclei included in this study were: the head of the caudate nucleus (CN), putamen (PUT), globus pallidus (GP), thalamus (THA), pulvinar thalamus (PT), red nucleus (RN), SN, and dentate nucleus (DN). Multi-slice 3D regions-of-interest (ROI) representing these structures were manually traced on QSM slices using SPIN (Signal Processing in NMR, SpinTech, Inc., Bingham Farms, MI, United States) by the first author (KG) with more than 5 years of relevant experience. Original magnitude and phase images were used as references to ensure accurate boundary drawings. An illustration of the 3D ROIs is given in **Figure 1**. Mean susceptibility values from the entire structures of both cohorts were then extracted and plotted as a function of age, also known as the global analysis. Similar to Liu et al.'s (2016) work, age-dependent susceptibility values were chosen as thresholds from the upper 95% prediction intervals based on their global analysis of 174 controls from which regional high iron (RII) content voxels were then estimated for a given structure at a given age for all the nuclei except the DN. For the DN, a similar process was performed on the global analysis established by Ghassaban et al.'s (2018) study from 81 healthy adults. Similarly, mean susceptibilities of the RII regions were calculated and plotted as a function of age, also known as the regional analysis. The global and regional analyses of both PD

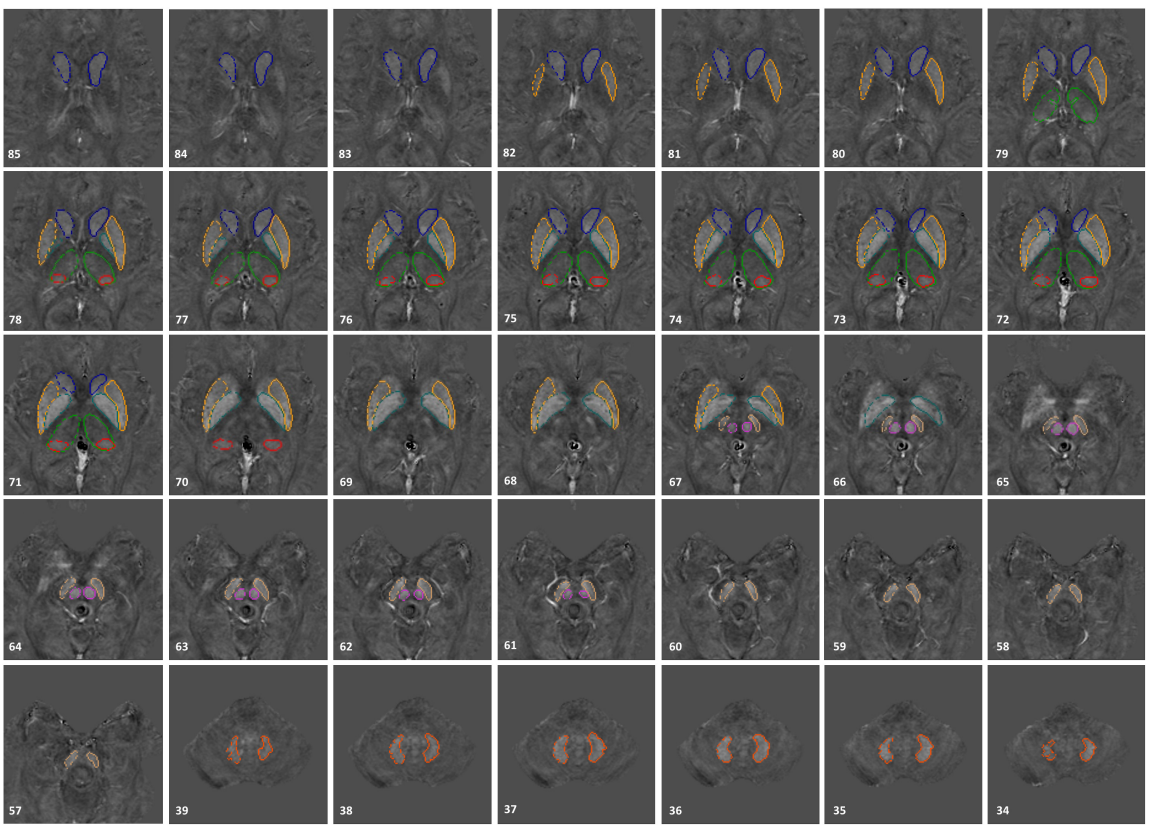

FIGURE 1 | 3D regions of interest (ROIs) traced on susceptibility maps of a 65-year-old male. Structures include the head of caudate nucleus (CN), globus pallidus (GP), putamen (PUT), thalamus (THA), pulvinar thalamus (PT), red nucleus (RN), substantia nigra (SN), and dentate nucleus (DN). The numbers in the lower left corner represent the slice numbers from 132 slices collected in this example.

and HC cohorts were then superimposed on the corresponding plots introduced by Liu et al. (2016) and Ghassaban et al. (2018). Additionally, the average values were compared for both global and RII susceptibilities between the PD and HC cohorts in both hemispheres and in all DGM nuclei.

R2* Processing

The R2* maps were also reconstructed using the first eight echoes through a pixel-by-pixel fit to an exponential curve. The exact same 3D ROIs traced on the QSM maps were also used on R2* maps. Similar to QSM data analysis, mean R2* values were extracted from each structure and plotted as a function of age (i.e., global analysis). These values were then superimposed and visually compared to the corresponding R2*-age baselines established by Li et al. (2014) for six DGM structures including the CN, GP, PUT, RN, SN, and DN. For each structure the fitted exponential regression equation and 95% confidence intervals provided by Li et al. (2014) were used to predict the mean R2* values as a function of age for the normal population. Moreover, similar to the analysis done in QSM processing, R2* values of

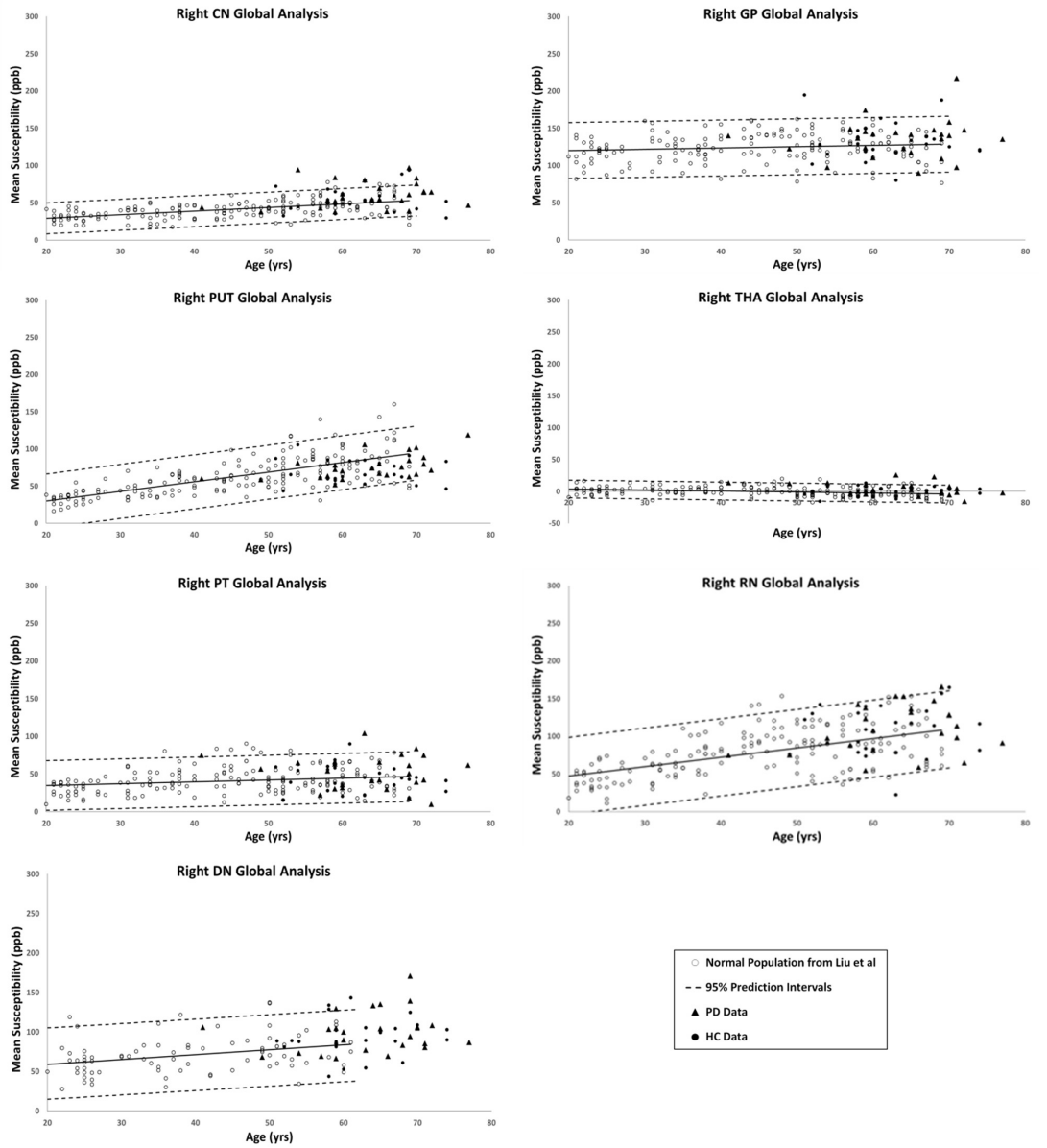

FIGURE 2 | Right hemisphere global analyses of HC and PD cohorts superimposed on the susceptibility-age baselines for different deep gray matter (DGM) structures published by Ghassaban et al. (2018) for the dentate nucleus and Liu et al. (2016) for the other six nuclei. CN, caudate nucleus; GP, globus pallidus; PUT, putamen; THA, thalamus; PT, pulvinar thalamus; RN, red nucleus; DN, dentate nucleus. Hollow circles, normal baselines; solid circles, HC data from this study; triangles, PD data from this study; solid lines, linear regression models associated with the normal population; dashed lines, 95% prediction intervals associated with the normal population.

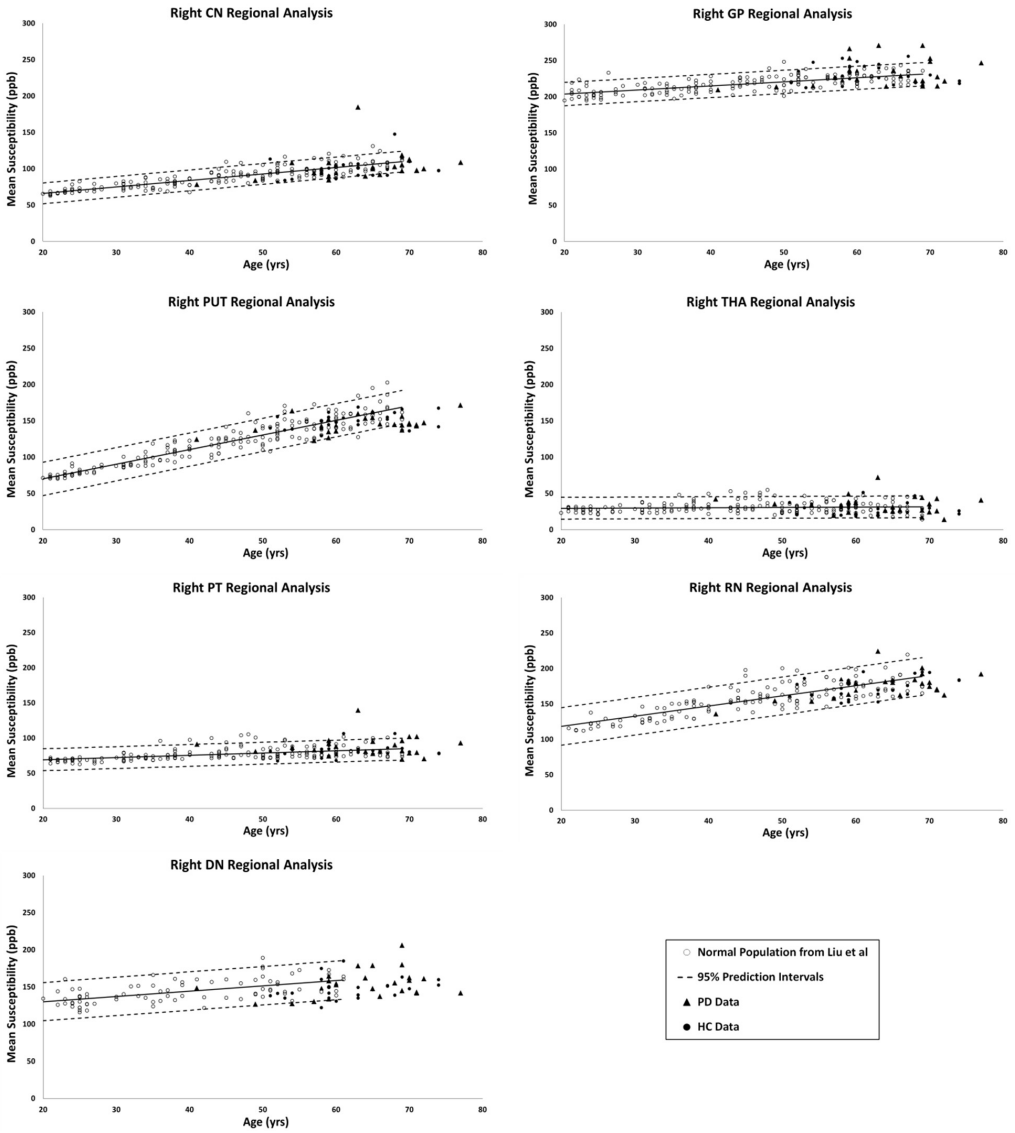

FIGURE 3 | Right hemisphere regional high iron (RII) analyses of HC and PD cohorts superimposed on the susceptibility-age baselines for different DGM structures published by Ghassaban et al. (2018) for the dentate nucleus and Liu et al. (2016) for the other six nuclei. CN, caudate nucleus; GP, globus pallidus; PUT, putamen; THA, thalamus; PT, pulvinar thalamus; RN, red nucleus; DN, dentate nucleus. Hollow circles, normal baselines; solid circles, HC data from this study; triangles, PD data from this study; solid lines, linear regression models associated with the normal population; dashed lines, 95% prediction intervals associated with the normal population.

both PD and HC cohorts were compared to each other in both hemispheres for all DGM structures.

Correlation Between Susceptibility and R2*

With both the QSM and R2* data available and in order to assess the relationship between these two parameters in the DGM structures, a linear regression model was fitted to the mean R2* as a function of mean susceptibility in all the nuclei. To avoid any sources of bias, only the healthy cohort was included for this correlation, the results of which were compared to those of Li et al.'s (2014) study.

Statistical Analysis

All statistical analyses were carried out using Microsoft Excel 2013 (Microsoft Corporation, Redmond, WA, United States) with a two-tailed significance level of 0.05. Two-sample *t*-test analyses were performed to compare the average global (for QSM and R2*) and regional (for QSM only) values of PD and HC cohorts in both hemispheres. Furthermore, paired sample *t*-tests were performed to compare susceptibility and R2* values between the left and right hemisphere of each DGM structure.

Additionally, a comparison between the mean susceptibility values of the SN and clinical status of the PD patients

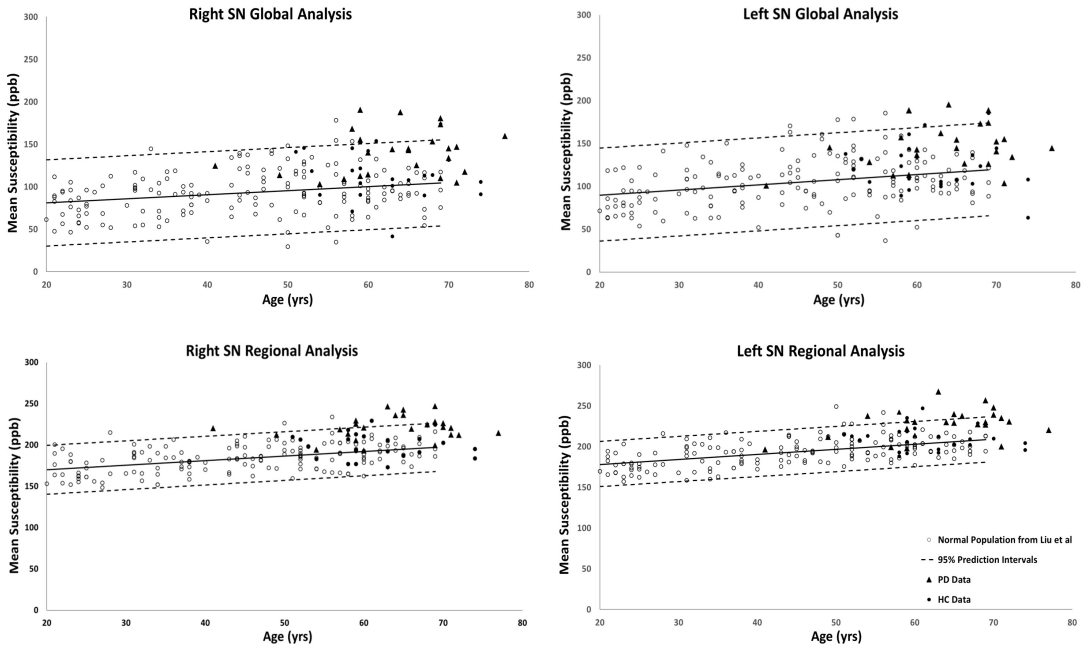

FIGURE 4 | Substantia nigra global (entire structure) and regional (RII high iron) analyses of HC and PD cohorts superimposed on the susceptibility-age baselines published by Liu et al. (2016). Hollow circles, normal baselines; solid circles, HC data from this study; triangles, PD data from this study; solid lines, linear regression models associated with the normal population; dashed lines, 95% prediction intervals associated with the normal population.

TABLE 1 | Two-sample *t*-test statistics comparing susceptibility means (ppb) of the global and regional analyses between the two cohorts in both hemispheres.

		Global analysis			RII analysis		
Hemisphere		**Right**	**Left**	***P*-value**	**Right**	**Left**	***P*-value**
CN	HC	54.6 ± 6.6	52.4 ± 7.6	0.27	99.1 ± 5.6	97.3 ± 6.1	0.32
	PD	59.3 ± 6.7	54.7 ± 6.9	0.16	102.0 ± 7.8	97.7 ± 8.6	**0.03**
	P-value	0.35	0.67	NA	0.56	0.95	NA
GP	HC	133.1 ± 10.1	127.8 ± 7.8	0.15	231.8 ± 5.2	231.1 ± 6.9	0.82
	PD	133.7 ± 10.0	127.6 ± 9.9	0.11	232.3 ± 7.2	231.6 ± 7.9	0.86
	P-value	0.94	0.97	NA	0.92	0.92	NA
PUT	HC	68.7 ± 6.4	72.8 ± 7.0	0.25	150.5 ± 4.3	144.9 ± 5.0	0.08
	PD	75.8 ± 6.6	73.6 ± 7.8	0.32	145.1 ± 4.8	142.1 ± 6.1	0.12
	P-value	0.15	0.87	NA	0.19	0.10	NA
THA	HC	2.3 ± 2.8	2.8 ± 2.9	0.71	30.2 ± 3.2	36.5 ± 3.0	**<0.001**
	PD	3.1 ± 3.7	2.2 ± 3.7	0.59	33.3 ± 4.8	36.8 ± 3.8	**<0.001**
	P-value	0.24	0.66	NA	0.30	0.88	NA
PT	HC	45.3 ± 7.0	45.6 ± 6.9	0.90	83.3 ± 3.7	85.4 ± 2.8	0.10
	PD	51.8 ± 8.8	47.7 ± 7.2	0.12	87.5 ± 5.5	86.4 ± 4.7	0.45
	P-value	0.27	0.68	NA	0.22	0.74	NA
RN	HC	108.1 ± 13.0	102.9 ± 12.9	0.31	173.2 ± 5.4	177.5 ± 6.1	**0.03**
	PD	112.8 ± 13.1	112.2 ± 13.8	0.85	175.8 ± 6.8	179.3 ± 6.8	**0.01**
	P-value	0.61	0.36	NA	0.55	0.69	NA
SN	HC	115.4 ± 11.6	127.5 ± 10.8	**0.04**	200.1 ± 6.1	210.3 ± 5.7	**<0.001**
	PD	139.8 ± 10.4	147.5 ± 10.5	**0.01**	220.7 ± 5.6	234.7 ± 5.9	**<0.01**
	P-value	**< 0.01**	**< 0.01**	NA	**< 0.001**	**< 0.001**	NA
DN	HC	93.1 ± 9.7	95.3 ± 11.0	0.41	147.6 ± 5.4	155.9 ± 6.2	**<0.001**
	PD	99.4 ± 10.2	102.1 ± 10.8	0.41	153.7 ± 7.2	159.1 ± 7.4	**<0.01**
	P-value	0.38	0.39	NA	0.20	0.52	NA

Numbers are reported in Mean ± 95% confidence intervals. CN, caudate nucleus; GP, globus pallidus; PUT, putamen; THA, thalamus; PT, pulvinar thalamus; RN, red nucleus; SN, substantia nigra; DN, dentate nucleus. P-values in bold show significant differences between the means.

was performed. The parameters to which SN global and regional susceptibility values were compared included the unified Parkinson's disease rating scale part III (UPDRS-III) and H&Y scores as well as the disease duration.

Finally, the same clinical status parameters along with patients' ages were used to compare a sub-group of PD patients with abnormal RII susceptibility values [i.e., higher than the corresponding upper 95% prediction interval from the susceptibility-age baseline (Liu et al., 2016)] to another sub-group whose RII susceptibilities fall within the normal ranges of the baseline.

RESULTS

Figures 2, **3** show the QSM global and regional analyses for the right hemisphere of both groups, respectively, superimposed on the corresponding previously established normal populations. These susceptibility-age baselines were published by Ghassaban et al. (2018) (for the DN only) and Liu et al. (2016) (for the rest of the DGM structures). The SN is the only structure showing elevated susceptibility values in both global and regional analyses (see **Figure 4**).

The results of the two-sample and paired-sample *t*-tests comparing the susceptibility means of HC and PD cohorts within and between the two hemispheres of different DGM structures are summarized in **Table 1**. Only the SN showed significantly higher susceptibility values in PD patients when compared with the HC cohort, with the regional analysis (PD: 221 ± 14 ppb, HC: 200 ± 15 ppb, $p < 0.001$ for the right and PD: 235 ± 15 ppb, HC: 210 ± 15 ppb, $p < 0.001$ for the left hemisphere) revealing more prominent differences compared to those of the global analysis (PD: 140 ± 26 ppb, HC: 115 ± 29 ppb, $p < 0.01$ for the right and PD: 147 ± 27 ppb, HC: 127 ± 27 ppb, $p < 0.01$ for the left hemisphere). The SN was also the only structure showing significant differences between the two hemispheres in both cohorts using both global and regional analyses. On the other hand, in addition to the SN, significant differences were seen between the hemispheres in both PD and HC groups in the THA, RN, and DN only using the regional analysis. Among all affected nuclei, the left hemisphere showed significantly higher susceptibility values.

The relationship between mean global and regional susceptibility changes in the SN of PD patients and clinical status parameters (i.e., disease duration, H&Y and UPDRS-III scores) resulted in no significant correlations (all *p*-values > 0.05). However, as shown in **Table 2**, dividing the PD cohort in two sub-groups with normal and abnormal RII susceptibility values showed that there were significantly higher UPDRS-III scores in patients with elevated RII iron content ($p < 0.05$ in both hemispheres).

The global measurements of R2* values superimposed on the corresponding age-dependent baselines published by Li et al. (2014) resulted in no abnormal values with most of the

TABLE 2 | Comparison of clinical status between two sub-groups of the PD cohort with normal and abnormal RII iron content in the SN.

Hemisphere	Right			Left		
Group	Abnormal iron (*N* = 10)	Normal iron (*N* = 14)	*p*-value	Abnormal iron (*N* = 10)	Normal iron (*N* = 14)	*P*-value
Age (years)	62.5 ± 8.6	64.9 ± 7.8	0.51	63.9 ± 5.6	63.1 ± 9.7	0.80
Disease duration (years)	4.7 ± 2.8	3.8 ± 3.3	0.49	5.1 ± 3.4	3.4 ± 2.9	0.29
UPDRS-III	30.4 ± 14.3	17.8 ± 9.6	**0.03**	28.6 ± 12.9	16.6 ± 9.7	**0.03**
H&Y	1.8 ± 0.6	1.4 ± 0.5	0.17	2.0 ± 0.75	1.5 ± 0.55	0.10

Normal and abnormal sub-groups are separated based on RII susceptibility values lower and higher than the baseline upper 95% prediction intervals, respectively. P-values in bold show significant differences between the means.

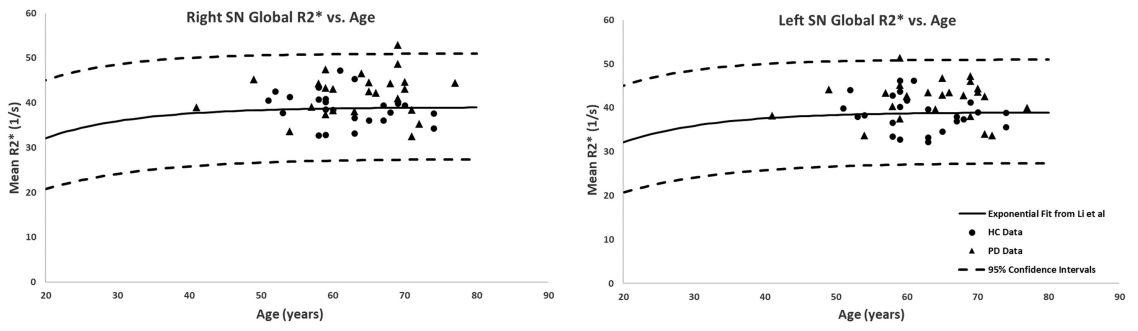

FIGURE 5 | Global analysis of the R2* measurements in the SN of PD patients and healthy adults superimposed on the corresponding R2*-age exponential fits provided by Li et al. (2014). Although most of the subjects fall within the 95% confidence intervals, the PD patients showed higher R2* values compared to those of the HC. Solid circles, HC data from this study; triangles, PD data from this study; solid lines, exponential regression models from the normal population (Li et al., 2014); dashed lines, 95% confidence intervals associated with the fitted curves.

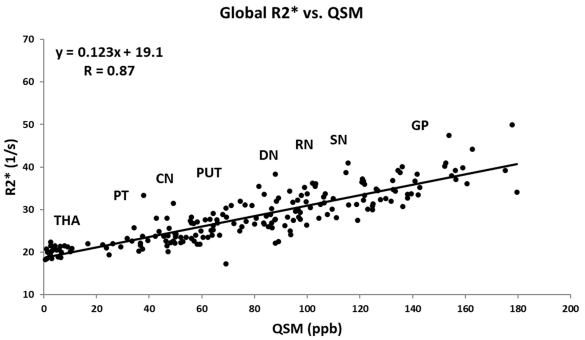

FIGURE 6 | Mean R2* as a function of mean QSM in deep gray matter nuclei of the HC group fitted by a linear regression model. The data points are the average means between the two hemispheres. Based on the estimated mean values, the labels show the approximate locations around which each structure falls. The regression parameters are shown on the plot. CN, caudate nucleus; GP, globus pallidus; PUT, putamen; THA, thalamus; PT, pulvinar thalamus; RN, red nucleus; DN, dentate nucleus. Solid circles, HC data from this study; solid line, linear regression fit.

means falling within the 95% confidence intervals. The only exception was the SN of the PD patients with R2* values slightly skewed upward but still most subjects were below the upper 95% confidence interval, as shown in **Figure 5**. Also, the two-sample *t*-tests between PD and HC cohorts revealed significant differences in the SN in both hemispheres (PD: 42 ± 4 s^{-1}, HC: 39 ± 4 s^{-1}, $p = 0.01$ for the right and PD: 43 ± 4 s^{-1}, HC: 39 ± 4 s^{-1}, $p = 0.01$ for the left hemisphere). The paired sample *t*-tests showed no significant differences between the hemispheres for any of the structures in either cohort.

Figure 6 shows the linear regression model fitted to the R2* values as a function of the corresponding QSM values for the HC group plotted for all the nuclei included in this study. The Pearson correlation coefficient (PCC) value of 0.87 is indicative of a strong linear relationship between these two parameters. Also, the linear slope of 0.123 s^{-1}/ppb is very close to the slope of 0.126 s^{-1}/ppb reported by Li et al. (2014).

DISCUSSION AND CONCLUSION

To date, there is no clear answer to the contributing factors in the pathogenesis of PD (Langkammer et al., 2016; Pietracupa et al., 2017). It is generally believed that the loss of neuromelanin content may initiate the process of increasing non-heme iron deposits in the midbrain which then leads to different forms of parkinsonism (Castellanos et al., 2015; Huddleston et al., 2017; Langley et al., 2017). On the other hand, there is also the hypothesis arguing that the depigmentation of the nigrosome-1 content in the posterolateral part of the SN might lead to the subsequent increase in iron deposition in this midbrain structure (Schwarz et al., 2018).

In this work, we have shown that there is an increase in iron in the SN over and above the normal increase due to age in PD patients. Although the average susceptibility value of the SN is seen to increase in the PD cohort, especially in the thresholded regions characterized by high iron content, we also note that there may, in fact, be two populations of PD patients, those that do not change iron content and those that do. For the abnormally high iron content group, there was a significantly higher UPDRS-III than the group showing normal iron content. Nevertheless, to draw a stronger conclusion will require investigating a considerably larger sample size.

The global and regional analyses in the SN of PD patients has previously been evaluated in Ghassaban et al. (2018) and Sethi et al. (2018) in which similar QSM reconstruction techniques were adopted using different scanners and field strengths. The regional analysis being more sensitive to local high iron content changes seen in the SN in this study is in accordance with their findings. This validates the consistency and reliability of using gradient echo imaging and the use of the threshold-based QSM reconstruction for data from different MR manufacturers' systems.

The comparison between the two hemispheres revealed significantly higher iron deposition in the left hemispheres of both PD and HC cohorts in the THA, RN, SN, and DN in the regional (RII) analysis and only in the SN for the global analysis. However, the largest effects in terms of absolute shifts in susceptibility were seen in the SN where the differences were on the order of 20 ppb compared to all other cases where the differences are on the order of less than 8 ppb. This is consistent with Liu et al.'s (2016) study where they showed that, except in the SN, small but significant differences between the hemispheres of all DGM structures would vanish if other sources of error (in their case excluding one slice from the top and/or bottom of the structures or changing the definition of RII from upper 95 to 99% prediction interval of the global analysis) were taken into account when measuring the susceptibility values. However, simulation results for the SN show that QSM has a systematic error of roughly 12 ppb in the SN due to streaking artifacts generated by the QSM reconstruction (Haacke et al., 2015). Additionally, low spatial frequency undulations seen in QSM techniques could also lead to asymmetry in the brain (Haacke et al., 2015). Therefore, by taking into consideration all these sources of systematic error, the asymmetries seen in the SN may disappear as well. Another QSM study in which lateral asymmetry was found in the SN of PD patients was done by Azuma et al. (2016) where the mean susceptibility was seen to be significantly higher in the more affected hemisphere compared to that of the less affected hemisphere although they had much larger errors compared to our data due in part to the distribution of iron and the small sample size. They also do not account for the other sources of systematic error mentioned above which may again remove any remaining small differences between left and right values of iron in the SN.

Evaluating R2* maps led to two major findings: first, in accordance with the literature, iron content characterized by R2* values was seen to be higher in the SN of PD patients compared to the healthy group. Second, even though these differences were statistically significant, considerably lower *p*-values from QSM results (both between the two groups and between the hemispheres within each group) showed higher sensitivity and

reliability of susceptibility-based techniques to pick up more subtle changes in brain iron. Additionally, the error analysis from both of these iron quantification techniques reveals that the variability of measurements associated with QSM is considerably less compared to that of R2* (Feng et al., 2018), especially in the high iron content (RII) region. Despite the fact that R2* correlates well with QSM measures of iron content, R2* measurements (especially from a limited number of echo times) is more prone to noise. One major advantage of QSM is that it is in theory independent of echo time, but the SNR of the R2* maps depends critically on the echo time (Haacke et al., 2015). Practically an echo time of roughly 20 ms is enough to give excellent susceptibility maps and in this case with 8 echoes excellent measurements of the DGM is possible.

Another key finding in this work that validates previous results is the tightness (higher r^2-values) of the iron growth with age in the different DGM structures in the regional iron content measures. The fact that regional changes are much tighter than global changes opens the door to a better separation of patient types, specifically in terms of separating high iron content patients from normal iron content patients. Averaging over all patients, especially in the global analysis, will reduce the shift in the mean iron content and may be the reason that some of the previous studies failed to show increased iron content in the SN (Yan et al., 2018). RII iron content may provide a new means to evaluate the role of regional changes in iron deposition. For example, it is believed that the loss of neuromelanin in the nigrosome-1 territory of the SN pars compacta leaves behind MR-visible iron (Zecca et al., 2004). Localizing where this high iron content occurs anatomically may help to answer this question.

Further, in this work, the ability to separate the high and normal RII iron content patients using QSM data led to the finding that there are in fact group differences in UPDRS-III scores. Similarly, by using R2*, Pesch et al. (2019) found a correlation between iron content and UPDRS-III scores in the SN of 35 PD patients. However, their R2* measurements were not corrected for age. Since R2* has been seen to increase as a function of normal aging, (Li et al., 2014) it is imperative to take this factor into account in iron quantification studies.

There are a number of limitations to this study. First, the number of samples is small and a much larger population should be studied to best demonstrate the presence of two groups of PD patients. Second, no clinical phenotypes were taken into consideration while analyzing imaging data. Third, ROI tracings were done manually which might have induced some unwanted errors when demarcating different DGM nuclei especially around the edges of the structures; this source of error, however, gets substantially reduced when thresholded low susceptibility values are excluded in the regional analysis. Nonetheless, the undesired errors associated with manual ROI tracing in the global analysis could be effectively minimized by using atlas-based automated DGM segmentation techniques (Li et al., 2019). Finally, the fairly low in-plane resolution used in the GRE sequence made it difficult to evaluate the sub-structures, especially the SN pars compacta whose abnormally high iron deposition is believed to be correlated with neuromelanin degeneration in the midbrain (Castellanos et al., 2015; Huddleston et al., 2017; Langley et al., 2017). Higher spatial resolution is recommended in future studies for this purpose.

In conclusion, the increase in iron in the SN in some PD patients is higher than the normal range in HC as found in both regional and global analyses. Using RII content may provide a means to separate two populations of PD patients; one with and one without iron increases in the SN. Separating the PD population into two groups may prove useful in understanding the etiology of the disease as well as monitoring the disease progression.

ETHICS STATEMENT

This study was carried out in accordance with the recommendations of the "ethics committee of Ruijin Hospital, Shanghai Jiao Tong University School of Medicine, Shanghai, China" with written informed consent from all subjects. All subjects gave written informed consent in accordance with the Declaration of Helsinki. The protocol was approved by the "ethics committee of Ruijin Hospital, Shanghai Jiao Tong University School of Medicine, Shanghai, China."

AUTHOR CONTRIBUTIONS

NH, FY, EMH, PH, and SC conceived the research project. NH, EMH, and FY organized the research project. KG and NH executed the research project. KG and SKS designed the statistical analysis. KG and SKS executed the statistical analysis. NH and EMH critically reviewed the statistical analysis. KG wrote the first draft of the manuscript. NH and EMH critically reviewed the manuscript.

FUNDING

This work was supported in part by a grant from the Science and Technology Commission of Shanghai Municipality (17411952700) for FY and NH, and a grant from the Shanghai Sailing Program (18YF1414700), and National Natural Science Fund (81801652) for NH.

REFERENCES

Abdul-Rahman, H. S., Gdeisat, M. A., Burton, D. R., Lalor, M. J., Lilley, F., and Moore, C. J. (2007). Fast and robust three-dimensional best path phase unwrapping algorithm. *Appl. Opt.* 46, 6623–6635.

Acosta-Cabronero, J., Cardenas-Blanco, A., Betts, M. J., Butryn, M., Valdes-Herrera, J. P., Galazky, I., et al. (2017). The whole-brain pattern of magnetic susceptibility perturbations in Parkinson's disease. *Brain* 140, 118–131. doi: 10.1093/brain/aww278

Azuma, M., Hirai, T., Yamada, K., Yamashita, S., Ando, Y., Tateishi, M., et al. (2016). Lateral asymmetry and spatial difference of iron deposition in the substantia nigra of patients with parkinson disease measured with quantitative susceptibility mapping. *AJNR Am. J. Neuroradiol.* 37, 782–788. doi: 10.3174/ajnr.A4645

Castellanos, G., Fernandez-Seara, M. A., Lorenzo-Betancor, O., Ortega-Cubero, S., Puigvert, M., Uranga, J., et al. (2015). Automated neuromelanin imaging as a diagnostic biomarker for Parkinson's disease. *Mov. Disord.* 30, 945–952. doi: 10.1002/mds.26201

Du, G., Liu, T., Lewis, M. M., Kong, L., Wang, Y., Connor, J., et al. (2016). Quantitative susceptibility mapping of the midbrain in Parkinson's disease. *Mov. Disord.* 31, 317–324. doi: 10.1002/mds.26417

Feng, X., Deistung, A., and Reichenbach, J. R. (2018). Quantitative susceptibility mapping (QSM) and R2(*) in the human brain at 3T: evaluation of intra-scanner repeatability. *Z. Med. Phys.* 28, 36–48. doi: 10.1016/j.zemedi.2017.05.003

Ghassaban, K., Liu, S., Jiang, C., and Haacke, E. M. (2018). Quantifying iron content in magnetic resonance imaging. *Neuroimage* 187, 77–92. doi: 10.1016/j.neuroimage.2018.04.047

Haacke, E. M., Liu, S., Buch, S., Zheng, W., Wu, D., and Ye, Y. (2015). Quantitative susceptibility mapping: current status and future directions. *Magn. Reson. Imaging* 33, 1–25. doi: 10.1016/j.mri.2014.09.004

Haacke, E. M., Tang, J., Neelavalli, J., and Cheng, Y. C. (2010). Susceptibility mapping as a means to visualize veins and quantify oxygen saturation. *J. Magn. Reson. Imaging* 32, 663–676. doi: 10.1002/jmri.22276

Hallgren, B., and Sourander, P. (1958). The effect of age on the non-haemin iron in the human brain. *J. Neurochem.* 3, 41–51.

Huddleston, D. E., Langley, J., Sedlacik, J., Boelmans, K., Factor, S. A., and Hu, X. P. (2017). In vivo detection of lateral-ventral tier nigral degeneration in Parkinson's disease. *Hum. Brain Mapp.* 38, 2627–2634. doi: 10.1002/hbm.23547

Langkammer, C., Pirpamer, L., Seiler, S., Deistung, A., Schweser, F., Franthal, S., et al. (2016). Quantitative susceptibility mapping in Parkinson's disease. *PLoS One* 11:e0162460. doi: 10.1371/journal.pone.0162460

Langley, J., Huddleston, D. E., Sedlacik, J., Boelmans, K., and Hu, X. P. (2017). Parkinson's disease-related increase of T2*-weighted hypointensity in substantia nigra pars compacta. *Mov. Disord.* 32, 441–449. doi: 10.1002/mds.26883

Li, W., Wu, B., Batrachenko, A., Bancroft-Wu, V., Morey, R. A., Shashi, V., et al. (2014). Differential developmental trajectories of magnetic susceptibility in human brain gray and white matter over the lifespan. *Hum. Brain Mapp.* 35, 2698–2713. doi: 10.1002/hbm.22360

Li, X., Chen, L., Kutten, K., Ceritoglu, C., Li, Y., Kang, N., et al. (2019). Multi-atlas tool for automated segmentation of brain gray matter nuclei and quantification of their magnetic susceptibility. *Neuroimage* 191, 337–349. doi: 10.1016/j.neuroimage.2019.02.016

Liu, M., Liu, S., Ghassaban, K., Zheng, W., Dicicco, D., Miao, Y., et al. (2016). Assessing global and regional iron content in deep gray matter as a function of age using susceptibility mapping. *J. Magn. Reson. Imaging* 44, 59–71. doi: 10.1002/jmri.25130

Martin-Bastida, A., Lao-Kaim, N. P., Loane, C., Politis, M., Roussakis, A. A., Valle-Guzman, N., et al. (2017). Motor associations of iron accumulation in deep grey matter nuclei in Parkinson's disease: a cross-sectional study of iron-related magnetic resonance imaging susceptibility. *Eur. J. Neurol.* 24, 357–365. doi: 10.1111/ene.13208

Pesch, B., Casjens, S., Woitalla, D., Dharmadhikari, S., Edmondson, D. A., Zella, M. A. S., et al. (2019). Impairment of motor function correlates with neurometabolite and brain iron alterations in parkinson's disease. *Cells* 8:E96. doi: 10.3390/cells8020096

Pietracupa, S., Martin-Bastida, A., and Piccini, P. (2017). Iron metabolism and its detection through MRI in parkinsonian disorders: a systematic review. *Neurol. Sci.* 38, 2095–2101. doi: 10.1007/s10072-017-3099-y

Schwarz, S. T., Mougin, O., Xing, Y., Blazejewska, A., Bajaj, N., Auer, D. P., et al. (2018). Parkinson's disease related signal change in the nigrosomes 1-5 and the substantia nigra using T2* weighted 7T MRI. *Neuroimage Clin.* 19, 683–689. doi: 10.1016/j.nicl.2018.05.027

Schweser, F., Deistung, A., Lehr, B. W., and Reichenbach, J. R. (2011). Quantitative imaging of intrinsic magnetic tissue properties using MRI signal phase: an approach to in vivo brain iron metabolism? *Neuroimage* 54, 2789–2807. doi: 10.1016/j.neuroimage.2010.10.070

Sethi, S. K., Kisch, S. J., Ghassaban, K., Rajput, A., Rajput, A., Babyn, P. S., et al. (2018). Iron quantification in Parkinson's disease using an age-based threshold on susceptibility maps: the advantage of local versus entire structure iron content measurements. *Magn. Reson. Imaging* 55, 145–152. doi: 10.1016/j.mri.2018.10.001

Shulman, J. M., and De Jager, P. L. (2009). Evidence for a common pathway linking neurodegenerative diseases. *Nat. Genet.* 41, 1261–1262.

Smith, S. M. (2002). Fast robust automated brain extraction. *Hum. Brain Mapp.* 17, 143–155.

Wang, J. Y., Zhuang, Q. Q., Zhu, L. B., Zhu, H., Li, T., Li, R., et al. (2016). Meta-analysis of brain iron levels of Parkinson's disease patients determined by postmortem and MRI measurements. *Sci. Rep.* 6:36669. doi: 10.1038/srep36669

Yan, F., He, N., Lin, H., and Li, R. (2018). Iron deposition quantification: applications in the brain and liver. *J. Magn. Reson. Imaging* 48, 301–317. doi: 10.1002/jmri.26161

Zecca, L., Youdim, M. B., Riederer, P., Connor, J. R., and Crichton, R. R. (2004). Iron, brain ageing and neurodegenerative disorders. *Nat. Rev. Neurosci.* 5, 863–873.

Conflict of Interest Statement: SKS and EMH have part time positions in Magnetic Resonance Innovations, Inc.

The remaining authors declare that the research was conducted in the absence of any commercial or financial relationships that could be construed as a potential conflict of interest.

frontiers in Aging Neuroscience

ORIGINAL RESEARCH
published: 25 June 2019
doi: 10.3389/fnagi.2019.00139

Altered Global Synchronizations in Patients With Parkinson's Disease: A Resting-State fMRI Study

Mengyan Li[1†], Yanjun Liu[2†], Haobo Chen[1], Guihe Hu[1], Shaode Yu[2,3], Xiuhang Ruan[4], Zhenhang Luo[5], Xinhua Wei[4*] and Yaoqin Xie[2*]*

[1]*Department of Neurology, Guangzhou First People's Hospital, School of Medicine, South China University of Technology, Guangzhou, China,* [2]*Institute of Biomedical and Health Engineering, Shenzhen Institutes of Advanced Technology, Chinese Academy of Sciences, Shenzhen, China,* [3]*Department of Radiation Oncology, Southwestern Medical Center, University of Texas, Dallas, TX, United States,* [4]*Department of Radiology, Guangzhou First People's Hospital, School of Medicine, South China University of Technology, Guangzhou, China,* [5]*GYENNO Technologies Co., Ltd., Shenzhen, China*

Background: Abnormalities of cognitive and movement functions are widely reported in Parkinson's disease (PD). The mechanisms therein are complicated and assumed to a coordination of various brain regions. This study explored the alterations of global synchronizations of brain activities and investigated the neural correlations of cognitive and movement function in PD patients.

Methods: Thirty-five age-matched patients with PD and 35 normal controls (NC) were enrolled in resting-state functional magnetic resonance imaging (rs-fMRI) scanning. Degree centrality (DC) was calculated to measure the global synchronizations of brain activity for two groups. Neural correlations between DC and cognitive function Frontal Assessment Battery (FAB), as well as movement function Unified Parkinson's Disease Rating Scale (UPDRS-III), were examined across the whole brain within Anatomical Automatic Labeling (AAL) templates.

Results: In the PD group, increased DC was observed in left fusiform gyrus extending to inferior temporal gyrus, left middle temporal gyrus (MTG) and angular gyrus, while it was decreased in right inferior opercular-frontal gyrus extending to superior temporal gyrus (STG). The DC in a significant region of the fusiform gyrus was positively correlated with UPDRS-III scores in PD ($r = 0.41$, $p = 0.0145$). Higher FAB scores were shown in NC than PD ($p < 0.0001$). Correlative analysis of PD between DC and FAB showed negative results ($p < 0.05$) in frontal cortex, whereas positive in insula and cerebellum. As for the correlations between DC and UPDRS-III, negative correlation ($p < 0.05$) was observed in bilateral inferior parietal lobule (IPL) and right cerebellum, whereas positive correlation ($p < 0.05$) in bilateral hippocampus and para-hippocampus gyrus ($p < 0.01$).

Conclusion: The altered global synchronizations revealed altered cognitive and movement functions in PD. The findings suggested that the global functional connectivity in fusiform gyrus, cerebellum and hippocampus gyrus are critical regions in the identification of cognitive and movement functions in PD. This study provides new insights on the interactions among global coordination of brain activity, cognitive and movement functions in PD.

Keywords: resting-state fMRI, global synchronizations, Parkinson's disease, cognitive function, movement function

OPEN ACCESS

Edited by:
Xun Chen,
University of Science and Technology of China, China

Reviewed by:
Liu Jun,
Shanghai Jiao Tong University, China
Ruiwang Huang,
South China Normal University, China

***Correspondence:**
Yanjun Liu
yj.liu1@siat.ac.cn
Xinhua Wei
weixinhua@aliyun.com
Yaoqin Xie
yq.xie@siat.ac.cn

[†]These authors have contributed equally to this work

Received: *30 January 2019*
Accepted: *23 May 2019*
Published: *25 June 2019*

Citation:
Li M, Liu Y, Chen H, Hu G, Yu S, Ruan X, Luo Z, Wei X and Xie Y (2019) Altered Global Synchronizations in Patients With Parkinson's Disease: A Resting-State fMRI Study. Front. Aging Neurosci. 11:139. doi: 10.3389/fnagi.2019.00139

INTRODUCTION

As one of the most common neurodegenerative diseases, people diagnosed with Parkinson's disease (PD) are widely reported with abnormalities consisting of motor and non-motor symptoms (Chaudhuri et al., 2006; Bunzeck et al., 2013; Villarreal et al., 2018). PD is known as a kind of movement disorder, including general motor symptoms and specific motor symptoms (Fox et al., 2018). However, non-movement aspects such as impairment of cognitive and executive functions have also gained great attention and have been the topic of a great number of researches on PD (Kudlicka et al., 2011; Litvan et al., 2011; Dirnberger and Jahanshahi, 2013; Delgado-Alvarado et al., 2016). Various methods are performed to explore the biomarkers for the diagnosis and progression monitoring of PD, including metabolomics profiling of blood (Bogdanov et al., 2008), cerebrospinal fluid (Hong et al., 2010), cognitive impairment (Svenningsson et al., 2012) and neuroimaging (Reijnders et al., 2010; Tessitore et al., 2016; Li et al., 2018).

Structural and functional changes in patients with PD are observed in many neuroimaging studies (Borroni et al., 2015; Wang et al., 2016; Prell, 2018). Structural changes are reported in various brain regions such as corpus callosum, hippocampus, basal ganglia, temporal cortex and frontal cortex by voxel-based morphometry (VBM) analysis (Camicioli et al., 2003; Summerfield et al., 2005; Wiltshire et al., 2010; Tessitore et al., 2016; Lee et al., 2018; Prell, 2018). In recent years, resting-state functional magnetic resonance imaging (rs-fMRI) has become a prevalent method to explore the alterations of spontaneous brain activities (Fox and Raichle, 2007; Van Eimeren et al., 2009) in patients with PD. For the functional neuroimaging aspect, the blood oxygen level dependent (BOLD) signal is widely employed to explore the differences of spontaneous brain activity between healthy people and PD patients (Göttlich et al., 2013; Pan et al., 2017a; Wang et al., 2018). Functional neuroimaging studies of PD are mainly focused on the spontaneous brain activity of amplitude of low frequency oscillations (Kwak et al., 2012; Hou et al., 2014; Pan et al., 2017b), regional synchronization (Wu et al., 2009; Li et al., 2016; Pan et al., 2017a) and functional connectivity (de Schipper et al., 2018; Wang et al., 2018).

The neuroimaging findings of PD are various and inconsistent. In the current stage, it is still unclear which structural or functional neuroimaging marker is reliable or convincing for understanding the pathological physiology of PD. While these findings suggest that the pathophysiological mechanisms in PD is complicated and assumed to a coordination of various brain regions. Degree centrality (DC), a voxel-wise measurement, is applied to evaluate the strengths of functional connectivity across the whole brain (Buckner et al., 2009). DC is a reliable rs-fMRI indicator (Zuo et al., 2013) and suggested to represent the global synchronizations or global functional connectivity density (Tomasi and Volkow, 2012). Using the DC method, alterations are found in brain regions associated with cognition and motor, with these regions being depressed in PD sufferers (Wang et al., 2018). Higher degrees are observed in the precuneus in PD patients with cognitive impairments than patients without cognitive impairment (Nagano-Saito et al., 2019). In the current study, we applied DC to investigate the differences of global synchronizations of brain activity between PD and normal controls (NC). Furthermore, the neural correlations between global synchronizations and cognitive function as well as movement function were explored in PD group across the whole brain.

MATERIALS AND METHODS

Participants

In this study, 35 NC and 35 patients diagnosed with PD were included in the investigation. Subjects of NC were included who had no history of neurological disease, no symptom of PD and no disorder of cognitive function and movement function. Diagnosis of PD was according to the clinical criteria of Movement Disorder Society (MDS; Postuma et al., 2015). PD patients included: those aged over 30 years old, no less than 1 year of disease duration, had received a stable dose of levodopa medication treatment for at least 30 days, without cardiovascular disease and respiratory disease, nor with a history of surgical operations or embedded with a pacemaker in the body. PD patients with severe symptoms of dementia, anxiety and depression were excluded. All of the PD patients were in a medication-on state during experimental data collection and no drug-naïve patient was included in this study. Both NC and PD subjects were recruited by Guangzhou First People's Hospital from May 2017 to September 2018. This study was approved by the Institutional Review Board (IRB) of Guangzhou First People's Hospital. Informed written consents were obtained from all subjects.

Clinical Assessments

Clinical assessments, including motor and non-motor symptoms, were measured across all subjects with PD. Hoehn & Yahr (H&Y) scale (Hoehn and Yahr, 1998) was collected from subjects of PD group to evaluate the severity of PD symptoms, with classifications of stages 1–5, with a higher H&Y stage indicating an advanced state of PD. Additionally, cognitive function and motor function were also measured. For both NC and PD, cognitive-related measurement was identified by the Frontal Assessment Battery (FAB) containing six sub-items that are associated with the frontal cortex (Dubois et al., 2000). Movement-related assessment was evaluated from PD (medication-on) by the motor part (Part three) of Unified Parkinson's Disease Rating Scale (UPDRS-III), which was developed by the MDS (Goetz et al., 2008). Higher UPDRS-III scores indicated decreased movement ability.

Data Acquisition

Two groups of subjects (35 NC and 35 PD) participated in the MRI scanning by 3.0T SIEMENS MRI machine system. All of the subjects were required to lie quietly and stayed awake with eye closed during the whole process of scanning. All of the PD patients were in medication-on state when the fMRI was performed. Functional images and structural images of the brain were obtained. The resting-state functional images were obtained with the following parameters: repetition time (TR) of 2,000 ms,

echo time (TE) of 21 ms, slice thickness of 4 mm, acquisition matrix of 64 × 64; flip angle (FA) of 78° and pixel spacing of 3.5 mm × 3.5 mm. Structural T1-weighted images were scanned with parameters: 1,900/2.22 ms TR/TE, acquisition matrix of 256 × 215, 9° FA, pixel spacing of 0.488 × 0.488 and 1 mm slice thickness.

Data Preprocessing

Data preprocessing was implemented on MATLAB platform based on toolkit package of DPABI (Yan et al., 2016) and Statistical Parametric Mapping (SPM12[1]). Preprocessing procedures included: removal of the first 10 of 220 time points; slice timing adjustment (33 slices); realign; segmentation using new segment (Ashburner and Friston, 2005) and Diffeomorphic Anatomical Registration through Exponentiated Lie Algebra (DARTEL; Ashburner, 2007); regression of nuisance covariates including while matter, cerebrospinal fluid and Friston 24 parameters of head motions (Friston et al., 1996; Satterthwaite et al., 2013; Yan et al., 2013); spatial normalization with resampling of 3 mm × 3 mm × 3 mm to Montreal Neurological Institute (MNI) space by DARTEL (Ashburner, 2007); temporal filtering with low frequency band pass of 0.01–0.1 Hz and linear detrend removal. Subjects with maximal translations exceeded 2.5 mm or rotations over 2.5° were excluded from analysis. According to this exclusion criteria, no subjects were excluded. Additionally, the mean framewise displacement (FD) Jenkinson (Jenkinson et al., 2002) was calculated, representing the head motions of every subject. No significant difference of FD Jenkinson between two groups was observed by two-sample t-test ($p = 0.1294$).

Global Signal Synchronization—Degree Centrality

DC is a voxel-wise measurement calculating the functional connectivity density between a voxel with the other voxels within the mask (Buckner et al., 2009). Pearson correlation is employed to evaluate the connectivity strength of all pairs of voxels. DC is conventionally calculated as weighted-sum DC or binarized-sum DC. The weighted-sum DC is defined as summing up the correlation coefficients that reach a given threshold, whereas the binarized-sum DC is defined as summing up the number of correlation coefficient that reaches a given threshold. Therefore, DC is also named global functional connectivity density, long range functional connectivity and global signal synchronization (Tomasi and Volkow, 2012). In this study, based on the preprocessed functional image, binarized-sum DC was calculated and the threshold was set at 0.3. For standardization, the DC maps of all subjects were transformed into Z-maps by subtracting the global mean value and then divided by standard deviation. After standardization transformation, the Z-maps were then smoothed with 4 mm of full width at half maximum (FWHM). The smoothed Z-maps were applied to the subsequent statistical analysis and correlative analysis.

[1]http://www.fil.ion.ucl.ac.uk/spm/

Statistical and Correlative Analysis

To explore global signal synchronization differences between NC and PD, a two-sample t-test was performed on DC maps of two groups, with age, sex, education time and mean FD Jenkinson as covariates within the mask of gray matter. The resultant statistical T-map was corrected with multiple comparisons of Gaussian Random Field (GRF) within gray matter mask, with voxel $p < 0.005$ and cluster $p < 0.05$, two-tailed test ($T > 2.91$, cluster size $> 1{,}350\ mm^3$).

The brain regions showing significant group differences were extracted as regions of interest (ROIs) to explore the neural correlates between global signal synchronization (DC) and cognitive function (FAB) as well as movement function (UPDRS-III). DC signals were extracted from ROIs by averaging the signals of all voxels within ROI. Pearson correlation (statistical significance level $p < 0.05$) was applied to calculate the correlations between DC and cognitive/movement function. Moreover, the correlation analysis was also analyzed across the whole brain, within Automated Anatomical Labeling (AAL) template, which contains 116 brain regions, including 90 cerebrum regions and 26 cerebellum regions (Tzourio-Mazoyer et al., 2002).

RESULTS

Demographic Characteristics and Clinical Assessments

Statistical results of demographic characteristics and clinical measurements were summarized in **Table 1**. No group difference ($p > 0.05$) was observed on age or mean FD Jenkinson. Significant group differences were demonstrated in FAB scores ($p < 0.0001$) and education time ($p = 0.0277$). NC were shown to have higher FAB scores and longer education time than PD (**Table 1**). It should be noted that the FAB scores were obtained

TABLE 1 | Demographic characteristics and clinical assessments.

	NC (n = 35)	PD (n = 35)	Statistical p-value
Age (years)	60 ± 6	63 ± 12	0.0989
Sex (female/male)	24/11	18/17	NA
Education time (years)	11.08 ± 2.84	9.43 ± 3.31	0.0277
Hand dominance (left/right)	0/35	2/33	NA
Disease duration (years)	NA	4.19 ± 3.97	NA
H&Y scores	NA	2.44 ± 0.72	NA
UPDRS-III scores (medication-on)	NA	31.93 ± 14.56	NA
FAB scores	17.17 ± 1.34	15.16 ± 2.44 (n = 31)	<0.0001
Levodopa equivalent daily dose (mg)	NA	431.95 ± 383.33	NA
Mean FD (mm)	0.088 ± 0.064	0.069 ± 0.031	0.1284

NC, normal controls; PD, Parkinson's disease; FD, framewise displacement of Jenkinson; H&Y, Hoehn & Yahr; UPDRS-III, Unified Parkinson's Disease Rating Scale (part three); FAB, Frontal assessment battery; NA, not applicable. Data was noted as average ± standard deviation. Statistical p-value was obtained by two-sample t-test with significance level of $p < 0.05$.

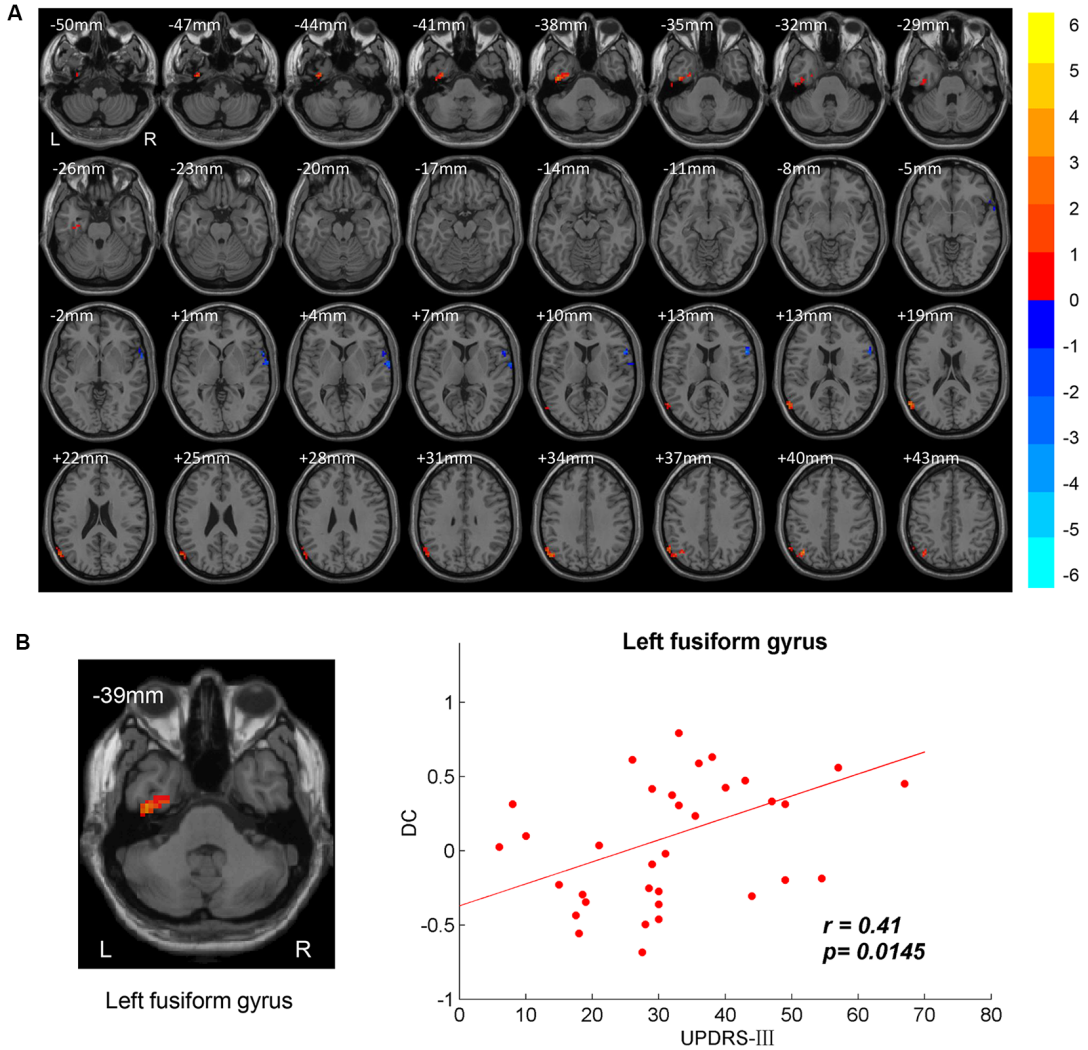

FIGURE 1 | Between-group degree centrality (DC) differences. **(A)** T-maps of DC differences between normal controls (NC) and patients with Parkinson's disease (PD). Multiple comparison corrections were implemented by Gaussian Random Field (GRF) with voxel $p < 0.005$ and cluster $p < 0.05$ within gray matter mask ($T > 2.91$, cluster size $> 1{,}350$ mm^3). The color bar indicated the statistical t-value. Warm/Cool overlays indicated increased/decreased DC in PD. L/R = left/right hemisphere. **(B)** Positive correlation between DC and motor part of Unified Parkinson's Disease Rating Scale (UPDRS-III) in left fusiform gyrus.

from 31 out of 35 PD patients because four PD patients refused to do the FAB assessment.

Differences of Global Synchronizations

DC differences between NC and PD were implemented by two-sample t-test. The significant brain regions were showed in **Table 2**, **Figure 1A**. The survival voxels of brain regions were identified based on CUI Xu's XjView[2]. For the PD group, increased DC was observed in left fusiform gyrus extending to inferior temporal gurus (ITG), left middle temporal gyrus (MTG) and angular gyrus, whereas it was decreased in right interior opercular-frontal gyrus (IFGoper) extending to superior temporal gyrus (STG).

[2]http://www.alivelearn.net/xjview/

Correlative Analysis

The brain regions showing significant DC differences (**Table 2**) between NC and PD were extracted as ROIs. The correlative analysis between DC and cognitive/movement functions was performed within these brain regions. Positive correlation was observed between DC and UPDRS-III in left fusiform gyrus ($r = 0.41$, $p = 0.0145$; **Figure 1B**), while no correlation ($p > 0.05$) was observed between DC and FAB scores. Additionally, the neural correlations of cognitive function (FAB) and movement function (UPDRS-III) were examined across the whole brain within AAL templates. The significant results were demonstrated in **Figures 2–4**.

Among the correlative analysis between DC and FAB scores in PD, negative correlations were observed in bilateral superior frontal gyrus (SFG; **Figures 2B,C**) and right medial SFG

TABLE 2 | Brain regions showing significant degree centrality (DC) differences between normal controls (NC) and patients with Parkinson's disease (PD).

Side	Brain regions	Brodmann area	Cluster size (mm^3)	Peak MNI coordinates (*x y z*)	Peak *t*-value
Left	Fusiform gyrus/Inferior temporal gyrus	20	1,890	−42 −15 −39	4.85
Left	Middle temporal gyrus/Angular gyrus	39	2,754	−60 −63 18	4.73
Right	Inferior opercular-frontal gyrus/Superior temporal gyrus	44/48	1,620	57 15 12	−4.59

MNI, Montreal Neurological Institute. Positive/Negative statistical t-value indicated increased/decreased DC in PD.

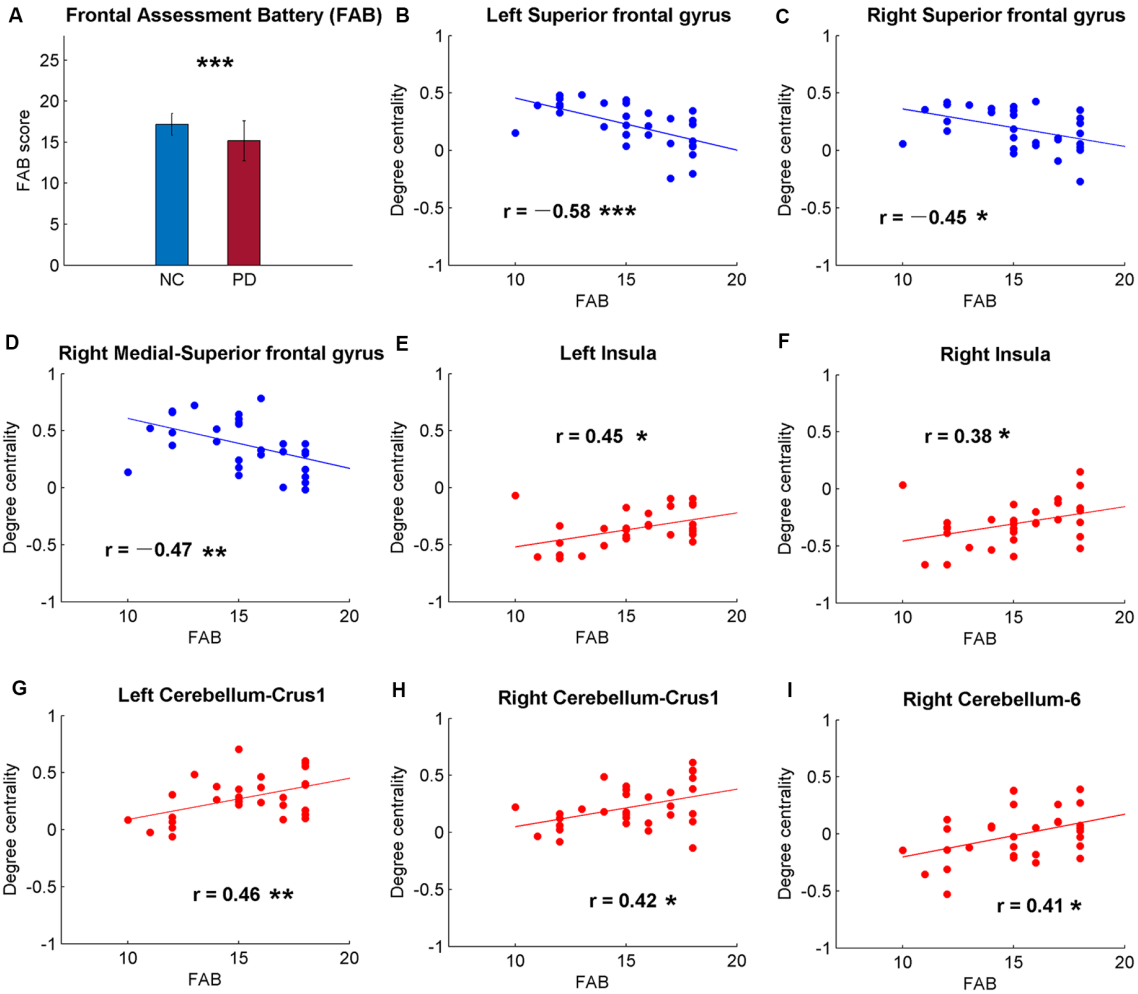

FIGURE 2 | Significant correlations between cognitive function and the global signal synchronizations within the whole brain [Automated Anatomical Labeling (AAL) templates] in patients with PD. **(A)** The Frontal Assessment Battery (FAB) scores of NC and PD. Significant correlations between FAB and DC in bilateral superior frontal gyrus (SFG; **B,C**), right medial-SFG **(D)**, bilateral insula **(E,F)**, bilateral cerebellum-curs1 **(G,H)** and right cerebellum-6 **(I)**. Significance notations: $^{*}p < 0.05$, $^{**}p < 0.01$, $^{***}p < 0.005$. The dots and lines were demonstrated in red/blue color for positive/negative correlations.

(**Figure 2D**). The results were shown to be positive in bilateral insula (**Figures 2E,F**), bilateral cerebellum-crus1 (**Figures 2G,H**) and right cerebellum-6 (**Figure 2I**). The results were insignificant ($p > 0.05$) in NC within these regions. Conversely, significant negative results ($p < 0.05$) were observed in the bilateral hippocampus in NC, while the results were unobvious ($p > 0.05$) in PD (**Figure 3**).

Significant correlative analysis between DC and movement function (UPDRS-III) of PD within AAL templates are demonstrated in **Figure 4**. Negative correlations were observed in bilateral inferior parietal lobule (IPL; **Figures 4A,D**), right AG (**Figure 4G**), and right cerebellum-6 (**Figure 4H**). DC were positively correlated with UPDRS-III in the bilateral hippocampus (**Figures 4B,E**) and para-hippocampus gyrus (**Figures 4C,F**).

DISCUSSION

In this study, the indicator of DC was adopted to compare the difference of global signal synchronizations of spontaneous brain

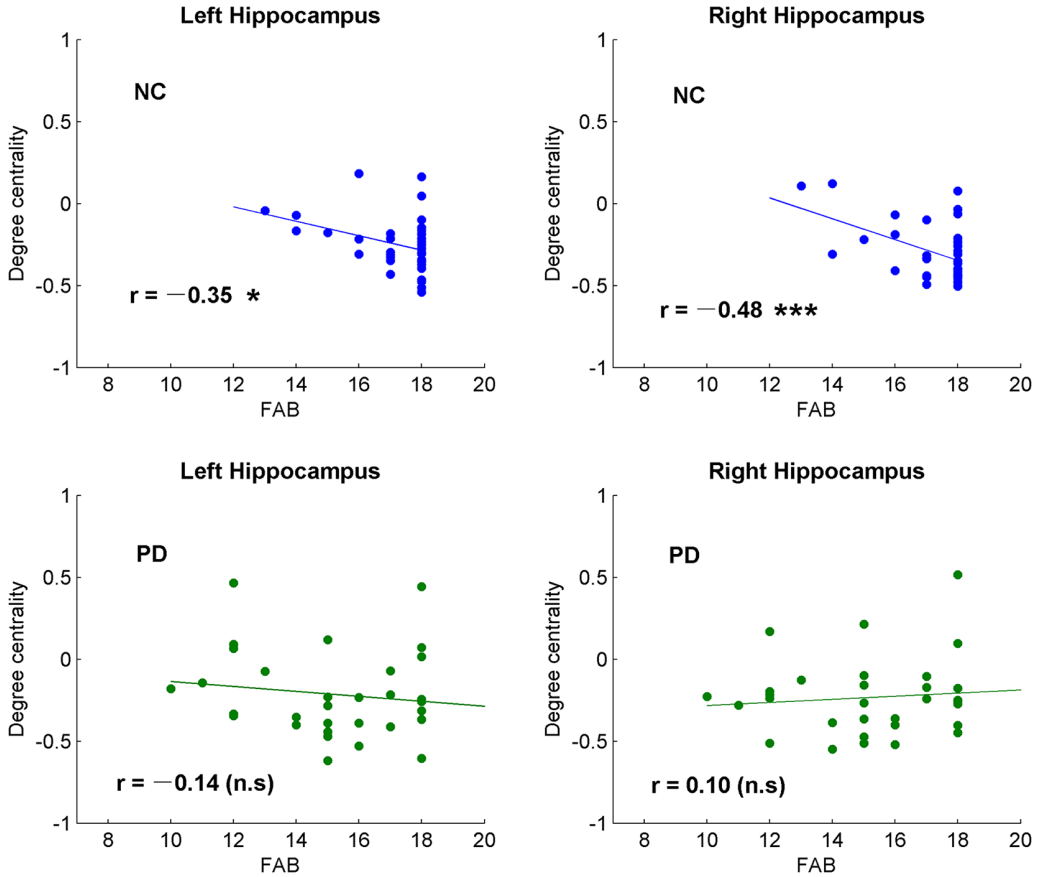

FIGURE 3 | Correlative analysis between cognitive function and the global signal synchronizations in bilateral hippocampus in both NC and patients with PD. Significance notations: $^{*}p < 0.05$, $^{***}p < 0.005$, n.s = no significance. The dots and lines were demonstrated in blue/green color for negative/no correlations.

activity between PD and NC. In addition, the neural correlations between global synchronizations and cognitive/movement functions were explored across the whole brain within AAL templates. Significant results were observed in both analysis of group DC differences and neural correlations.

More Sticky to Default Mode State in Parkinson's Disease

Significant DC differences between PD and DC were observed in left fusiform gyrus extending to ITG, left MTG/angular gyrus and right IFGoper/STG (**Table 2**, **Figure 1A**). Posterior MTG and angular gyrus, together with medial prefrontal cortex (MPFC) and precuneus/posterior cingulate cortex (PCu/PCC), are identified as critical brain regions that constitute default mode network (DMN; Raichle et al., 2001; Laird et al., 2009). Brain activities in DMN are task-negative, which means deactivations during task-related state and activations in resting state (Raichle et al., 2001). DMN is also thought to be associated with self-referential processing (de Groot et al., 2000; Gusnard and Raichle, 2001). In our results, increased DC was demonstrated in left MTG and angular gyrus compared to in the NC group in a resting state. Dysfunctional DMN was also reported in other neuropsychiatric disorders like schizophrenia (Calhoun et al., 2008) and Alzheimer's disease (Lustig et al., 2003). Additionally, less deactivations of DMN in PD were also observed in executive tasks than those in NC (Van Eimeren et al., 2009). DC evaluates global synchronizations and global functional connectivity density, therefore, higher DC activities indicate higher binding between inter-regions collaboration. Therefore, higher global synchronizations of DMN in PD may result in decreased ability to be self-referential, more likely to remain the default mode state and less control of interactions between brain regions.

Cognitive impairment is commonly present in PD patients. A VBM study on PD reports gray matter atrophy in left fusiform gyrus, and the fusiform atrophy is associated with poor memory (Camicioli et al., 2009). Fusiform gyrus is famous for its face area and face perception (Kanwisher et al., 1997; George et al., 1999). PD patients have an impairment in recognizing facial expression and visuospatial dysfunctions (Levin et al., 1991; Sprengelmeyer et al., 2003). In our results, increased DC was also observed in left fusiform gyrus and the DC in the fusiform is positively correlated with movement function for PD patients (**Figure 1**, **Table 2**). Consistent with previous study, increased activity is shown in the fusiform gyrus in response to the paradigm of facial perception

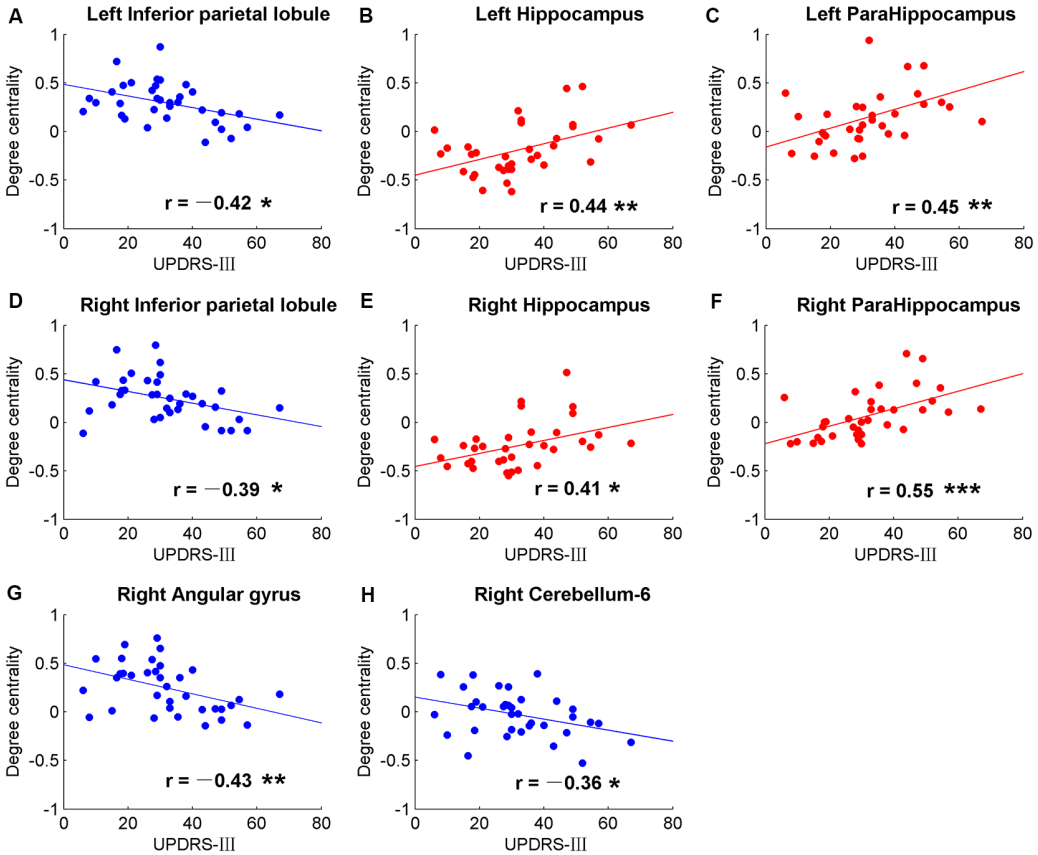

FIGURE 4 | Significant correlations between movement measurements and the global signal synchronizations within the whole brain (AAL templates) in patients with PD. Correlations between Part three of UPDRS-III and DC in bilateral inferior parietal lobule (IPL; **A,D**), right angular gyrus **(G)**, right cerebellum-6 **(H)**, bilateral hippocampus **(B,E)** and bilateral para-hippocampus gyrus **(C,F)**. The dots and lines were demonstrated in red/blue color for positive/negative correlations.

(Cardoso et al., 2010). Visuospatial dysfunctions have an impact on the movement of PD especially those with freezing gait. The correlation between DC in fusiform gyrus and movement function may be explained by impaired vision in balance (Day and Guerraz, 2007).

Neural Correlations of Cognitive and Movement Function in Parkinson's Disease

Patients with PD are not only reported with abnormalities of motor symptoms but also with decreased cognitive function (Dubois and Pillon, 1996; Kehagia et al., 2010). As expected, the FAB scores of PD were significantly lower than NC ($p < 0.0001$; **Figure 2A**), suggesting decreased frontal-related of cognitive function in PD. The correlative analysis between global synchronizations and cognitive function scores across the whole brain showed significant correlations in frontal cortex, insula and cerebellum in PD patients (**Figure 2**), while there was no significant result in NC. The DC of PD was negatively correlated with FAB scores in bilateral SFG and medial SFG, and positively correlated with bilateral insula and cerebellum. The frontal cortex is always associated with cognitive and executive functions (Miller and Cohen, 2001). Cortical thickness changes and gray matter volume reductions were reported in frontal cortex of PD (Pan et al., 2012; Tessitore et al., 2016). Therefore, negative correlations between DC and FAB scores reveal altered frontal-cognitive function in PD.

Contrary to frontal cortex, the correlations between DC and FAB scores were positive in the insula (**Figure 2**). Though the insula is a well-known brain region that is associated with self-representation (Burgmer et al., 2013) and awareness (Craig, 2009), it is also suggested to be related to non-motor symptoms of PD (Christopher et al., 2014a). In addition, patients with PD were observed with reduced gray matter volume in insula (Pan et al., 2012) and decreased DC in bilateral insula in medication-off state (Zhong et al., 2018). Insular dysfunction is also related to PD with cognitive impairment (Christopher et al., 2014b). These findings suggest higher DC in insula of PD suggests higher cognitive function.

Positive correlations between DC and FAB scores were also shown in the cerebellum (**Figure 2**). However, negative correlations were observed between DC and movement function (UPDRS-III) in PD (**Figure 4**). Cerebellum is both associated with sensorimotor processing (Baumann et al., 2015; Kansal et al., 2017) and cognitive/emotional processing (Schmahmann, 2010; Adamaszek et al., 2017). Decreased DC in cerebellum-6

was also observed in PD (Wang et al., 2018). Positive results in neural correlations of cognitive function and negative neural correlations of movement function were found in the cerebellum, suggesting that the cerebellum plays both cognitive and motor function roles in the pathology of PD.

The hippocampus is well known for its role in memory (Squire, 1992). Interestingly, negative correlations were observed between DC and FAB scores in the hippocampus of NC, while no correlation was observed ($p > 0.05$) in PD (**Figure 3**). Moreover, positive correlations were shown between DC and movement function (UPDRS-III) in the hippocampus/para-hippocampus in PD (**Figure 4**). These findings seem to suggest that the global synchronizations in the hippocampus reveal both cognitive and movement functions of PD. Hippocampus atrophy is found in PD patients with depressive symptoms, cognitive impairment and dementia (van Mierlo et al., 2015; Delgado-Alvarado et al., 2016). A longitudinal study on PD patients suggests that the hippocampus is related to the progression of cognitive impairment and dementia (Kandiah et al., 2014). Decoupled correlation between hippocampal DC and FAB scores of PD (**Figure 3**) may imply cognitive decline in PD. The findings of PD studies in reference to hippocampus/para-hippocampus are extensively focused on non-motor symptoms, mostly on depression, cognitive decline and memory impairment, and are rarely related to motor symptoms or movement function. The hippocampus is involved in motor tasks and perturbed movements (Devan et al., 2015; Kerr et al., 2017) which are not general movements. No direct evidence supports the influence of hippocampus on motor effect in PD. Our finding of increased hippocampal signal synchronization comes with increased motor performance in PD (**Figure 4**) suggests that the hippocampus has an important role in the motor symptoms of PD.

In our results, negative correlations between DC and movement function (UPDRS-III) were observed in bilateral IPL (**Figure 4**). Altered brain activities of parietal lobe are widely reported in PD studies. Decreased inter-hemispheric functional connectivity in IPL was demonstrated in PD and negative neural correlation was observed in interaction with motor scores (Li et al., 2018). Meta-analysis also suggests that IPL is a robust brain region that showed significant differences in regional synchronizations between PD and NC (Pan et al., 2017a). Therefore, IPL may be a critical brain region in the motor symptom of PD.

The findings of this study suggest the global synchronizations of the fusiform, hippocampus and cerebellum-6 are critical brain regions for both cognitive function and movement function of PD. However, the exact pathology remains unclear and needs further studies on it.

CONCLUSION

Alterations of global synchronization in the left fusiform gyrus and right opercular-frontal cortex reveal altered cognitive and movement functions in PD. The findings of neural correlations suggest that the global functional connectivity in fusiform gyrus, cerebellum and hippocampus are critical in the identification of cognitive and movement functions in PD. This study provides new insights on the interaction among global coordination of brain activity, cognitive function and movement function in PD.

ETHICS STATEMENT

This study was approved by the Institutional Review Board (IRB) of Guangzhou First People's Hospital. Informed written consents were obtained from all subjects.

AUTHOR CONTRIBUTIONS

ML and YL wrote the manuscript and designed the experiment. YL, XW and YX conceived the idea and performed the literature review. YL, ML, HC, GH and SY performed the data analysis. HC, GH, XR, ZL and XW contributed to data collection. All authors reviewed the manuscript and joined the discussion of the manuscript.

FUNDING

This work was supported in part by grants from the National Key Research and Develop Program of China (2016YFC0105102), National Science Foundation of China (81871846), Science and Technology Planning Project of Guangzhou (201804010032), Guangzhou Municipal Health Bureau Project (20171A010247), Guangzhou Key Project of R&D Innovation (2016201604030018), Leading Talent of Special Support Project in Guangdong (2016TX03R139), Shenzhen Key Technical Research Project (JSGG20160229203812944), Science Foundation of Guangdong (2017B020229002, 2015B020233011, 2014A030312006), Shenzhen Basic Technology Research Project (JCYJ20170413162458312), and Beijing Center for Mathematics and Information Interdisciplinary Sciences.

REFERENCES

Adamaszek, M., D'Agata, F., Ferrucci, R., Habas, C., Keulen, S., Kirkby, K. C., et al. (2017). Consensus paper: cerebellum and emotion. *Cerebellum* 16, 552–576. doi: 10.1007/s12311-016-0815-8

Ashburner, J. (2007). A fast diffeomorphic image registration algorithm. *Neuroimage* 38, 95–113. doi: 10.1016/j.neuroimage.2007.07.007

Ashburner, J., and Friston, K. J. (2005). Unified segmentation. *Neuroimage* 26, 839–851. doi: 10.1016/j.neuroimage.2005.02.018

Baumann, O., Borra, R. J., Bower, J. M., Cullen, K. E., Habas, C., Ivry, R. B., et al. (2015). Consensus paper: the role of the cerebellum in perceptual processes. *Cerebellum* 14, 197–220. doi: 10.1007/s12311-014-0627-7

Bogdanov, M., Matson, W. R., Wang, L., Matson, T., Saunders-Pullman, R., Bressman, S. S., et al. (2008). Metabolomic profiling to develop blood biomarkers for Parkinson's disease. *Brain* 131, 389–396. doi: 10.1093/brain/awm304

Borroni, B., Premi, E., Formenti, A., Turrone, R., Alberici, A., Cottini, E., et al. (2015). Structural and functional imaging study in dementia with Lewy bodies

and Parkinson's disease dementia. *Parkinsonism Relat. Disord.* 21, 1049–1055. doi: 10.1016/j.parkreldis.2015.06.013

Buckner, R. L., Sepulcre, J., Talukdar, T., Krienen, F. M., Liu, H., Hedden, T., et al. (2009). Cortical hubs revealed by intrinsic functional connectivity: mapping, assessment of stability and relation to Alzheimer's disease. *J. Neurosci.* 29, 1860–1873. doi: 10.1523/jneurosci.5062-08.2009

Bunzeck, N., Singh-Curry, V., Eckart, C., Weiskopf, N., Perry, R. J., Bain, P. G., et al. (2013). Motor phenotype and magnetic resonance measures of basal ganglia iron levels in Parkinson's disease. *Parkinsonism Relat. Disord.* 19, 1136–1142. doi: 10.1016/j.parkreldis.2013.08.011

Burgmer, M., Kugel, H., Pfleiderer, B., Ewert, A., Lenzen, T., Pioch, R., et al. (2013). The mirror neuron system under hypnosis—Brain substrates of voluntary and involuntary motor activation in hypnotic paralysis. *Cortex* 49, 437–445. doi: 10.1016/j.cortex.2012.05.023

Calhoun, V. D., Maciejewski, P. K., Pearlson, G. D., and Kiehl, K. A. (2008). Temporal lobe and "default" hemodynamic brain modes discriminate between schizophrenia and bipolar disorder. *Hum. Brain Mapp.* 29, 1265–1275. doi: 10.1002/hbm.20463

Camicioli, R., Gee, M., Bouchard, T. P., Fisher, N. J., Hanstock, C. C., Emery, D. J., et al. (2009). Voxel-based morphometry reveals extra-nigral atrophy patterns associated with dopamine refractory cognitive and motor impairment in parkinsonism. *Parkinsonism Relat. Disord.* 15, 187–195. doi: 10.1016/j.parkreldis.2008.05.002

Camicioli, R., Moore, M. M., Kinney, A., Corbridge, E., Glassberg, K., and Kaye, J. A. (2003). Parkinson's disease is associated with hippocampal atrophy. *Mov. Disord.* 18, 784–790. doi: 10.1002/mds.10444

Cardoso, E. F., Fregni, F., Maia, F. M., Melo, L. M., Sato, J. R., Cruz, A. C., et al. (2010). Abnormal visual activation in Parkinson's disease patients. *Mov. Disord.* 25, 1590–1596. doi: 10.1002/mds.23101

Chaudhuri, K. R., Healy, D. G., and Schapira, A. H. V. (2006). Non-motor symptoms of Parkinson's disease: diagnosis and management. *Lancet Neurol.* 5, 235–245. doi: 10.1016/S1474-4422(06)70373-8

Christopher, L., Koshimori, Y., Lang, A. E., Criaud, M., and Strafella, A. P. (2014a). Uncovering the role of the insula in non-motor symptoms of Parkinson's disease. *Brain* 137, 2143–2154. doi: 10.1093/brain/awu084

Christopher, L., Marras, C., Duff-Canning, S., Koshimori, Y., Chen, R., Boileau, I., et al. (2014b). Combined insular and striatal dopamine dysfunction are associated with executive deficits in Parkinson's disease with mild cognitive impairment. *Brain* 137, 565–575. doi: 10.1093/brain/awt337

Craig, A. D. (2009). How do you feel—now? The anterior insula and human awareness. *Nat. Rev. Neurosci.* 10, 59–70. doi: 10.1038/nrn2555

Day, B. L., and Guerraz, M. (2007). Feedforward versus feedback modulation of human vestibular-evoked balance responses by visual self-motion information. *J. Physiol.* 582, 153–161. doi: 10.1113/jphysiol.2007.132092

de Groot, N. M., Bootsma, M., van der Velde, E. T., and Schalij, M. J. (2000). Three-dimensional catheter positioning during radiofrequency ablation in patients: first application of a real-time position management system. *J. Cardiovasc. Electrophysiol.* 11, 1183–1192. doi: 10.1046/j.1540-8167.2000.01183.x

Delgado-Alvarado, M., Gago, B., Navalpotro-Gomez, I., Jiménez-Urbieta, H., and Rodriguez-Oroz, M. C. (2016). Biomarkers for dementia and mild cognitive impairment in Parkinson's disease. *Mov. Disord.* 31, 861–881. doi: 10.1002/mds.26662

de Schipper, L. J., Hafkemeijer, A., van der Grond, J., Marinus, J., Henselmans, J. M. L., and van Hilten, J. J. (2018). Altered whole-brain and network-based functional connectivity in Parkinson's disease. *Front. Neurol.* 9:419. doi: 10.3389/fneur.2018.00419

Devan, B. D., Magalis, C., and McDonald, R. J. (2015). Hippocampal development and the dissociation of cognitive-spatial mapping from motor performance. *F1000Res.* 4:625. doi: 10.12688/f1000research.6966.2

Dirnberger, G., and Jahanshahi, M. (2013). Executive dysfunction in Parkinson's disease: a review. *J, Neuropsychol.* 7, 193–224. doi: 10.1111/jnp.12028

Dubois, B., and Pillon, B. (1996). Cognitive deficits in Parkinson's disease. *J. Neurol.* 244, 2–8. doi: 10.1007/PL00007725

Dubois, B., Slachevsky, A., Litvan, I., and Pillon, B. (2000). The FAB: a frontal assessment battery at bedside. *Neurology* 55, 1621–1628. doi: 10.1212/wnl.55.11.1621

Fox, S. H., Katzenschlager, R., Lim, S. Y., Barton, B., de Bie, R. M. A., Seppi, K., et al. (2018). International Parkinson and movement disorder society evidence-based medicine review: update on treatments for the motor symptoms of Parkinson's disease. *Mov. Disord.* 33, 1248–1266. doi: 10.1002/mds.27372

Fox, M. D., and Raichle, M. E. (2007). Spontaneous fluctuations in brain activity observed with functional magnetic resonance imaging. *Nat. Rev. Neurosci.* 8, 700–711. doi: 10.1038/nrn2201

Friston, K. J., Williams, S., Howard, R., Frackowiak, R. S. J., and Turner, R. (1996). Movement-related effects in fMRI time-series. *Magn. Reson. Med.* 35, 346–355. doi: 10.1002/mrm.1910350312

George, N., Dolan, R. J., Fink, G. R., Baylis, G. C., Russell, C., and Driver, J. (1999). Contrast polarity and face recognition in the human fusiform gyrus. *Nat. Neurosci.* 2, 574–580. doi: 10.1038/9230

Goetz, C. G., Tilley, B. C., Shaftman, S. R., Stebbins, G. T., Fahn, S., Martinez-Martin, P., et al. (2008). Movement disorder society-sponsored revision of the unified Parkinson's disease rating scale (MDS-UPDRS): scale presentation and clinimetric testing results. *Mov. Disord.* 23, 2129–2170. doi: 10.1002/mds.22340

Göttlich, M., Münte, T. F., Heldmann, M., Kasten, M., Hagenah, J., and Krämer, U. M. (2013). Altered resting state brain networks in Parkinson's disease. *PLoS One* 8:e77336. doi: 10.1089/brain.2018.0659

Gusnard, D. A., and Raichle, M. E. (2001). Searching for a baseline: functional imaging and the resting human brain. *Nat. Rev. Neurosci.* 2, 685–694. doi: 10.1038/35094500

Hoehn, M. M., and Yahr, M. D. (1998). Parkinsonism: onset, progression and, mortality. *Neurology* 50:318. doi: 10.1212/wnl.50.2.318

Hong, Z., Shi, M., Chung, K. A., Quinn, J. F., Peskind, E. R., Galasko, D., et al. (2010). DJ-1 and α-synuclein in human cerebrospinal fluid as biomarkers of Parkinson's disease. *Brain* 133, 713–726. doi: 10.1093/brain/awq008

Hou, Y., Wu, X., Hallett, M., Chan, P., and Wu, T. (2014). Frequency-dependent neural activity in Parkinson's disease. *Hum. Brain Mapp.* 35, 5815–5833. doi: 10.1002/hbm.22587

Jenkinson, M., Bannister, P., Brady, M., and Smith, S. (2002). Improved optimization for the robust and accurate linear registration and motion correction of brain images. *Neuroimage* 17, 825–841. doi: 10.1016/s1053-8119(02)91132-8

Kandiah, N., Zainal, N. H., Narasimhalu, K., Chander, R. J., Ng, A., Mak, E., et al. (2014). Hippocampal volume and white matter disease in the prediction of dementia in Parkinson's disease. *Parkinsonism Relat. Disord.* 20, 1203–1208. doi: 10.1016/j.parkreldis.2014.08.024

Kansal, K., Yang, Z., Fishman, A. M., Sair, H. I., Ying, S. H., Jedynak, B. M., et al. (2017). Structural cerebellar correlates of cognitive and motor dysfunctions in cerebellar degeneration. *Brain* 140, 707–720. doi: 10.1093/brain/aww327

Kanwisher, N., McDermott, J., and Chun, M. M. (1997). The fusiform face area: a module in human extrastriate cortex specialized for face perception. *J. Neurosci.* 17, 4302–4311. doi: 10.1523/jneurosci.17-11-04302.1997

Kehagia, A. A., Barker, R. A., and Robbins, T. W. (2010). Neuropsychological and clinical heterogeneity of cognitive impairment and dementia in patients with Parkinson's disease. *Lancet Neurol.* 9, 1200–1213. doi: 10.1016/s1474-4422(10)70212-x

Kerr, M. S. D., Sacré, P., Kahn, K., Park, H.-J., Johnson, M., Lee, J., et al. (2017). The role of associative cortices and hippocampus during movement perturbations. *Front. Neural Circuits* 11:26. doi: 10.3389/fncir.2017.00026

Kudlicka, A., Clare, L., and Hindle, J. V. (2011). Executive functions in Parkinson's disease: systematic review and meta-analysis. *Mov. Disord.* 26, 2305–2315. doi: 10.1002/mds.23868

Kwak, Y., Peltier, S. J., Bohnen, N. I., Müller, M. L. T. M., Dayalu, P., and Seidler, R. D. (2012). L-DOPA changes spontaneous low-frequency BOLD signal oscillations in Parkinson's disease: a resting state fMRI study. *Front. Syst. Neurosci.* 6:52. doi: 10.3389/fnsys.2012.00052

Laird, A. R., Eickhoff, S. B., Li, K., Robin, D. A., Glahn, D. C., and Fox, P. T. (2009). Investigating the functional heterogeneity of the default mode network using coordinate-based meta-analytic modeling. *J. Neurosci.* 29, 14496–14505. doi: 10.1523/jneurosci.4004-09.2009

Lee, P. L., Chou, K. H., Lu, C. H., Chen, H. L., Tsai, N. W., Hsu, A. L., et al. (2018). Extraction of large-scale structural covariance networks from grey matter volume for Parkinson's disease classification. *Eur. Radiol.* 28, 3296–3305. doi: 10.1007/s00330-018-5342-1

Levin, B. E., Llabre, M. M., Reisman, S., Weiner, W. J., Sanchez-Ramos, J., Singer, C., et al. (1991). Visuospatial impairment in Parkinson's disease. *Neurology* 41, 365–369. doi: 10.1212/wnl.41.3.365

Li, Y., Liang, P., Jia, X., and Li, K. (2016). Abnormal regional homogeneity in Parkinson's disease: a resting state fMRI study. *Clin. Radiol.* 71, e28–e34. doi: 10.1016/j.crad.2015.10.006

Li, J., Yuan, Y., Wang, M., Zhang, J., Zhang, L., Jiang, S., et al. (2018). Decreased interhemispheric homotopic connectivity in Parkinson's disease patients with freezing of gait: a resting state fMRI study. *Parkinsonism Relat. Disord.* 52, 30–36. doi: 10.1016/j.parkreldis.2018.03.015

Litvan, I., Aarsland, D., Adler, C. H., Goldman, J. G., Kulisevsky, J., Mollenhauer, B., et al. (2011). MDS task force on mild cognitive impairment in Parkinson's disease: critical review of PD-MCI. *Mov. Disord.* 26, 1814–1824. doi: 10.1002/mds.23823

Lustig, C., Snyder, A. Z., Bhakta, M., O'Brien, K. C., McAvoy, M., Raichle, M. E., et al. (2003). Functional deactivations: change with age and dementia of the Alzheimer type. *Proc. Natl. Acad. Sci. U S A* 100, 14504–14509. doi: 10.1073/pnas.2235925100

Miller, E. K., and Cohen, J. D. (2001). An integrative theory of prefrontal cortex function. *Annu. Rev. Neurosci.* 24, 167–202. doi: 10.1146/annurev.neuro.24.1.167

Nagano-Saito, A., Bellec, P., Hanganu, A., Jobert, S., Mejia-Constain, B., Lafontaine, A.-L., et al. (2019). Why is aging a risk factor for cognitive impairment in Parkinson's disease? a resting state fMRI study. *Front. Neurol.* 10:267. doi: 10.3389/fneur.2019.00267

Pan, P. L., Song, W., and Shang, H. F. (2012). Voxel-wise meta-analysis of gray matter abnormalities in idiopathic Parkinson's disease. *Eur. J. Neurol.* 19, 199–206. doi: 10.1111/j.1468-1331.2011.03474.x

Pan, P. L., Zhan, H., Xia, M. X., Zhang, Y., Guan, D. N., and Xu, Y. (2017a). Aberrant regional homogeneity in Parkinson's disease: a voxel-wise meta-analysis of resting-state functional magnetic resonance imaging studies. *Neurosci. Biobehav. Rev.* 72, 223–231. doi: 10.1016/j.neubiorev.2016.11.018

Pan, P. L., Zhang, Y., Liu, Y., Zhang, H., Guan, D., and Xu, Y. (2017b). Abnormalities of regional brain function in Parkinson's disease: a meta-analysis of resting state functional magnetic resonance imaging studies. *Sci. Rep.* 7:40469. doi: 10.1038/srep40469

Postuma, R. B., Berg, D., Stern, M., Poewe, W., Olanow, C. W., Oertel, W., et al. (2015). MDS clinical diagnostic criteria for Parkinson's disease. *Mov. Disord.* 30, 1591–1601. doi: 10.1002/mds.26424

Prell, T. (2018). Structural and functional brain patterns of non-motor syndromes in Parkinson's disease. *Front. Neurol.* 9:138. doi: 10.3389/fneur.2018.00138

Raichle, M. E., MacLeod, A. M., Snyder, A. Z., Powers, W. J., Gusnard, D. A., and Shulman, G. L. (2001). A default mode of brain function. *Proc. Natl. Acad. Sci. U S A* 98, 676–682. doi: 10.1073/pnas.98.2.676

Reijnders, J. S. A. M., Scholtissen, B., Weber, W. E. J., Aalten, P., Verhey, F. R. J., and Leentjens, A. F. G. (2010). Neuroanatomical correlates of apathy in Parkinson's disease: a magnetic resonance imaging study using voxel-based morphometry. *Mov. Disord.* 25, 2318–2325. doi: 10.1002/mds.23268

Satterthwaite, T. D., Elliott, M. A., Gerraty, R. T., Ruparel, K., Loughead, J., Calkins, M. E., et al. (2013). An improved framework for confound regression and filtering for control of motion artifact in the preprocessing of resting-state functional connectivity data. *Neuroimage* 64, 240–256. doi: 10.1016/j.neuroimage.2012.08.052

Schmahmann, J. D. (2010). The role of the cerebellum in cognition and emotion: personal reflections since 1982 on the dysmetria of thought hypothesis and its historical evolution from theory to therapy. *Neuropsychol. Rev.* 20, 236–260. doi: 10.1007/s11065-010-9142-x

Sprengelmeyer, R., Young, A. W., Mahn, K., Schroeder, U., Woitalla, D., Büttner, T., et al. (2003). Facial expression recognition in people with medicated and unmedicated Parkinson's disease. *Neuropsychologia* 41, 1047–1057. doi: 10.1016/s0028-3932(02)00295-6

Squire, L. R. (1992). Memory and the hippocampuss: a synthesis from findings with rats, monkeys and humans. *Psychol. Rev.* 99, 195–231. doi: 10.1037//0033-295x.99.2.195

Summerfield, C., Junqué, C., Tolosa, E., Salgado-Pineda, P., Gómez-Ansón, B., Martí, M. J., et al. (2005). Structural brain changes in Parkinson disease with dementia: a voxel-based morphometry study. *Arch. Neurol.* 62, 281–285. doi: 10.1001/archneur.62.2.281

Svenningsson, P., Westman, E., Ballard, C., and Aarsland, D. (2012). Cognitive impairment in patients with Parkinson's disease: diagnosis, biomarkers and treatment. *Lancet Neurol.* 11, 697–707. doi: 10.1016/S1474-4422(12)70152-7

Tessitore, A., Santangelo, G., De Micco, R., Vitale, C., Giordano, A., Raimo, S., et al. (2016). Cortical thickness changes in patients with Parkinson's disease and impulse control disorders. *Parkinsonism Relat. Disord.* 24, 119–125. doi: 10.1016/j.parkreldis.2015.10.013

Tomasi, D., and Volkow, N. D. (2012). Aging and functional brain networks. *Mol. Psychiatry* 17, 549–558. doi: 10.1038/mp.2011.81

Tzourio-Mazoyer, N., Landeau, B., Papathanassiou, D., Crivello, F., Etard, O., Delcroix, N., et al. (2002). Automated anatomical labeling of activations in SPM using a macroscopic anatomical parcellation of the MNI MRI single-subject brain. *Neuroimage* 15, 273–289. doi: 10.1006/nimg.2001.0978

Van Eimeren, T., Monchi, O., Ballanger, B., and Strafella, A. P. (2009). Dysfunction of the default mode network in Parkinson disease: a functional magnetic resonance imaging study. *Arch. Neurol.* 66, 877–883. doi: 10.1001/archneurol.2009.97

van Mierlo, T. J., Chung, C., Foncke, E. M., Berendse, H. W., and van den Heuvel, O. A. (2015). Depressive symptoms in Parkinson's disease are related to decreased hippocampus and amygdala volume. *Mov. Disord.* 30, 245–252. doi: 10.1002/mds.26112

Villarreal, M. F., Huerta-Gutierrez, R., and Fregni, F. (2018). Parkinson's disease. *Neuromethods* 138, 139–181.doi: 10.1007/978-1-4939-7880-9_5

Wang, H., Chen, H., Wu, J., Tao, L., Pang, Y., Gu, M., et al. (2018). Altered resting-state voxel-level whole-brain functional connectivity in depressed Parkinson's disease. *Parkinsonism Relat. Disord.* 50, 74–80. doi: 10.1016/j.parkreldis.2018.02.019

Wang, M., Jiang, S., Yuan, Y., Zhang, L., Ding, J., Wang, J., et al. (2016). Alterations of functional and structural connectivity of freezing of gait in Parkinson's disease. *J. Neurol.* 263, 1583–1592. doi: 10.1007/s00415-016-8174-4

Wiltshire, K., Concha, L., Gee, M., Bouchard, T., Beaulieu, C., and Camicioli, R. (2010). Corpus callosum and cingulum tractography in Parkinson's disease. *Can. J. Neurol. Sci.* 37, 595–600. doi: 10.1017/s0317167100010751

Wu, T., Long, X., Zang, Y., Wang, L., Hallett, M., Li, K., et al. (2009). Regional homogeneity changes in patients with Parkinson's disease. *Hum. Brain Mapp.* 30, 1502–1510. doi: 10.1002/hbm.20622

Yan, C. G., Cheung, B., Kelly, C., Colcombe, S., Craddock, R. C., Di Martino, A., et al. (2013). A comprehensive assessment of regional variation in the impact of head micromovements on functional connectomics. *Neuroimage* 76, 183–201. doi: 10.1016/j.neuroimage.2013.03.004

Yan, C. G., Wang, X. D., Zuo, X. N., and Zang, Y. F. (2016). DPABI: data processing & analysis for (resting-state) brain imaging. *Neuroinformatics* 14, 339–351. doi: 10.1007/s12021-016-9299-4

Zhong, M., Yang, W., Huang, B., Jiang, W., Zhang, X., Liu, X., et al. (2018). Effects of levodopa therapy on voxel-based degree centrality in Parkinson's disease. *Brain Imaging Behav.* doi: 10.1007/s11682-018-9936-7 [Epub ahead of print].

Zuo, X. N., Xu, T., Jiang, L., Yang, Z., Cao, X. Y., He, Y., et al. (2013). Toward reliable characterization of functional homogeneity in the human brain: preprocessing, scan duration, imaging resolution and computational space. *Neuroimage* 65, 374–386. doi: 10.1016/j.neuroimage.2012.10.017

Conflict of Interest Statement: ZL was employed by the company GYENNO Technologies Co., Ltd.

The remaining authors declare that the research was conducted in the absence of any commercial or financial relationships that could be construed as a potential conflict of interest.

frontiers in Aging Neuroscience

ORIGINAL RESEARCH
published: 15 October 2019
doi: 10.3389/fnagi.2019.00276

Alterations of Regional Homogeneity in Parkinson's Disease Patients With Freezing of Gait: A Resting-State fMRI Study

Yanjun Liu[1], Mengyan Li[2], Haobo Chen[2], Xinhua Wei[3]*, Guihe Hu[2], Shaode Yu[1,4], Xiuhang Ruan[3], Jin Zhou[2], Xiaoping Pan[2], Ze Li[2], Zhenhang Luo[5] and Yaoqin Xie[1]**

[1] Institute of Biomedical and Health Engineering, Shenzhen Institutes of Advanced Technology, Chinese Academy of Sciences, Shenzhen, China, [2] Department of Neurology, Guangzhou First People's Hospital, School of Medicine, South China University of Technology, Guangzhou, China, [3] Department of Radiology, Guangzhou First People's Hospital, School of Medicine, South China University of Technology, Guangzhou, China, [4] Department of Radiation Oncology, Southwestern Medical Center, University of Texas, Dallas, TX, United States, [5] GYENNO Technologies Co., Ltd., Shenzhen, China

OPEN ACCESS

Edited by:
Xun Chen,
University of Science and Technology of China, China

Reviewed by:
Yu-Feng Zang,
Hangzhou Normal University, China
Xiaodong Zhu,
Tianjin Medical University General Hospital, China
Martin J. McKeown,
The University of British Columbia, Canada

***Correspondence:**
Mengyan Li
doclmy@163.com
Xinhua Wei
weixinhua@aliyun.com
Yaoqin Xie
yq.xie@siat.ac.cn

Received: 27 February 2019
Accepted: 25 September 2019
Published: 15 October 2019

Citation:
Liu Y, Li M, Chen H, Wei X, Hu G, Yu S, Ruan X, Zhou J, Pan X, Li Z, Luo Z and Xie Y (2019) Alterations of Regional Homogeneity in Parkinson's Disease Patients With Freezing of Gait: A Resting-State fMRI Study. Front. Aging Neurosci. 11:276. doi: 10.3389/fnagi.2019.00276

Objective: The purposes of this study are to investigate the regional homogeneity (ReHo) of spontaneous brain activities in Parkinson's disease (PD) patients with freeze of gait (FOG) and to investigate the neural correlation of movement function through resting-state functional magnetic resonance imaging (RS-fMRI).

Methods: A total of 35 normal controls (NC), 33 PD patients with FOG (FOG+), and 35 PD patients without FOG (FOG−) were enrolled. ReHo was applied to evaluate the regional synchronization of spontaneous brain activities. Analysis of covariance (ANCOVA) was performed on ReHo maps of the three groups, followed by *post hoc* two-sample *t*-tests between every two groups. Moreover, the ReHo signals of FOG+ and FOG− were extracted across the whole brain and correlated with movement scores (FOGQ, FOG questionnaire; GFQ, gait and falls questionnaire).

Results: Significant ReHo differences were observed in the left cerebrum. Compared to NC subjects, the ReHo of PD subjects was increased in the left angular gyrus (AG) and decreased in the left rolandic operculum/postcentral gyrus (Rol/PostC), left inferior opercular-frontal cortex, left middle occipital gyrus, and supramarginal gyrus (SMG). Compared to that of FOG−, the ReHo of FOG+ was increased in the left caudate and decreased in the left Rol/PostC. Within the significant regions, the ReHo of FOG+ was negatively correlated with FOGQ in the left SMG/PostC ($r = -0.39$, $p < 0.05$). Negative correlations were also observed between ReHo and GFQ/FOGQ ($r = -0.36/-0.38$, $p < 0.05$) in the left superior temporal gyrus (STG) of the whole brain analysis based on AAL templates.

Conclusion: The ReHo analysis suggested that the regional signal synchronization of brain activities in FOG+ subjects was most active in the left caudate and most hypoactive in the left Rol/PostC. It also indicated that ReHo in the left caudate and left Rol/PostC was critical for discriminating the three groups. The correlation between

ReHo and movement scores (GFQ/FOGQ) in the STG has the potential to differentiate FOG+ from FOG−. This study provided new insight into the understanding of PD with and without FOG.

Keywords: resting-state fMRI, Parkinson's disease, freezing of gait, regional homogeneity, movement function

INTRODUCTION

Parkinson's disease (PD) is a kind of neurodegenerative disease characterized by motor deficits (Villarreal et al., 2018). Freezing of gait (FOG) is a disabling symptom characterized by brief episodes of an inability to take a step or taking extremely short steps that typically occurs on initiating gait or on turning while walking (Nutt et al., 2011). Although FOG is more commonly observed in PD patients with advanced disease stages and old age, it may also occur in the early stage of idiopathic PD. Nearly 50% of PD patients suffer from FOG (Macht et al., 2007). Though FOG is transient and lasts for only a few seconds, it greatly impacts the quality of life of affected patients.

In the most recent decade, an increasing number of neuroimaging studies have focused on exploring the pathophysiology of PD patients with FOG by using different imaging modalities (Bartels and Leenders, 2008; Fasano et al., 2015) such as positron emission tomography (PET) (Park et al., 2009; Bohnen et al., 2014), functional near-infrared spectroscopy (fNIRS) (Maidan et al., 2015), diffusion tensor imaging (DTI) (Schweder et al., 2010; Herman et al., 2013), and functional magnetic resonance imaging (fMRI) (Tessitore et al., 2012b; Wang et al., 2016; Li et al., 2018). FOG in PD patients is suggested to be associated with abnormalities in motor, executive, cognitive, and affective functions (Amboni et al., 2008; Shine et al., 2013b). It has been synthesized that freezing occurs through a neural pathway in which the transient increase in inhibitory basal ganglia output leads to hypoactivity within the gait-coordinated brainstem, which may be caused by dopaminergic depletion in the striatum and hyperactivity in the subthalamic nucleus (Lewis and Shine, 2016). However, the pathophysiological mechanisms of FOG are not yet fully understood.

Resting-state fMRI (RS-fMRI) reflects alterations in spontaneous brain activities by measuring blood-oxygen-level-dependent (BOLD) signals (Fox and Raichle, 2007), and regional homogeneity (ReHo) evaluates signal synchronization by calculating the concordance of temporal change in BOLD signals within local brain regions (Zang et al., 2004). ReHo has been used to evaluate the differences between PD patients and normal controls (NC) (Li et al., 2016; Pan et al., 2017), and significant differences have been observed in the motor- and executive-related brain regions of PD patients, including the prefrontal cortex (Choe et al., 2013; Borroni et al., 2015), inferior parietal lobule (Wu et al., 2009), basal ganglia (Wang et al., 2018), precentral gyrus (Li et al., 2016; Wang et al., 2016), and cerebellum (Jiang et al., 2016). PD patients with gait disturbance are observed to have impaired coordination of movement and locomotion (Plotnik et al., 2008; Peterson et al., 2012). Therefore, it is hypothesized that PD with FOG (FOG+) may exhibit altered local signal synchronizations of neural activities in comparison to PD without FOG (FOG−) and NC. In this study, ReHo was employed to investigate the regional synchronizations of spontaneous brain activities in FOG+. Moreover, due to the altered movement performance in PD, the neural correlations of movement function in clinical assessment were also explored within the whole brain for both FOG+ and FOG−.

MATERIALS AND METHODS

Subjects and Clinical Assessments

In this study, 37 NC and 72 subjects with a diagnosis of PD were investigated. The NC were healthy subjects with no history of neurological disease, no symptoms of PD, and no disorder of cognitive function. PD patients were diagnosed according to the clinical criteria of the Movement Disorder Society (Postuma et al., 2015). The exclusion criteria for PD patients: severe comorbidity disease (cardiovascular disease, respiratory disease, and malignant tumor, etc.), a history of surgical operations (thalamotomy and posteroventral pallidotomy, deep brain stimulation (DBS), and organ transplantation, etc.), or a pacemaker/metal implanted in their body, which is forbidden in MRI scanning. Among the 72 PD patients, 35 patients were included as FOG+ according to two criteria: (1) rating scores >0 for the third item in the freezing of gait questionnaire (FOGQ), which was described by Giladi et al. (2000) as "Do you feel that your feet get glued to the floor while walking, making a turn or when trying to initiate walking (freezing)?"; (2) based on the former criteria, OFF-FOG patients whose symptoms of FOG were improved after drug therapy were included. The other 37 patients were grouped as PD without freezing of gait (FOG−). In addition, FOGQ was employed to evaluate the severity of FOG performance (Giladi et al., 2000). Other clinical assessments were also made across all subjects with PD. Ratings on the Hoehn and Yahr system (H&Y) (Hoehn and Yahr, 1998) were collected to evaluate the severity of PD symptoms. The gait and falls questionnaire (GFQ) was applied to evaluate the gait and falls risk (Giladi et al., 2000). The motor part of the Unified Parkinson's Disease Rating Scale (UPDRS-III) was also applied. For the motor assessments of PD patients, both FOGQ and GFQ assessments were made for the most severe OFF medication state based on their experience over the last week, and the UPDRS-III rating was assessed for the ON medication state. Non-motor symptoms of cognitive function were evaluated by montreal cognitive assessment (MOCA) (Nasreddine et al., 2005) and mini-mental state examination (MMSE) (Folstein et al., 1975). The levodopa equivalent daily dose (LEDD) of all of the PD patients was also collected. All subjects were recruited by the Guangzhou First People's Hospital from May 2017 to September 2018.

Data Acquisition

All subjects (37 NC, 37 FOG−, and 35 FOG+) were enrolled in 3.0T SIEMENS MRI scanning and were required to lie quietly in the scanner, staying awake with eyes closed. All of the PD patients were in the ON medication state when the MRI scanning was performed. Both functional and structural MRI images were obtained. The RS-fMRI was obtained by echo-planar imaging (EPI) with the following parameters: repetition time (TR) = 2000 ms; echo time (TE) = 21 ms; slice thickness/gap = 4 mm/0.6 mm; acquisition matrix = 64 × 64; flip angle = 78°; in-plane resolution = 3.5 mm × 3.5 mm; FOV = 224 × 224 mm^2. Sagittal T1-weighted images were obtained with the following parameters: TR/TE = 1900 ms/2.22 ms; acquisition matrix = 256 × 215; flip angle = 9°; in-plane resolution = 0.488 mm × 0.488 mm; slice thickness/gap = 1 mm/0.5 mm.

Data Preprocessing

The functional images were preprocessed using the toolkits of DPABI (Yan et al., 2016), the RS-fMRI Data Analysis Toolkit (REST)[1], and Statistical Parametric Mapping (SPM12)[2], implemented on a MATLAB platform. Data preprocessing included removal of the first 10 of the 220 time points in case of unstable signal quality, slice-timing adjustment (33 slices), head-motion correction, segmentation using a new segment (Ashburner and Friston, 2005) and diffeomorphic anatomical registration through Exponentiated Lie Algebra (DARTEL) (Ashburner, 2007), regression of nuisance covariates (including white matter, cerebrospinal fluid, and Friston's 24 parameters of head motion) (Friston et al., 1996; Satterthwaite et al., 2013; Yan et al., 2013), spatial normalization to Montreal Neurological Institute (MNI) space by resampling to 3mm × 3mm × 3mm by DARTEL (Ashburner, 2007), a temporal filter with a bandpass of 0.01–0.1 Hz, and removal of linear detrending. Six parameters of head motion (three directions each of rotation and translation) were recorded during the scanning. Subjects with maximal translations exceeding 2.5 mm or rotations over 2.5 degrees were excluded. According to this exclusion criterion, a total of six subjects were excluded from three groups, leaving 35/35/33 subjects for NC/FOG−/FOG+, respectively. Additionally, the mean frame-wise displacement (FD) (Jenkinson et al., 2002) was calculated, which represents the head motion. The mean FD was added as a covariate in the statistical analysis.

[1]http://www.restfmri.net/forum/REST

[2]http://www.fil.ion.ucl.ac.uk/spm/

Regional Homogeneity

ReHo evaluates local signal synchronizations by assessing the similarity between the time series of a chosen voxel and those of its neighboring voxels, and Kendall's coefficient concordance (KCC) is applied to ReHo calculation between a voxel and its 26 neighboring voxels (Zang et al., 2004). KCC-ReHo is a value between 0 and 1. Higher values indicate better local synchronization. Voxel-wise ReHo maps were calculated, and the ReHo maps were then spatially smoothed with a full width at half maximum (FWHM) of 4 mm. Additionally, *Z*-transformation was applied to the ReHo maps for standardization by subtracting the global mean value and then dividing by the global standard deviation. The standardized ReHo Z-maps were applied to the subsequent statistical and correlative analysis.

Statistical and Correlative Analysis

Analysis of covariance (ANCOVA) was applied to explore the ReHo differences among NC, FOG−, and FOG+, with

TABLE 1 | Demographic characteristics and clinical assessments.

	NC (n = 35)	FOG− (n = 35)	FOG+ (n = 33)	Statistical p
Age (years)	59.57 ± 5.94	62.60 ± 10.22	68.91 ± 8.17	$0.0001^{a\#\Delta}$
(range)	(47∼81)	(35∼82)	(54∼85)	
Sex (female/male)	24/11	16/19	12/21	0.0232^{b}
Education length (years)	11.08 ± 2.84	9.73 ± 3.21	10.64 ± 3.93	0.2416^{a}
Disease duration (years)	NA	3.30 ± 3.04	5.81 ± 3.88	0.0077^{c}
H&Y scores	NA	2.03 ± 0.52	2.70 ± 0.74	0.000^{c}
GFQ (OFF medication)	NA	3.03 ± 2.57	17.41 ± 12.43(n = 32)	$<0.0001^{c}$
FOGQ (OFF medication)	NA	1.29 ± 1.32(n = 34)	10.55 ± 6.41(n = 31)	$<0.0001^{c}$
UPDRS-III (ON medication)	NA	27.48 ± 13.36	31.80 ± 18.35	0.2830^{c}
MMSE	27.88 ± 2.10	26.09 ± 3.95	25.39 ± 4.24	$0.0153^{a*\#}$
MOCA	25.80 ± 3.13	22.82 ± 5.08	22.29 ± 4.90	$0.0034^{a*\#}$
LEDD	NA	319 ± 131	591 ± 387	0.0004^{c}
Mean FD (mm)	0.088 ± 0.064	0.076 ± 0.015	0.097 ± 0.069	0.2096^{a}

*NC, normal controls; FOG+/FOG−, Parkinson's disease with/without freezing of gait; H&Y, Hoehn and Yahr; FOGQ, freezing of gait questionnaire; GFQ, gait and falls questionnaire; UPDRS-III, Unified Parkinson's Disease Rating Scale (part three); MMSE, mini-mental state examination; MOCA, montreal cognitive assessment; LEDD, levodopa equivalent daily dose; FD, framewise displacement; NA, not applicable. Data are given as mean ± standard deviation. [a]Statistical p-value by one-way ANOVA test. [b]Statistical p-value by chi-square test. [c]Statistical p-value by two-sample t-test. *Significant group differences between NC and FOG− indicated by post hoc comparisons. [#]Significant group differences between NC and FOG+ indicated by post hoc comparisons. [Δ]Significant group differences between FOG− and FOG+ indicated by post hoc comparisons. Statistical significance level $p < 0.05$ for all tests.*

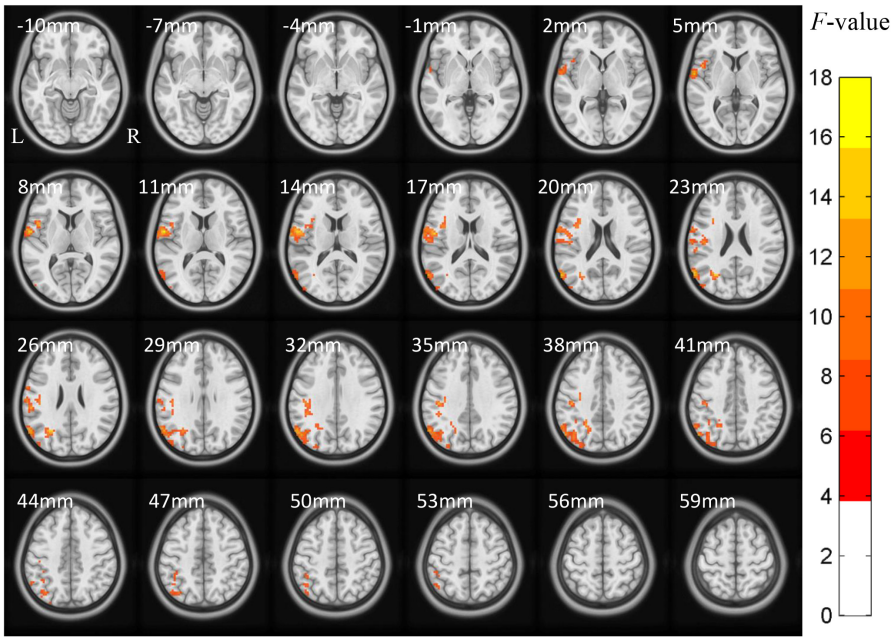

FIGURE 1 | ACONVA analysis of regional homogeneity (ReHo) among NC, FOG–, and FOG+ within gray matter. The *F*-map was corrected by GRF with voxel $p < 0.05$ and cluster $p < 0.05$ ($F > 3.83$, cluster size >6750 mm^3) within a gray matter mask. L/R, left/right hemisphere; NC, normal controls; FOG+/FOG–, Parkinson's disease with/without freezing of gait.

age, sex, and mean FD Jenkinson as covariates. The resultant *F*-map was corrected by multiple comparisons of the Gaussian Random Field (GRF) with voxel $p < 0.05$ and cluster $p < 0.05$ within a gray matter mask, two-tailed ($F > 3.83$ and cluster size >6750 mm^3). The surviving voxels were then extracted as a mask in the *post hoc* analysis of ReHo differences between every two groups by two-sample *t*-test with the covariates of age, sex, and mean FD. For the ReHo differences between FOG+ and FOG−, the clinical assessments that demonstrated significant group difference were also controlled as covariates. The resultant *T*-maps were further corrected by GRF with voxel $p < 0.001$ and cluster $p < 0.05$, which is beneficial for avoiding false positives (Woo et al., 2014).

In addition to the whole-brain gray matter, ReHo differences were also investigated within certain brain regions that have frequently been reported in previous motor- and gait-related PD studies, including the basal ganglia (caudate, putamen, and pallidum), sensorimotor cortices, cerebellum, hippocampus, para-hippocampus, and fusiform gyrus (Camicioli et al., 2003; Herman et al., 2014; Pan et al., 2017; Wang et al., 2018; Li et al., 2019). These brain regions were, respectively, extracted from the Automated Anatomical Labeling (AAL) template, which contains 116 brain regions, including 90 cerebrum regions and 26 cerebellum regions (Tzourio-Mazoyer et al., 2002). The corresponding AAL atlas regions were: the bilateral precentral gyrus (PreC, AAL-1,2), postcentral gyrus (PostC, AAL-57,58), supplementary motor area (SMA, AAL-19,20), cerebellum (AAL-91 to 116), caudate (AAL-71,72), putamen (AAL-73,74), pallidum (AAL-75,76), hippocampus (AAL-37,38), para-hippocampus (AAL-39,40), and fusiform gyrus (AAL-55,56). Both ANCOVA and *post hoc* analysis were performed within these regions, respectively, with covariates as in the analysis within whole-brain gray matter. Both ANCOVA and *post hoc* two-sample *t*-test were corrected by GRF with voxel $p < 0.05$ and cluster $p < 0.05$, two-tailed.

Brain regions showing significant differences were extracted as regions of interest (ROIs) for exploring the correlative relationship between signal synchronization and movement function (FOGQ, GFQ). The ReHo value was extracted from ROIs by averaging the values of all voxels within ROI. The Pearson correlation coefficient (statistical significance level $p < 0.05$) was used to quantify the correlation between ReHo and FOGQ/GFQ. Moreover, correlations were also analyzed within AAL templates to examine the neural interactions between regional signal synchronization and movement function across the whole brain.

RESULTS

Demographic Characteristics and Clinical Assessments

After exclusion of subjects with excessive head motion, 35 NC, 35 FOG−, and 33 FOG+ remained. There was no significant difference in head motion (mean FD) among the three groups ($p = 0.2096$). **Table 1** summarizes the demographic characteristics and clinical assessments of the

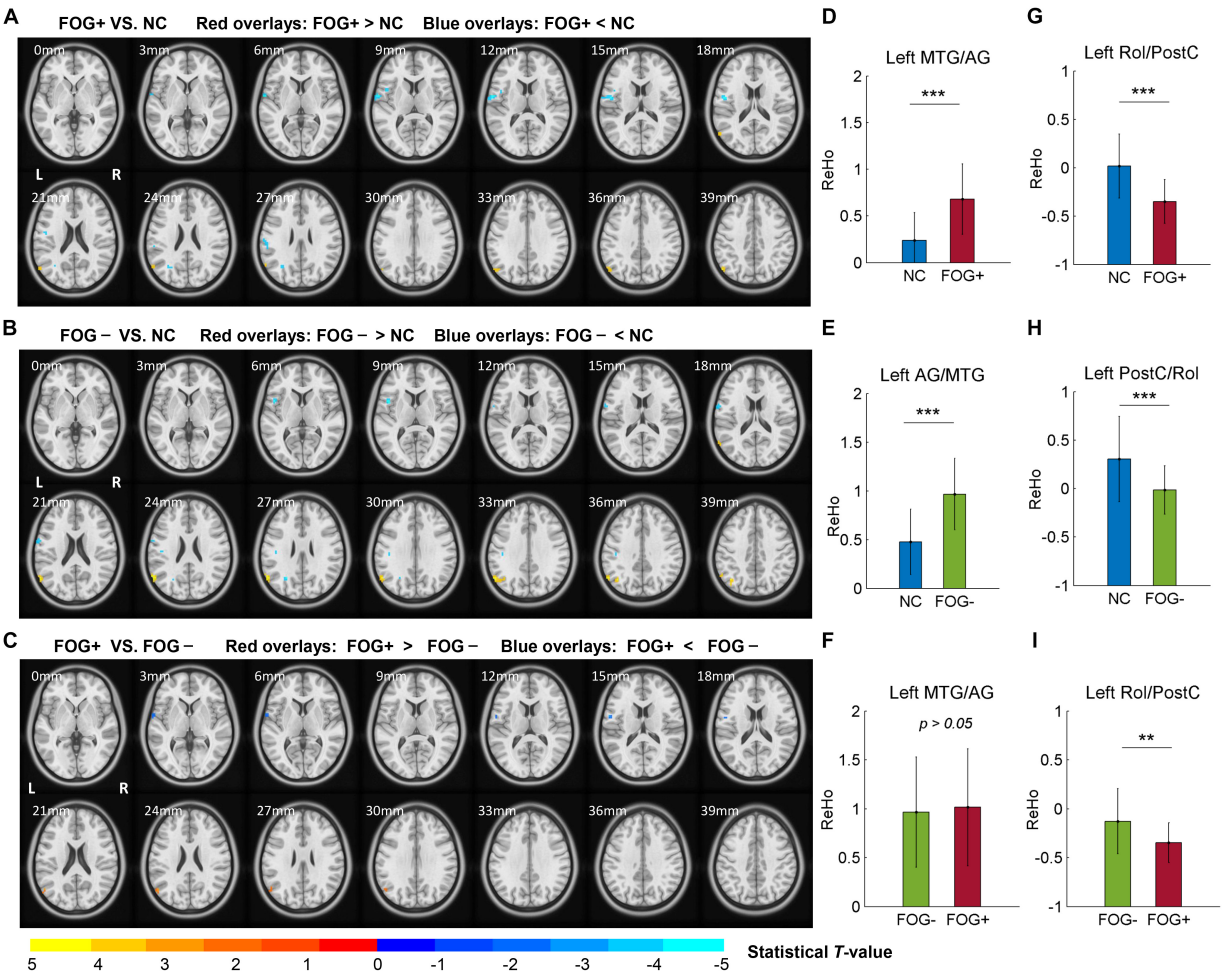

FIGURE 2 | *Post hoc* analysis of ReHo differences among NC, FOG–, and FOG+. **(A)** ReHo differences between FOG+ and NC. **(B)** ReHo differences between FOG– and NC. **(C)** ReHo differences between FOG+ and FOG– (voxel $p < 0.05$, uncorrected). *T*-maps **(A,B)** were corrected by GRF with voxel $p < 0.001$ and cluster $p < 0.05$ ($T > 3.45$, cluster size >135 mm^3) within the mask of significant brain regions identified by ANCOVA. ReHo signals were extracted from the left MTG/AG **(D–F)** and left Rol/PostC **(G–I)**, which were identified by *post hoc* analysis. L/R, left/right hemisphere; NC, normal controls; FOG+/FOG–, Parkinson's disease with/without freezing of gait; MTG, middle temporal gyrus; AG, angular gyrus; Rol, rolandic operculum; PostC, postcentral gyrus; $^{**}p < 0.005$; $^{***}p < 0.0005$.

subjects. A significant difference in age was observed among the three groups ($p = 0.0001$). Specifically, FOG+ showed higher ages than FOG− and NC, while no age difference was found between FOG− and NC ($p > 0.05$). Compared to FOG−, FOG+ had experienced longer disease durations and had higher severity of PD symptoms (H&Y scores) and higher ratings for GFQ and FOGQ. However, FOG+ and FOG− demonstrated no significant differences ($p > 0.05$) on UPDRS-III, MMSE, and MOCA. Note that some PD subjects refused to answer the GFQ and FOGQ and thereby, 35/32 GFQ results remained for FOG−/FOG+ and 34/31 FOGQ results for FOG−/FOG+, respectively.

Group Differences of Regional Homogeneity

The ACONVA analysis demonstrated significant ReHo differences among NC, FOG−, and FOG+. The identification of significant brain regions was based on XjView[3]. It was observed that all significant regions were located in the left cerebrum, including the sensorimotor area of PostC and rolandic operculum (Rol), the posterior middle temporal gyrus (MTG), the parietal gyrus with the angular gyrus (AG) and supramarginal gyrus (SMG), the middle occipital gyrus (MOG), and the opercular part of the inferior frontal gyrus (IFGoper) (**Figure 1**). Within these significant regions, *post hoc* analysis of two-sample *t*-test was performed between every two groups, corrected by GRF with voxel $p < 0.001$ and cluster $p < 0.05$, two-tailed ($T > 3.45$, cluster size >135 mm^3). The *T*-map between FOG+ and FOG− was thresholded with an uncorrected $p < 0.05$ (**Figure 2C**), which failed to survive under GRF correction. The results of between-group ReHo differences are shown in **Table 2** and **Figure 2**.

[3]http://www.alivelearn.net/xjview/

TABLE 2 | Brain regions showing significant regional homogeneity (ReHo) differences among NC, FOG−, and FOG+ within gray matter.

Brain regions	BA	Cluster size (mm^3)	Peak MNI coordinates (x y z)	Peak *T*-value
FOG+ vs. NC (Positive/Negative T-value indicates increased/decreased ReHo in FOG+)				
L-AG	39	567	–54 –69 39	4.32
L-MTG	39	378	–60 –66 21	4.13
L-Rol/PostC	48/22	1269	–60 –3 9	–4.92
L-IFGoper	48	189	–45 6 12	–4.01
L-MOG	19	243	–30 –63 27	–4.14
L-SMG/PostC	48	270	–57 –30 27	–4.15
FOG− vs. NC (Positive/Negative T-value indicates increased/decreased ReHo in FOG−)				
L-AG/MTG	39	2268	–60 –66 24	4.83
L-IFGoper	48	297	–48 9 6	–4.71
L-PostC/Rol	43	486	–63 0 18	–4.04
L-MOG	19	162	–27 –63 27	–4.45
L-PostC/SMG	48	270	–45 –21 27	–4.16
FOG+ vs. FOG− (Positive/Negative T-value indicates increased/decreased ReHo in FOG+)				
L-MTG/AG	39	405	–54 –66 24	2.70
L-PostC	48	216	–57 0 15	–2.62
L-Rol	48	243	–63 0 3	–2.38

NC, normal controls; FOG+/FOG−, Parkinson's disease with/without freezing of gait; L, left hemisphere; BA, Brodmann area; MNI, montreal neurological institute; AG, angular gyrus; MTG/MOG, middle temporal/occipital gyrus; Rol, rolandic operculum; PostC, postcentral gyrus; IFGoper, opercular part of the inferior frontal gyrus; SMG, supramarginal gyrus. T-value was the statistical t by post hoc analysis of two-sample t-test.

TABLE 3 | Brain regions showing significant ReHo differences among NC, FOG−, and FOG+ within the bilateral caudate.

Groups	Multiple comparison correction	Cluster size (mm^3)	Peak MNI coordinates (x y z)	Peak statistical value
NC, FOG−, FOG+	GRF $p < 0.05$	1566	–15 0 24	$F = 15.00$
FOG+ vs. NC	GRF $p < 0.05$	1458	–15 0 24	$T = 5.16$
FOG− vs. NC	Uncorrected $p < 0.05$	351	–15 21 9	$T = 3.44$
FOG+ vs. FOG−	GRF $p < 0.05$	918	–18 0 24	$T = 4.03$

NC, normal controls; FOG+/FOG−, Parkinson's disease with/without freezing of gait; MNI, montreal neurological institute; GRF, gaussian random field. The F-value indicates the statistical value among the three groups according to ANCOVA. The T-value indicates the statistical value of the between-group differences according to post hoc two-sample t-test.

Both FOG+ and FOG− showed higher ReHo than the NC in the left AG, and lower ReHo in the left IFGoper, left MOG, left Rol/PostC, and left SMG/PostC (**Table 2** and **Figures 2A,B**). Moreover, FOG+ achieved higher ReHo than the FOG− in the left MTG and left AG (**Table 2** and **Figure 2A**) and lower ReHo than the FOG− in the left Rol/PostC (**Table 2** and **Figure 2C**).

Furthermore, ReHo differences were also examined in the bilateral PreC, PostC, SMA, cerebellum, caudate, putamen, pallidum, hippocampus, para-hippocampus, and fusiform gyrus, respectively. However, significant results were only observed in the caudate (**Table 3** and **Figure 3**). The *F*-map acquired by ANCOVA among the three groups was corrected by GRF with voxel $p < 0.05$ and cluster $p < 0.05$ (threshold of $F > 3.84$ and cluster size >1566 mm^3) (**Figure 3B**). ReHo differences were demonstrated between the three groups in the left caudate (**Figures 3B,C**). *Post hoc* two-sample *t*-testing on the pair groups were performed within the significant left caudate, and the resultant *T*-maps were corrected by GRF with voxel $p < 0.05$ and cluster $p < 0.05$ (threshold of $T > 2.00$ and cluster size >486 mm^3). FOG+ was observed to have higher ReHo than FOG− (**Figures 3F,I**) and NC (**Figures 3D,G**) in the left caudate. While no cluster survived the GRF correction for the *T*-map between FOG− and NC, thresholding with an uncorrected voxel $p < 0.05$ and cluster size of 351 mm^3 demonstrated higher ReHo in the left caudate in FOG− than in NC (**Figures 3E,H**).

Correlative Analysis

The correlative analysis between local signal synchronization (ReHo) and movement function (GFQ/FOGQ) was performed within significant brain regions identified by *post hoc* two-sample *t*-tests. Among the regions, significant results were observed in the left SMG/PostC (**Figure 4A**), which was visualized by BrainNet Viewer (Xia et al., 2013). The ReHo values of FOG+ and FOG− were significantly lower than those of NC ($p < 0.0001$), while no difference was found between those of FOG+ and FOG− ($p = 0.2408$) (**Figure 4B**). The ReHo of FOG+ was negatively correlated with FOGQ in the left SMG/PostC ($r = -0.39$, $p < 0.05$) (**Figure 4D**), while no significant correlation was found between the ReHo of FOG− and FOGQ (**Figure 4C**). In addition, neither the ReHo of FOG+ nor the ReHo of FOG− was correlated with GFQ.

As well as from the ROIs identified by the *post hoc* analysis (**Tables 2**, **3**), ReHo signals were also extracted from AAL

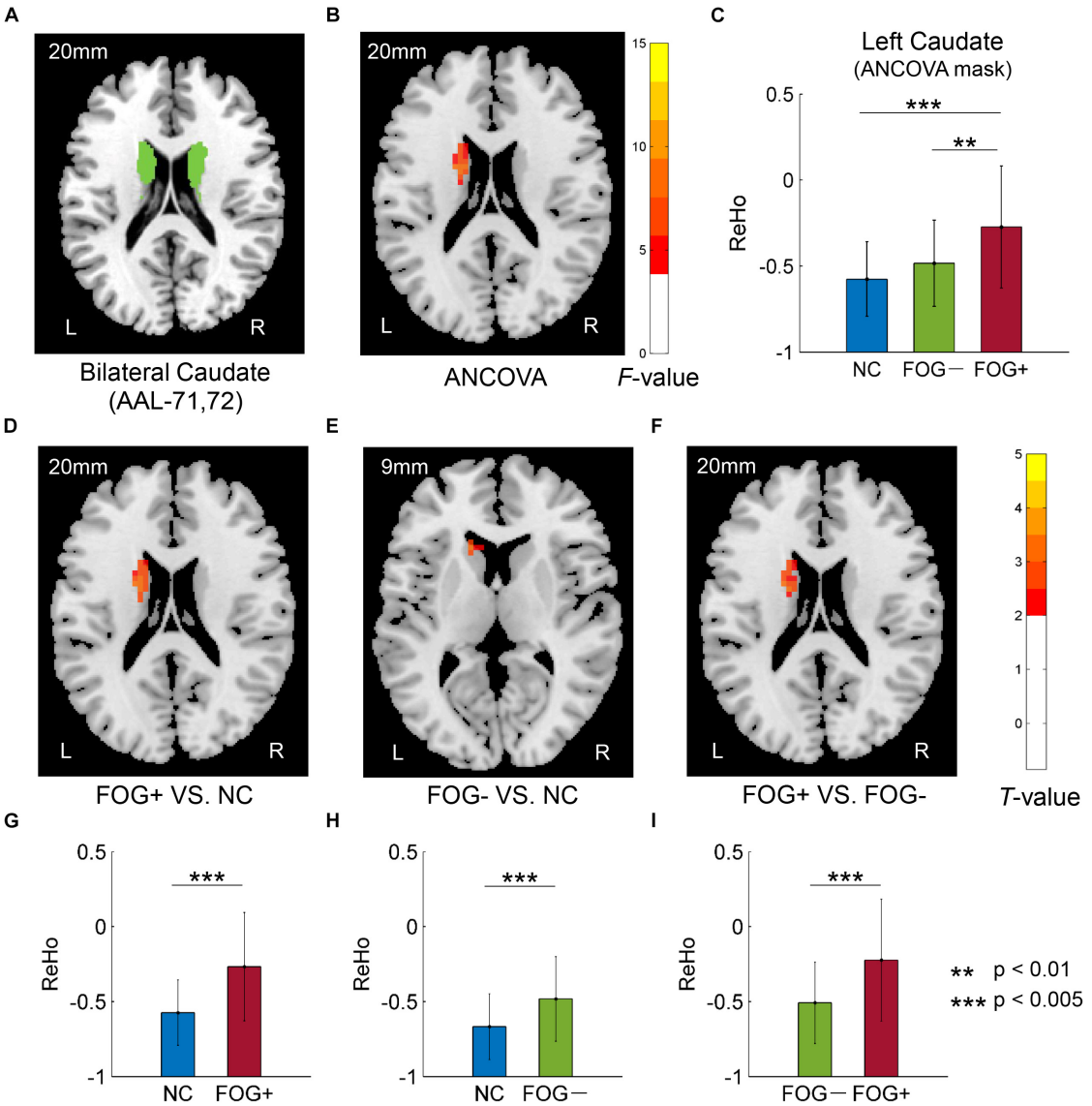

FIGURE 3 | Regional homogeneity differences among NC, FOG–, and FOG+ within the bilateral caudate. **(A)** Bilateral caudate. **(B)** *F*-map of ANCOVA analysis of the three groups, corrected by GRF with voxel $p < 0.05$, threshold of $F > 3.84$ and cluster size >1566 mm^3. **(C)** FOG+ subjects showed higher ReHo within the left caudate than did FOG– and NC. *Post hoc* two-sample *t*-tests on FOG+ and NC **(D,G)**, FOG– and NC **(E,H)**, and FOG+ and FOG– **(F,I)**. The *T*-map in **(E)** was with a threshold of an uncorrected voxel $p < 0.05$, **(D,F)** were corrected by GRF with voxel $p < 0.05$, threshold of $T > 2.00$ and cluster size >486 mm^3. L/R, eft/right hemisphere; NC, normal controls; FOG+/FOG–, Parkinson's disease with/without freezing of gait.

templates and correlated with GFQ and FOGQ, respectively. Significant results were observed in the left superior temporal gyrus (STG, AAL-81), left orbital part of the medial prefrontal cortex (MPFCorb, AAL-25), left gyrus rectus (AAL-27), right inferior temporal gyrus (ITG, AAL-90), and left cerebellum anterior lobe (CAL, AAL-97) (**Figure 5**). The ReHo values of FOG+ in the left STG were observed to have negative correlations ($p < 0.05$) with GFQ ($r = -0.36$) and FOGQ ($r = -0.38$) (**Figure 5A**). The ReHo values of FOG−, meanwhile, were observed to have negative correlations with GFQ/FOGQ in the left MPFCorb (**Figure 5B**), left gyrus rectus (**Figure 5C**), and right ITG (**Figure 5D**) and to be positively correlated with GFQ/FOGQ in the left CAL (**Figure 5E**). Though significant correlations were observed in the above five brain regions, the ReHo signals extracted from the five sub-templates showed no significant difference ($p > 0.05$) between FOG− and FOG+ according to two-sample *t*-test (**Figure 5**).

DISCUSSION

In this study, we assessed ReHo to explore differences in local synchronization among NC, FOG+, and FOG− subjects, and significant results were observed in the left cerebrum. In

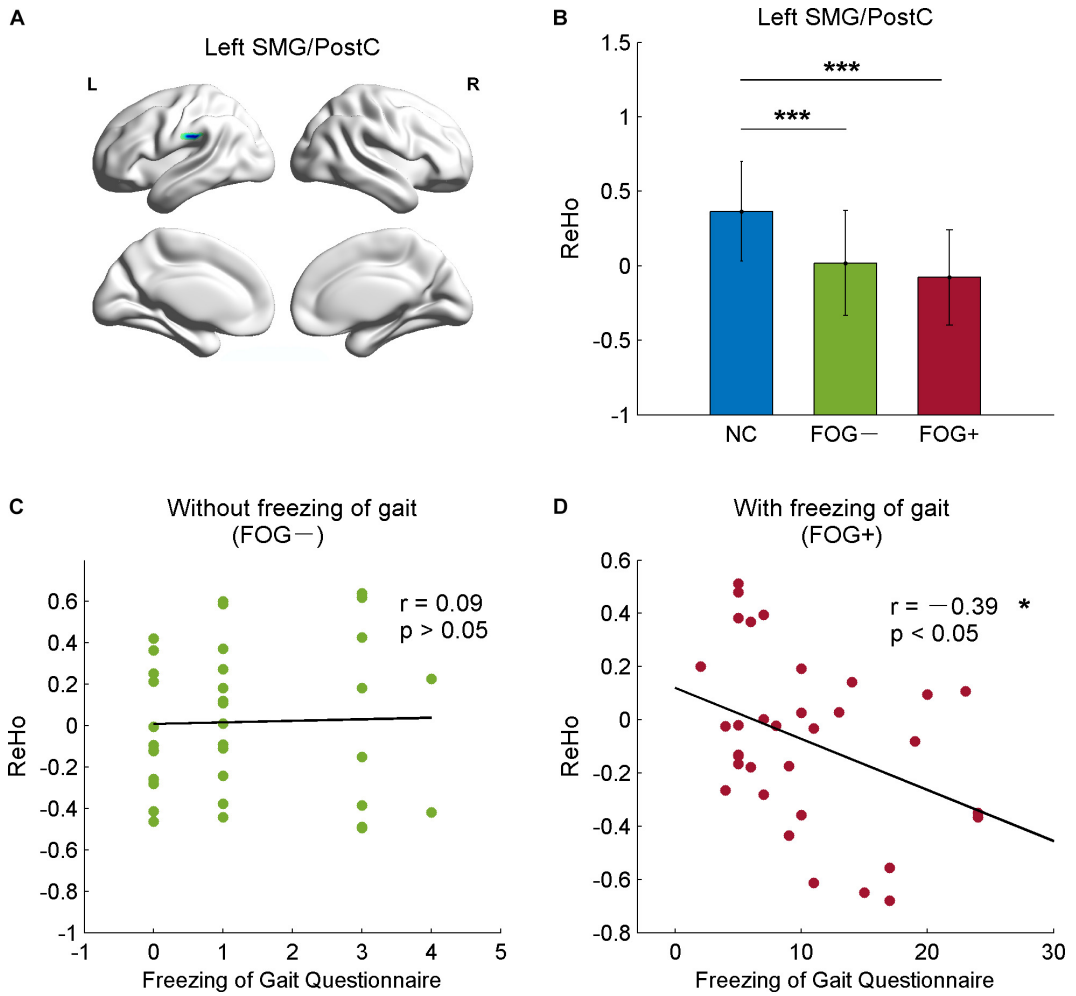

FIGURE 4 | Correlation between ReHo and movement function in the left supramarginal gyrus/postcentral gyrus (SMG/PostC). **(A)** Visualization of left SMG/PostC. **(B)** ReHo of left SMG/PostC. ***$p < 0.0001$ between FOG+/FOG– and NC, $p = 0.2408$ between FOG+ and FOG–. **(C)** Correlation between ReHo of FOG– and movement function. **(D)** Correlation between ReHo of FOG+ and movement function.

comparison to NC, FOG+, and FOG− showed increased ReHo in the left AG but decreased ReHo in the left IFGoper, left Rol/PostC, left MOG, and left SMG (**Table 2** and **Figures 2A,B**). Compared to FOG−, the ReHo in FOG+ was decreased in the left Rol/PostC (**Figure 2C**) and increased in the left caudate (**Figure 3**). Neural correlation analysis showed that the ReHo of FOG+ was negatively correlated with FOGQ ($r = -0.39$) in the left SMG/PostC (**Figure 4**) and negatively correlated with GFQ/FOGQ ($r = -0.36/-0.38$) in the STG (**Figure 5A**).

Previous studies have reported structural changes in FOG+ vs. FOG−, with gray matter volume reductions in the posterior cingulate cortex/precuneus (PCC/PCu) (Tessitore et al., 2012a), left IFG (Pan et al., 2012), inferior parietal lobule (IPL) (Kostić et al., 2012), and AG (Herman et al., 2014). The PCC/PCu, medial prefrontal cortex (MPFC), AG, and posterior MTG are major parts of the default mode network (DMN), where brain activities are active in the resting state but passive in the task-induced state (Raichle et al., 2001). Gray-matter atrophy of the DMN in FOG+ probably leads to dysfunctional brain activities in the resting state. Meta-analysis of the ReHo of PD has been reported to give consistent results in the DMN and motor networks, with increased ReHo in the bilateral IPL, bilateral MPFC, and left cerebellum and decreased ReHo in the right putamen and right PreC (Pan et al., 2017; Wang et al., 2018). Our findings are consistent with the results showing increased ReHo in the DMN, observing increased ReHo in the left MTG/AG (**Figures 2A,B,D,E**). However, no gait-specificity of ReHo in the DMN was found in PD patients. Under a threshold of an uncorrected voxel $p < 0.05$, FOG+ were observed to have increased ReHo in the left MTG/AG (**Figure 2C**), while no difference was found between FOG+ and FOG− when the averaged ReHo was extracted from these regions (**Figure 2F**). A previous study on FOG+ also reported decreased ReHo in the frontal cortex and motor area (Zhou et al., 2018), which suggests that FOG+ subjects have decreased cognitive function and motor function. Our findings also demonstrated decreased ReHo in the

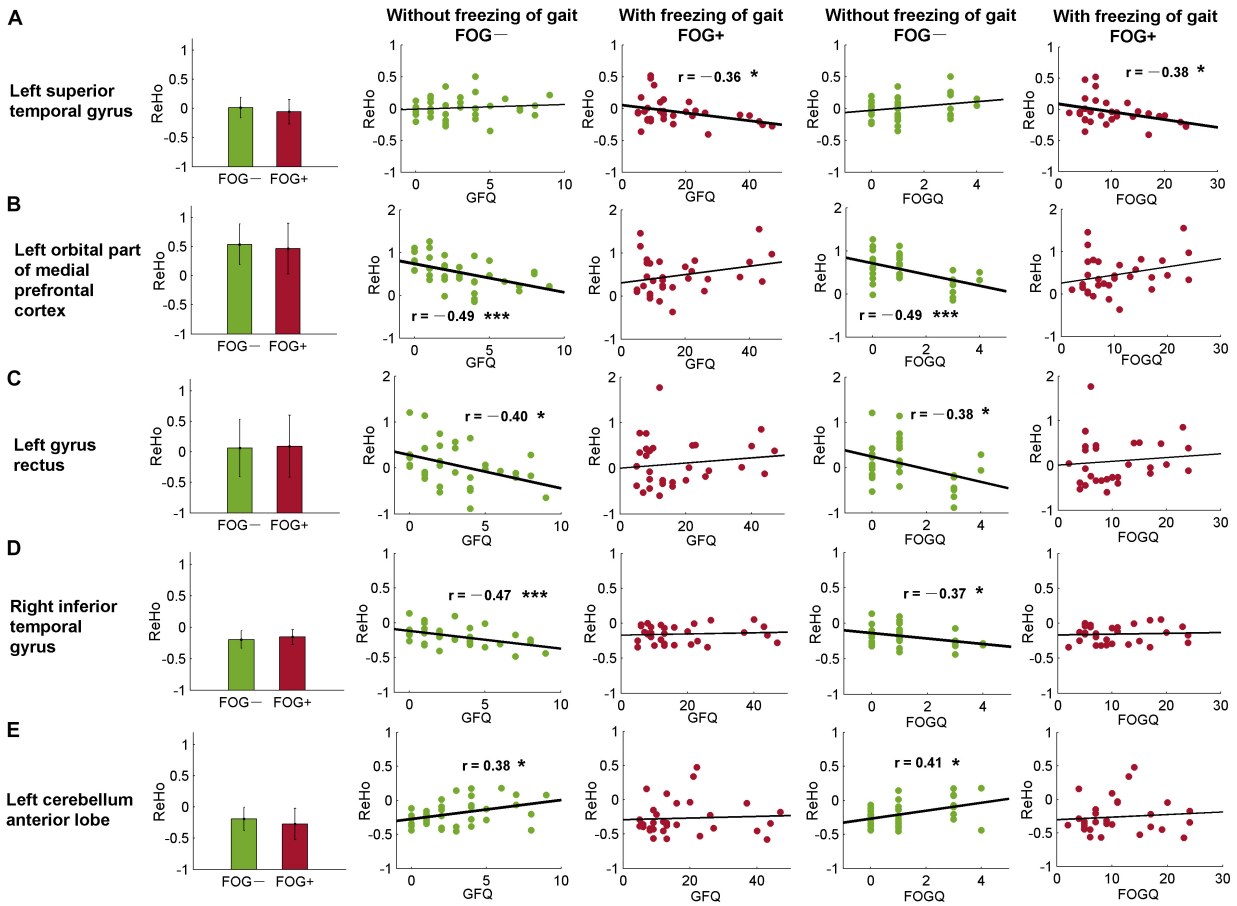

FIGURE 5 | Correlative analysis between ReHo and movement function within automated anatomical labeling (AAL) templates. Significant correlation was found in the **(A)** left superior temporal gyrus, **(B)** left orbital part of the medial prefrontal cortex, **(C)** left gyrus rectus, **(D)** right inferior temporal gyrus, and **(E)** left cerebellum anterior lobe. FOGQ, freezing of gait questionnaire; GFQ, gait and falls questionnaire. Statistical significance notation: $^{*}p < 0.05$, $^{***}p < 0.005$.

IFG and MOG. A resting-state study with connectivity analysis of FOG+ observed decreased connectivity in the frontal and occipital lobes, which correspond to the executive and visual networks (Tessitore et al., 2012b). These findings suggest the disruption of executive and visual functions in FOG+.

One of the most critical findings of this study is that for ReHo in the left Rol/PostC, FOG+ <FOG− <NC, which suggests that this region is most hypoactive in FOG+ (**Figures 2G–I**). However, when using a threshold of an uncorrected voxel $p < 0.05$ when comparing the ReHo of FOG+ and FOG−, significant difference ($p < 0.005$) was observed in the left Rol/PostC by extracting the averaged ReHo from the surviving voxels (**Figure 2I**). This suggests that ReHo values in the left Rol/PostC, the sensorimotor areas, are critical features for discriminating the three groups. One interesting finding comes from the fact that all of the significant ROIs among FOG+, FOG−, and NC were located in the left hemisphere of the cerebrum (**Figures 1, 2** and **Table 2**). An fMRI study of emotional picture stimuli reported activations of left-brain activities in response to positive pictures and hence suggested that the left hemisphere of the brain is associated with positive emotions (Canli et al., 1998). Altered ReHo in the left hemisphere may reveal decreased positive emotion in FOG+. Previous studies also demonstrate that emotional state affects the motor control of gait (Naugle et al., 2011). Depression and anxiety are also the major emotional symptoms in PD, which exacerbate poor motor performance (Macht et al., 2005; Avanzino et al., 2018). Therefore, cognitive behavioral therapy is recommended for the treatment of patients with FOG (Berardelli et al., 2015).

The basal ganglia, sensorimotor area, cerebellum, hippocampus, parahippocampus, and fusiform gyrus are critical regions involved in the pathophysiology of PD. ReHo differences were also examined within these brain regions. However, significant results were only observed in the left caudate: FOG+ >FOG− >NC (**Table 3** and **Figure 3**). Gray matter atrophy in the left caudate (Jia et al., 2019) and consistently decreased ReHo in the putamen (Pan et al., 2017; Wang et al., 2018) have been observed in PD patients. In our results, meanwhile, PD showed increased ReHo in the left caudate, with FOG+ being the most active. Decreased ReHo may indicate functional deficits caused by diseases, while increased ReHo may be related to a compensatory mechanism for maintaining normal function

(Pan et al., 2017). It is suggested that FOG in PD is associated with functional decoupling between the cognitive control network and the basal ganglia (Shine et al., 2013a). Increased ReHo in the left caudate may reflect a compensation of the cognitive control function in PD patients.

Within the significant brain regions, the ReHo of FOG+ was negatively correlated ($r = -0.39$) with FOGQ in the left SMG/PostC (**Figure 4**). Negative correlation was also observed between ReHo and GFQ/FOGQ ($r = -0.36/-0.38$) in the STG based on the whole-brain analysis (**Figure 5A**). A DBS study on the effect of sub-thalamic nucleus stimulation in PD reported a positive correlation between motor scores and metabolic activity in parietal-temporal sensory-related brain areas (Chul et al., 2007). Activation of brain activity was found in the temporal lobe during a memory paradigm fMRI study after rehabilitation (Díez-Cirarda et al., 2017). These findings indicate that brain activities in the motor area and temporal lobe are associated with an improvement in motor performance.

There are two limitations to this study. The demographic characteristics of age and sex are not properly matched among FOG+, FOG−, and NC. The age of FOG+ is significantly higher than that of FOG− and NC. PD patients with advanced age and a higher stage of disease progression are more likely to experience FOG (Zhang et al., 2016). In this study, age and sex were included as covariates in the statistical analysis to regress out the unmatched confounds. The second limitation comes from the insufficient sample size. In our future work, more subjects will be enrolled for a better understanding of the neuroimaging features of PD patients with freezing of gait.

CONCLUSION

ReHo was used to explore the regional signal synchronization of brain activities in PD patients. The results suggest that the brain activities of PD patients with FOG were the most active in the left caudate and the most hypoactive in the left Rol/PostC. The correlation analysis between ReHo and movement scores (GFQ/FOGQ) in the left STG provides the potential to stratify PD patients with and without FOG. This study provides new insight for understanding PD patients.

DATA AVAILABILITY STATEMENT

The datasets generated for this study are available on request to the corresponding author.

ETHICS STATEMENT

This study was approved by the Institutional Review Board (IRB) of Guangzhou First People's Hospital. Written informed consent was obtained from all subjects.

AUTHOR CONTRIBUTIONS

YL wrote the manuscript. YL, ML, and XW conceived of the idea and performed the literature review. YL, ML, XW, HC, GH, and SY performed the data analysis. XW, XR, ZLuo, and JZ contributed to the data collection. All authors interpreted the results, reviewed the manuscript and joined the discussion of the manuscript.

FUNDING

This work was supported in part by grants from the Shenzhen Matching Project (GJHS20170314155751703), the National Key Research and Development Program of China (2016YFC0105102), the National Science Foundation of China (61871374 and 81871846), the Science Foundation of Guangdong (2017B020229002, 2015B020233011, and 2014A030312006), the Leading Talent of Special Support Project in Guangdong (2016TX03R139), the Science and Technology Planning Project of Guangzhou (201804010032), the Guangzhou Municipal Health Bureau Project (20171A010247), the Guangzhou Key Project of R&D Innovation (2016201604030018), the Shenzhen Key Technical Research Project (JSGG20160229203812944), the Shenzhen Basic Technology Research Project (JCYJ20170413162458312), and the Shenzhen Engineering Laboratory for Key Technologies on Intervention Diagnosis and Treatment Integration.

REFERENCES

Amboni, M., Cozzolino, A., Longo, K., Picillo, M., and Barone, P. (2008). Freezing of gait and executive functions in patients with Parkinson's disease. *Mov. Disord.* 23, 395–400. doi: 10.1002/mds.21850

Ashburner, J. (2007). A fast diffeomorphic image registration algorithm. *Neuroimage* 38, 95–113. doi: 10.1016/j.neuroimage.2007.07.007

Ashburner, J., and Friston, K. J. (2005). Unified segmentation. *Neuroimage* 26, 839–851. doi: 10.1016/j.neuroimage.2005.02.018

Avanzino, L., Lagravinese, G., Abbruzzese, G., and Pelosin, E. (2018). Relationships between gait and emotion in Parkinson's disease: a narrative review. *Gait Posture* 65, 57–64. doi: 10.1016/j.gaitpost.2018.06.171

Bartels, A. L., and Leenders, K. L. (2008). Brain imaging in patients with freezing of gait. *Mov. Disord.* 23, S461–S467. doi: 10.1002/mds.21912

Berardelli, I., Fabbrini, G., Pasquini, M., Biondi, M., Berardelli, A., and Roselli, V. (2015). Cognitive behavioral therapy in movement disorders: a review. *Mov. Disord. Clin. Pract.* 2, 107–115. doi: 10.1002/mdc3.12160

Bohnen, N. I., Frey, K. A., Studenski, S., Kotagal, V., Koeppe, R. A., Constantine, G. M., et al. (2014). Extra-nigral pathological conditions are common in Parkinson's disease with freezing of gait: an in vivo positron emission tomography study. *Mov. Disord.* 29, 1118–1124. doi: 10.1002/mds.25929

Borroni, B., Premi, E., Formenti, A., Turrone, R., Alberici, A., Cottini, E., et al. (2015). Structural and functional imaging study in dementia with lewy bodies and Parkinson's disease dementia. *Park. Relat. Disord.* 21, 1049–1055. doi: 10.1016/j.parkreldis.2015.06.013

Camicioli, R., Moore, M. M., Kinney, A., Corbridge, E., Glassberg, K., and Kaye, J. A. (2003). Parkinson's disease is associated with hippocampal atrophy. *Mov. Disord.* 18, 784–790. doi: 10.1002/mds.10444

Canli, T., Desmond, J. E., Zhao, Z., Glover, G., and Gabrieli, J. D. E. (1998). Hemispheric asymmetry for emotional stimuli detected with fMRI. *Neuroreport* 9, 3233–3239. doi: 10.1097/00001756-199810050-199810019

Choe, I. H., Yeo, S., Chung, K. C., Kim, S. H., and Lim, S. (2013). Decreased and increased cerebral regional homogeneity in early Parkinson's disease. *Brain Res.* 1527, 230–237. doi: 10.1016/j.brainres.2013.06.027

Chul, H. L., Aalto, S., Rinne, J. O., Ki, O. L., Seung, H. O., Jin, W. C., et al. (2007). Different cerebral cortical areas influence the effect of subthalamic nucleus stimulation on Parkinsonian motor deficits and freezing of gait. *Mov. Disord.* 22, 2176–2182. doi: 10.1002/mds.21609

Díez-Cirarda, M., Ojeda, N., Peña, J., Cabrera-Zubizarreta, A., Lucas-Jiménez, O., Gómez-Esteban, J. C., et al. (2017). Increased brain connectivity and activation after cognitive rehabilitation in Parkinson's disease: a randomized controlled trial. *Brain Imaging Behav.* 11, 1640–1651. doi: 10.1007/s11682-016-9639-x

Fasano, A., Herman, T., Tessitore, A., Strafella, A. P., and Bohnen, N. I. (2015). Neuroimaging of freezing of gait. *J. Parkinsons Dis.* 5, 241–254. doi: 10.3233/JPD-150536

Folstein, M. F., Folstein, S. E., and McHugh, P. R. (1975). Mini-mental state". a practical method for grading the cognitive state of patients for the clinician. *J. Psychiatr. Res.* 12, 189–198. doi: 10.1016/0022-3956(75)90026-90026

Fox, M. D., and Raichle, M. E. (2007). Spontaneous fluctuations in brain activity observed with functional magnetic resonance imaging. *Nat. Rev. Neurosci.* 8, 700–711. doi: 10.1038/nrn2201

Friston, K. J., Williams, S., Howard, R., Frackowiak, R. S. J., and Turner, R. (1996). Movement-related effects in fMRI time-series. *Magn. Reson. Med.* 35, 346–355. doi: 10.1002/mrm.1910350312

Giladi, N., Shabtai, H., Simon, E. S., Biran, S., Tal, J., and Korczyn, A. D. (2000). Construction of freezing of gait questionnaire for patients with Parkinsonism. *Park. Relat. Disord.* 6, 165–170. doi: 10.1016/S1353-8020(99)00062-60

Herman, T., Rosenberg-Katz, K., Jacob, Y., Auriel, E., Gurevich, T., Giladi, N., et al. (2013). White matter hyperintensities in Parkinson's disease: do they explain the disparity between the postural instability gait difficulty and tremor dominant subtypes? *PLoS One* 8:e55193. doi: 10.1371/journal.pone.0055193

Herman, T., Rosenberg-Katz, K., Jacob, Y., Giladi, N., and Hausdorff, J. M. (2014). Gray matter atrophy and freezing of gait in Parkinson's disease: is the evidence black-on-white? *Mov. Disord.* 29, 134–139. doi: 10.1002/mds.25697

Hoehn, M. M., and Yahr, M. D. (1998). Parkinsonism: onset, progression, and mortality. *Neurology* 50, 318–318. doi: 10.1212/WNL.50.2.318

Jenkinson, M., Bannister, P., Brady, M., and Smith, S. (2002). Improved optimization for the robust and accurate linear registration and motion correction of brain images. *Neuroimage* 17, 825–841. doi: 10.1016/S1053-8119(02)91132-91138

Jia, X., Li, K., Fu, X., Liang, P., and Li, Y. (2019). Precuneus dysfunction in Parkinson's disease with mild cognitive impairment. *Front. Aging Neurosci.* 10:427. doi: 10.3389/fnagi.2018.00427

Jiang, S., Wang, M., Zhang, L., Yuan, Y., Tong, Q., Ding, J., et al. (2016). Regional homogeneity alterations differentiate between tremor dominant and postural instability gait difficulty subtypes of Parkinson's disease. *J. Neural. Transm.* 123, 219–229. doi: 10.1007/s00702-015-1490-1495

Kostić, V. S., Agosta, F., Pievani, M., Stefanova, E., Ječmenica-Lukić, M., Scarale, A., et al. (2012). Pattern of brain tissue loss associated with freezing of gait in Parkinson disease. *Neurology* 78, 409–416. doi: 10.1212/WNL.0b013e318245d23c

Lewis, S. J. G., and Shine, J. M. (2016). The next step: a common neural mechanism for freezing of gait. *Neuroscientist* 22, 72–82. doi: 10.1177/1073858414559101

Li, J., Yuan, Y., Wang, M., Zhang, J., Zhang, L., Jiang, S., et al. (2018). Decreased interhemispheric homotopic connectivity in Parkinson's disease patients with freezing of gait: a resting state fMRI study. *Park. Relat. Disord.* 52, 30–36. doi: 10.1016/j.parkreldis.2018.03.015

Li, M., Liu, Y., Chen, H., Hu, G., Yu, S., Ruan, X., et al. (2019). Altered global synchronizations in patients with Parkinson's disease: a resting-state fMRI study. *Front. Aging Neurosci.* 11:139. doi: 10.3389/fnagi.2019.00139

Li, Y., Liang, P., Jia, X., and Li, K. (2016). Abnormal regional homogeneity in Parkinson's disease: a resting state fMRI study. *Clin. Radiol.* 71, 28–34. doi: 10.1016/j.crad.2015.10.006

Macht, M., Kaussner, Y., Möller, J. C., Stiasny-Kolster, K., Eggert, K. M., Krüger, H. P., et al. (2007). Predictors of freezing in Parkinson's disease: a survey of 6,620 patients. *Mov. Disord.* 22, 953–956. doi: 10.1002/mds.21458

Macht, M., Schwarz, R., and Ellgring, H. (2005). Patterns of psychological problems in Parkinson's disease. *Acta Neurol. Scand.* 111, 95–101. doi: 10.1111/j.1600-0404.2005.00375.x

Maidan, I., Bernad-Elazari, H., Gazit, E., Giladi, N., Hausdorff, J. M., and Mirelman, A. (2015). Changes in oxygenated hemoglobin link freezing of gait to frontal activation in patients with Parkinson disease: an fNIRS study of transient motor-cognitive failures. *J. Neurol.* 262, 899–908. doi: 10.1007/s00415-015-7650-7656

Nasreddine, Z. S., Phillips, N. A., Bédirian, V., Charbonneau, S., Whitehead, V., Collin, I., et al. (2005). The montreal cognitive assessment, MoCA: a brief screening tool for mild cognitive impairment. *J. Am. Geriatr. Soc.* 53, 695–699. doi: 10.1111/j.1532-5415.2005.53221.x

Naugle, K. M., Hass, C. J., Joyner, J., Coombes, S. A., and Janelle, C. M. (2011). Emotional state affects the initiation of forward gait. *Emotion* 11, 267–277. doi: 10.1037/a0022577

Nutt, J. G., Bloem, B. R., Giladi, N., Hallett, M., Horak, F. B., and Nieuwboer, A. (2011). Freezing of gait: moving forward on a mysterious clinical phenomenon. *Lancet Neurol.* 10, 734–744. doi: 10.1016/S1474-4422(11)70143-70140

Pan, P. L., Song, W., and Shang, H. F. (2012). Voxel-wise meta-analysis of gray matter abnormalities in idiopathic Parkinson's disease. *Eur. J. Neurol.* 19, 199–206. doi: 10.1111/j.1468-1331.2011.03474.x

Pan, P. L., Zhan, H., Xia, M. X., Zhang, Y., Guan, D. N., and Xu, Y. (2017). Aberrant regional homogeneity in Parkinson's disease: a voxel-wise meta-analysis of resting-state functional magnetic resonance imaging studies. *Neurosci. Biobehav. Rev.* 72, 223–231. doi: 10.1016/j.neubiorev.2016.11.018

Park, H. K., Kim, J. S., Im, K. C., Oh, S. J., Kim, M. J., Lee, J. H., et al. (2009). Functional brain imaging in pure Akinesia with gait freezing: [18F] FDG PET and [18F] FP-CIT PET analyses. *Mov. Disord.* 24, 237–245. doi: 10.1002/mds.22347

Peterson, D. S., Plotnik, M., Hausdorff, J. M., and Earhart, G. M. (2012). Evidence for a relationship between bilateral coordination during complex gait tasks and freezing of gait in Parkinson's disease. *Park. Relat. Disord.* 18, 1022–1026. doi: 10.1016/j.parkreldis.2012.05.019

Plotnik, M., Giladi, N., and Hausdorff, J. M. (2008). Bilateral coordination of walking and freezing of gait in Parkinson's disease. *Eur. J. Neurosci.* 27, 1999–2006. doi: 10.1111/j.1460-9568.2008.06167.x

Postuma, R. B., Berg, D., Stern, M., Poewe, W., Olanow, C. W., Oertel, W., et al. (2015). MDS clinical diagnostic criteria for Parkinson's disease. *Mov. Disord.* 30, 1591–1601. doi: 10.1002/mds.26424

Raichle, M. E., MacLeod, A. M., Snyder, A. Z., Powers, W. J., Gusnard, D. A., and Shulman, G. L. (2001). A default mode of brain function. *Proc. Natl. Acad. Sci. U.S.A.* 98, 676–682. doi: 10.1073/pnas.98.2.676

Satterthwaite, T. D., Elliott, M. A., Gerraty, R. T., Ruparel, K., Loughead, J., Calkins, M. E., et al. (2013). An improved framework for confound regression and filtering for control of motion artifact in the preprocessing of resting-state functional connectivity data. *Neuroimage* 64, 240–256. doi: 10.1016/j.neuroimage.2012.08.052

Schweder, P. M., Hansen, P. C., Green, A. L., Quaghebeur, G., Stein, J., and Aziz, T. Z. (2010). Connectivity of the pedunculopontine nucleus in parkinsonian freezing of gait. *Neuroreport* 21, 914–916. doi: 10.1097/WNR.0b013e32833ce5f1

Shine, J. M., Matar, E., Ward, P. B., Frank, M. J., Moustafa, A. A., Pearson, M., et al. (2013a). Freezing of gait in Parkinson's disease is associated with functional decoupling between the cognitive control network and the basal ganglia. *Brain* 136, 3671–3681. doi: 10.1093/brain/awt272

Shine, J. M., Naismith, S. L., and Lewis, S. J. G. (2013b). The differential yet concurrent contributions of motor, cognitive and affective disturbance to freezing of gait in Parkinson's disease. *Clin. Neurol. Neurosurg.* 115, 542–545. doi: 10.1016/j.clineuro.2012.06.027

Tessitore, A., Amboni, M., Cirillo, G., Corbo, D., Picillo, M., Russo, A., et al. (2012a). Regional gray matter atrophy in patients with Parkinson disease and freezing of gait. *Am. J. Neuroradiol.* 33, 1804–1809. doi: 10.3174/ajnr.A3066

Tessitore, A., Amboni, M., Esposito, F., Russo, A., Picillo, M., Marcuccio, L., et al. (2012b). Resting-state brain connectivity in patients with Parkinson's disease and freezing of gait. *Park. Relat. Disord.* 18, 781–787. doi: 10.1016/j.parkreldis.2012.03.018

Tzourio-Mazoyer, N., Landeau, B., Papathanassiou, D., Crivello, F., Etard, O., Delcroix, N., et al. (2002). Automated anatomical labeling of activations in SPM using a macroscopic anatomical parcellation of the MNI MRI single-subject brain. *Neuroimage* 15, 273–289. doi: 10.1006/nimg.2001.0978

Villarreal, M. F., Huerta-Gutierrez, R., and Fregni, F. (2018). "Parkinson's disease," in *Clinical Trials in Neurology*, Vol. 138, ed. F. Fregni, (New York, NY: Humana Press).

Wang, J., Zhang, J. R., Zang, Y. F., and Wu, T. (2018). Consistent decreased activity in the putamen in Parkinson's disease: a meta-analysis and an independent validation of resting-state fMRI. *Gigascience* 7, 1–13. doi: 10.1093/gigascience/giy071

Wang, M., Jiang, S., Yuan, Y., Zhang, L., Ding, J., Wang, J., et al. (2016). Alterations of functional and structural connectivity of freezing of gait in Parkinson's disease. *J. Neurol.* 263, 1583–1592. doi: 10.1007/s00415-016-8174-8174

Woo, C. W., Krishnan, A., and Wager, T. D. (2014). Cluster-extent based thresholding in fMRI analyses: pitfalls and recommendations. *Neuroimage* 91, 412–419. doi: 10.1016/j.neuroimage.2013.12.058

Wu, T., Long, X., Zang, Y., Wang, L., Hallett, M., Li, K., et al. (2009). Regional homogeneity changes in patients with parkinson's disease. *Hum. Brain Mapp.* 30, 1502–1510. doi: 10.1002/hbm.20622

Xia, M., Wang, J., and He, Y. (2013). BrainNet viewer: a network visualization tool for human brain connectomics. *PLoS One* 8:e68910. doi: 10.1371/journal.pone.0068910

Yan, C. G., Cheung, B., Kelly, C., Colcombe, S., Craddock, R. C., Di Martino, A., et al. (2013). A comprehensive assessment of regional variation in the impact of head micromovements on functional connectomics. *Neuroimage* 76, 183–201. doi: 10.1016/j.neuroimage.2013.03.004

Yan, C. G., Wang, X., Zuo, X. N., and Zang, Y. F. (2016). DPABI: data processing & analysis for (resting-state) brain imaging. *Neuroinformatics* 14, 339–351. doi: 10.1007/s12021-016-9299-9294

Zang, Y., Jiang, T., Lu, Y., He, Y., and Tian, L. (2004). Regional homogeneity approach to fMRI data analysis. *Neuroimage* 22, 394–400. doi: 10.1016/j.neuroimage.2003.12.030

Zhang, H., Yin, X., Ouyang, Z., Chen, J., Zhou, S., Zhang, C., et al. (2016). A prospective study of freezing of gait with early Parkinson disease in chinese patients. *Medicine* 95:e4056. doi: 10.1097/MD.0000000000004056

Zhou, C., Zhong, X., Yang, Y., Yang, W., Wang, L., Zhang, Y., et al. (2018). Alterations of regional homogeneity in freezing of gait in Parkinson's disease. *J. Neurol. Sci.* 387, 54–59. doi: 10.1016/j.jns.2018.01.021

Conflict of Interest: ZLuo was employed by the company of GYENNO Technologies Co., Ltd.

The remaining authors declare that the research was conducted in the absence of any commercial or financial relationships that could be construed as a potential conflict of interest.

frontiers in Neuroscience

ORIGINAL RESEARCH
published: 07 February 2020
doi: 10.3389/fnins.2019.01450

Motion Biomarkers Showing Maximum Contrast Between Healthy Subjects and Parkinson's Disease Patients Treated With Deep Brain Stimulation of the Subthalamic Nucleus. A Pilot Study

*Andreas Kuhner[1,2], Isabella Katharina Wiesmeier[2,3], Massimo Cenciarini[2,3], Timo Leon Maier[2,3], Stefan Kammermeier[4], Volker Arnd Coenen[2,5], Wolfram Burgard[1,2] and Christoph Maurer[2,3]**

[1] Department of Computer Science, University of Freiburg, Freiburg im Breisgau, Germany, [2] BrainLinks BrainTools, Cluster of Excellence, University of Freiburg, Freiburg im Breisgau, Germany, [3] Department of Neurology and Neurophysiology, University Medical Center Freiburg, Medical Faculty, Freiburg im Breisgau, Germany, [4] Klinikum der Universität München, Ludwig-Maximilians-Universität LMU, Neurologische Klinik und Poliklinik, Munich, Germany, [5] Department of Stereotactic and Functional Neurosurgery, University Medical Center Freiburg, Medical Faculty, Freiburg im Breisgau, Germany

OPEN ACCESS

Edited by:
Martin J. McKeown,
University of British Columbia, Canada

Reviewed by:
Maria Eugenia Caligiuri,
University of Magna Graecia, Italy
Dejan Georgiev,
University Medical Centre,
Ljubljana, Slovenia
Jean-Francois Daneault,
Rutgers, The State University of New Jersey, United States

***Correspondence:**
Christoph Maurer
christoph.maurer@uniklinik-freiburg.de

Specialty section:
This article was submitted to Neurodegeneration, a section of the journal Frontiers in Neuroscience

Received: 12 January 2019
Accepted: 30 December 2019
Published: 07 February 2020

Citation:
Kuhner A, Wiesmeier IK, Cenciarini M, Maier TL, Kammermeier S, Coenen VA, Burgard W and Maurer C (2020) Motion Biomarkers Showing Maximum Contrast Between Healthy Subjects and Parkinson's Disease Patients Treated With Deep Brain Stimulation of the Subthalamic Nucleus. A Pilot Study. Front. Neurosci. 13:1450. doi: 10.3389/fnins.2019.01450

Background: Classic motion abnormalities in Parkinson's disease (PD), such as tremor, bradykinesia, or rigidity, are well-covered by standard clinical assessments such as the Unified Parkinson's Disease Rating Scale (UPDRS). However, PD includes motor abnormalities beyond the symptoms and signs as measured by UPDRS, such as the lack of anticipatory adjustments or compromised movement smoothness, which are difficult to assess clinically. Moreover, PD may entail motor abnormalities not yet known. All these abnormalities are quantifiable via motion capture and may serve as biomarkers to diagnose and monitor PD.

Objective: In this pilot study, we attempted to identify motion features revealing maximum contrast between healthy subjects and PD patients with deep brain stimulation (DBS) of the nucleus subthalamicus (STN) switched off and on as the first step to develop biomarkers for detecting and monitoring PD patients' motor symptoms.

Methods: We performed 3D gait analysis in 7 out of 26 PD patients with DBS switched off and on, and in 25 healthy control subjects. We computed feature values for each stride, related to 22 body segments, four time derivatives, left–right mean vs. difference, and mean vs. variance across stride time. We then ranked the feature values according to their distinguishing power between PD patients and healthy subjects.

Results: The foot and lower leg segments proved better in classifying motor anomalies than any other segment. Higher degrees of time derivatives were superior to lower degrees (jerk > acceleration > velocity > displacement). The averaged movements across left and right demonstrated greater distinguishing power than left–right asymmetries. The variability of motion was superior to motion's absolute values.

Conclusions: This small pilot study identified the variability of a smoothness measure, i.e., jerk of the foot, as the optimal signal to separate healthy subjects' from PD patients' gait. This biomarker is invisible to clinicians' naked eye and is therefore not included in current motor assessments such as the UPDRS. We therefore recommend that more extensive investigations be conducted to identify the most powerful biomarkers to characterize motor abnormalities in PD. Future studies may challenge the composition of traditional assessments such as the UPDRS.

Keywords: Parkinson's disease, machine learning, motion, algorithm, accelerometry

INTRODUCTION

Technology-based assessments of Parkinson's disease (PD) symptoms can provide valid and accurate parameters of the disease's clinically relevant features (Maetzler et al., 2016). Moreover, they may deliver an additional benefit by detecting, quantifying, and ranking signs and symptoms that have not been considered, or of which we have been unaware before. Motion capture techniques as a typical example for technology-based assessments have already been tested in PD (e.g., Lorincz and Welsh, 2005). One reason for PD being a pioneering disease for motion capture is that PD presents rather clear-cut, familiar motor deficits (Braak et al., 1996; Fahn, 2003; Bloem et al., 2004; Vaugoyeau and Azulay, 2010). They include the classical symptoms such as bradykinesia, rigidity and tremor, freezing, and falling (Bloem et al., 2004; Lewis and Barker, 2009). In addition, PD patients have difficulty in initiating movements and maintaining fluid sequential or repetitive movements. All these motor abnormalities converge to abnormal movement patterns, e.g., during gait. Specifically, PD patients' gait abnormalities consist of decreased gait velocity with shuffling, dragging steps, short step lengths, forward-stooped posture, decreased arm swing, and a wide step variability (Hausdorff et al., 1998; Dietz et al., 2001; Gutnik et al., 2005). Motor deficits usually appear one-sided and remain dominant on one side throughout disease progression (Lewek et al., 2010; Roggendorf et al., 2012; Boonstra et al., 2014, 2016; Plate et al., 2015).

Motion capture techniques were applied in the past to reproduce clinical findings by using either single sensors (accelerometers, inertial sensors, or gyroscopes), e.g., placed on the lower back (Hubble et al., 2015; Bernad-Elazari et al., 2016) or multiple sensors like the Xsens MVN suit used in the present study.

Despite the abundance of available motion data in PD patients, motion capture techniques have not been regularly used in hospitals thus far. One reason for this may be the "big data" problem. Motion data from the Xsens MVN suit used here delivers data on 22 segments, in 6 dimensions (3 rotations, 3 translations), with a frame rate of 120 Hz, so 5 min recording time leads to about 5 million data points. To characterize PD patients' motor abnormalities meaningfully, the amount of data must be considerably reduced, e.g., via feature extraction (Hester et al., 2006; Patel et al., 2009).

Resulting motion features may include parameters such as mean displacements, velocities, and accelerations, or smoothness, represented by jerk (third time derivative of displacement). There is already evidence that jerk is abnormal in PD (Teulings et al., 1997; Hogan and Sternad, 2009). Other methods of data reduction by feature extraction involve signal processing methods, e.g., wavelet analysis (Joshi et al., 2017), stochastic models, like the Hidden Markov Model (Joshi et al., 2017), or machine-learning algorithms (Wouda et al., 2016), i.e., using Random Forests (Wahid et al., 2015; Kuhner et al., 2016, 2017).

Simple machine-learning algorithms like Random Forests may be able to deliver a classification strategy and successfully separate healthy subjects from patients. However, the process by which machine-learning algorithms favor certain features over others is not necessarily instructive. For example, features not applied for a given classification task may either correlate very closely with features already in use (and that were therefore disregarded) or, on the contrary, on features that do not facilitate the classification task at all. As a consequence, machine-learning algorithms are usually unsuitable to advance the understanding of a certain abnormality.

When experimenting with machine-learning algorithms for feature extraction in PD subjects (Kuhner et al., 2016, 2017), we came up with a very simple question that machine-learning classification methods alone cannot answer, namely, which signals or features best describe the difference between healthy subjects on the one hand and PD patients on the other hand.

For this study, we collected gait data of patients with deep brain stimulation (DBS) electrodes in place, switched on or off. For the sake of simplicity, we report here the maximum contrast between healthy subjects, and PD patients with DBS switched on or off. We attempted to optimize a computational model based on a minimally reduced number of ideally one optimal body segment, one single optimal time derivative (displacement, velocity, acceleration, or jerk), and one optimal signal entity (single channels vs. left–right difference) as either absolute values or their variability. In addition, we used AdaBoost to determine the most valuable feature combination to characterize PD patients' state.

MATERIALS AND METHODS

Subjects

This study involved 26 PD patients and 25 healthy control subjects. PD patients stayed in the Department of Neurology and Neurophysiology of the University Hospital Freiburg for their first post-implantation parameter setting of DBS. Among the

recorded 26 patients, 7 patients [3 female, 4 male; mean age 58 ± 14.5 years (± SD), age range 40–74 years] with rather long disease duration (see **Table 1**) were able to complete the 10 m walk test with DBS both in the ON and OFF condition. The remaining 19 patients could not walk 10 m in the OFF condition due to severe postural instability and gait disturbance, and were thus excluded from data analysis.

Mean Unified Parkinson's Disease Rating Scale (UPDRS) in the DBS OFF condition was 44 [±11.7 (±SD)], and in the ON condition, 24 [±6.5 (±SD)]. Disease duration ranged from 8 to 14 years [mean 10.5 years ± 1.9 (±SD), **Table 1**]. The PD patients were measured twice (in the DBS ON and OFF condition) in order to balance on and off DBS conditions. Healthy control subjects [13 female, 12 male; mean age 52 ± 6.8 years (±SD), age range 37–63 years] were recruited from relatives and department staff. All patients and subjects gave their written informed consent in accordance with the Declaration of Helsinki. The study protocol was approved by the Ethics Committee of the University of Freiburg. All the included data were anonymized.

Experimental Setup

The Xsens MVN suit is a human motion capture system (see **Figure 1**) consisting of 17 MEMS (microelectro-mechanical systems) which merge the signals of 3D inertial measurement units (IMUs), i.e., linear accelerometers, 3D magnetometers, and 3D rate gyroscopes. Each MEMS was attached to a specific body region, i.e., the head, upper or lower arms, spine or upper or lower legs, etc. The sensors were positioned next to bigger joints (e.g., knee, wrist, shoulder). Data were sampled at 120 Hz and sent to two wireless receivers. Both receivers delivered the data to a portable computer. Custom-made software employed the data from the sensor trajectories to extrapolate segment size, segment movements, and orientations, as well as joint positions. That data were then used to reconstruct 3D segmental movements and joint angles. Furthermore, the program provided velocity and acceleration for each segment/joint, as well as the orientation. **Figure 1** shows a subject's reconstructed avatar as a visualization of the segment and joint positions at a given moment.

Data Analysis

For data analysis, we applied the absolute values of position, velocity, acceleration, and jerk vectors of segments and joints. The reconstructed skeleton (see right panel in **Figure 1**) consisted of 22 segments, including 3D positions and orientations in space, which were represented in quaternions. The data sets covering gait were split into individual steps and strides ($j \in S$). We first identified the exact moment when the swinging leg passes the standing leg. Starting from that point in time, we went both forwards and backwards in time until we identified the moments where the foot segment's absolute velocity dropped below 5% of its maximum velocity, which then identified the start and end of a given step. Each stride served as an individual data set for further processing.

Data Preprocessing

We denoted with $p_i^{(t)}$ the position of segment i at time step t. A Gaussian filter with several time dependent positions was used to filter sensor-related noise to compute a smoothed position trace $\underline{p}_i^{(t)} = \frac{\left(\sum_{n=-\tau}^{\tau} \frac{1}{\sqrt{2\cdot\pi\cdot\sigma^2}} \cdot e^{-\frac{1}{2}\cdot\frac{n^2}{\sigma^2}} \cdot p_i^{(t+n)}\right)}{\left(\sum_{n=-\tau}^{\tau} \frac{1}{\sqrt{2\cdot\pi\cdot\sigma^2}} \cdot e^{-\frac{1}{2}\cdot\frac{n^2}{\sigma^2}}\right)}$, where the index i denotes the segment ID. In the next step, we transformed position traces into the local frame of the hip, namely $\hat{p}_i^{(t)} = \underline{p}_i^{(t)} - \underline{p}_0^{(t)}$, where $\underline{p}_0^{(t)}$ is the smoothed position of the hip frame. This transformation allowed us to evaluate data such as the arm swing in relation to the lower trunk to guarantee independence from the main movement direction.

Features

The 22 segments consisted of 6 midline segments (trunk) and 8 segments with left and right specificity in each case, e.g., left and right hand, thus 16 segments with left and right specificity in total. We can reformulate the segment positions as $\left\{\hat{p}_1^{(t)}, \ldots, \hat{p}_6^{(t)}, \hat{p}_{7,l}^{(t)}, \hat{p}_{7,r}^{(t)}, \ldots, \hat{p}_{14,l}^{(t)}, \hat{p}_{14,r}^{(t)}\right\}$.

The first group of features includes the means between the left and right side of the segments with left and right specificity, i.e.,

$$f_{i,m}^{(t)} = \frac{1}{2} \cdot \left(\hat{p}_{i,l}^{(t)} + \hat{p}_{i,r}^{(t)}\right) \text{ for } i \in \{7, \ldots, 14\}.$$

TABLE 1 | Summary of clinical data: Parkinson's disease (PD) patients are shown with type [one patient tremor dominant (TD), six patients akinetic-rigid with dominant postural instability and gait disturbance over tremor (PIGD)], age, disease duration, Unified Parkinson's Disease Rating Scale (UPDRS), with modified subscore III when nucleus subthalamicus (STN) simulation was switched on and off, levodopa equivalent daily dosage (LEDD), most affected side, and of freezing of gait (FOG).

Patient	PD type	Age (years)	Disease dur. (years)	UPDRS deep brain stimulation (DBS) On	UPDRS DBS Off	LEDD	Affected side	FOG
P002	TD	74	9	15	20	300	Left	–
P013	PIGD	69	8	29	38	400	Left	–
P017	PIGD	74	12	22	43	320	Right	+
P018	PIGD	49	9	32	51	250	Left	+
P020	PIGD	57	14	15	47	200	Right and left	–
P021	PIGD	40	10	16	61	350	Right	+
P022	PIGD	43	10	28	45	450	Right	–
Mean		58	10,5	24	44	324		
SD		14.5	2.0	6.5	12	79		

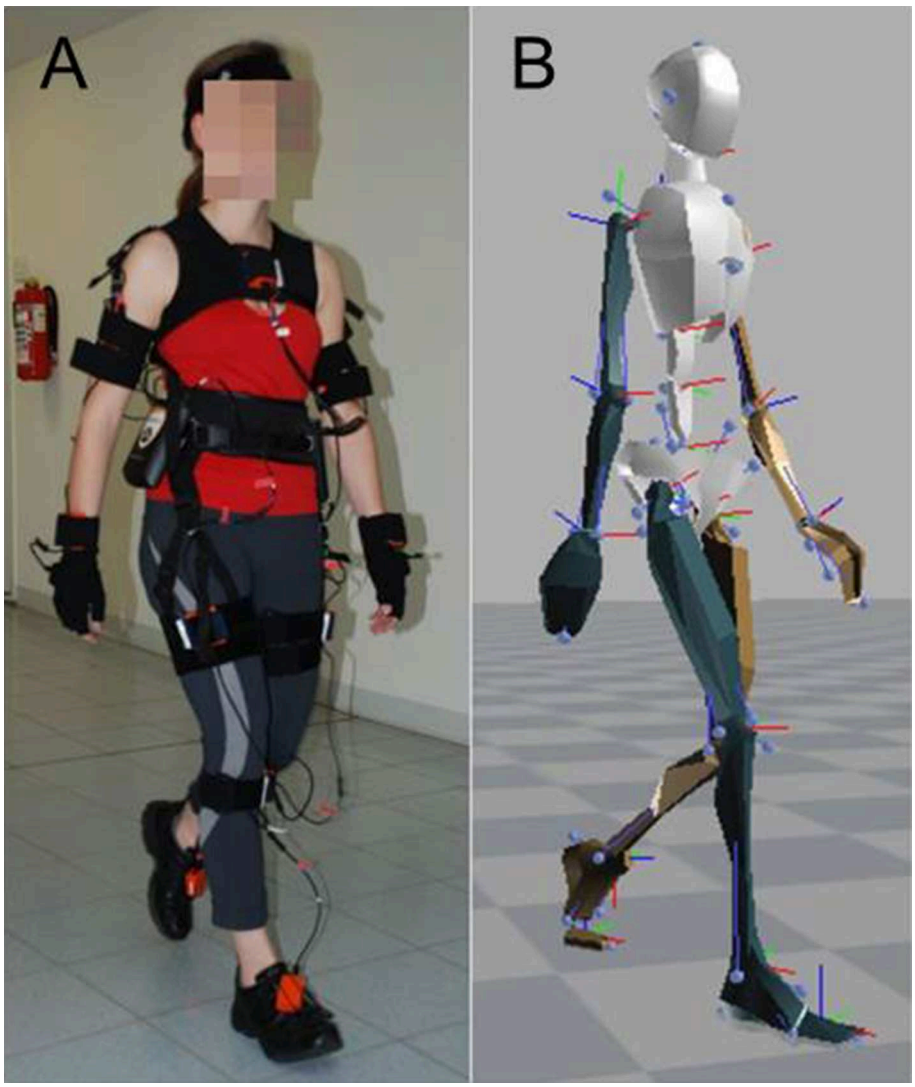

FIGURE 1 | Experimental setup. **(A)** Subject wearing the Xsens sensor suit, consisting of 17 MEMS (microelectro-mechanical systems) which merge the signals of 3D inertial measurement units (IMUs), i.e., linear accelerometers, 3D magnetometers, and 3D rate gyroscopes. Data were sampled at 120 Hz and used to reconstruct 3D segmental movements and joint angles. **(B)** Reconstructed avatar of the subject as a visualization of the segment and joint positions at a given moment.

The second group of features covers the left/right differences, i.e., $f_{i,d}^{(t)} = \left(\hat{p}_{i,l}^{(t)} - \hat{p}_{i,r}^{(t)}\right)$ for $i \in \{7, \ldots, 14\}$. Using the second feature, we evaluated differences between the more and less affected side.

Furthermore, we computed the first and second moment of each feature for each body segment i over the whole trajectory, yielding each feature's mean and variance. The mean is computed by

$\mu_i = \frac{1}{T} \cdot \sum_{t=1}^{T} d_i^{(t)}$ for $i \in \{1, \ldots, 22\}$ and the variance with $\sigma_i^2 = \frac{1}{T-1} \cdot \sum_{t=1}^{T} \left(\mu_i - d_i^{(t)}\right)^2$ for $i \in \{1, \ldots, 22\}$ where d is either p, f_i or f_m.

Thus, the total number of features is the product of the absolute mean and variance (2) of a single stride, times body segments (22), times displacement and three orders of time derivative of displacement (4), times left–right mean and left–right difference (2) of 8 out of 22 segments, resulting in 264 features. One subject's data set consisted of values for all 264 features for each stride. Since we evaluated about 30 strides for each subject, the total amount of data points of one subject amounted to a value of about $30 \times 264 = 7{,}920$.

Weak Classifiers

A weak classifier (C_W) relates to a separating algorithm which splits a certain feature of the data into two categories with an accuracy of at least 50% (e.g., a specific segment's slow vs. fast velocity). Parameters $\{-1, 1\}$ are chosen as class labels. Weak classifiers were used to detect a specific threshold that delivered the best separation results between PD patients and healthy control subjects. We calculated the highest classification rate by uniting data sets of healthy subjects and PD patients into

one, sorting the elements according to the value of the current separating algorithm, and taking the value ε as a threshold between two elements in the set. The final weak classifier is calculated by $WC_i(x) = 1$ *if* $x < \varepsilon_i$ *and* $WC_i(x) = -1$ *if* $x \geq \varepsilon_i$.

The classifiers' performance was quantified by a leave-one-subject-out cross-validation, i.e., one subject was removed from the data set, and the residual data set was used to predict the missing data sample. This procedure was repeated for each subject.

Meta-Classifier AdaBoost

We used AdaBoost to evaluate which types of feature combinations ameliorated the classification results as compared to single features. AdaBoost works as a meta-classifier and combines multiple classifiers, i.e., features plus respective thresholds, into one, by weighting the output of this set of weak classifiers. In this case, the meta-classifier represents an optimal mix of features for maximum differences between PD patients and healthy subjects. If the result is smaller than zero, the data set belongs to the first group (here, PD patients); otherwise it belongs to the second group (healthy subjects). In principle, AdaBoost repeats the following two steps: First, the algorithm identifies a classifier C_m which contributes the most information to the current weighted sum of chosen weak classifiers

$$C^{(m-1)} = \sum_{k=1}^{m-1} \alpha_k C_k, \text{ i.e., } C_m = \underset{c \in C_W}{argmin} \sum_{c(x_i) \neq y_i} \omega_i^{(m)}$$

where $\omega_i^{(1)} := 1, \omega_i^{(m)} := e^{-y_i \cdot C^{(m-1)}(x_i)}$ for $m > 1$.
Then, the sum runs over the total training set. Thereby, $\{(x_i, y_i)\}_{i=1}^{N}$ denotes the set of training data points x_i and the corresponding labels y_i. The concept of this algorithm is to add the classifier which maximizes information acquisition. In this way, the algorithm categorizes the wrongly classified elements of $C^{(m-1)}$ correctly. The second step of the AdaBoost involved the computation of a weight for the selected classifier. Let $\xi^{(m)} = \sum_{i=1}^{N} \omega_i^{(m)}$ be the total error. Note that the optimal weight α_m for the classifier C_m is given by

$\alpha_m = \frac{1}{2} \cdot log\left(\frac{1-\epsilon_m}{\epsilon_m}\right)$ with $\epsilon_m = \frac{\sum_{C_m(x_i) \neq y_i} \omega_i^{(m)}}{\xi^{(m)}}$. The resulting function to classify a sample x is: $C^{(m)}(x) = \sum_{k=1}^{m} \alpha_k \cdot C_k(x)$.
The algorithm chooses the most accurate weak classifier as first classifier. Each succeeding classifier is not necessarily a classifier with high accuracy, but it does add the highest amount of information to the existing (chosen) set. As a result, a set of weak classifiers represents one of the best combinations for separating the data.

Our classifier accuracy values were statistically analyzed using the JMP® statistic program by SAS Institute Inc., Cary, NC, USA. We tested normal distribution and homogeneity of variances with the Kolmogorov–Smirnov test and parametric methods for further analyses. Due to the expected dependency between the outcome measures within motor behavior, statistical significance was tested by an analysis of variance (ANOVA). The within-subjects factors were: (i) absolute values vs. variance of absolute values, (ii) displacement vs. velocity vs. acceleration vs. jerk-related measures, (iii) mean absolute values vs. left–right difference, and (iv) segments (e.g., head, neck, shoulder). The level of statistical significance was set at $p = 0.05$. Differences between groups were tested using Tukey's *post-hoc* test, if multiple comparisons were considered.

RESULTS

Overall, our study yielded a total of four different time derivatives: displacement, velocity, acceleration, and jerk (**Figure 2**). Hereby, displacement relied on the position vectors between the hip and the analyzed segment. Velocity, acceleration and jerk were the first, second, and third derivation of that position. **Figure 2A** depicts the accuracy, which we defined as the percentage of correctly classified subjects as PD patients: Here, nearly all features [except for the displacement of the midline segments (trunk) and the mean between left and right limbs] attained accuracy rates between 80 and 90%.

Figure 2B displays the results of the variance of features. Again, features of the midline segments and the mean between more and less affected limb performed across all time derivatives equally with accuracy rates of 80% to 90%.

Systematic Evaluation of Feature Characteristics

We applied accuracy values to determine the effects of different degrees of freedom in our feature matrix, i.e.,:

- Absolute values vs. variance of absolute values (**Figure 3A**)
- Displacement vs. velocity vs. acceleration vs. jerk-related measures (**Figure 3B**)
- Mean absolute values vs. left–right difference (**Figure 3C**)
- Segments (e.g., head, neck, shoulder, **Figure 3D**).

We found that variance of a certain feature determined significantly higher accuracy values than the raw feature ($F = 26$, $p < 0.0001$, **Figure 3A**). Jerk measures displayed significantly higher accuracy values than acceleration, velocity, and displacement-related measures ($F = 32$, $p < 0.0001$, **Figure 3B**). *Post-hoc* tests showed that displacement-related measures reveal significantly less accuracy than all other time derivatives ($p < 0.0001$ between displacement, and all other time derivatives). The limbs' mean values demonstrated significantly higher accuracy values than the differences between the more and less affected limb ($F = 210$, $p < 0.0001$, **Figure 3C**). Finally, the accuracy of segments varied: lower leg, foot, and toe measures revealed the greatest accuracy, followed by trunk measures (L5, L3, T12, T8); the upper arm, shoulders, head, hand, and forearm were lowest ($F = 2.3$, $p = 0.01$, **Figure 3D**). *Post-hoc* tests revealed that both the foot and lower leg showed significantly higher accuracies than the forearm ($p = 0.043$ and $p = 0.045$, respectively). All other pairwise comparisons between segments did not reach a significance level below $p = 0.05$. These findings were in line with the overall highest accuracy value (variance of jerk of the mean of the left and right foot).

Meta-Classifier AdaBoost

When evaluating the performance of combinations of classifiers using AdaBoost, we observed the following rules: The feet yielded the highest accuracy by applying a combination of variance of

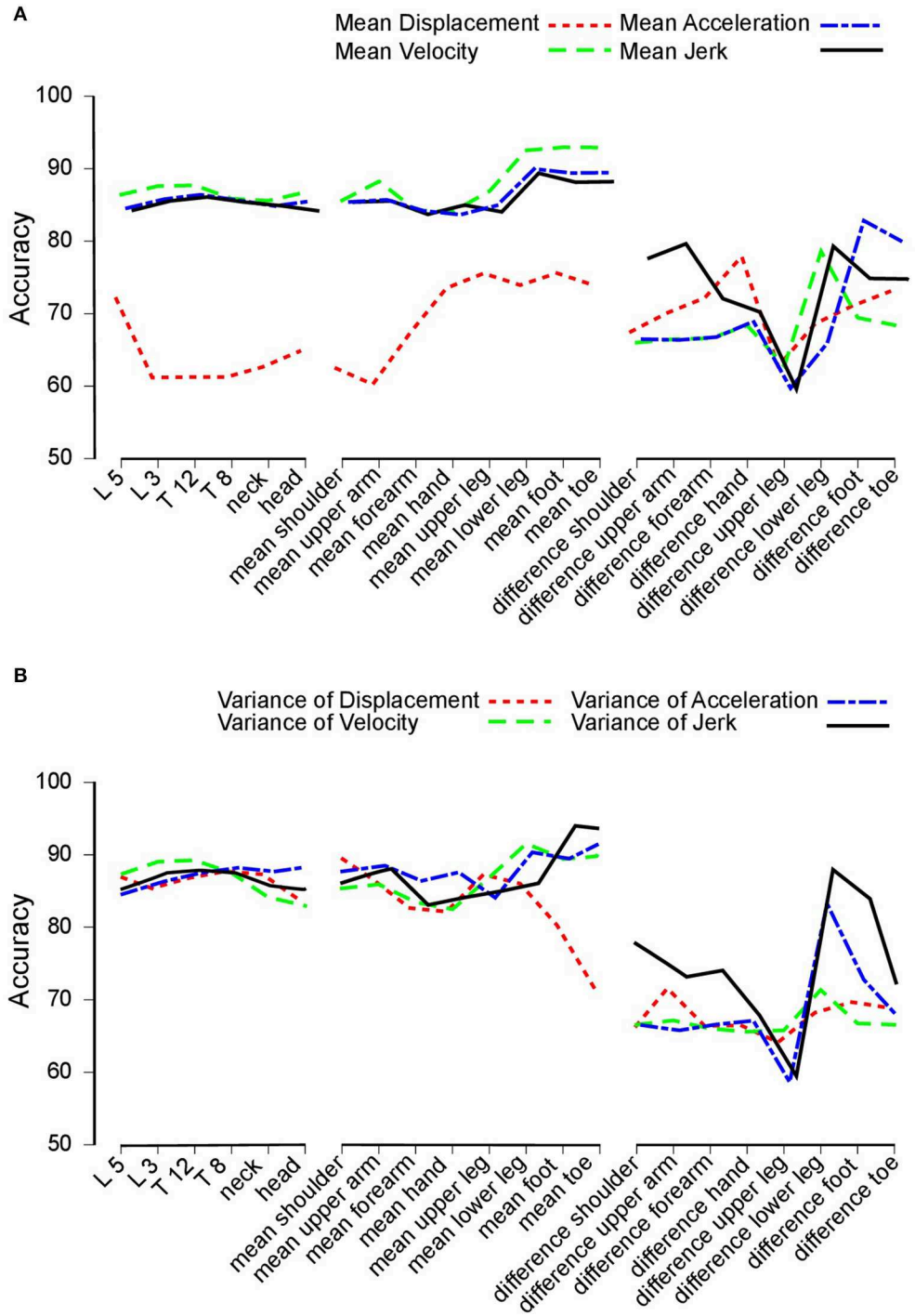

FIGURE 2 | Accuracy. **(A)** Accuracy achieved to distinguish between Parkinson's disease (PD) patients and healthy control subjects. Accuracy for trunk segments (left section), limb segments (central section), and limb segment asymmetries (right section) using mean displacement (dotted line), velocity (dashed line), acceleration (dashed and dotted line), and jerk (solid line). **(B)** Accuracy values based on variance measures. This figure is based on variance measures instead of mean values for displacement (dotted line), velocity (dashed line), acceleration (dashed and dotted line), and jerk (solid line).

jerk, variance of acceleration, and mean of velocity. Concerning the left–right difference, the combination of variance of jerk and the mean of displacement displayed the highest accuracy. The segment with the overall highest accuracy was the lower leg using the combination of variance of acceleration, jerk, and mean of velocity. Of the head and trunk segments, the head

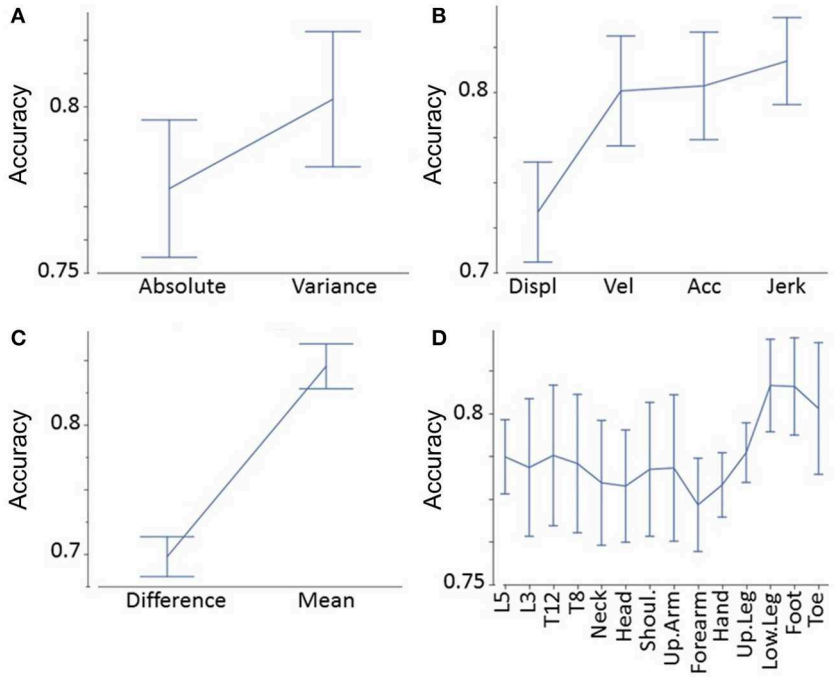

FIGURE 3 | Accuracy analyses. Accuracy as a function of absolute values vs. variance of absolute values **(A)**, displacement vs. velocity vs. acceleration vs. jerk-related measures **(B)**, mean absolute values vs. left–right difference **(C)**, and segments **(D)**.

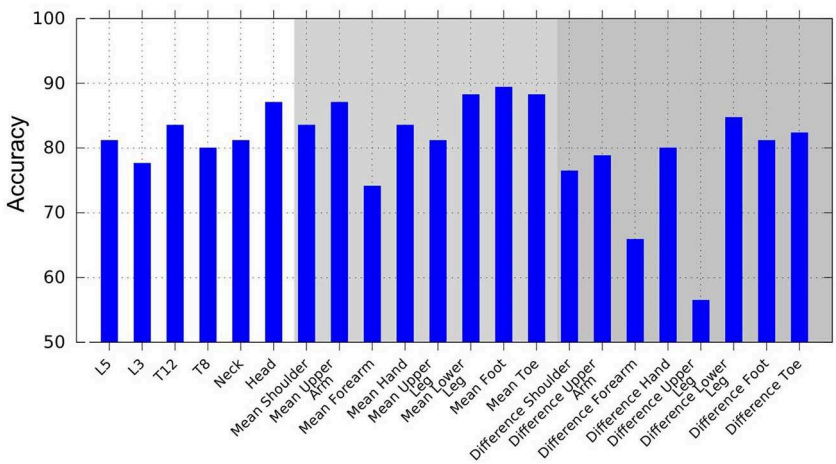

FIGURE 4 | Accuracy achieved using AdaBoost, based on combinations of multiple weak classifiers to create a stronger classification hypothesis. Weak classifiers are displacement, velocity, acceleration, and jerk mean, and variance features.

yielded the highest accuracy rate based on the combination of variance and mean of acceleration and displacement. Overall, the head and trunk segments' best feature combination was mean of displacement, variance of jerk, and acceleration. As an example of feature combinations, **Figure 4** illustrates the combined AdaBoost accuracy rates separated by segments. Note that due to the cross-validation procedure, the overall performance of AdaBoost is lower than the best feature of each segment.

DISCUSSION

Gait deficits are one of the major problems that determine PD patients' quality of life. PD patients report them as the most debilitating disease features (Horak et al., 2005). While gait disturbances occur in all PD subtypes, they are the leading symptom in the postural instability and gait disturbance type of PD, PIGD. The patient group studied here mainly presented

akinetic types of the disease. In this paper, we analyzed gait because it involves movements of all body segments. Other motion tasks, e.g., getting up from a chair or doing accuracy tasks with the hand, require specific instructions. In addition, they represent a minor portion of overall motion deficits and vary widely.

The aim of this pilot study was to compare features from sensor suit data (segments, time derivatives, variance, left–right difference) that enable optimal discrimination between the gait patterns of advanced-stage PD patients with DBS electrodes in the nucleus subthalamicus (STN) switched on or off, and healthy subjects. Other approaches to classify PD patients' gait employed data from considerably different sources for different purposes. While Khorasani and Daliri (2014) and Joshi et al. (2017) analyzed data of force-sensitive insoles provided by Hausdorff et al. (1998), Wahid et al. (2015) used whole body gait data and force platform outcomes to optimize classification results. Here, we report the maximum contrast between healthy subjects and PD patients with DBS switched on or off. In theory, one could calculate the contrast between many different subgroups of this cohort. For example, another potential question is which parameter best separates PD patients with DBS switched off from those with DBS switched on. Such a contrast would provide information on the treatment effect of DBS which might deliver another favorable signal. Here, we focused on the aforementioned contrast for simplicity's sake.

In our approach, we calculated weak classifiers for each feature separately in order to compare the quality of different features. In the next step, we systematically analyzed the accuracy of those classifiers to correctly distinguish PD patients from healthy subjects. In general, we identified an obvious grade of classifier accuracies: (i) variance was superior to absolute values of body motion, (ii) jerk (third time derivative of displacement) was superior to acceleration, velocity, and displacement, (iii) average motion across left and right was superior to the differences, i.e., asymmetries between left and right markers, and (iv) feet and lower leg segments were superior to trunk, head, and hand movements. These principles were in line with the overall highest accuracy value (variance of jerk of the mean of the left and right foot).

In addition, we evaluated the accuracy outcomes from AdaBoost and the respective sets of weak classifiers to extract the combination of features displaying maximum discriminative power. The main purpose of this approach was to potentially enhance the quality of discrimination by combining different features across different segments.

Meta-classifiers like AdaBoost deliver a set of classifiers that optimally separate the group of PD patients from healthy subjects. We found that a combination of two to three features is optimal. In most cases, the combination consisted of a feature related to absolute values with a low order of time derivative, like displacement or velocity, and a variance-related feature of a high order of time derivative like acceleration or jerk. This proved to be true for the trunk and limb, as well as for the asymmetry features. Out of all head and trunk segments, the head delivered the highest accuracy rates.

In a previous study, we showed that machine-learning approaches significantly correlate with known clinical measures such as the UPDRS (Kuhner et al., 2017).

Our selection of a small set of features instead of using the entire body data set is specifically interesting since a full sensor suit is obtrusive for everyday use. On the other hand, very few sensors (e.g., at the belt, or as a collar, at the wrist, near the trunk) to monitor motion patterns in PD patients (Horak et al., 2005) and other diseases (Bonora et al., 2015) might neglect important information of certain motor tasks, particularly considering the growth in wearable technology in conjunction with modern smartphones. Our findings may facilitate the development of motion capture systems based on commercial-grade wearable sensors and "smartphone apps" to observe motor features in PD patients. In addition, data reduction is often done locally, which means next to the sensor (IMU), before the information is transferred to a collecting unit and further processed, due to the usually limited rate of data transfer. Such data reduction means the signals of interest must be pre-selected. We aimed here to make recommendations as to where best to place sensors and which type of signals should ideally be processed so as to exploit the available motion data to the maximum.

Limitations

In this study, PD patients were suffering from advanced-stage PD and were undergoing recent DBS of the STN. Most study participants were not able to walk 10 m in the OFF condition independently, which greatly reduced our sample size and potentially biased our data. This severely affected group was chosen to analyze the strongest expressions of pathological features. Early-stage PD gait deficits, PD patients without DBS, and the variability of the defined features during medication were not the focus of the present study. Additional investigations should explore whether our study's optimal-parameter findings also apply to less severely affected PD patients and other treatment conditions.

CONCLUSIONS

Our approach proposes a specific marker position (foot, lower leg) and certain data processing algorithms (variance of jerk) to optimally characterize PD patients' motion abnormalities during walking. Using AdaBoost, we identified sets of classifiers that optimally separate PD from healthy subjects. For walking, a useful combination of classifiers may refer to the head and a foot segment. Moreover, this combination should include an absolute value derived from a low order of time derivative and a variance-related feature from a high order of time derivative.

In the future, we aim to evaluate the differential effect of treatment (e.g., STN DBS) in order to characterize the optimal set of features for monitoring intervention effects, before we extend this approach to different motion patterns, e.g., standing up from a chair, turning around, and interacting with the surroundings. In future studies, our results may help to develop a low-threshold and objective analysis tool for diagnosing and monitoring motor abnormalities in PD. Given our latest findings, a simplified and

small sensor attachable to the shoe may suffice to analyze PD gait abnormalities.

More generally, this small pilot study ranked motion features according to their distinguishing power and identified the variability of a smoothness measure i.e., jerk of the foot as the most favorable signal from which to separate healthy subjects' from PD patients' gait. This biomarker is imperceptible to clinicians' naked eye and, therefore, is not incorporated in current motor assessments such as the UPDRS. Consequently, we believe that more extensive investigations are warranted to identify the most powerful biomarkers for characterizing motor abnormalities in PD. Future studies may ultimately challenge how traditional assessments such as the UPDRS are composed.

DATA AVAILABILITY STATEMENT

The datasets generated for this study are available on request to the corresponding author.

ETHICS STATEMENT

All patients and subjects gave their written informed consent in accordance with the Declaration of Helsinki. This study protocol was approved by the Ethics Committee of the University of Freiburg. All data was included anonymized.

AUTHOR CONTRIBUTIONS

AK and CM were responsible for the concept and design of the work, the analysis and interpretation of data, and the first draft of the manuscript. AK and TM were responsible for data acquisition. MC contributed to conceiving and designing the work, and critically revised the manuscript. IW drafted the manuscript, edited the final manuscript for submission, and revised the work critically. SK, VC, and WB contributed to the concept and critical revision of the work. All authors approved the final manuscript.

FUNDING

CM was partially funded by the BrainLinks-BrainTools Cluster of Excellence of the German Research foundation (DFG, Grant No. ADV139) and by EC grant H2020-SC1–2017-CNECT-1 (HOLOBALANCE: Project ID 769574).

REFERENCES

Bernad-Elazari, H., Herman, T., Mirelman, A., Gazit, E., Giladi, N., and Hausdorff, J. M. (2016). Objective characterization of daily living transitions in patients with Parkinson's disease using a single body-fixed sensor. *J. Neurol.* 263, 1544–1551. doi: 10.1007/s00415-016-8164-6

Bloem, B. R., Hausdorff, J. M., Visser, J. E., and Giladi, N. (2004). Falls and freezing of gait in Parkinson's disease: a review of two interconnected, episodic phenomena. *Mov. Disord. Off. J. Mov. Disord. Soc.* 19, 871–884. doi: 10.1002/mds.20115

Bonora, G., Carpinella, I., Cattaneo, D., Chiari, L., and Ferrarin, M. (2015). A new instrumented method for the evaluation of gait initiation and step climbing based on inertial sensors: a pilot application in Parkinson's disease. *J. Neuroengineering Rehabil.* 12, 45. doi: 10.1186/s12984-015-0038-0

Boonstra, T. A., Schouten, A. C., van Vugt, J. P. P., Bloem, B. R., and van der Kooij, H. (2014). Parkinson's disease patients compensate for balance control asymmetry. *J. Neurophysiol.* 112, 3227–3239. doi: 10.1152/jn.00813.2013

Boonstra, T. A., van Kordelaar, J., Engelhart, D., van Vugt, J. P. P., and van der Kooij, H. (2016). Asymmetries in reactive and anticipatory balance control are of similar magnitude in Parkinson's disease patients. *Gait Posture* 43, 108–113. doi: 10.1016/j.gaitpost.2015.08.014

Braak, H., Braak, E., Yilmazer, D., de Vos, R. A., Jansen, E. N., and Bohl, J. (1996). Pattern of brain destruction in Parkinson's and Alzheimer's diseases. *J. Neural Transm.* 103, 455–490. doi: 10.1007/BF01276421

Dietz, V., Fouad, K., and Bastiaanse, C. M. (2001). Neuronal coordination of arm and leg movements during human locomotion. *Eur. J. Neurosci.* 14, 1906–1914. doi: 10.1046/j.0953-816x.2001.01813.x

Fahn, S. (2003). Description of Parkinson's disease as a clinical syndrome. *Ann. N. Y. Acad. Sci.* 991, 1–14. doi: 10.1111/j.1749-6632.2003.tb07458.x

Gutnik, B., Mackie, H., Hudson, G., and Standen, C. (2005). How close to a pendulum is human upper limb movement during walking? *Homo Int. Z. Vgl. Forsch. Am Menschen* 56, 35–49. doi: 10.1016/j.jchb.2004.09.002

Hausdorff, J. M., Cudkowicz, M. E., Firtion, R., Wei, J. Y., and Goldberger, A. L. (1998). Gait variability and basal ganglia disorders: stride-to-stride variations of gait cycle timing in Parkinson's disease and Huntington's disease. *Mov. Disord.* 13, 428–437. doi: 10.1002/mds.870130310

Hester, T., Sherrill, D. M., Hamel, M., Perreault, K., Boissy, P., and Bonato, P. (2006). Identification of tasks performed by stroke patients using a mobility assistive device. *Conf. Proc. Annu. Int. Conf. IEEE Eng. Med. Biol. Soc.* 1, 1501–1504. doi: 10.1109/IEMBS.2006.259437

Hogan, N., and Sternad, D. (2009). Sensitivity of smoothness measures to movement duration, amplitude, and arrests. *J. Mot. Behav.* 41, 529–534. doi: 10.3200/35-09-004-RC

Horak, F. B., Dimitrova, D., and Nutt, J. G. (2005). Direction-specific postural instability in subjects with Parkinson's disease. *Exp. Neurol.* 193, 504–521. doi: 10.1016/j.expneurol.2004.12.008

Hubble, R. P., Naughton, G. A., Silburn, P. A., and Cole, M. H. (2015). Wearable sensor use for assessing standing balance and walking stability in people with Parkinson's disease: a systematic review. *PLoS ONE* 10:e0123705. doi: 10.1371/journal.pone.0123705

Joshi, D., Khajuria, A., and Joshi, P. (2017). An automatic non-invasive method for Parkinson's disease classification. *Comput. Methods Programs Biomed.* 145, 135–145. doi: 10.1016/j.cmpb.2017.04.007

Khorasani, A., and Daliri, M. R. (2014). HMM for classification of Parkinson's disease based on the raw gait data. *J. Med. Syst.* 38:147. doi: 10.1007/s10916-014-0147-5

Kuhner, A., Schubert, T., Cenciarini, M., Maurer, C., and Burgard, W. (2016). "A probabilistic approach based on Random Forests to estimating similarity of human motion in the context of Parkinson's Disease," in *2016 IEEE/RSJ International Conference on Intelligent Robots and Systems (IROS)* (Daejeon), 1851–1856. doi: 10.1109/IROS.2016.7759294

Kuhner, A., Schubert, T., Cenciarini, M., Wiesmeier, I. K., Coenen, V. A., Burgard, W., et al. (2017). Correlations between motor symptoms across different motor tasks, quantified via Random-Forest feature classification in Parkinson's disease. *Front. Neurol.* 8:607. doi: 10.3389/fneur.2017.00607

Lewek, M. D., Poole, R., Johnson, J., Halawa, O., and Huang, X. (2010). Arm swing magnitude and asymmetry during gait in the early stages of Parkinson's disease. *Gait Posture* 31, 256–260. doi: 10.1016/j.gaitpost.2009.10.013

Lewis, S. J. G., and Barker, R. A. (2009). A pathophysiological model of freezing of gait in Parkinson's disease. *Parkinsonism Relat. Disord.* 15, 333–338. doi: 10.1016/j.parkreldis.2008.08.006

Lorincz, K., and Welsh, M. (2005). "MoteTrack: a robust, decentralized approach to RF-based location tracking," in *Location- and Context-Awareness*, eds T. Strang and C. Linnhoff-Popien (Berlin; Heidelberg: Springer), 63–82. doi: 10.1007/11426646_7

Maetzler, W., Klucken, J., and Horne, M. (2016). A clinical view on the development of technology-based tools in managing Parkinson's disease. *Mov. Disord.* 31, 1263–1271. doi: 10.1002/mds.26673

Patel, S., Lorincz, K., Hughes, R., Huggins, N., Growdon, J., Standaert, D., et al. (2009). Monitoring motor fluctuations in patients with Parkinson's disease using wearable sensors. *IEEE Trans. Inf. Technol. Biomed.* 13, 864–873. doi: 10.1109/TITB.2009.2033471

Plate, A., Sedunko, D., Pelykh, O., Schlick, C., Ilmberger, J. R., and Bötzel, K. (2015). Normative data for arm swing asymmetry: how (a)symmetrical are we? *Gait Posture* 41, 13–18. doi: 10.1016/j.gaitpost.2014.07.011

Roggendorf, J., Chen, S., Baudrexel, S., van de Loo, S., Seifried, C., and Hilker, R. (2012). Arm swing asymmetry in Parkinson's disease measured with ultrasound based motion analysis during treadmill gait. *Gait Posture* 35, 116–120. doi: 10.1016/j.gaitpost.2011.08.020

Teulings, H. L., Contreras-Vidal, J. L., Stelmach, G. E., and Adler, C. H. (1997). Parkinsonism reduces coordination of fingers, wrist, and arm in fine motor control. *Exp. Neurol.* 146, 159–170. doi: 10.1006/exnr.1997.6507

Vaugoyeau, M., and Azulay, J.-P. (2010). Role of sensory information in the control of postural orientation in Parkinson's disease. *J. Neurol. Sci.* 289, 66–68. doi: 10.1016/j.jns.2009.08.019

Wahid, F., Begg, R. K., Hass, C. J., Halgamuge, S., and Ackland, D. C. (2015). Classification of Parkinson's disease gait using spatial-temporal gait features. *IEEE J. Biomed. Health Inform.* 19, 1794–1802. doi: 10.1109/JBHI.2015.2450232

Wouda, F. J., Giuberti, M., Bellusci, G., and Veltink, P. H. (2016). Estimation of full-body poses using only five inertial sensors: an eager or lazy learning approach? *Sensors* 16:E2138. doi: 10.3390/s16122138

Conflict of Interest: The authors declare that the research was conducted in the absence of any commercial or financial relationships that could be construed as a potential conflict of interest.

Advantages of publishing in Frontiers

OPEN ACCESS
Articles are free to read for greatest visibility and readership

FAST PUBLICATION
Around 90 days from submission to decision

HIGH QUALITY PEER-REVIEW
Rigorous, collaborative, and constructive peer-review

TRANSPARENT PEER-REVIEW
Editors and reviewers acknowledged by name on published articles

Frontiers
Avenue du Tribunal-Fédéral 34
1005 Lausanne | Switzerland

Visit us: www.frontiersin.org
Contact us: info@frontiersin.org | +41 21 510 17 00

REPRODUCIBILITY OF RESEARCH
Support open data and methods to enhance research reproducibility

DIGITAL PUBLISHING
Articles designed for optimal readership across devices

FOLLOW US
@frontiersin

IMPACT METRICS
Advanced article metrics track visibility across digital media

EXTENSIVE PROMOTION
Marketing and promotion of impactful research

LOOP RESEARCH NETWORK
Our network increases your article's readership